

# The determination of the mixing height - current progress and problems. Proceedings

**Gryning, Sven-Erik; Beyrich, F.; Batchvarova, E.**

*Publication date:*
1997

*Document Version*
Publisher's PDF, also known as Version of record

RISØ BTU Cottbus NIMH

Risø-R-997(EN)

# The Determination of the Mixing Height - Current Progress and Problems



## EURASAP Workshop Proceedings
## 1-3 October 1997
## Risø National Laboratory

Editors
Sven-Erik Gryning, Frank Beyrich and Ekaterina Batchvarova



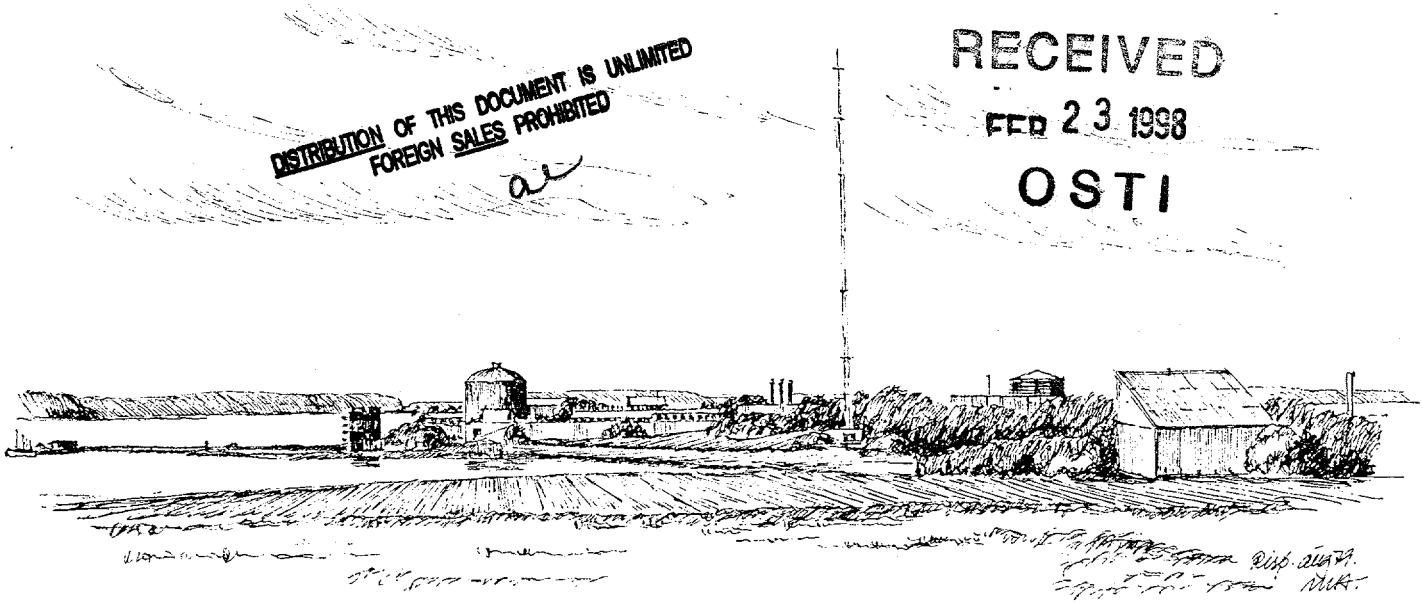

Risø National Laboratory, Roskilde, Denmark
October 1997

## DISCLAIMER

Portions of this document may be illegible electronic image products. Images are produced from the best available original document.

Risø-R-997(EN)

# The Determination of the Mixing Height - Current Progress and Problems

## EURASAP Workshop Proceedings
## 1-3 October 1997
## Risø National Laboratory

Editors

Sven-Erik Gryning,
Risø National Laboratory, Roskilde, Denmark

Frank Beyrich,
Brandenburg Technical University, Cottbus, Germany

Ekaterina Batchvarova,
National Institute of Meteorology and Hydrology, Sofia, Bulgaria

Risø National Laboratory, Roskilde, Denmark
October 1997

**Preface** This report contains extended abstracts of presentations given at a EURASAP Workshop on The Determination of the Mixing Height - Current Progress and Problems. The Workshop, initiated from discussions with Peter Builtjes, was held at Risø National Laboratory 1-3 October 1997 within the framework of EURASAP (European Association for the Sciences of Air Pollution). The specific topics and chairpersons of the Workshop were: Theoretical Considerations (Sven-Erik Gryning), Mixing Height Estimation from Turbulence Measurements and In-Situ Soundings (Douw Steyn), Mixing Height Determination from NWP-Models (Han van Dop), Climatology and Global Aspects (Werner Klug), Mixing Height Determination from Remote Systems (Werner Klug), Verification of Mixing Height Parameterizations and Models (Frank Beyrich), Mixing Height over Complex Terrain (Ekaterina Batchvarova), Internal Boundary Layers: Mixing Height in Coastal Areas and Over Cities (Allen White). The discussion at the end of the Workshop was chaired by Robert Bornstein.

As Organizers and Editors, we should like to record our gratitude to all the participants who made the meeting so successful. Our thanks are also extended to EURASAP, Risø National Laboratory, the Nordic Council of Ministers, The Brandenburg Technical University and the National Institute of Meteorology and Hydrology for their support to the Workshop.

ISBN 87-550-2325-8
ISSN 0106-2840

Information Service Department, Risø, 1997

## Contents

**Session I - Theoretical Considerations** *7*

K. Nyrén and S.-E. Gryning
Nomogram for the height of the daytime mixed layer *9*

J. Bergmann
Mixing height determination from the momentum balance of the neutral or stable PBL *13*

E. Fedorovich and R. Kaiser
A model study of mixing and entrainment in the horizontally evolving atmospheric convective boundary layer *17*

**Session II - Mixing Height estimation from Turbulence Measurements and In-Situ Soundings** *21*

M. Piringer
Experiences of ZAMG on mixing height determination *23*

J. Højstrup, R. J. Barthelmie and B. Källstrand
Boundary layer heights derived from velocity spectra *27*

A:A: Samah
Modelling the development of mixing height in near equatorial region *31*

S.E. Gryning and E. Batchvarova
Determination of regional heat fluxes from the growth of the mixing layer *35*

**Session III - Mixing Height Determination from NWP-Models** *39*

J.H. Sørensen and A. Rasmussen
Mixing Height Derived from the DMI-HIRLAM NWP Model, and used for ETEX Dispersion Modelling *41*

T. Iversen and H.A. Jakobsen
An operational routine for off-line diagnostic determination of the mixing-layer depth *45*

G. Wotawa and A. Stohl
Boundary layer heights and surface fluxes of momentum and heat derived from ECMWF data for use in pollutant dispersion models - problems with data accuracy *47*

H. Klein Baltink and A.A.M. Holtslag
A comparison of boundary-layer heights inferred from windprofiler backscatter profiles with diagnostic calculations using regional model forecasts *51*

B. Fay, R. Schrodin, I. Jacobsen and D. Engelbart
Validation of mixing heights derived from the operational NWP models at ther German Weather Service *55*

**Session IV - Climatology and Global Aspects** *59*

H. van Dop, M. Krol and B. Holtslag
A global boundary-layer height climatology *61*

A-M Sempreviva and S-E Gryning
Climatology and evolution of the mixing height over water *65*

**Session V - Mixing Height Determination from Remote Sensing Systems** *69*

F. Beyrich
Mixing height determination using remote sensing systems - general remarks *71*

W.M. Angevine and A.W. Grimsdell
Mixing height measurements from UHF wind profiling radar *75*

M. Bennett and G.C. Hunter
Variation of Lidar backscatter as an indicator of boundary layer structure *79*

A.B. White, C. Senff and R.M. Banta
A comparison of mixing depths observed by ground-based wind profilers and an airborne lidar *83*

M.A. Kallistratova and M.A. Lokoshchenko
On determination of the urban mixing height for air quality application *87*

J. Walczewski
Some aspects of estimation of mixing height using vertical sodar records *91*

**Session VI - Verification of Mixing Height Parameterizations and Models** *95*

P. Faggian, G. M. Riva and G. Brusasca
Comparison of Mixed layer Models predictions with experimental data *97*

A. Rasmussen, J. H. Sørensen and N. Woetmann Nielsen
Validation of Mixing Height Determined from Vertical Profiles of Wind and Temperature from the DMI-HIRLAM NWP Model in Comparison with radiosoundings *101*

A. Jaquier, R. Stübi and Ph. Tercier
Comparison of mixing height parameterizations with profiles measurements *105*

T. Mikkelsen, H.E. Jørgensen, P. Astrup, S. Ott and J. H, Sørensen
Comparison of measured and modelled mixing heights during the BOREX-95 Experiment *109*

A Bielak, J. Burzynski, W. Kaszowski and J. Walcewski
Some parameterization formulae for mixing height compared with joint Sodar and Lidar observations *113*

D. Yordanov, D. Syrakov and M. Kolarova
On the parameterization of the planetary boundary layer of the atmosphere *117*

**Session VII - Mixing Height over Complex Terrain** *121*

A.B. White and C.W. King
A comparison of mixing depths observed over horizontally inhomogeneous terrain *123*

K. Baumann
Mixing heights over hilly terrain - a case study in northern Austria *127*

S. Galmarini, D. Anfossi, P. Salin, G. Schayes and S. Trini-Castelli
Effect on tracer concentration of ABL depth models in complex terrain *131*

**Session VIII - Internal Boundary Layers: Mixing Height in Coastal Areas and Over Cities** *135*

D. G. Steyn
Interaction between the Thermal Internal Boundary Layer and Sea Breezes *137*

E. Batchvarova, D. Steyn, X. Cai, S.-E. Gryning and M. Baldi
Modelling the Internal Boundary Layer over the Lower Fraser Valley, British Columbia *141*

H.P. Frank
Simulation of the convective mixed layer in Athens *145*

G. Schayes and P. Grossi
Sensitivity analysis of the Boundary Layer Height on idealised Cities (model study) *149*

E.A. Shurygin
Sodar measurements of the mixed-layer depth over a large city *153*

F.R. Freedman and R.D. Bornstein
Turbulent structure of the nighttime atmospheric boundary layer and its application to vertically dependent mixing heights *157*

# Session I - Theoretical Considerations
# Chairperson: Sven-Erik Gryning

# NOMOGRAM FOR THE HEIGHT OF THE DAYTIME MIXED LAYER

Kenneth Nyrén[1] and Sven-Erik Gryning[2]

[1] *Ericsson EriSoft AB, Box 4205, S-904 06 Umeå, Sweden*
[2] *Risø National Laboratory, DK-4000 Roskilde, Denmark*

## Introduction

The height of the daytime mixed layer, $h$, is an essential parameter for air pollution assessment studies, because it forms a barrier for the vertical dispersion of pollutants in the air. Also it is an essential scaling length parameter for the turbulence structure in the atmospheric boundary layer. It has in combination with the Monin-Obukhov length, $L$, and the height, $z$, been used by Holtslag and Nieuwstadt (1986) to give a framework of scaling regimes for the atmospheric boundary layer forms the physical basis adopted for applied dispersion modelling in Gryning et al. (1987).

In this paper we present a nomogram that provide information about the general behaviour of the mixed layer at a given location. The nomogram is meant to be a practical and easy to use tool to determine the height of the mixed layer for i.e. weather forecaster, air pollution studies and planning of meteorological experiments. Use of the nomogram is restricted to flat, relatively homogeneous terrain. Inhomogeneous terrain with patch scales of 10 km or more might create organised circulation like i.e. lake breezes. The data represented in the nomogram is computed using a meteorological preprocessor and climatological temperature data for the location. The nomogram is simplified but retain main physical processes that control the evolution of the mixed layer and can be easily constructed for any chosen location on land. Nomogram of the mixed layer behaviour at the location of Cabauw, the Netherlands is shown and discussed.

## Nomogram

The nomograms were inspired by figure 6.5 on page 319 in Pasquill and Smith (1983). It is divided into three parts. The first part represents curves of the integrated sensible heat flux from dawn for cloudless day as a function of local time on a monthly basis. The second part takes the effect of cloud cover (oktas) into account and links the integrated heat flux with the third part giving the height of the mixed layer for different wind speeds.

In order to construct a nomogram for a specific location, information on the air temperature on a climatological basis, surface albedo, surface roughness, $z_o$, and surface moisture, usually expressed by the surface moisture availability parameters $\alpha$ (de Bruin and Holtslag, 1982) is required. Through the use of a meteorological pre-processor this information is used to calculate the Monin-Obukhov length, the friction velocity, and the sensible surface kinematic heat flux, as a function of time. This forms the input to the model of the mixed layer height evolution. It is characteristic that the application is based on climatological data. Having calculated the nomogram, the mixed layer height evolution during a specific day can be estimated knowing the month, cloud cover and wind speed.

**Meteorological Pre-Processing**

A validated model for estimation of the height of the daytime mixed layer has been reported by i.e. Batchvarova and Gryning (1991). Their method gives an accessible tool to compute the evolution of the mixed-layer height, knowing the Monin-Obukhov length, the friction velocity, $u_*$, kinematic heat flux at the surface, $(\overline{w\theta})_s$, and the potential temperature gradient above the mixed layer, $\gamma_\theta$. The model can be used to study individual cases of mixed layer evolution, provided sufficient detailed meteorological data is available.

The meteorological pre-processing adopted in the present study has been applied in the following sequence (Holtslag and van Ulden, 1983, 1985):
First the radiation budget for the site is established. From the site position in latitude and longitude the local solar elevation is derived as a function of time, Sellers, (1965). This information is used to calculate the albedo as a function of time and surface type, Paltridge and Platt (1976). Next the short wave radiation is estimated from Karsten and Czeplak, (1980), taking the effect of cloud cover into account. Knowing the albedo and the short wave radiation, the net radiation can be derived following Stull (1988).The net radiation is the main driving entity of the surface energy budget.
It is now possible to derive the sensible heat flux, which is an essential parameter for the growth of the mixed layer, using the modified Priestley-Taylor method suggested by DeBruin and Holtslag (1982) is used. The moisture dependence is addressed by the moisture availability parameter, $\alpha$. The partition of the latent heat flux and sensible heat flux is sensitive to temperature. At relative low temperatures the sensible heat flux is greater than the latent heat flux and at relative high temperatures the opposite is found. Climatological temperature data for the locations is therefore an essential part of the calculation of the sensible heat flux.
The momentum flux and the Monin-Obukhov length is iteratively determined for differing classes of wind speed by using the wind profile and a derived value of the sensible heat flux. Finally the nomogram data for the mixed layer evolution is calculated from the model of Batchvarova and Gryning (1991).

**Example of Nomogram**

In order to illustrate the use of the described procedures and the variation of the mixed-layer height, a nomogram was calculated for the location of Cabauw in the Netherlands, figure 1. The parameters used in the construction of the nomogram is given in Table I.

**TABLE I.** Parameters used in the simulation of the growth of the day-time mixed layer represented in the nomograms in figure 1.

| Parameters | | | Cabauw |
|---|---|---|---|
| position | latitude | | 52.0°N |
| | longitude | | 4.9°E |
| high solar radiation albedo | $A_1$ | | 0.23 |
| moisture availability factor | $\alpha$ | wet | 0.95 |
| | | dry | - |
| surface roughness | $z_o$ | | 0.1 m |
| potential temperature gardient above the mixed layer | $\gamma_\theta$ | | 0.007 K $m^{-1}$ |

## Discussion

In this study the growth of the mixed-layer starts at the ground when surface heat flux becomes positive in the morning. It grows fairly fast, in the beginning proportional to $u_*$ and later is controlled by the production of mechanical turbulence. Later the mixed layer dependence of mechanical turbulence ceases, and the sensible heat flux starts to control the growth process.

The nomogram presented in figure 1 are meant as illustrations of typical features of mixed layer growth. When constructing nomograms representing a specific site, an appropriate set of parameters, table I, must be applied.

The nomogram was tested for the site of Cabauw (52.0°N, 4.9°E) on data from a comprehensive study by Driedonks, (1981) of the dynamics of the mixed boundary layer. The data tables are divided in initial conditions, forcing functions and mixed layer data. The measurement period start after sunrise and ends in the afternoon.

The data from Driedonks, (1981) does not contain cloud-cover, but this has been adopted by implicitly estimating the cloud cover from the given net radiation by the use of the meteorological pre-processor described above. The resulting cloud cover values have been used in a nomogram for the position of Cabauw to estimate the mixed layer height. In fig. 1 (lower right graph) the compared mixed layer height values are illustrated in the form of a correlogram. The cloud cover estimated from the net radiation data presented by Driedonks (1981) are marked by different symbols. The overall agreement is fair, considering that the nomogram is constructed with the standard values, and no attempts to include the specific meteorological conditions during the experiment has been done.


## Acknowledgements

The study was supported by the Ericsson Erisoft Educational Foundation (UKP 21:02) and the Danish Environmental Research Programme 1992-96.


## References


Batchvarova, E. and Gryning, S. E.: 1991 Applied Model for the Growth of the Daytime Mixed Layer. Boundary-Layer Met. 56, 261-274.

de Bruin, H. A. and Holtslag, A. A. M.: 1982 A Simple Parameterization of the Surface Fluxes of Sensible and Latent Heat During Daytime Compared with the Penman-Monteith concept. J. Appl. Meteor., 21, 1610-1621.

Driedonks, A.G.M., 1981: Dynamics of the Well-Mixed Atmospheric Boundary Layer. Scientific Report W.R. 81-2.

Gryning, S. E., Holtslag A. A. M., Irwin J. S. and Siversen B.:, 1987 Applied Dispersion Modelling Based on Meteorological Scaling Parameters. Atmospheric Environment, 21, 79-89.

Holtslag, A. A. M., and Nieuwstadt F. T. M.: 1986 Scaling the atmospheric boundary layer. Boundary-Layer Met. 36, 201-209.

Holtslag, A. A. M., and van Ulden A. P.: 1983: A simple scheme for daytime estimates of the surface fluxes from routine weather data. J. of Climate and Appl. Meteor., 22, 517-529.

Kasten, F. and Czeplak G.: 1980 Solar and terrestial radiation dependent on the amount and type of cloud. Solar energy, 24, 177-189.

Paltridge, G. W. and Platt C. M. R.: 1976 Radiative Processes in Meteorology and Climatology, Elsevier, 318 pp.

Pasquill, F., and Smith F. B.: 1983 Atmopheric Diffusion. Third ed. Wiley, 437 pp.

Sellers, W. D., 1965: Physical Climatology. The University of Chicago Press, 272 pp.

Stull, R. B., 1988: An Introduction to Boundary Layer Meteorology. Kluwer Academic Publisher, 666 pp.

Van Ulden, A. P., and Holtslag A. A. M.:, 1985 Estimation of Atmospheric Boundary Layer Parameters for Diffusion Applications. J. of Climate and Appl. Meteor., 24, 1196-1207.

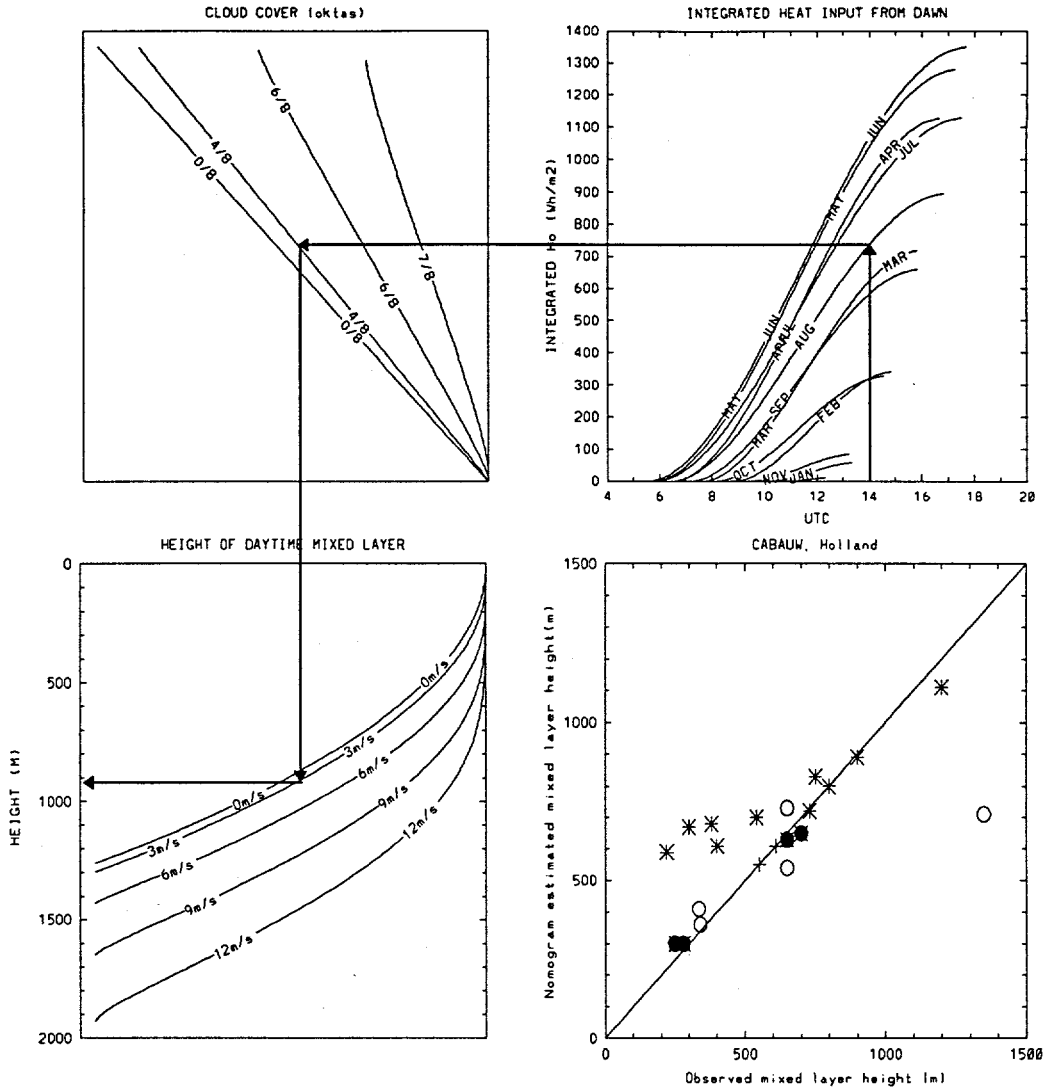


Fig. 1 An estimate of the mixed layer height at Cabauw in August 14 UTC is illustrated by a thick line. Starting at 14 UTC in August, 4 oktas cloud cover and mean wind speed at 10m height of 3m $s^{-1}$ results in a mixed layer height estimate of 910m. The observed mixed layer heights from measured data by Driedonks, (1981) versus estimated mixed layer height from a the nomogram for the site of Cabauw (52.0°N, 4.9°E) are collected in the lower right graph. The different symbols represent the cloud cover (• 75% cloud cover, * 50% cloud cover, + 25% cloud cover and o no clouds).

# Mixing Height Determination from the Momentum Balance of the Neutral or Stable PBL

J.C. Bergmann

Risø National Laboratory - VEA, P.O.Box 49, DK-4000 Roskilde, Denmark

## Introduction

The mixing height is defined by the top of the layer of turbulent mixing. This height is equal to the height H of turbulent vertical momentum transport (friction) in neutral or stable stratification. In very stable cases, the wave induced momentum transport must be excluded if the waves do not have mixing effects (e.g. break) within the frictional layer. Thus the conditions provided by the momentum balance determine the mixing height in most cases of mechanical turbulence.

Mixing is a time dependent process and depends also on the height of release of substance to be mixed. It depends on the specific form of the exchange coefficient function whether the mixing time for the mixed layer is finite or infinite. If this time is infinite, an additional mixing time criterion for a substance released close to the ground must be applied for the determination of the corresponding mixing height.

## Mixing Time Considerations

The usual profiles of PBL exchange coefficients K have a linear increase at the ground, a maximum at about ¼ of the PBL height and decrease linearly to zero at the top of the PBL. This type of K function has a typical mixing time of order 10 hours. However, a linear decrease at the top of the PBL is not realistic because it corresponds to the characteristic of a phase boundary as it is found at the ground. More detailed physical reasoning (Bergmann 1997) leads to a decrease with a square function of the distance to the PBL top, cf. figure 1a. This K function has an infinite mixing time, and a time criterion must be chosen in order to determine the fraction of H that will be mixed within this time. Figure 1b shows the diffusion resistance of the PBL. The integral of this function over dz with the mixing height as upper integration limit yields the mixing time. A mixing time of 10 hours is related to a mixing height of min. 96% of H.

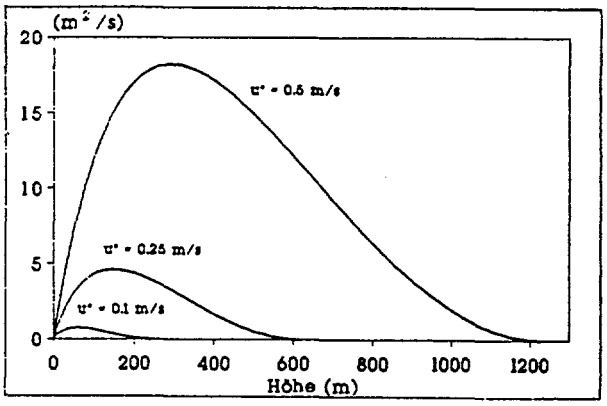


**Figure 1a**

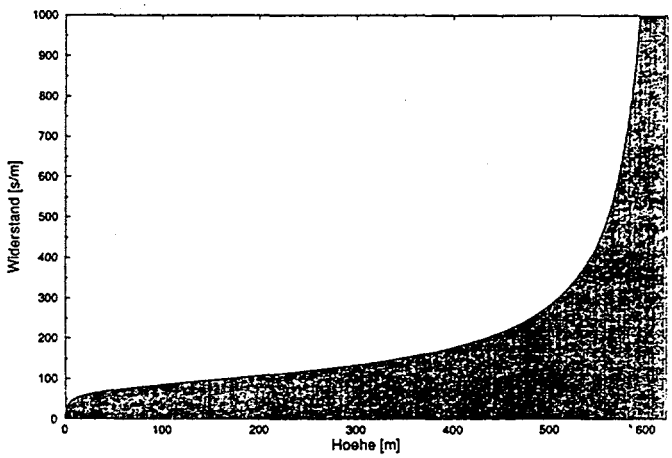


**Figure 1b**

**Iterative Determination of the Neutral PBL Height**

The details of this procedure can be studied in (Bergmann 1997).
An iteration of the momentum balance equation of the PBL is performed with varying PBL heights until the momentum conservation condition at the surface is satisfied in the form of a momentum flux density equal to that presumed by u* in the velocity profile (cf. eq (4). The result is a scaling factor for eq (1) of 0.295 which is exactly in the range of the experimental values of approximately 0.3.

**Non-Iterative Determination of the Neutral PBL Height**

The momentum balance, i.e. the integration over the real net force contributions of elements of volume of height dz, represents only one component of the apparent forces. The virtual component is excluded from the momentum balance. On the basis of the apparent forces, a boundary layer height $H_{app} = u^*/f$ should be expected, however, with the difficulty of formulation of a 'momentum' balance because only the real momentum flux enters the velocity profile in the form of u*. A solution can be found if the scaling factor for the real boundary layer height is interpreted as the ratio of real momentum flux to flux of apparent momentum at the surface.

$$H = \tau/\tau_{app}\ u^*/f \qquad (1)$$

with H the (real) height of the boundary layer, u* the friction velocity, f the Coriolis parameter and $\tau$ the momentum flux density at the surface. $\tau$ is known from the momentum balance as (Bergmann 1997)

$$\tau' = \tau/\rho = Hf/u_g\ (u_g^2 - \langle u_s^2 \rangle) \qquad (2)$$

with $u_g$ the geostrophic velocity and $\langle u_s^2 \rangle$ the average of the speed squares in the boundary layer. The corresponding apparent quantity is (Bergmann 1997)

$$\tau'_{app} = Hf\ (u_g^2 - \langle u_s^2 \rangle)^{1/2} \qquad (3)$$

Momentum conservation requires

$$\tau' = u^{*2} \qquad (4)$$

Eqs (2)-(4) can be transformed to

$$\tau/\tau_{app} = (u^{*2}/Hfu_g)^{1/2} \qquad (5)$$

and eq (1) transforms to

$$H = (u^*/u_g)^{1/3}\ u^*/f \qquad (6)$$

This result for the boundary layer height is physically very plausible because the scaling factor is formulated in terms of surface momentum flux (u*) and atmospheric pressure gradient as driving force of the PBL ($u_g$). $u_g$ can be calculated from the surface parameters u* and $z_0$ (Bergmann 1997) if it is not known a priori

$$u_g = u^*/\kappa\ (\ln(H/z_0) - \tfrac{1}{2}) \qquad (7)$$

In table 1, eq (6) has been compared to iterative results with a step width of 10 m using eq (7) for $u_g$. The calculations refer to a surface of small roughness length (approx. $10^{-4}$ m) at north European latitudes.

The deviations at large u* indicate a minor problem with the exact formulation of the velocity profile for a given value of the geostrophic velocity. This problem is more relevant in case of very rough surfaces and requires further investigations. For roughness lengths of 1 meter, the deviations amount to 15% - 20%. However, eq (6) can be expected to be less sensitive to velocity profile problems than the iteration which depends on $\langle u_s^2 \rangle$ which is quite different from the corresponding average of u(z) with the high turbulence intensity in case of rough surfaces.

Table 1

| u* | H Iteration | H Equation (6) |
|---|---|---|
| 0.10 m/s | 250 m | 249 m |
| 0.25 m/s | 620 m | 610 m |
| 0.50 m/s | 1230 m | 1201 m |
| 1.00 m/s | 2460 m | 2370 m |

**Determination of the Stable PBL Height**

The same momentum balance calculations have been performed for the stable case for $u^* = 0.25$ m/s. The velocity profile used for the iteration (step width 5 m) applies the same modulation function for the surface layer profile as in the neutral case. However, the slope factor of the constant gradient term is taken as $b = 1/\kappa$, the inverse von Karman constant (Bergmann 1995). Table 2 displays the results in comparison to a scaling derived from these results in the form

$$H_S = (u^*/u_g)^{1/3} (Lu^{*2}/f^2)^{1/3} \approx 0.26 (Lu^{*2}/f^2)^{1/3} \quad (8)$$

and to the famous Zilitinkevich (1972) formula

$$H_S = 0.37 (Lu^*/f)^{1/2} \quad (9)$$

Table 2

| L | $H_S$ Iteration | $H_S$ Equation (8) | $H_S$ Equation (9) |
|---|---|---|---|
| 200 m | 270 m | 269 m | 240 m |
| 100 m | 210 m | 209 m | 169 m |
| 50 m | 160 m | 161 m | 120 m |
| 25 m | 120 m | 123 m | 85 m |

Table 2 demonstrates that for stable stratification not too close to neutrality, there is an excellent approximation of the iteration results by eq (8). Eq (9) shows systematically lower results with increasing relative deviation for decreasing L.
Lamentably, the transition to near neutral stratification is still not included in both equations.

For a decision of the question whether eq (8) is better than eq (9), the two equations are compared to the famous Cabauw data (Nieuwstadt 1984). The comparison is not based on selected half-hour averages as it is in Nieuwstadt's article. The reason is that the measured fluxes vary too much from interval to interval. The data have been selected after the following criteria:
- Averaging time min. 1.5 h, max. 4.5 h. The min. corresponds to 60% of the time scale 1/f, the max. shall avoid integration over trends in the data.
- Only near constant height and flux data are included if they fit the time criterion.
- Very low heat fluxes are excluded because of little resolution and high measuring errors.

Figures 2 and 3 demonstrate that eq (8) fits the data better than eq (9).

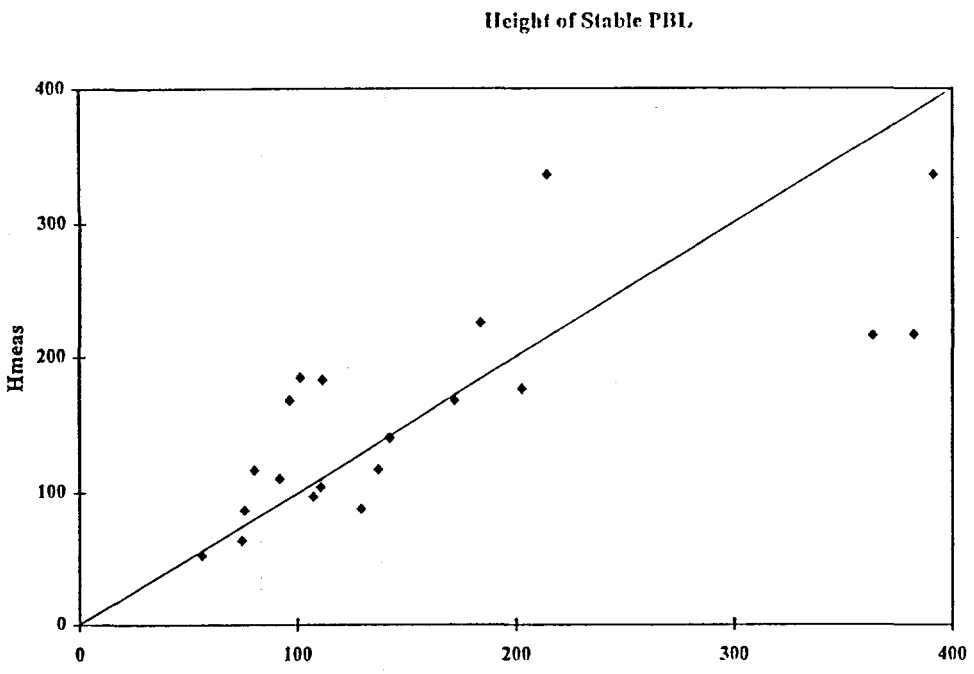


**Figure 2:** Comparison of the Cabauw data to eq (8).

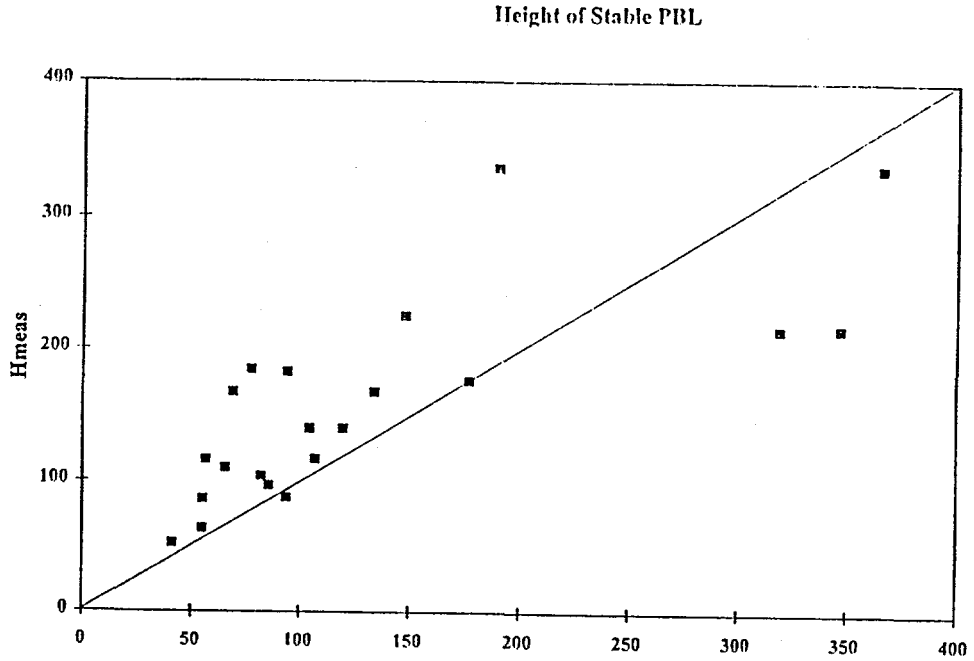


**Figure 3:** Comparison of the Cabauw data to eq (9).

## References

Bergmann, J.: 1995, Zur Quantifizierung des vertikalen Austausches in einer idealisierten neutralen oder stabilen Planetarischen Grenzschicht - Ein Konzept zur Herleitung des vertikalen Austauschkoeffizienten, PhD thesis, Faculty of Geo-Sciences, University of Hamburg, January 1995.

Bergmann, J.: 1997, On the Quantification of Vertical Exchange in an Idealized Neutral PBL - A Physical Derivation of the Exchange Coefficient, Contr. Atmosph. Phys. **70**, 65-77.

Nieuwstadt, F.T.M.: 1984, Some Aspects of the Turbulent Stable Boundary Layer, Boundary Layer Meteorology **30**, 31-55.

Zilitinkevich, S.S.: 1972, On the determination of the height of the Ekman Boundary Layer, Boundary Layer Meteorology **3**, 141-145.

# A Model Study of Mixing and Entrainment in the Horizontally Evolving Atmospheric Convective Boundary Layer

E. Fedorovich, R. Kaiser

Institut für Hydrologie und Wasserwirtschaft, Universität Karlsruhe, Germany

## Introduction

We present results from a parallel wind-tunnel / large-eddy simulation (LES) model study of mixing and entrainment in the atmospheric convective boundary layer (CBL) longitudinally developing over a heated surface. The advection-type entrainment of warmer air from upper turbulence-free layers into the growing CBL has been investigated. Most of numerical and laboratory model studies of the CBL carried out so far dealt with another type of entrainment, namely the non-steady one, regarding the CBL growth as a non-stationary process. In the atmosphere, both types of the CBL development can take place, often being superimposed.

## Experimental Facility

The experimental facility employed in the study is a thermally stratified wind tunnel specially designed to simulate turbulent penetrative convection developing on the background of imposed stable stratification. The tunnel was constructed at the Institut für Hydrologie und Wasserwirtschaft (IHW), Universität Karlsruhe. Its test section is 10 m long, 1.5 m wide, and 1.5 m high. Design and operating ranges of the tunnel are presented in Rau and Plate (1995). Detailed analysis of turbulence properties in the simulated CBL is given in Fedorovich et al. (1996), and Kaiser and Fedorovich (1997). Compared to water-tank models, which are traditional laboratory tools for simulating the atmospheric convection (Deardorff and Willis 1985, Cenedese and Querzoli 1994), the wind-tunnel approach provides an advantageous opportunity to study sheared convection regimes, when the buoyant production of turbulence is accompanied by the shear production. The sheared convection is much more common case in the atmospheric planetary boundary layer than the shear-free convection. Profiles of the mean-flow temperature and velocity at the inlet of the IHW tunnel are preshaped in a way to make them similar to their counterparts in the atmospheric CBL. The preshaped flow proceeds downstream over the heated floor of the tunnel, with convective turbulence penetrating into the flow and adjusting its mean structure to a local turbulent regime. This allows to achieve a developed CBL over comparatively short fetches. Different forcings affecting the CBL turbulence field can be investigated by varying flow profiles at the inlet.

## Scaling Considerations

Studied flow configurations were corresponding to moderate values of Richardson numbers $\mathrm{Ri}_{\Delta T}$ ($\leq 10$) and $\mathrm{Ri}_N$ ($\leq 20$), representing the effects of temperature increment $\Delta T$ across the capping inversion, and stable stratification in the free atmosphere characterized by the buoyancy frequency $N$. These Richardson numbers are expressed as $\mathrm{Ri}_{\Delta T} = \beta w_*^{-2} z_i \Delta T$ and $\mathrm{Ri}_N = N^2 z_i^{\,2} w_*^{-2}$, where $z_i$ is the CBL depth, $w_* = \left(\beta Q_s z_i\right)^{1/3}$ is the Deardorff (1970) convective velocity scale, $\beta = g / T_0$ is the buoyancy parameter ($g$ is the acceleration due to the gravity, $T_0$ is the reference temperature value), and $Q_s$ is the near-surface value of the turbulent kinematic heat flux. To account for the effects of the surface shear, the above numbers have to be complemented by the ratio $u_* / w_*$

contributions to the turbulence production in the CBL (Meroney and Melbourne 1992). In the atmospheric CBL, typical $Ri_{\Delta T}$ and $Ri_N$ are within the range of 0 to 100. Thus, the wind-tunnel Richardson numbers refer to atmospheric convection regimes with comparatively weak damping effects of stable stratification in the upper portion of the CBL and above it. Turbulence production in the CBL is dominated by convection when the ratio $u_* / w_*$ is sufficiently small. Based on classification proposed by Holtslag and Nieuwstadt (1986), $u_* / w_*$=0.34 may be obtained as a conventional boundary value separating the regimes of sheared and shear-free convection. Typical values of $u_* / w_*$ in the wind tunnel are within the range of 0.2 to 0.5. For relating temporal and spatial scales of turbulent motions in the simulated CBL we invoke the Taylor hypothesis, which is satisfied fairly well in the wind tunnel model (Fedorovich et al. 1996).

**Development of Mixing**

Evolution of the mean-temperature and turbulence fields in the tunnel is shown in Fig. 1. At $x$=3.98 m and at two downstream measurement locations, the temperature pattern displays the structure characteristic of the developed atmospheric CBL: a sharp decrease of temperature in the near-surface layer; an approximate thermal uniformity within the mixed layer; temperature increase with height across the inversion; and a quiescence of temperature field in the stably stratified flow aloft. The mixed-layer depth, which can be roughly estimated from the elevation of the capping inversion midpoint, as well as from the vertical extension of the turbulized zone, increases progressively with distance. This growth is accompanied by cooling of the stably stratified layer due to the entrainment of warmer air from above the inversion into the bulk of the mixed layer.

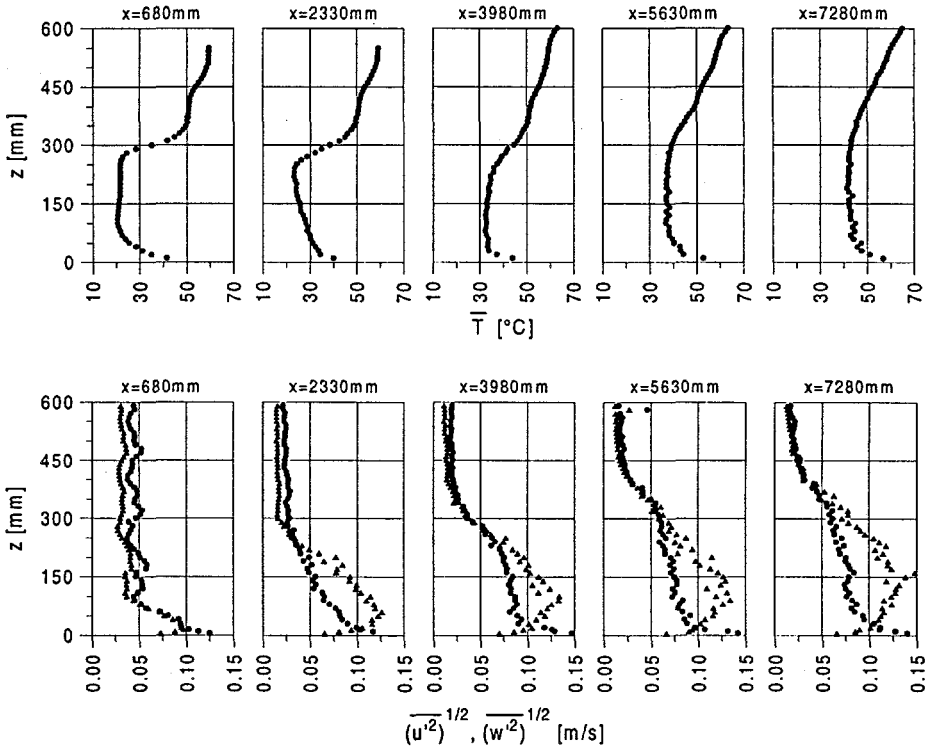


Fig. 1. Evolution of mean-flow temperature (upper plot), and turbulence intensity (lower plot) along the tunnel. Dots represent the longitudinal velocity and triangles the vertical velocity r.m.s. values.

A variety of convective flow regimes reproduced in the wind tunnel were simulated using a modified version of the Nieuwstadt and Brost (1986) LES model. The model

modification involved a reformulation of the boundary conditions, adaptation of the Poisson solver for the pressure-field calculations, and alteration of the near-surface parameterization to account for horizontal inhomogeneity of the surface layer. The finite-difference numerical scheme was used to solve the three-dimensional grid-volume-averaged Navier-Stokes equations for incompressible fluid. The buoyancy forcing was parameterized using the Boussinesq approximation.

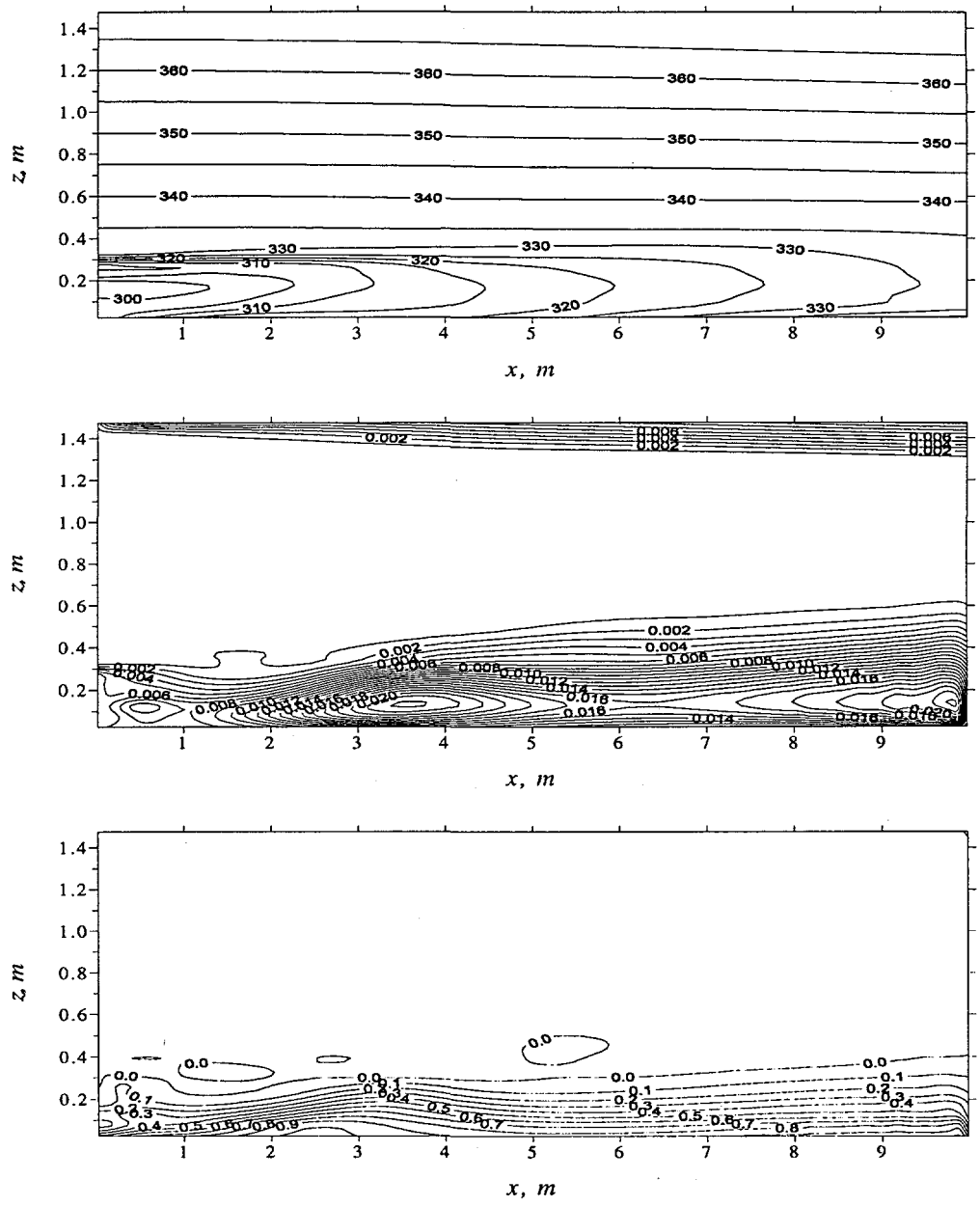


Fig. 2. Large-eddy simulation patterns of mean-flow temperature (in K, upper plot), vertical velocity variance (in $m^2 / s^2$, middle plot), and vertical heat flux (in m·K/s, lower plot) averaged across the tunnel.

Strong longitudinal variability of the entrainment dynamics has been observed in results from both physical and numerical models. Transition regions associated with turbulence enhancement, and overturning of the temperature profile have been discovered in the CBL evolution pattern. The LES model has shown that with some initial flow configurations the transitional turbulence enhancement may have a form of the turbulence blow-up. Peculiar features of entrainment and mixing-height dynamics have been observed in the vicinity of transition regions, see Fig. 2.

## Summary of Results

Turbulent mixing in the simulated CBL turned out to be essentially affected by the flow shear. With $u_* / w_*$ of >0.3, velocity components variances in the lower portion of the CBL are noticeably larger than their counterparts in the shear-free CBL. Wind-tunnel experiments with elevated shear revealed its impeding effect on the CBL growth, see Fig. 3. Behavior of different turbulence statistics near the CBL top have been analyzed in a search for an optimal predictor for the mixed-layer height.

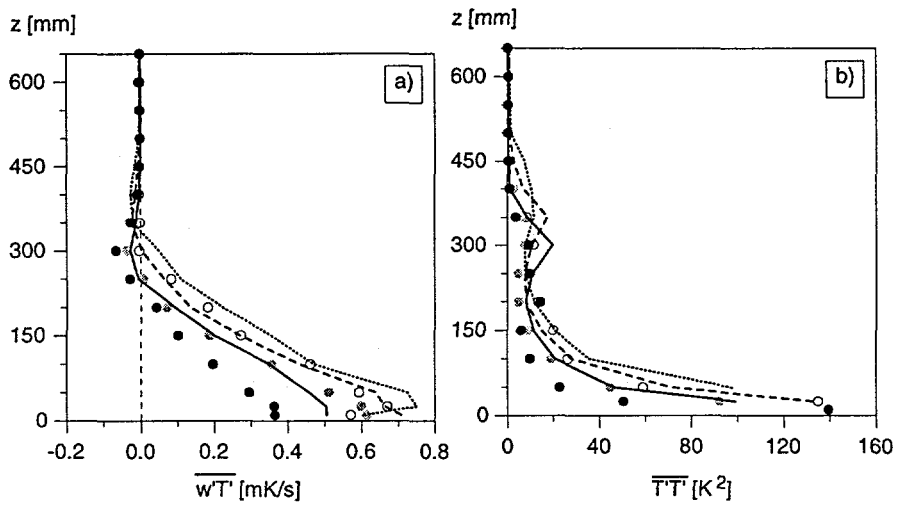


Fig. 3. Vertical heat flux (a), and temperature variance (b) in the CBL with the elevated shear (points) and without the elevated shear (lines). Data refer to $x$=3.98 m (solid lines and black symbols), $x$=5.63 m (dashed lines and gray symbols), and to $x$=7.28 m (dotted lines and empty symbols).

We found that compared to data from studies of the shear-free CBL, more energy in the wind-tunnel velocity spectra refer to larger wave numbers which is probably a result of the turbulence production by shear. At all elevations within the mixed core of the simulated CBL, the apparent linear -5/3 parts were discovered in the log-scaled velocity and temperature spectra, however the velocity fluctuations were not found to be purely isotropic even at large wave numbers. Wind-tunnel turbulence spectra obtained at different levels across the entrainment zone displayed a scale redistribution in turbulent motions within this zone.

## References


Cenedese, A., and G. Querzoli, 1994: A laboratory model of turbulent convection in the atmospheric boundary layer. *Atmos. Environ.*, **28**, 1901-1914.

Deardorff, J. W., 1970: Convective velocity and temperature scales for the unstable planetary boundary layer and for Raleigh convection. *J. Atmos. Sci.*, **27**, 1211-1213.

Deardorff, J. W., and G. E. Willis, 1985: Further results from a laboratory model of the convective planetary boundary layer. *Bound.-Layer Meteor.*, **32**, 205-236.

Fedorovich, E., R. Kaiser, M. Rau, and E. Plate, 1996: Wind tunnel study of turbulent flow structure in the convective boundary layer capped by a temperature inversion. *J. Atmos. Sci.*, **53**, 1273-1289.

Holtslag, A. A. M., and F. T. M. Nieuwstadt, 1986: Scaling the atmospheric boundary layer. *Bound.-Layer Meteor.*, **36**, 201-209.

Kaiser, R., and E. Fedorovich, 1997: Turbulence spectra and dissipation rates in a wind tunnel model of the atmospheric convective boundary layer. *J. Atmos. Sci.*, in press.

Meroney, R. N., and W. H. Melbourne, 1992: Operating ranges of meteorological wind tunnels for the simulation of convective boundary layer (CBL) phenomena. *Bound.-Layer Meteor.*, **61**, 145-174.

Nieuwstadt, F. T. M., and R. A. Brost, 1986: Decay of convective turbulence. *J. Atmos. Sci.*, **43**, 532-546.

Rau, M., and E. Plate, 1995: Wind tunnel modelling of convective boundary layers. *Wind Climate in Cities*, J. Cermak et al., Eds., Kluwer, 431-456.

# Session II - Mixing Height estimation from Turbulence Measurements and In-Situ Soundings
# Chairperson: Douw Steyn

# Experiences of ZAMG on Mixing Height Determination

Martin Piringer

Zentralanstalt für Meteorologie und Geodynamik (ZAMG), Vienna, Austria

## Introduction

Temperature inversions in the boundary layer occur quite often, esp. in mountainous terrain by which Austria is covered to a large extent, and can lead to enhanced pollution at the surface because the air volume available for dilution is then vertically limited. The Department of Environmental Meteorology of ZAMG therefore set up several field programs in the past to study such conditions at a variety of sites in Austria, using tethersondes and Sodars. Early investigations aimed at comparing Sodar echo profiles to the tethersonde temperature profiles to derive mixing heights from the Sodar echo structure. More recently, evolving from KONGEX, the „convective boundary layer experiment" (Piringer et al., 1996), mixing heights calculated for Vienna by the OML model (Olesen and Brown, 1992) were compared to those derived from radiosonde and tethersonde potential temperature profiles. Results of these investigations will be presented, focussing on the problems when using the different methods. New efforts to derive mixing heights from Sodar data were also undertaken and are discussed separately (K. Baumann, this volume).

## Early Investigations

The manual of the A0 Doppler Sodar (Remtech, 1985) which was used by ZAMG between 1986 and 1992 contained a detailed catalogue of vertical profiles of the echo intensity (and related components) and how they are related to an inversion top or bottom. From a comparison of Sodar echo profiles and tethersonde temperature profiles during wintertime in Southern Austria (Piringer, 1989), the maximal vertical decrease in the echo profile ($\partial E/\partial z$ max) above the first echo maximum coincided better with the inversion top determined by the tethersonde (Fig. 1) then the first minimum of echo intensity which would result in too high estimates of the top of a ground-based inversion. The same analysis undertaken at Vienna (Piringer, 1988) showed ambiguous results: sometimes the $\partial E/\partial z$ max-criterion worked well, sometimes several echo maxima were present although only one inversion was detected by the tethersonde. This ambiguity and large variations in the echo profiles from sounding to sounding pose severe restrictions to an automated Sodar inversion detection routine.

## Mixing Height Estimation During KONGEX

Vertical profiles of potential temperature were measured during the summer of 1995 in the Vienna area, Austria, by routine radiosoundings and additionally by tethersondes during the aforementioned field experiment KONGEX. Estimation of mixing heights from radio- and tethersonde soundings were done by use of Heffter's method (Marsik et al., 1995) and by the parcel method of Stull (1991). Mixing heights were also calculated with the mixing height routine of the Danish dispersion model OML (Olesen et al., 1992).

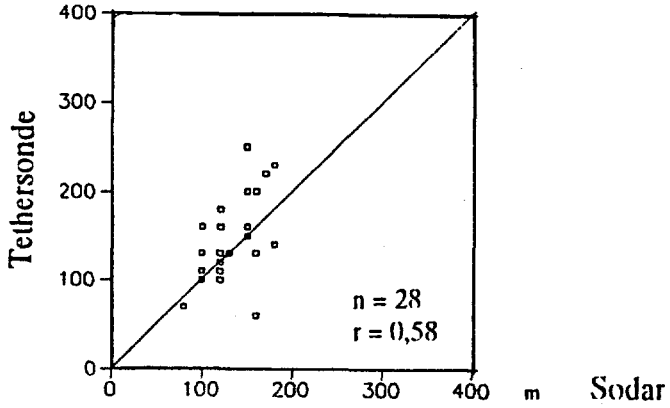


Fig. 1: Comparison of inversion tops detected by Sodar and tethersonde
Mellach, Austria, 17. - 23. 2. 1988

The OML preprocessor calculates convective mixing heights by taking into account heating from the ground and entrainment of warm air from the capping inversion aloft. Mechanical mixing heights are derived via a diagnostic relation where mixing height is determined by the friction velocity multiplied with a constant. During daytime, the actual mixing height is the larger of the mechanical or the convective mixing height.

Heffter's method consists of analyzing potential temperature profiles for the existence of a *critical inversion*, which is assumed to mark the top of the mixed layer. It is defined as the lowest inversion whose potential temperature lapse rate is equal to or larger than 5 K $km^{-1}$, and the temperature difference between inversion basé and inversion top must exceed 2 K. Stull's method is confined to determine regions of different static stability by air parcel movement based on parcel buoyancy. The convective mixing height is that height where the neutral buoyancy line, starting at a relative maximum of potential temperature, intersects the temperature profile for the first time.

**KONGEX Results**

A statistical comparison of the mixing heights determined by the three methods at 12:00 UTC during July and August 1995 is given in Table 1. $\sigma$ is the standard deviation, R is the linear correlation coefficient, rmsd is the root mean square difference.

**TABLE 1**

| 12:00 UTC | OML | Stull | Heffter |
|---|---|---|---|
| Cases | 62 | 62 | 58 |
| Mean (m) and $\sigma$ (m) | 1286 +/- 497 | 1389 +/- 570 | 1422 +/- 524 |
| Maximum (m) | 2389 | 2820 | 2717 |
| Minimum (m) | 286 | 248 | 519 |
| Comparison | OML/Stull | Stull/Heff | Heff/OML |
| Sample bias (m) | -103 | -52 | 149 |
| rmsd (m) | 412 | 181 | 429 |
| R | 0,74 | 0,97 | 0,72 |

The largest mixing heights, on average, are those derived by the Heffter method, closely followed by Stull; OML, on average, calculates values which are about 100 m lower. For the Stull and Heffter comparison, the sample bias and the root mean square difference are much lower and the correlation is very high, compared to the cases when OML is included in the statistical analysis. The agreement between all three methods is best on convective days with a well-defined capping inversion.

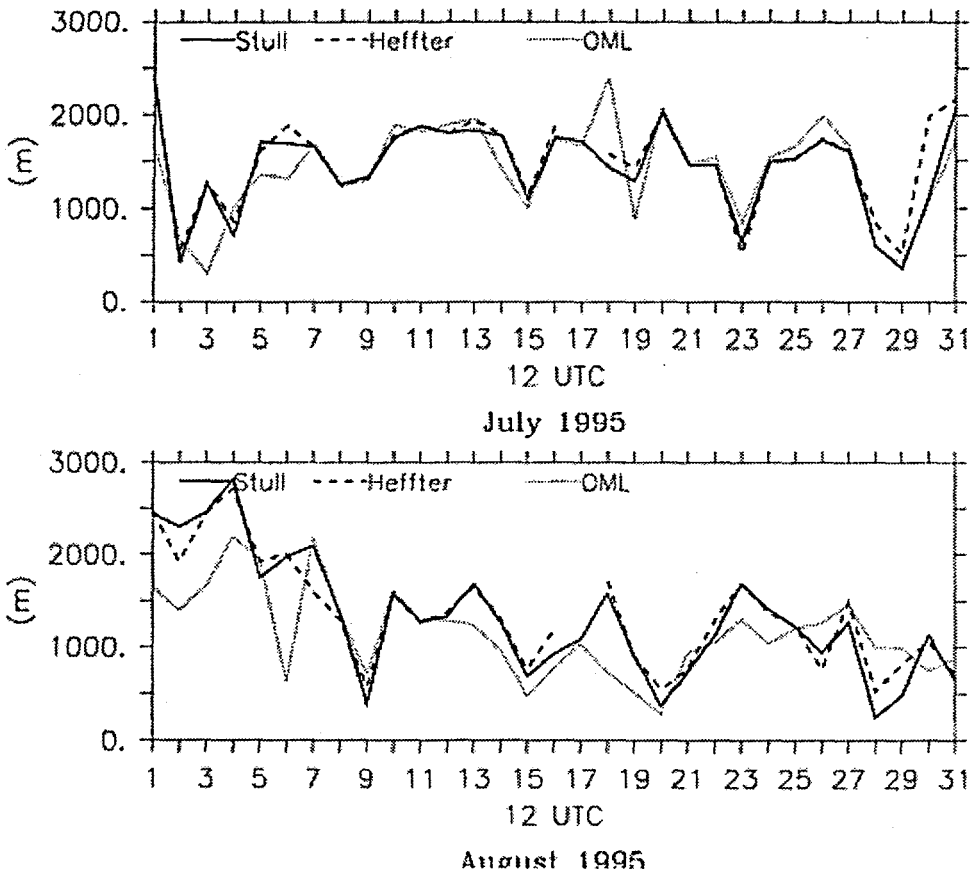


Figure 2: Daily mixing heights at Vienna during July and August 1995, 12 UTC

With a few exceptions (especially July 30, August 2 and August 7), the Stull and Heffter estimates are in good agreement (Fig. 2). OML sometimes deviates considerably, esp. at the beginning and in mid-July, and during a large part of August. These deviations occur to a great extent during periods of changeable weather. The second half of August was the most extended of these periods, when cloudiness, high windspeeds, and precipitation occurred frequently.

**Discussion**

All the three methods used have their deficiencies or need additional assumptions before they can be applied. The OML meteorological preprocessor uses a very strong criterion to accept an elevated inversion to be the top of the mixed layer in the noon radionsonde profile. If no such lid is found (which was true for the large majority of cases during July and August 1995), OML cannot match the time-integrated mixing

heights to an observed value, which may be one of the reasons for the differences to other methods (Table 1, Fig. 2).

The application of Heffter's method is also subject to a certain inversion strength, but the criterion is weaker than that used by the OML preprocessor and therefore more effective to detect a mixing height from a radiosonde profile. The inversion strength of at least 2 K is taken to account for entrainment of warm air by rising parcels at the inversion bottom. In only 4 cases out of 62 the Heffter method was not successful to detect the mixing height from the noon radiosonde profile. It is intended to improve OML mixing height predictions for Austria by using the Heffter method in the preprocessor. One has to remember, however, that both the OML preprocessor as well as the Heffter method use subjective criteria to detect the mixing height based on an analysis of observed vertical potential temperature profiles which might be representative for a limited area only.

The strength in Stull's parcel method is given by the fact that no assumptions about gradients in the vertical temperature profile are needed. However, the determination of a so-called excess temperature at the surface is necessary if the radiosonde potential temperature profile shows an adiabatic or stable layer from the start, which is quite common also during convective conditions. In our case, this excess temperature was determined from an average urban - suburban surface temperature difference of 1 K at Vienna during summer, thus giving an estimate of the mixing height above the urban area. More sophisticated approaches to calculate the surface excess temperature depending on the heat flux and a scaling velocity are proposed in the literature (e.g. Beljaars and Betts, 1992).

**Acknowledgements.** - This research was funded by the Austrian National Bank under contract 5522/1995. We thank H. R. Olesen (National Environmental Research Institute, Denmark) for making available the OML code.

## References

Beljaars, A. C. M., A. K. Betts, 1992: Validation of the boundary layer representation in the ECMWF model. *ECMWF Seminar Proceedings: Validation of Models over Europe, Vol. II, Reading (UK), 7-11 September 1992.*

Marsik, F. J., K. W. Fischer, T. D. McDonald, P. J. Samson, 1995: Comparison of methods for estimating mixing height used during the 1992 Atlanta field intensive. *J. Appl. Meteor.* **34**, 1802 - 1814.

Olesen, H. R., N. Brown, 1992: The OML meteorological preprocessor. *MST LUFT-A122*, National Environmental Research Institute, Roskilde, Denmark.

Olesen, H. R., A. B. Jensen, N. Brown, 1992: An operational procedure for mixing height estimation. *MST LUFT-A96*, National Environmental Research Institute, Roskilde, Denmark.

Piringer, M., K. Baumann, M. Langer, A. Stohl, G. Wotawa, 1996: Forschungsprojekt KONGEX - Konvektives Grenzschicht-Experiment. Report No. 5522, sponsored by the Austrian National Bank.

Piringer, M., 1989: Vergleichende Stabilitäts- und Windanalysen der bodennahen Grenzschicht mittels Sodar und Fesselballon. ZAMG Vienna, Austria, internal report.

Piringer, M., 1988: The determination of mixing heights by Sodar in an urban environment. In: *K. Grefen and J. Löbel (eds.), Environmental Meteorology,* 425 - 444. Kluwer Academic Publishers.

Remtech, 1985: Doppler Sodar Operating Manual. Document Nr. 85/038 A, June 17, 1985.

Stull, R. B., 1991: Static stability - an update. *Bull. Am. Met. Soc.* **72**, 1521 - 1529.

# Boundary Layer Heights derived from Velocity Spectra

J.Højstrup[1] , R.J.Barthelmie[1], B.Källstrand[2]

[1]Risø National Laboratory, Roskilde, Denmark
[2]University of Uppsala, Uppsala, Sweden

## Introduction

It is a well-known fact that the height of the mixed layer determines the size of the largest and most energetic eddies that can be observed in the unstable boundary layer *[Panofsky et al 1977, Kaimal 1978, Højstrup 1982]*, and consequently a peak can be observed in the the power spectra of the alongwind velocity component at scales comparable to the mixed layer depth. We will now show how the mixed layer depth can be derived from the u-spectra and the results will be compared with direct measurements using pibal and tethersonde measurements.

## Deriving peak frequencies from velocity spectra

The velocity spectrum in the unstable boundary layer can be modelled as a sum of two portions, one scaling with surface layer parameters (shear production), and the other scaling with mixed layer parameters (buoyancy production) *[Højstrup 1982]*:

$$fS_u(f) = u_* A(fz/u) + w_* B(fz_i/u),$$

where f is the frequency in Hz, z the height above ground, $z_i$ the height of the lowest inversion and u the windspeed. Near neutral the first term will be dominant and it will difficult to find $z_i$ but in more unstable conditions the second term will be of a significant size and we will be able to see the peak associated with it in the power spectra. It is quite difficult to make reliable fits to a spectral form due to large statistical variantions in spectral shape, but instead we have chosen another method involving two steps:

1) Find a characteristic frequency of the spectrum for which half of the variance lies at higher frequencies and the other half at lower frequencies, $f_{50\%}$. In very unstable conditions this frequency is close to the peak of the convective part of the spectrum.

2) Correct the found peak for the fact that we do not always have very unstable conditions. The magnitude of the correction is computed from the spectral model in Højstrup (1982), using height and stability. In fig.1 is shown the resulting spectral peak lengthscale for different stabilities at one measuring height, and in fig.2 we see the effect of varying stability for three different values of $z_i$. To a good approximation the spectral length scale can be found as:

$$\Gamma_{spectrum} = \frac{20z}{1+3\frac{z}{L}} + \frac{z_i}{1+\left(3\frac{z}{L}\right)^{-1}}$$

The correction derived from this equation was applied to sonic anemometer data at 5 and 10m from a field campaign at Östergarnsholm (small island East of Gotland), the resulting comparison between the two heights are shown in fig 3.

**Comparison with balloon and tethersonde**

Pibal and tethersonde measurements were taken as part of the Gotland field campaign (18-25 September 1996). Availability of these data depends on weather conditions permitting access to Østergarnsholm. In addition, the tethersonde cannot be launched if surface wind speeds are high. In total, there are five days of tethersonde data and eight days of pibal data taken approximately every two to three hours.

The tethersonde package included instrumentation to measure wind speed and direction, pressure, temperature and relative humidity and was able to reach heights of 3000m. A subjective procedure was used to determine mixed layer depth from the tethersonde measurements. If one ascent and descent were made within one hour, a composite profile was calculated. The composite profiles were examined, placing the greatest emphasis on temperature profiles. The height of the temperature inversion was assumed to be the height of the mixed layer. The remaining measurements were used as confirmation, looking for a major discontinuity in wind speed, and direction (using the u- and v- components) and a reduction in relative humidity.

For the pibals a similar procedure was used. Since three pibals were launched within a 15 minute interval, the average value was taken for each height (plotted at 50m intervals below 550m and 100m intervals above this height). The height of the mixed layer was estimated as the height at which a concomitant change in both wind speed and direction occurred.

There are few overlapping data points and therefore it is not possible to assess whether there are major differences between the mixed layer depth estimates from the tethersonde and pibal estimates (shown in Figure 4 together with the spectral estimates). There seems to be reasonable consistency between the spectral estimates and balloon measurements except after 23 September, when the flow was over the island istead of undisturbed onshore flow, causing the sonic measurements to represent other conditions than what the balloons see.

**Comparison with modelling of the mixed layer depth**

The parameterisation incorporated for mixed layer depth under convective conditions is from [*Batchvarova and Gryning*, 1990] where subsidence velocity is disregarded. Surface observations were used to determine the friction velocity, $u_*$, the Monin-Obukhov length, L, the kinematic heat flux at the surface $(w'\theta')_S$, and the buoyancy parameter, g/T. The potential temperature gradient above the mixed layer was determined from the tethersonde measurements. The growth of the mixed layer (h) with time (t) is *dh/dt:*

$$\left\{\frac{h^2}{(1+2A)h-2BkL}+\frac{Cu_*^2T}{\gamma g\left[(1+A)h-BkL\right]}\right\}\left(\frac{dh}{dt}\right)=\frac{\left(\overline{w'\theta'}\right)_s}{\gamma} \qquad (1)$$

where:
A, B and C are constants 0.2, 2.5 and 8, respectively
$\kappa$ is the von karman constant

For each half-hour for which surface observations were available the mixed layer depth was calculated using (1) unless conditions were close to neutral or unstable in which case the following equation was employed [*Nieuwstadt*, 1981]:

$$\frac{h}{L} = \frac{\left(1+2.28(u_*/fL)\right)^{\frac{1}{2}} - 1}{3.8} \qquad (2)$$

The major problem in implementing this scheme for Østergarnsholm is that the mixed layer continues to grow while atmospheric conditions are unstable since subsidence is disregarded. Using the parameterization of [*Batchvarova and Gryning*, 1990] over land, the model can be re-initialised each morning at sunrise. However, conditions offshore can be unstable at night and more stable during the day [*Barthelmie et al.*, 1996] and it is not clear at which time of day model re-initialisation should occur. Running the model without reinitialisation (as shown in Figure 5) allows the predicted mixed layer depth to become very large if conditions remain convective. The collapse of the mixed layer is brought about by transition to near-neutral or unstable conditions.

The model was initialised at 0430 on September 18 using the measured lapse rate above the mixed layer (at 1200 on the same day) and mixed layer depth from the pibal measurements at 0800. The mixed layer depth then follows a pattern of increasing while conditions remain convective or maintaining relatively low values while conditions are close to neutral or stable. Due to a break in the surface measurements it was necessary to re-initialise the model at 0800 on September 24 (using mixed layer depth estimated from the pibal measurement at 0900).

Despite the re-initialisation difficulty in the model, there is reasonably good agreement between modelled values and those estimated from the tethersonde and pibal measurements particularly on September 22.

## Conclusions

There is a fair agreement between spectral estimates of mixed layer height and direct measurements for these offshore measurements. Due to the fact that these were offshore measurements the mixed layer height was not as well defined as it would have been over land, making it difficult to interpret the balloon data, which is believed to cause much of the scatter in the data.


## Acknowledgements

The Risø measurements at Gotland were supported by the ONR


## References


Barthelmie, R.J., B. Grisogono, and S.C. Pryor, Observations and simulations of diurnal cycles of near-surface wind speeds over land and sea., *Journal of Geophysical Research (Atmospheres)*, *101* (D16), 21,327-21,337, 1996.

Batchvarova, E., and S.E. Gryning, Applied model for the growth of the daytime mixed layer, *Boundary Layer Meteorology*, *56* (3), 261-274, 1990.

Højstrup, J., Velocity spectra in the unstable boundary layer. *J. Atmos. Sci.* **39**, 2239-2248. 1982

Kaimal, J.C., Horizontal velocity spectra in an unstable surface layer. *J. Atmos. Sci.*, **35**, 18-24, 1978

Panofsky, H.A., Tennekes, H., Lenschow, D.H., and Wyngaard, J.C., The characteristics of turbulent velocity components in the surface layer under convective conditions. *Boundary Layer Meteorol.* **11**, 355-361, 1977

Nieuwstadt, F., The steady-state height and resistance laws of the nocturnal boundary layer: theory compared with Cabauw observations, *Boundary Layer Meteorology*, *30*, 31-55, 1981.

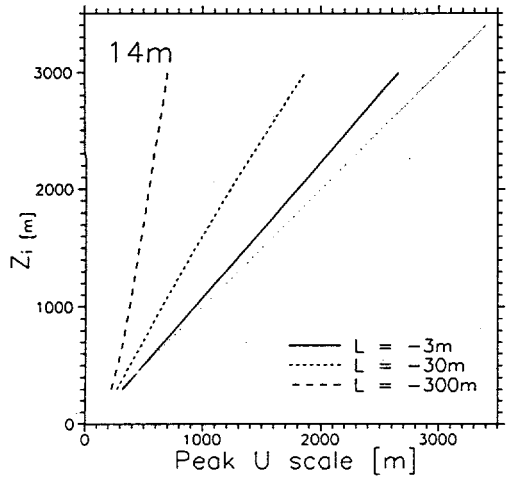


**Figure 1** Variation of spectral peak with stability. Height 14m

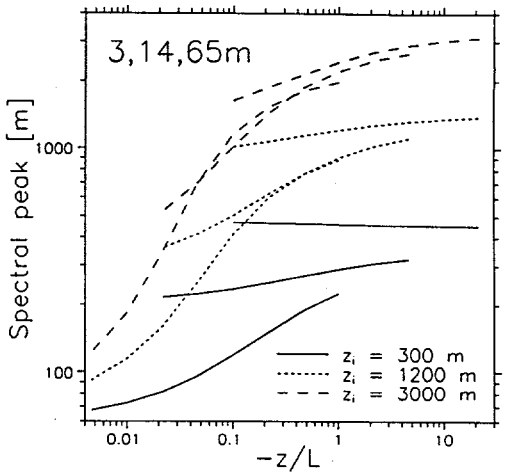


**Figure 2** Spectral peak as a function of stability for three different $z_i$'s.

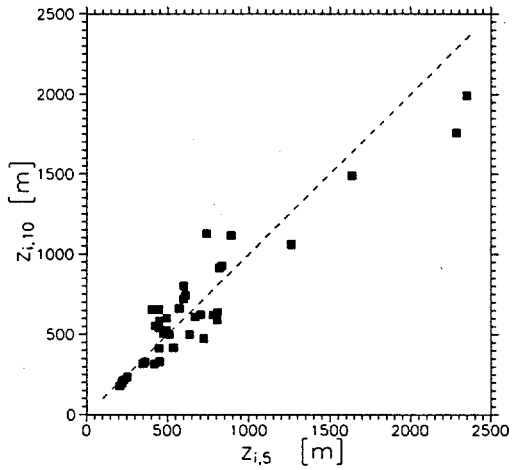


**Figure 3** Mixed layer heights calculated from sonic spectra at 5m and 10m.

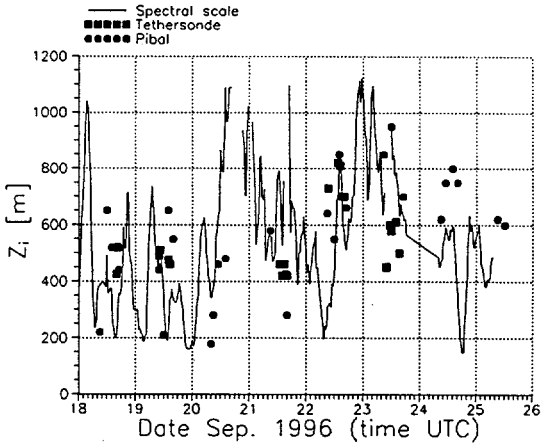


**Figure 4** Mixed layer heights from spectra compared with balloon measurements.

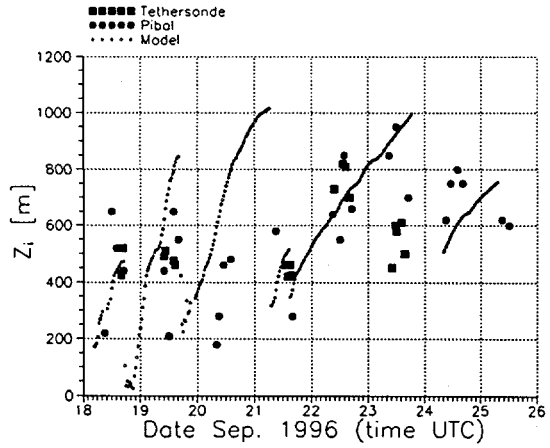


**Figure 5** Modelled mixed layer heights compared with balloon measurements

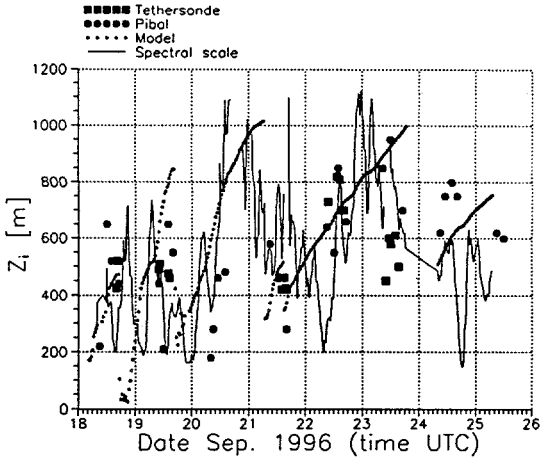


**Figure 6** All mixed layer height estimates compared

## Modelling the development of mixing height in near equatorial region.

A. A. Samah.

Air Pollution Research Unit, University of Malaya, Kuala Lumpur, Malaysia.

### Introduction.

Most current air pollution models were developed for midlatitude conditions and as such many of the empirical parameters used were based on observations taken in the midlatitude boundary layer which is physically different from that of the equatorial boundary layer. In the equatorial boundary layer the Coriolis parameter *f* is small or zero and moisture plays a more important role in the control of stability and the surface energy balance. Therefore the applications of air pollution models such as the OMLMULTI or the ADMS which were basically developed for midlatitude conditions must be with some caution and would need some adaptation to properly simulate the properties of equatorial boundary layer. This works elucidate some of the problems of modelling the evolution of mixing height in the equatorial region. These mixing height estimates were compared with routine observations taken during a severe air pollution episodes in Malaysia.

### The Model.

The model used in this study is the OML meteorological preprocessor developed by NERI described by Olesen and Brown, 1992. The evolution of the convective boundary layer were based on the set of equations derived by Tennekes, 1973 and Tennekes and Driedonks, 1981. In this adaption a small change was made to the set of equations in which the potential temperature was replaced with virtual potential temperature to include the effects of moisture. Hence the development of the mixing height h is given as,

$$dh/dt = 1/\Delta\theta_v \, (A_e \, (\theta_v{}'w')_s + A_m u_*{}^3 \, T_v/(gh))$$

with the temperature jump $\Delta\theta_v$ as,

$$d\Delta\theta_v/dt = (A_e/\Delta\theta_v - (1+ A_e)/h) \, (\theta_v{}'w')_s + (\gamma/\Delta\theta_v - 1/h) \, A_m u_*{}^3 \, T_v/(gh)$$

The development of the stable mixing height due to mechanical mixing in this preprocessor is scaled by *f* and was found to be unrealistic. A number of alternatives representation as given in the COST710 report were attempted. These estimates were observed to be too dependent on the friction velocity which could have very small values during the night. Hence under such a situation the predicted mixing height would be small. Alternatively representation using the concept developed Stull, 1982 based on the time history of surface heat flux may provide a better alternative. Any development however must include a detail observation of the equatorial boundary layer to verify these estimates.

**Observations.**
Due to a lack of detail observation of the boundary layer in Kuala Lumpur, the observations used in this study were those observed in the ABRACOS experiment which took place in Rondonia, Brazil in July and August 1993 and was described by Nobre et al, 1996. This was used to contsruct the energy and momentum fluxes at the surface. This was assume to be typical for equatorial situation. The radiosondes ascents used in the mixing height estimates were that taken in Kuala Lumpur during a severe episode of aerosol pollution from 18th September 1994 to 6 October 1994. These were chosen since a clear lid in the form of a mid-level temperature inversion was observed on the 28th of Sept. 1994 (see figure 1) and to test the sensitivity and robustness of the mixing height calculation scheme in capturing this lid. Thermodynamic analysis of the radiosonde ascent showed the importance of moist processes in the equatorial boundary layer. This was clearly elucidated when a comparison was made between the variation of the the equivalent potential temperature and moist static energy shown in figures 2a and 2b with the potential temperature and dry static energy in figure 2c and 2d. It was observed that for the equatorial atmosphere there is a rapid adjustment of the dry temperature field hence producing near uniform fields of potential temperature and dry static energy with very little variation. Therefore the stratification observed was defined more by the moisture field and hence the stability of the boundary layer and such parameters as energy flux and mixing height would be strongly influenced by moist processes.

**Discussion.**
Comparison was initially made between the hourly variation of the convective mixing height calculated using the OML meteorological preprocessor and the mixing height calculated in the ABRACOS experiment. There was a good agreement between the two calculations. The variation of the mixing height during the air pollution episodes were then calculated and a comparison was made with the observed radiosonde analysis. The convective mixing height calculated was found to be insensitive to the stratification inferred by the radiosonde analysis. This could be due to many factors, the first obvious factor was that the turbulence input base on the Amazonian data did not reflect the true state and the second was that the stratification observed were dominated more by the vertical variation of moisture than by temperature and that the current scheme to test for possible lid need to be improve to include some measure of moisture stratification. The predicted nocturnal mixing heights were shallow due to the slower wind speed and as a consequent a small frictional velocity. This resulted in a very skewed diurnal variation of the mixing height with a rapid drop during the night.
Clearly this preliminary study indicate that there is need to develop a better parameterisation of the mixing height estimate for tropical boundary layer.

**Acknowledgements.**
This study was made possible by DANCED and the Malaysian IRPA grant which sponsored the research in NERI. Helge Olesen assisted in changing of the OML meteorological preprocessor program to include the above adaptations.

## References.

Nobre et al 1996, Amazonian Deforestation and Climate

Olesen H.R. Jensen A.B.and Brown N. 1992, An operational Procedure for mixing height estimation. MSTLUFT-A96, National Environmental Research Institute, Denmark.

Nobre et 1996

Tenekes, H. 1973, A model for the dynamics of the inversion above a convective boundary layer. J. Atmos Sci., 30, 558-567.

Tenekes, H and A.G. M. Drierdonks 1981, Basic entrainment equations for atmospheric boundary layer. Boun. Layer Meteor., 20, 515-531.

Stull, R.B. 1983, A heat-flux history length scale for the nocturnal boundary layer. Tellus, 35A, 219-230.

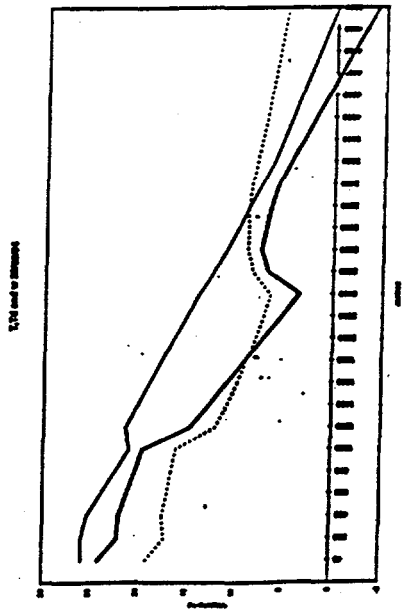

**Figure 1.** The profile of the temperature, dew point temperature and mixing ratio on the 28th of Sept. Two possible distinct stratification at 1000m and 2400m could be observed in this profile.

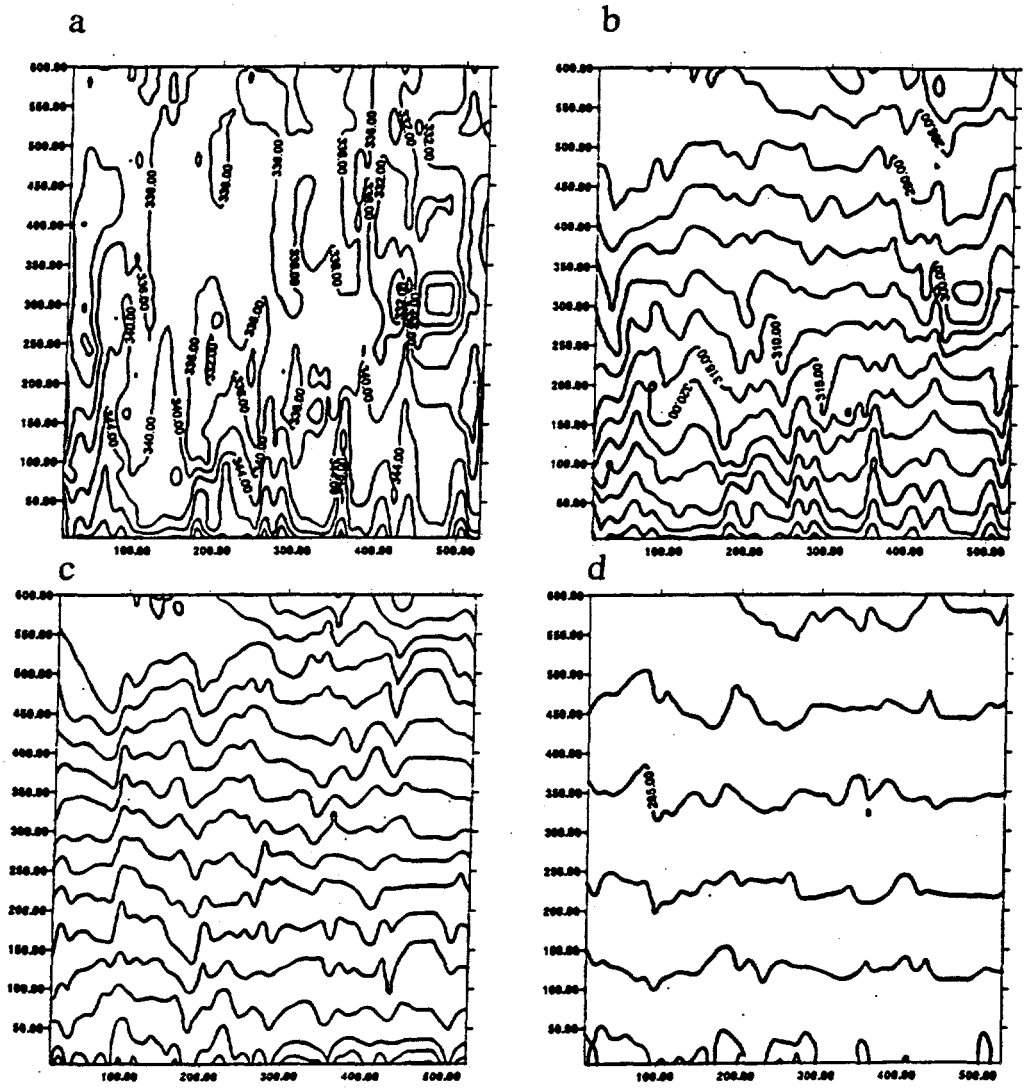


**Figure 2. a:** The time(hr), height (10xm) variation of equivalent potential beginning on the 18th of Sept 1994. Note a distinct blob of drier layer around the period of 200 hr (28 Sept (-+ 1 day) centred at about 2500 km. This layer coincide with the top layer stratification observed in figure 1. **b:** the same format but for moist static energy **c:** potential temperature. **d:** dry static energy. Note that for the case in which moisture was not included the variation was nearly uniform daily. The dry analysis fail to capture the blob of drier air observed.

# Determination of regional heat fluxes from the growth of the mixed layer

S.-E. Gryning[1], E. Batchvarova[1,2]

[1] *Risø National Laboratory, DK-4000 Roskilde, Denmark*
[2] *National Institute of Meteorology and Hydrology, 1784 Sofia, Bulgaria*

## Introduction

The distribution of surface sensible heat flux is a critical factor in producing and modifying the mesoscale atmospheric flows, turbulence and evaporation. Parameterizations that assume homogeneous land characteristics are inappropriate to represent the spatial variability often found in nature. One possibility to overcome this problem is to increase the resolution of the model grid which demands unrealistic computing resources and data for model initialization. Area averaged fluxes can be obtained from aircraft measurements. It is essential that the flights are performed at a height where the individual surface features are not felt. A large number of flights and appropriate pattern to meet the task are needed in order to achieve a fair statistics (Jochum, 1993; Tjernström and Smedman, 1993). The mixed layer grows in response to the regional turbulent fluxes including the aggregation and small scale processes. The region of influence in upwind direction is typically 20 times the height of the mixed layer for convective and 100 times the height of the mixed layer for atmospheric near neutral conditions. In this study we determine the regional integrated sensible heat flux from information on the evolution of the mixed layer over the area. The required information to use the method can be derived from wind speed and temperature profiles obtained by radiosoundings when performed frequently enough to provide a reasonably detailed structure of the development of the mixed-layer. The method is applied to estimate the regional heat flux over the NOPEX experimental area for three days during the campaign in 1994.

## Mixed-layer growth model

The theoretical framework is the zero-order mixed-layer growth model for near neutral and unstable atmospheric conditions suggested by Batchvarova and Gryning (1991) and (1994):

$$\left\{\frac{h^2}{(1+2A)h-2B\kappa L}+\frac{Cu_*^2T}{\gamma g[(1+A)h-B\kappa L]}\right\}\left(\frac{dh}{dt}-w_s\right)=\frac{\left(\overline{w'\theta'}\right)_s}{\gamma} \qquad (1)$$

where t is time, L the Monin-Obukhov length, $\kappa$ - the von Karman constant, g/T - the buoyancy parameter, A, B and C are parameterization constants. Commonly accepted values are A=0.2, B=2.5, and C=8.

Knowing the potential temperature gradient $\gamma$, the height of the boundary layer, h, and its growth rate, dh/dt, the friction velocity, $u_*$, and the mean vertical motion at the top of the mixed layer, $w_s$, Eq. (1) can be solved numerically for the

vertical turbulent kinematic sensible heat flux at the surface, $\left(\overline{w'\theta'}\right)_s$, that is forcing the growth of the boundary layer. The estimated heat flux represents a regional average when the top of the mixed layer is above the height where the properties of the flow are spatially invariant.

**NOPEX region and measuring sites**

The NOPEX region represents the northern landscape, the boreal zone. It is a mosaic type flat terrain with patches of forest (54%), agricultural fields (38%), lakes (4%), towns and villages (4%). The region is located north-west of Stockholm, Sweden. The region extended 80 kilometers in West-East and 40 km in South-North direction, Fig. 1.

The measurements used in this paper were carried out during the experiment in 1994 at two agricultural (Marsta and Tisby) and two forest (Norunda and Siggefora) sites.

The Marsta site (Smedman-Högström and Högström, 1973) is located at 17°35'E, 59°57' N in a grass covered area, surrounded by agricultural fields. The observational program performed at Marsta by the Department of Meteorology, Uppsala University, included atmospheric turbulence measurements at a height of 10 meters with a Solent Ultrasonic Anemometer 1012R2 and boundary-layer profile measurements by launches of radiosondes type Vaisala 80 with a vertical resolution of about 4 meters. During the selected days the radiosoundings were performed at intervals of one or two hours.

The Tisby site is located 35 km West of Uppsala at 16°57'E and 59°46'N within agricultural fields of barley and wheat. A very comprehensive measuring program was carried out at this site. Turbulent fluxes were measured by an ultrasonic anemometer (type Kaijo Denki DAT/TR-61B) at a height of 6.5 meters.

The Norunda site is situated 35 km North of Uppsala at 17°25'E and 60°05'N in a 100-year old forest consisting of pine (60%) and spruce (40%). Measurements of turbulent fluxes with Solent ultrasonic anemometers were carried out at several heights on a 102-meter mast by the Swedish University of Agricultural Sciences. The heat flux measurements used in this paper were taken at 35 m height.

The Siggefora site is located 30 km North-West from Uppsala at 17°08'E and 59°59'N in a coniferous forest consisting of mature stands of pine and spruce. Measurements of turbulent fluxes were carried out at 31 m height with a Solent ultrasonic anemometer by the Swedish University of Agricultural Sciences.

On the 13, 14 and 21 of June 1994, an extensive radiosounding program was carried out at Marsta. The soundings typically started at 6 a.m. and continued throughout the day until 4 p.m. Radiosondes were launched every hour or every second hour.

**Results**

Figure 2 introduces the measured sensible heat flux at the forest and agricultural sites for the three analyzed days. It can be noted that the heat fluxes at the two agricultural sites are comparable and both show the characteristic daily cycle,

being low in the morning and evening with a maximum around noon. The heat flux at the forest sites reaches 2-3 times higher values than at the agricultural sites.

An estimate of the regional heat flux over the area weighting the forest data (Norunda) with 54 % and the agricultural data (Tisby) with 42 % for the three days is given in Fig. 3. For towns and villages (4%) the heat flux was assigned as for agricultural areas. The sensible heat flux over the lakes (4%) was assumed to be negligible.

An appropriate friction velocity is taken as 0.1u, where u is the wind speed at Tisby. The regional heat flux is then derived from Eq. (1) based on half-hour interpolated values of the mixed-layer height. The results are shown in Fig. 3. A comparison with Fig. 2 clearly shows that the regional heat flux determined on the basis of the growth of the mixed layer is typically twice bigger than the contemporary heat flux at the agricultural sites and significantly smaller than at the forest sites. The agreement with the area-weighted average heat flux is generally good, Fig. 3.

The method proposed here can be used at stationary synoptic conditions when information on the mixed-layer evolution is available.

**Acknowledgments**

The measurements at Marsta performed by the Department of Meteorology, Uppsala University, were kindly made available for us by Ulf Högström. We are thankful to Anders Lindroth, Swedish University of Agricultural Sciences, for providing the data from Norunda and Siggefora. We also express our sincere thanks to Hans Bergström, responsible for the sonic anemometer measurements at Marsta, to Achim Grelle, responsible for the sonic anemometer measurements at Norunda and Siggefora, and to Birgitta Källstrand who participated in the job with radiosonde launches. The study was supported by the Nordic Council of Ministers and the National Environmental Research Program 1992-1996.

**References**

Batchvarova, E. and Gryning, S.E.,1991. Applied model for the growth of the daytime mixed layer. Boundary-Layer Meteorology, 56: 261-274.

Batchvarova, E. and Gryning, S.E., 1994. An applied model for the height of the daytime mixed layer and the entrainment zone. Boundary-Layer Meteorology, 71: 311-323.

Jochum, A.M., 1993. Estimation of area-averaged fluxes from aircraft measurements using different observational techniques. Proc. eight Symposium on Meteorological Observations and Instrumentation, 17-22 January, Anaheim. American Meteorological Society, 467-472.

Smedman-Högström,A.-S. and Högström, U., 1973. The Marsta micro-meteorological field project. Profile measurements system and some preliminary data. Boundary-Layer Meteorology, 5: 259-273.

Tjernström, M. and Smedman, A.-S., 1993. The vertical turbulence structure of the coastal marine atmospheric boundary layer. J. Geophys. Res., 98: 4809-4826.

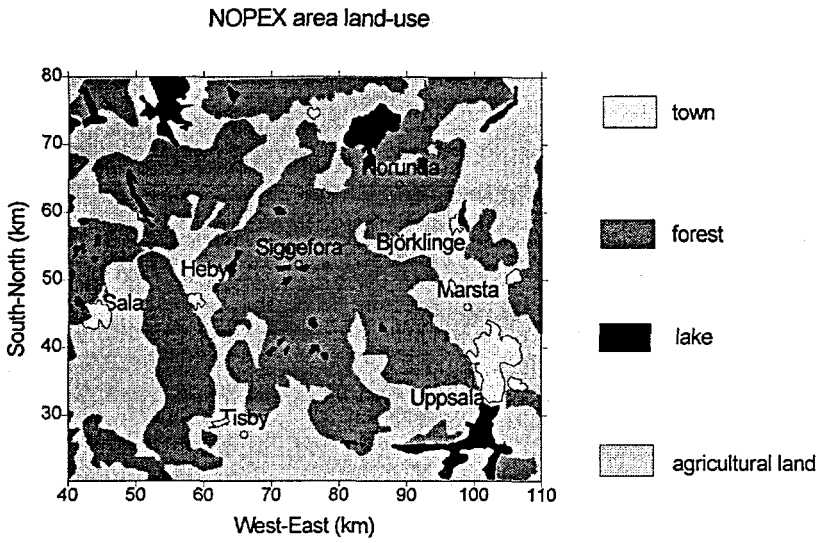


Figure 1. The spatial distribution of lakes, towns, prevailing forests, and prevailing agricultural fields for the NOPEX region. The location of the measuring sites is shown by open circles.

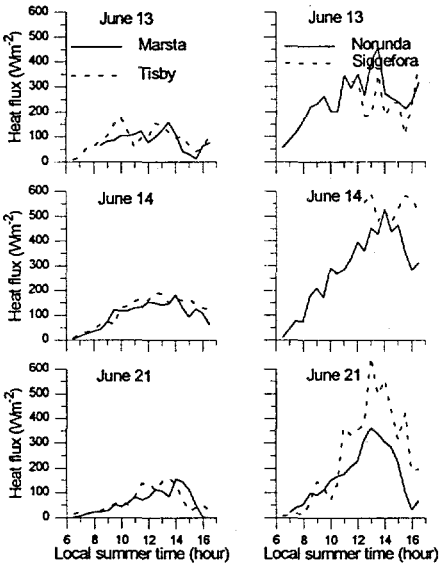


Figure 2. Measured heat flux over agricultural fields (Marsta and Tisby) and over forest (Norunda and Siggefora).

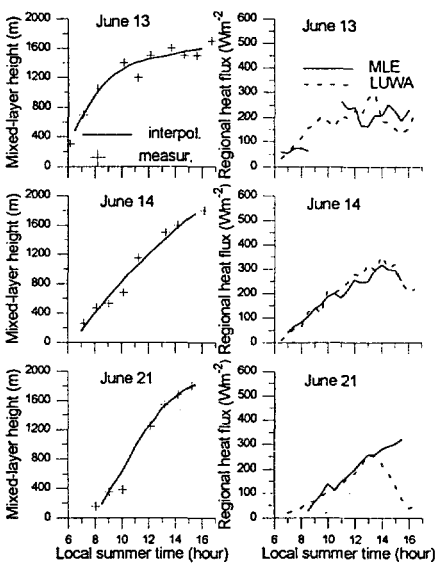


Figure 3. Mixed-layer evolu-tion and regional heat fluxes derived by the Mixed-Layer-Evolution method (MLE) and by Land-Use-Weighted-Average method (LUWA) .

# Session III - Mixing Height Determination from NWP-Models
# Chairperson: Han van Dop

# Mixing Height Derived from the DMI-HIRLAM NWP Model, and Used for ETEX Dispersion Modelling

J.H. Sørensen, A. Rasmussen

Danish Meteorological Institute (DMI), Copenhagen, Denmark

## Introduction

For atmospheric dispersion modelling it is of great significance to estimate the mixing height well. Mesoscale and long-range diffusion models using output from numerical weather prediction (NWP) models may well use NWP model profiles of wind, temperature and humidity in computation of the mixing height. This is dynamically consistent, and enables calculation of the mixing height for predicted states of the atmosphere.

In autumn 1994, the European Tracer Experiment (ETEX) (Nodop *et al.,* 1997) was carried out with the objective to validate atmospheric dispersion models. The Danish Meteorological Institute (DMI) participates in the model evaluations with the Danish Emergency Response Model of the Atmosphere (DERMA) (Sørensen *et al.,* 1997b; Sørensen 1997; Sørensen and Rasmussen, 1995) using NWP model data from the DMI version (Rasmussen and Sørensen, 1997; Sass, 1994) of the High Resolution Limited Area Model (HIRLAM) (Källén *et al.,* 1996) as well as from the global model of the European Centre for Medium-Range Weather Forecast (ECMWF). In DERMA, calculation of mixing heights are performed based on a bulk Richardson number approach.

Comparing with tracer gas measurements for the first ETEX experiment, a sensitivity study is performed for DERMA. Using DMI-HIRLAM data, the study shows that optimum values of the critical bulk Richardson number in the range 0.15–0.35 are adequate. These results are in agreement with recent mixing height verification studies against radiosonde data (Sørensen *et al.,* 1997a; Sørensen and Rasmussen, 1997). The fairly large range of adequate critical values is a signature of the robustness of the method.

Direct verification results against observed mixing heights from operational radiosondes released under the ETEX plume are presented.

## Bulk Richardson Number Method

The mixing height is estimated by a bulk Richardson number approach (Sørensen *et al.,* 1997a; Sørensen and Rasmussen, 1997; Vogelezang and Holtslag, 1996). The method is robust and fairly accurate, and it is suited for use in situations where the vertical resolution of temperature and wind is limited as e.g. output from NWP models. The bulk Richardson number at height $z$ above ground is given by the following expression,

$$\mathrm{Ri_B} = \frac{gz\,(\theta_v - \theta_s)}{\theta_s\,(u^2 + v^2)}. \qquad (1)$$

The quantities $\theta_s$ and $\theta_v$ are the virtual potential temperature at surface and at height $z$, respectively, $u$ and $v$ are the horizontal wind components at height $z$, and $g$ is the gravitational acceleration. The top of the ABL is given by the height at which the bulk Richardson number reaches a critical value.

In a recent study involving comparisons with radiosonde data (Sørensen *et al.,* 1997a; Sørensen and Rasmussen, 1997), a critical value of 0.24 was found most appropriate (with a correlation of 68%) for the DMI-HIRLAM model. From this study it furthermore

appears that critical values of the bulk Richardson number in the range 0.15–0.35 are adequate for DMI-HIRLAM data.

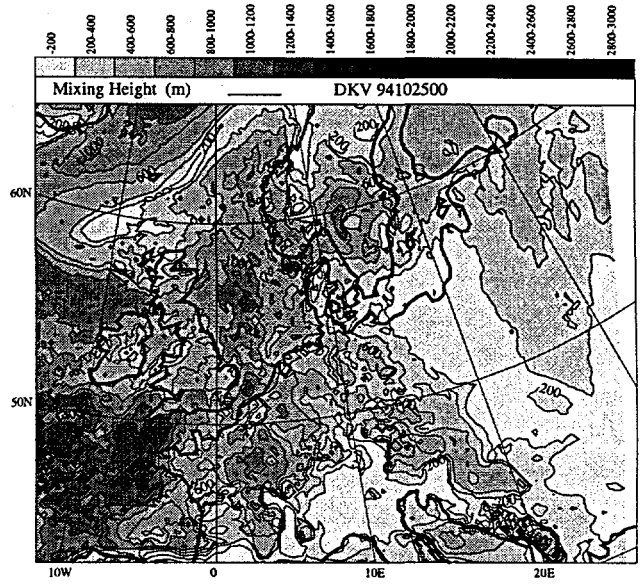


FIG. 1. Boundary layer height at 0 UTC on October 25, 1994, calculated from analysed DMI-HIRLAM data.

In Fig. 1 an example is shown of a calculation of the mixing height over Europe. The calculation which is valid at 0 UTC on October 25, 1994, is based on analysed DMI-HIRLAM data.

## Indirect Verification Against ETEX Tracer Gas Measurements

Comparisons are performed of DERMA simulations of the first ETEX experiment with observed concentrations (ETEX data set version: etex1_v1.1.960505). In Fig. 2, DERMA simulations of the first ETEX experiment are shown. The results are obtained by using high-resolution DMI-HIRLAM data. In Fig. 3, global values of normalised mean square error (NMSE), correlation and bias are shown for the DERMA simulations based on analysed DMI-HIRLAM and analysed ECMWF data, respectively. The statistical parameters are shown as functions of the critical value of the bulk Richardson number. From the figures it appears that critical values in the range 0.15–0.35 are adequate for DMI-HIRLAM data while it is 0.30–0.60 for ECMWF data. The difference between the two ranges of critical values owes to differences in vertical resolution and physical parametrisations of the corresponding NWP models. The fairly large range of critical values is in accordance with the above-mentioned verifications against radiosonde data.

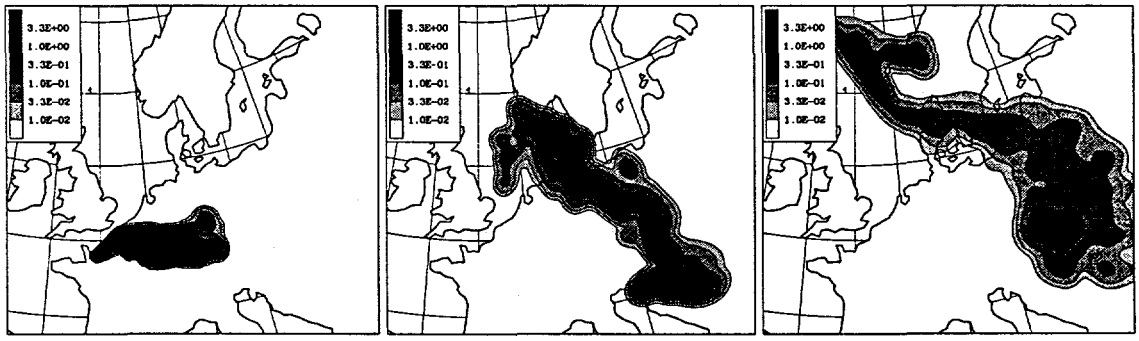


FIG. 2. Three-hour average surface concentrations from the DERMA simulation based on analysed DMI-HIRLAM data. On the sub-figures, the concentration patterns are shown in units of $\mathrm{ng\,m^{-3}}$ at 24, 48 and 72 hours, respectively, after the start of the first release.

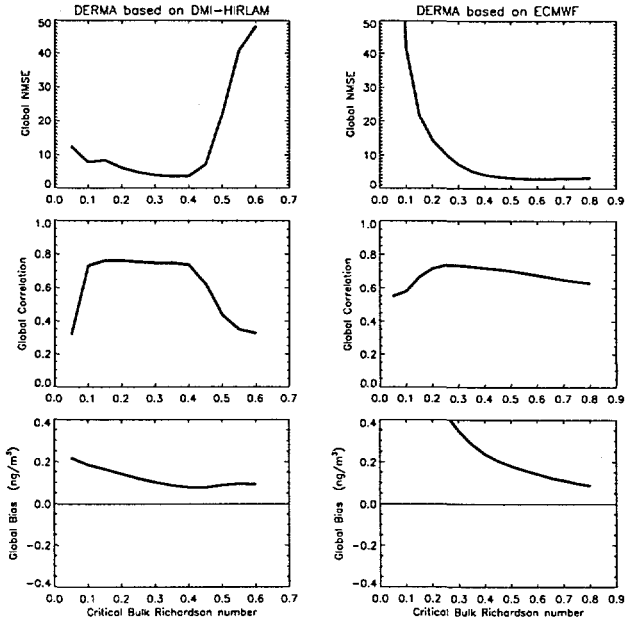


FIG. 3. Global values of normalised mean square error (NMSE), correlation and bias for DERMA simulations using analysed DMI-HIRLAM data (left column), and analysed ECMWF data (right column). Results are shown as a function of the critical bulk Richardson number.

## Direct Verification Against Radiosoundings under ETEX Plume

The routine radiosondes which were released under the ETEX plume have been located. Most radiosoundings correspond to 0 and 12 UTC, only few radiosondes are released at 6 and 18 UTC. By inspection of measured profiles of temperature, humidity and wind corresponding to well-defined boundary layers, a set of observations of mixing heights is obtained. In Fig. 4 observations are compared with model results derived by using the bulk Richardson number approach with a critical value of 0.25 applied to DMI-HIRLAM vertical profiles. The NWP profiles include analysed data as well as forecasts relevant to dispersion simulations of the first tracer gas experiment.

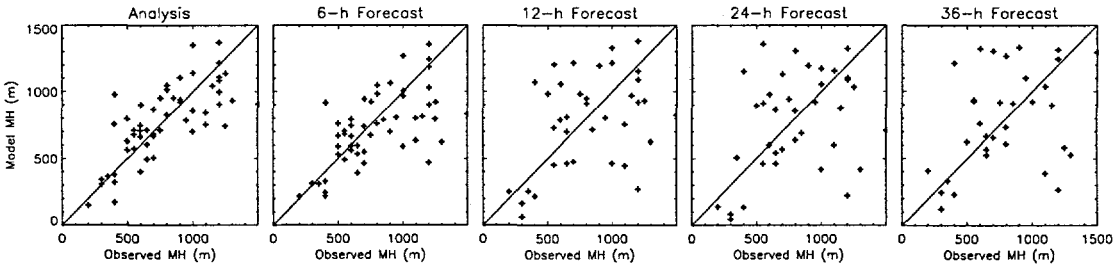


FIG. 4. Comparisons of modelled and observed mixing heights. The model results shown are derived from analysed as well as from 6, 12, 24 and 36 hour forecasts from the DMI-HIRLAM NWP model. From left to right, the number of data points in the scatter plots are 55, 54, 38, 38 and 34, respectively.

At the time the ETEX tracer gas experiments were carried out, the operational DMI-HIRLAM model produced analysed states of the atmosphere corresponding to 0, 6, 12 and 18 UTC. For the 0 and 12 UTC analyses, up to 36-hour forecasts were produced while the forecast length was only 6 hours corresponding to the 6 and 18 UTC analyses.

In Fig. 5 statistical parameters are shown as a function of forecast length. The correlation drops from 0.75 to a minimum value of 0.3, and the NMSE increases from 0.08 to a maximum of 0.35. The bias varies between 0 (analysis) and $-100$ m.

## Conclusions

The sensitivity of DERMA to the critical bulk Richardson number is studied by comparing model calculations with tracer gas measurements from the first ETEX experiment.

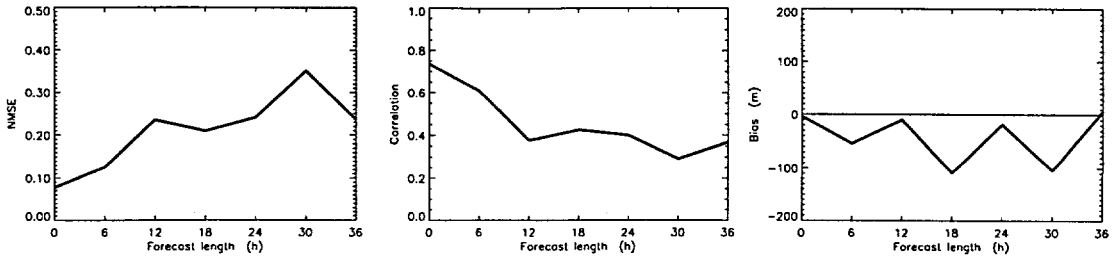


FIG. 5. Normalised mean square error (NMSE), correlation and bias calculated from observed mixing heights and model results derived from DMI-HIRLAM using the bulk Richardson number method with a critical value of 0.25. The statistical parameters are shown as functions of forecast length. The number of data points corresponding to analysed results and 6, 12, 18, 24, 30 and 36 hour forecasts are 55, 54, 38, 16, 38, 14 and 34, respectively.

Using DMI-HIRLAM data, optimum values of the critical number in the range 0.15–0.35 are obtained.

Direct comparisons are made of modelled and observed mixing heights. The observed mixing heights are obtained from routine radiosoundings within the ETEX tracer gas plume. The corresponding modelled mixing heights are derived from analysed as well as forecast DMI-HIRLAM profiles.

## References

Källén E. (Ed.), 1996: HIRLAM documentation manual, System 2.5. Available from the Swedish Meteorological and Hydrological Institute (SMHI).

Nodop K. (Ed), 1997: *ETEX Symposium on Long-Range Atmospheric Transport, Model Verification and Emergency Response, Proceedings.* Vienna, Austria, 13–16 May, 1997, *EUR 17346 EN.*

Rasmussen A. and Sørensen J.H., 1997: Quality Validation of Analyzed and Forecast Vertical Profiles of Wind and Temperature from the DMI-HIRLAM Model in Comparison with Radiosoundings. In: *Proceedings of the Sixth Topical Meeting on Emergency Preparedness and Response.* San Fransisco, California, April 22–25, 1997, pp. 31–34 (ISBN 0-89448-623-3).

Sass B.H., 1994: The DMI Operational HIRLAM Forecasting System, Version 2.3. *DMI Technical Report* **94–8**. Available from DMI.

Sørensen J.H., 1997: Sensitivity of DERMA to Boundary-Layer Parameters, and Evidence for Mesoscale Influence on Long-Range Transport. In: *ETEX Symposium on Long-Range Atmospheric Transport, Model Verification and Emergency Response, Proceedings.* Ed: Nodop K., Vienna, Austria, 13–16 May, 1997, *EUR 17346 EN,* pp. 207–210.

Sørensen J.H. and Rasmussen A., 1995: Calculations Performed by the Danish Meteorological Institute. In: *Report of the Nordic Dispersion/Trajectory Model Comparison with the ETEX-1 Fullscale Experiment.* Eds: Tveten U. and Mikkelsen T., *Risø-R-847(EN), NKS EKO-4(95)1,* pp. 16–27.

Sørensen J.H. and Rasmussen A., 1997: Method for Calculation of Atmospheric Boundary-Layer Height used in ETEX Dispersion Modeling. In: *Proceedings of the Sixth Topical Meeting on Emergency Preparedness and Response.* San Fransisco, California, April 22–25, 1997, pp. 503–506 (ISBN 0-89448-623-3).

Sørensen J.H., Rasmussen A. and Svensmark H., 1997a: Forecast of Atmospheric Boundary Layer Height Utilised for ETEX Real-time Dispersion Modelling. Accepted for publication in *Physics and Chemistry of the Earth.*

Sørensen J.H., Rasmussen A., Ellermann T. and Lyck E., 1997b: Mesoscale Influence on Long-range Transport; Evidence from ETEX Modelling and Observations. Accepted for publication in *Atmos. Environ.*

Vogelezang D.H.P. and Holtslag A.A.M., 1996: Evaluation and model impacts of alternative boundary-layer height formulations. *Boundary-Layer Meteorol.* **81**, 245–269.

# An Operational Routine for Off-Line diagnostic determination of the mixing height depth

T. Iversen[1,2] and H. A. Jakobsen[1]

[1]*EMEP / MSC-W, The Norwegian Meteorological Institute, P.O.Box 43, Blindern N-0313 OSLO, NORWAY*

[2]*c/o Department of Geophyics, P.O. Box 1022, Blindern, N-0315 Oslo, Norway*

**Abstract**

As a modelling center for the European Monitoring and Evaluation Programme (EMEP), The Norwegian Meteorological Institute has for more than 15 years been running models for long-range transport of air-pollutants in Europe. These models have used the height of the well mixed layer (MH) as a key determining parameter along with other met-data such as winds and precipitation.

In this paper we investigate the possibility to determine the MH at intermittent times by using data from a NWP-model run with intermittent data-assimilation, and with data taken out after 12 hours forecasts (to avoid spin-up problems). The model, which is run with 50 km grid-resolution, does not calculate the MH explicitely. Since data on MH are not frequently available from NWP-output, we have designed a diagnostic procedure to estimate the MH from the NWP-data at main synoptic hours. The method separates between the unstable (upward heatflux) ABL and the neutral and stable ABL. In the former case, the heat-input from the surface-layer over one hour is distributed vertically assuming a resulting dry-adiabatic lapse-rate. In the the latter, the MH is determined from a vertical exchange coefficient for heat using the Blackadar (1979) formulaes. Furthermore, the minimum MH is set to 200m and the maximum to 2500m. Data for MH are obtained four times daily, and results for 1992 are compared with MH "observed" from radio-sondes at 00 and 12 UT. These are determined as the height where the lapse rate becomes larger than half of the dry adiabat. Estimates of MH are also obtained by running Cressman-analysis of the radiosonde-data with the model-data as background.

The first choice of parameter-values for the MH-determination yields considerable underestimations of the modelled MH compared to those "observed". Sensitivity tests shows that the "observed" MH is very sensitive to the choice of maximum lapse rate in the ABL. It is thus questionable how well the MH really can be observed from radiosondes. The modelled MH is sensitive to the choice of minimum permitted vertical exchange coefficient in the ABL (giving MH in the stable case), but relatively insensitive to the choice of time-step for theheat-influx in the unstable case. The systematic under-estimations are consider-ably redused after a crude tuning of parameters based on the sensitivity tests.

# Boundary layer heights and surface fluxes of momentum and heat derived from ECMWF data for use in pollutant dispersion models - problems with data accuracy

G. Wotawa[1], A. Stohl[2]

[1] University of Agricultural Sciences, Institute of Meteorology and Physics, Vienna, Austria
[2] Ludwig-Maximilians-Universitaet Muenchen, Munich, Germany

## Introduction

Certain boundary layer parameters, especially boundary layer heights, are very important for pollutant dispersion modelling. On the regional scale (≥ 100 km), data of the numerical weather prediction model of the European Centre for Medium-Range Weather Forecasts (ECMWF, 1995) are often used for that purpose. Based on ECMWF data, the meteorological preprocessor FLEXTRA for Lagrangian air quality simulation models (Stohl et al., 1995; Wotawa et al., 1996) and the Lagrangian particle diffusion model FLEXPART (Stohl et al., 1997) have been developed. Using analyses and short term forecasts, a temporal resolution of three hours can be achieved. Some alternative methods to obtain boundary layer parameters can be applied, producing different results which affect all subsequent calculations, for instance the calculation of boundary layer trajectories (Stohl and Wotawa, 1995) and the dispersion of air pollutants.

## Boundary layer height calculation

In the convective case, boundary layer heights h are calculated analytically making use of the lifting parcel method (e.g., Beljaars and Bets, 1992) based on ECMWF temperature profiles and the calculation of an eddy excess temperature at the surface. The eddy excess temperature calculation requires as input friction velocities (u*) and surface sensible heat fluxes (SHF).

In the stable case, h can either be calculated from the values of u* ($h=C\,u^*/f$ with f being the Coriolis parameter and C a constant with values between 0.07 and 0.25) as done, e.g., in the OML model (Olesen and Brown, 1988), or, alternatively, using critical Richardson numbers. It was demonstrated that the boundary layer heights calculated with the latter method are in better accordance with measurement data (Vogelezang and Holtslag, 1996).

## Calculation of friction velocities and surface sensible heat fluxes

Values of u* and SHF can be calculated from ECMWF two meter temperatures, ten meter wind speeds and the respective quantities on the first model level (approximately 30 meters) applying the profile method as described by Olesen and Brown (1988). Alternatively, accumulated values of u* and SHF are available from the ECMWF short-term forecasts (temporal resolution: three hours). In this paper, a comparison is done between the values of u* and SHF taken from short-term forecasts and the respective quantities computed from temperature and wind profiles. This comparison is done for five different grid points in Europe (Atlantic Ocean, Eastern Alps, Southern Alps, Pannonian Lowland,

Siberia). Afterwards, the values of u* and SHF derived from ECMWF data are compared to the respective quantities obtained from routine observation data using the OML model.

Except for the grid point „Atlantic", a very bad accordance between short-term forecasts and profile method results for u* and SHF was observed. The correlation coefficients are quite low and the mean deviations are very high (see table 1). These results are surprising, since it was expected that both alternative methods to obtain the surface fluxes should yield comparable results. As worst accordance is observed in September, one possible reason for that behaviour could be that the first model layer of ECMWF model (approximately 33 m) is frequently above the surface layer (h/10), especially during stable conditions. This assumption is supported by the fact that the accordance is best for the grid point „Atlantic", which shows the highest values of h during night-time.

Wotawa et al. (1996) showed that there is a reasonably good statistical relationship between ECMWF short-term forecasts of u* and SHF and the respective quantities calculated from routine observations applying the OML model. This study was based on data from the summer of 1994. Typical correlation coefficients found were 0.7-0.8 for u* and 0.8-0.9 for SHF. To see whether the findings of this study are valid for another year and another cycle of the ECMWF model, the OML model was used to calculate u* and SHF based on routine observations for the grid point „Eastern Alps". The following conclusions can be drawn (see Table 2): The findings of Wotawa et al. (1996) were fully confirmed. There is reasonable correspondence between the ECMWF short term-forecasts and the OML results for u* and SHF. u* from the ECMWF model is higher by a factor of 2, but the correlation coefficient is 0.77. The SHF values show high correlation coefficients and almost no systematic error. On the other hand, the correlation coefficients between OML results and the ECMWF values obtained with the profile method are much lower. Thus, it can be concluded that surface fluxes obtained from ECMWF short-term forecasts should be used instead of fluxes obtained with the profile method, especially during stable meteorological conditions and outside the summer period.

**Comparisons of boundary layer heights**

First of all, differences between stable boundary layer heights calculated from friction velocities and from critical Richardson numbers are investigated. For that purpose, only 0 UTC fields during the calculation period are used. The following results are obtained (see table 3): The friction velocity method (the constant C is given the value of 0.125 instead of 0.25 used in the OML model to account for the higher u* values of the ECMWF model) yielded higher values of h. The correlation coefficients are reasonably high for the grid points in the Atlantic Ocean and the Alpine region, but small for the grid points in the Pannonian flatland and Siberia. The systematic differences between the h values obtained depend very much on the (more or less arbitrary) selection of C.

The method using critical Richardson numbers shows two major advantages: First, it is less sensitive to systematic deviations of friction velocities between ECMWF model and observation-based calculations and to the choice of the constant C. Second, the boundary layer heights calculated using this method are in better accordance with measurement data (Vogelezang and Holtslag, 1996). Therefore, the critical Richardson number method is used for the computation of an operational boundary layer height h in the stable case further on. The sensitivity of the operational boundary layer height to the calculation of u* and SHF was investigated for the grid points (see table 4). As a result, it can be seen that using profile

method values of u* and SHF as input data leads to a systematic reduction of h at most grid points. The correlation coefficients between the h-values are approximately 0.9 for the whole data set, but smaller than 0.5 if only stable cases are considered. The mean deviation is approximately 100 m. Thus, there is a significant sensitivity of h to the calculation of u* and SHF in the stable case, whereas the sensitivity in the convective case is small, supporting once more the conclusion that problems using the profile method are more or less restricted to stable meteorological conditions.

At last, the operational boundary layer heights (using u* and SHF from short-term forecasts as input data) were compared to h calculated from routine observations applying the OML model at the grid point „Eastern Alps". The comparison yields the following results (Table 5): The boundary layer heights are reasonably well correlated, but ECMWF values are approximately 15% lower than OML values. A comparable underestimation of boundary layer heights from the ECMWF data was shown by Wotawa et al. (1996) using data of the summer 1994.

| Grid point | $u^*_{(1)}$ | $u^*_{(2)}$ | r | $\Delta u^*$ | $SHF_{(1)}$ | $SHF_{(2)}$ | r | $\Delta SHF$ |
|---|---|---|---|---|---|---|---|---|
| Atlantic | 0.26 | 0.31 | 0.71 | 0.08 | -5.9 | -13.9 | 0.93 | 11.3 |
| Eastern Alps | 0.44 | 0.36 | 0.38 | 0.27 | -16.9 | 5.0 | 0.63 | 41.6 |
| Southern Alps | 0.41 | 0.20 | 0.52 | 0.26 | -16.3 | -25.5 | 0.59 | 30.7 |
| Pannonian lowland | 0.32 | 0.31 | 0.47 | 0.18 | -19.2 | 7.0 | 0.60 | 39.1 |
| Siberia | 0.40 | 0.33 | 0.36 | 0.23 | -18.2 | 13.8 | 0.56 | 44.2 |

Table 1: Comparison of the values of u* and SHF calculated from accumulated short-term forecasts (1) and using the profile method (2). Calculation period July 1 to October 1, 1996. Seasonal averages, correlation coefficients (r) and mean deviations ($\Delta$).

| | | $u^*_{ecm}$ | $u^*_{oml}$ | r | $SHF_{ecm}$ | $SHF_{oml}$ | r |
|---|---|---|---|---|---|---|---|
| Short term forecasts | all values | 0.44 | 0.22 | **0.77** | -16.9 | -17.6 | **0.82** |
| | convective | 0.53 | 0.27 | **0.73** | -65.5 | -66.0 | **0.63** |
| Profile method | all values | 0.36 | 0.22 | **0.25** | 5.0 | -17.6 | **0.54** |
| | convective | 0.43 | 0.27 | **0.29** | -49.7 | -66.0 | **0.18** |

Table 2: Comparison between ECMWF surface fluxes (ecm) and the respective observation based values calculated with the OML model (oml) for the grid point „Eastern Alps". Calculation period July 1 to October 1, 1996. Seasonal averages of u* and SHF and correlation coefficients (r). Results for convective conditions ($SHF_{oml}<0$) are tabulated additionally to eliminate the mean daily variations.

| Grid point | h(u*) | h(Ri) | $\Delta h$ | r |
|---|---|---|---|---|
| Atlantic | 396 | 473 | 129 | 0.80 |
| Eastern Alps | 414 | 323 | 165 | 0.70 |
| Southern Alps | 408 | 298 | 150 | 0.66 |
| Pannonian lowland | 297 | 247 | 122 | 0.44 |
| Siberia | 332 | 258 | 129 | 0.44 |

Table 3: Difference between stable boundary layer heights h calculated from friction velocity (u*) and critical Richardson numbers (Ri). Calculation period July 1 to October 1, 1996, only 0 UTC fields. Seasonal averages, mean deviation ($\Delta h$), correlation coefficient (r).

| Grid point | $h_1$ | $h_2$ | $\Delta h$ | r |
|---|---|---|---|---|
| Atlantic | 501 | 524 | 54 | 0.95 |
| Eastern Alps | 588 | 565 | 120 | 0.91 |
| Southern Alps | 587 | 535 | 109 | 0.92 |
| Pannonian lowland | 571 | 567 | 85 | 0.95 |
| Siberia | 627 | 603 | 128 | 0.90 |

Table 4: Difference between operational boundary layer heights h calculated using accumulated values of u* and SHF from ECMWF short-term forecasts (1) and using values calculated applying the profile method. Calculation period July 1 to October 1, 1996 (every 3 hours). Seasonal averages, mean deviation ($\Delta h$), correlation coefficient (r).

| | $h_{ecm}$ | $h_{oml}$ | r |
|---|---|---|---|
| all values | 588 | 689 | **0.77** |
| convective | 833 | 968 | **0.72** |

Table 5: Comparison between ECMWF boundary layer heights (ecm) and the respective observation based values calculated with the OML model (oml) for the grid point „Eastern Alps". Calculation period July 1 to October 1, 1996. Seasonal averages and correlation coefficients (r). Results for convective conditions ($SHF_{oml}<0$) are tabulated additionally.

## References


Beljaars A.C.M. and Betts A.K., 1992: *Validation of the Boundary Layer Representation in the ECMWF Model.* Seminar Proceedings Validation of Models over Europe, Vol II, Reading (UK), 7-11 September 1992.

European Centre for Medium Range Weather Forecasts (ECMWF), 1995: *User guide to ECMWF products 2.1.* ECMWF, Reading, UK.

Olesen H.R. and Brown N., 1988: *The OML Meteorological Preprocessor.* National Agency of Environmental Protection, Air Pollution Laboratory, DK-4000 Roskilde, Denmark.

Stohl A. and Wotawa G., 1995: A method for computing single trajectories representing boundary layer transport. *Atmos. Environ.*, **29**, 3235-3238.

Stohl A., Hittenberger M. and Wotawa G., 1997: Validation of the Lagrangian particle dispersion model FLEXPART against large scale tracer experiment data. *Atmos. Environ.*, special issue ETEX, in preparation.

Stohl A., Wotawa G., Seibert P. and Kromp-Kolb H., 1995: Interpolation errors in wind fields as a function of spatial and temporal resolution and their impact on different types of kinematic trajectories. *J. Appl. Meteor.* **34**, 2149-2165.

Vogelezang D.H.P. and Holtslag A.A.M., 1996: Evaluation and model impacts of alternative boundary-layer height formulations. Boundary-Layer Meteor. **81**, 245-269.

Wotawa G., Stohl A. and Kromp-Kolb H., 1996: Parameterization of the planetary boundary layer over Europe - a data comparison between the observation based OML preprocessor and ECMWF model data. *Contr. Atmos. Phys.* **69**, 10, 273-284.

# A comparison of boundary-layer heights inferred from windprofiler backscatter profiles with diagnostic calculations using regional model forecasts

H. Klein Baltink and A.A.M. Holtslag

Royal Netherlands Meteorological Institute (KNMI), De Bilt, the Netherlands.

## 1. Introduction

From October 1994 through January 1997 the Tropospheric Energy Budget Experiment (TEBEX) was executed by KNMI. The main objectives are to study boundary layer processes and cloud variability on the subgrid scale of present Global Climate Models and to improve the related subgrid parametrizations. A suite of instruments was deployed to measure a large number of variables. Measurements to characterize ABL processes were focussed around the 200 m high meteorological observation tower of the KNMI in Cabauw. In the framework of TEBEX a 1290 MHz windprofiler/RASS was installed in July 1994 at 300 m from the tower.

Data collected during TEBEX are used to assess the performance of a Regional Atmospheric Climate Model (RACMO). This climate model runs also in a operational forecast mode once a day. The diagnostic ABL-height ($h_{model}$) is calculated from the RACMO forecast output. A modified Richardson's number method extended with an excess parcel temperature is applied for all stability conditions. We present the preliminary results of a comparison of $h_{model}$ from forecasts with measured $h_{rs}$ derived from profiler and sodar data for July 1995. First we briefly describe the TEBEX dataset and the RACMO-model respectively.

## 2. TEBEX instruments and data

The systems from which data are used in the intercomparison of the ABL-height are a boundary-layer windprofiler/RASS, TEBEX in-situ surface sensors at Cabauw and the instruments deployed in the Cabauw operational continuous measuring program. The profiler/RASS is a Radian 1290 MHz LAP™3000 system (5 beams, 2.7 x 2.7 $m^2$ phased array antenna). The hourly measuring cycle consisted of 55 min wind measurements in alternated low and high mode and 5 min RASS measurements respectively. Raw spectral data were stored on optical disk. The three spectral moments (radial velocity, spectral width and SNR) of the (atmospheric) peak of the Doppler spectrum are used in this study.

The procedure to extract $h_{rs}$ from the windprofiler backscatter profiles is as follows. The height $h_{rs}$ is characterized by a (local) maximum in the range corrected SNR profiles (RCSNR) (Angevine et al 1994). We use the SNR-profiles from the low mode and oblique beams only (60 m gate height, range 100 - 1450 m agl.). The first step is to remove obvious outliers. Secondly 10 min. median RCSNR profiles are retrieved. The median RCSNR profiles are spline interpolated to create (smooth) profiles with a vertical resolution of 15 m. Next, all local maxima of every single profile are determined. The local maximum associated with $h_{rs}$ is selected by applying several criteria. Finally, sodar and profiler boundary layer height estimates are combined to a continuous $h_{rs}$ time series.

The Cabauw operational continuous measuring program includes 10 min. averaged data from the tower, surface instruments and a monostatic sodar. The ABL-height is derived automatically from the sodar backscatter profiles (Beljaars and Agterberg 1988). A "30 min." database is created from the quality controlled 10 min. data and includes also derived variables e.g. $u_*$ and sensible heatflux H. During TEBEX

additional instruments were deployed, e.g. sonic anemometers, ceilometers, infrared-radiometers and a time-lapse video cassette recorder (one sky image frame every 3 sec.). Furthermore high time resolution data are available from the 6-hourly radiosonde ascents at De Bilt, about 25 km North-east of Cabauw.

## 3. RACMO-model and boundary-layer height routine

RACMO is a regional version of the ECHAM global climate model (Christensen and Van Meijgaard 1992). The operational RACMO-model is based on ECHAM4 and has presently 19 levels in the vertical, a grid size of ≈ 50 x 50 km² and 92 x 81 points in the horizontal plane. For the comparison for July 1995 RACMO was runned with 31 levels. Basic timestep is 5 min. but the radiation module is activated only at a two hourly time interval. Lateral boundaries are taken from the ECMWF-analyses. The model uses a 1.5 order turbulence closure scheme, i.e. a prognostic turbulent kinetic energy equation and a diagnostic length scale (Roeckner et al 1996). A one-column version of the model is available to study the impact of the different parametrizations schemes. For the Cabauw gridbox single level data are stored every timestep, multi-level fields (e.g. U,T,q) are stored every 30 min.

The boundary layer height $h_{model}$ is calculated from the forecast outputs every timestep. There is no feedback on the mixing processes in the ABL (as was the case in the studies by Vogelezang and Holtslag (1996) and Holtslag et al (1995) for the same location). A modified Richardson's number method is applied to calculate $h_{model}$ (Vogelezang and Holtslag 1996). Its generalised form reads:

$$R_{ih} = \frac{g}{\theta_{vs}} \frac{(\theta_{vh} - \theta_{vs}')(h - z_s)}{(u_h - u_s)^2 + (v_h - v_s)^2 + bu_*^2}$$

where b=100 and s indicates a level at $z \approx 0.1\ h$. In RACMO the height of the first model level (≈ 30 m) is chosen as $z_s$ instead. If $(w'\theta')_o < 0$ then $\theta'_{vs} \equiv \theta_{vs}$, otherwise $\theta'_{vs}$ includes a parcel excess temperature (Troen and Mahrt 1986):

$$\theta_{vs}' = \theta_{vs} + b_s \frac{\overline{(w'\theta_v')_o}}{w_m}$$

where $b_s = 8.5$, and $w_m$ is a turbulent velocity scale ($w_m^3 = u_*^3 + cw_*^3$). The height h where $R_{ih} = R_{icr}$ yields the ABL-height $h_{model}$ (here: $R_{icr} = 0.25$).

## 4. Intercomparison results

At present we have RACMO output available from 5th to 31st of July 1995. Forecast output ranges from t+00 upto t+72 hours. We restrict the comparison of ABL-height h to the first 24 hours. We selected 10 days for which $h_{rs}$ was (easily) determined from the profiler data. Intercomparison shows that $h_{model}$ can differ from the measured $h_{rs}$ by as much as a factor of two at the maximum of h around noon. Furthermore, measured and model heat fluxes can differ also quite significantly. For the selected days model heat flux H was typically overestimated while the latent heatflux λE was too small (see e.g. data for 25th July, dotted lines in fig. 1D and 1E respectively). The differences indicate a problem with model soil moisture availability (Van den Hurk et al 1997). Therefore the 1-D model version is used to make a new run for 25th of July with the soil moisture adjusted such that the model fluxes for H and λE more or less coincided with the observations. In this case $h_{model}$ and $h_{rs}$ do compare favourable (full line in fig. 1C), while with the full 3D model the boundary layer height is overpredicted (dotted line).

Analysis of the other selected days is planned to investigate the sensitivity of the 1D-model outputs for initial soil moisture.

## 5. Concluding remarks

Combined measurements of remote sensing, surface and tower instruments collected in July 1995 during TEBEX have been used to assess the diagnostic ABL height $h_{model}$ derived from regional atmospheric climate model (RACMO) forecasts. Preliminary results show that the measured and model ABL-heights can differ significantly. The diagnostic $h_{model}$ from RACMO was in general too high for daytime hours as compared to measured $h_{rs}$ derived from profiler backscatter profiles. It is known that soil moisture availability plays an important role and also that the 3-D RACMO model tends to dry out the soil too much, resulting in unrealistic value for the Bowen ratio for Cabauw as compared with measurements. Improved soil moisture representation and assimilation is currently being developed (van den Hurk et al 1997). The TEBEX dataset will be used to assess the effects of the latter.

The ABL-height can be derived from profiler backscatter profiles with a high resolution in time and height in clear-sky conditions. During precipitation the backscatter is dominated by Rayleigh scatter and ABL-height estimation is not possible from profiler SNR-profiles. When (non-precipitating) clouds are present it may also become difficult to extract an ABL-height without additional measurements of cloudbase height. Therefore it is recommended to operate a ceilometer collocated with the profiler to determine cloud base height.

Further work will concentrate on testing the model boundary layer height routine in "all weather" conditions. Also the boundary layer height estimation from profiler data will be optimized and the determination of the depth of entrainment zone will be studied.

## Acknowledgements.

We would like to thank Erik van Meijgaard and Bart van den Hurk for their help in performing the RACMO runs.

## References.

Angevine W.M., A.B. White, S.K. Avery, 1994: Boundary-layer depth and entrainment zone characterization with a boundary-layer profiler, *Boundary-Layer Met.*, **68**, 375-385.

Beljaars A.C.M. and R.Agterberg, 1988: Automatische detektie van inversies met sodar, (in Dutch), KNMI Technical Report TR-106.

Christensen J.H. and E. van Meijgaard, 1992: On the construction of a regional atmospheric climate model, KNMI Technical Report TR-147.

Holtslag A.A.M., E. van Meijgaard, W.C. de Rooy, 1995: A comparison of boundary layer diffusion schemes in unstable conditions over land, *Boundary-Layer Met.*, **76**, 69-95.

Roeckner E., K. Arpe, I. Bengtsson, M.Christoph, M. Claussen, L. Dumenil, M.Esch, M. Giorgetta, U. Schlese, U. Schulzweida, 1996: The atmospheric general circulation model ECHAM-4: Model description and simulation of present-day climate, Report No. 218, MPI für Met., Hamburg.

Troen I. and L. Mahrt, 1986: A simple model of the atmospheric boundary layer; sensitivity to surface evaporation, *Boundary-Layer Met.*, **37**, 129-148.

Van den Hurk B.J.J.M, W Bastiaanssen, H. Pelgrum, E. van Meijgaard, 1997: A new methodology for initialization of soil moisture fields in numerical weather prediction models using METEOSAT and NOAA data, *J. Applied Meteor.*, **36**, 1271-1283.

Vogelezang D.H.P. and A.A.M. Holtslag, 1996: Evaluation and model impacts of alternative boundary-layer height formulations, *Boundary Layer Met.*, **81**, 245-269.

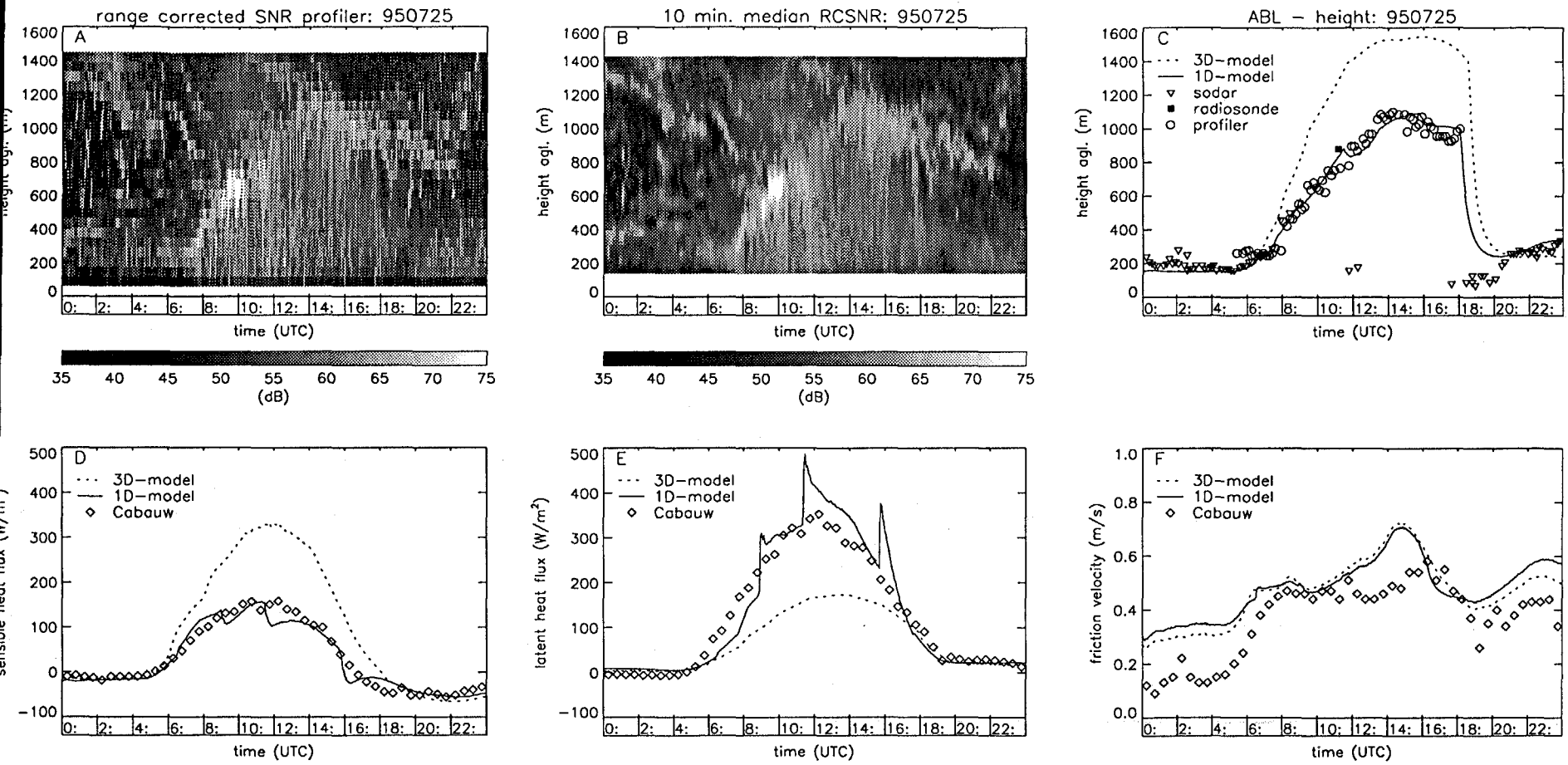


g. 1. Data for 25th July 1995: A) range corrected SNR data profiler, oblique beams only, B) spline interpolated 10 minutes median range corrected SNR data, C) retrieved ABL-heights from profiler (circle), sodar (triangle), radiosonde (filled square) and diagnostic ABL-height for gridbox Cabauw from 3D model (dotted line) and 1D model (solid line), D) surface heat flux Cabauw derived with profile method (diamond) and model heat fluxes H (as in fig. 1C), E) latent heat flux λE (as in fig. 1D) and F) friction velocity $u_*$ (as in fig. 1D).

# Validation of Mixing Heights Derived from the Operational NWP Models at the German Weather Service

B. Fay, R. Schrodin, I. Jacobsen, D. Engelbart[1]

Deutscher Wetterdienst, Offenbach, Germany
[1]Deutscher Wetterdienst, Meteorol. Observ. Lindenberg, Germany

## Introduction

NWP models incorporate an ever-increasing number of observations via four-dimensional data assimilation and are capable of providing comprehensive information about the atmosphere both in space and time. They describe not only near surface parameters but also the vertical structure of the atmosphere. They operate daily, are well verified and successfully used as meteorological pre-processors in large-scale dispersion modelling. Applications like ozone forecasts, emission or power plant control calculations require highly resolved, reliable, and routine values of the temporal evolution of the mixing height (MH) which is a criticial parameter in determining the mixing and transformation of substances and the resulting pollution levels near the ground.

The purpose of development at the German Weather Service is a straightforward mixing height scheme that uses only parameters derived from NWP model variables and thus automatically provides spatial and temporal fields of mixing heights on an operational basis.

An universal parameter to describe stability is the Richardson number Ri. Compared to the usual diagnostic or rate equations, the Ri number concept of determining mixing heights has the advantage of using not only surface layer parameters but also regarding the vertical structure of the boundary layer resolved in the NWP models.

## The Bulk Richardson Number Scheme

The current scheme is diagnostic and devised for automatic description of the temporal evolution of mixing heights (MH) from analyses and forecasts of the operational Europa-Modell (about 50 km resolution) and the Deutschland-Modell (DM, 14km resolution) of the German Weather Service. The atmosphere is divided into 20 layers (30 for DM from September) starting with 60m depth and increasing in thickness with height. Meso-$\alpha$-scale phenomena like cumulus convection cannot be dealt with explicitly but have to be parameterized, and complex BL structures cannot be modelled.

In the NWP-models, bulk Richardson numbers (Ri) are determined at each model grid point, height level, and time step as part of the calculation of exchange coefficients according to a modified turbulence closure scheme of order 2 of Mellor and Yamada (1974). It assumes equilibrium between the generation of turbulent kinetic energy due to mechanical and thermal forcing and its dissipation. The critical Richardson number is set to 0.38 following the given choice of constants and length scales in the turbulence scheme.

The Richardson number scheme (Schrodin (1995)) simply defines boundary surfaces at a height where a transition from laminar to turbulent conditions with height and v.v. is diagnosed. From the surface upwards the atmosphere is searched for Richardson numbers rising above or falling below the critical Richardson number $Ri_c$ to provide the heights of these boundary surfaces. The bulk Richardson number is used as parameter because it incorporates the dynamic and thermal characteristics of the fluid. $Ri_c$ thus delimits laminar from turbulent regions. The basic concept to be investigated is whet-

her these transition layers can be identified with a stable nighttime and a turbulent, possibly convective MH and their temporal evolution as outlined in Stull (1988) to provide a meaningful input for dispersion calculations.

From the ground upwards at each layer and above each grid point, the scheme searches for the first transition from a laminar to a turbulent layer as condition for the stable (nocturnal) MH henceforth called PBS and determines its height. Then it checks for the first transition from a turbulent to a laminar regime interpreting it as the height of the turbulent or convective boundary layer (called PBL) during the day or possibly the residual layer at night. MHs between discrete model layers are approximated with a stability-weighted interpolation scheme.

The Richardson number scheme includes some basic assumptions. Typical nocturnal stable boundary heights are found between 100 and 500m (Stull (1988)). In order to prevent the PBS from extending above, a preliminary maximum stable MH is set to model level 18 occuring at about 320m above ground. If the lowest model layer is turbulent, no stable MH exists. An exception is made during the daytime phase of dissolution of the stable boundary layer.

**Validation**

The Ri scheme is run daily on EM and DM model output with additional diagnostics. Analyses and forecasts with hourly resolution, mainly of DM, are examined using radiosoundings, weather reports, and satellite images. At the Meteorological Observatory Lindenberg of the German Weather Service, windprofiler/RASS measurements are performed and the backscatter intensity profiles are automatically converted to MHs and compared to the DM-derived MHs. The evaluation includes several clear days with the formation of a high convective daytime MH (PBL) and a stable nocturnal MH (PBS) but also cloudy days with some rain in August 1997.

Inspection of the overall hourly evolution of MHs over Central Europe determined with the Ri scheme (automatically smoothed by the graphics module) gives the following general picture for August 1997: The turbulent MH (PBL) reaches a nighttime minimum (undefined or below 500m in most areas). It starts increasing in area and value gradually from sunrise with maximum heights (up to more than 2000m) and area coverage in the afternoon and a sharp decrease by 18 UTC with a further gradual decline. PBL heights are clearly lower in regions with clouds or reduced local (maximum) temperatures. Higher mountain areas generally show a reduced average PBL ($<$ 1200m above ground) which is also low or often non-existent above the sea. During overcast days the daily cycle of the PBL is diminished. An example of the PBL for 12 Aug 1997,16 UTC (a mainly clear and anticyclonic day), is shown in Fig.1.

The stable MH (PBS) only covers some areas above the sea or few high mountains during the day while at night the large PBS areas contain mainly assumed maximum PBS heights (for planned improvements see discussion).

Looking into detail at these MHs at individual stations, the development is basically similar but less smooth. For use in sensitive dispersion models some smoothing or filtering of the MH fields or time series may be convenient.

As principal reference for validation, MHs were determined from radiosoundings by inspection of temperature and humidity profiles and of maximum temperatures.

PBL and PBS were computed with the Ri number scheme for DM grid points above Central Europe using 00 and 12 UTC analyses in order to avoid NWP forecast errors. The results are being compared to 00 and 12 UTC radiosoundings for 10 German pilot stations for mainly clear and some overcast days in August. A preliminary evaluation shows that on hot convective days the PBL tends to be underestimated but often only

within 150m. The calculated PBS heights are around the assumed maximum compared to near-surface radiosonde inversions between 100 and 400m above ground. In overcast conditions calculated PBL and PBS tend to agree with radiosoundings, a few even being too high, and underestimation is reduced. It is well known that the large turbulence of convective summer days is underestimated in diagnostic turbulence schemes.

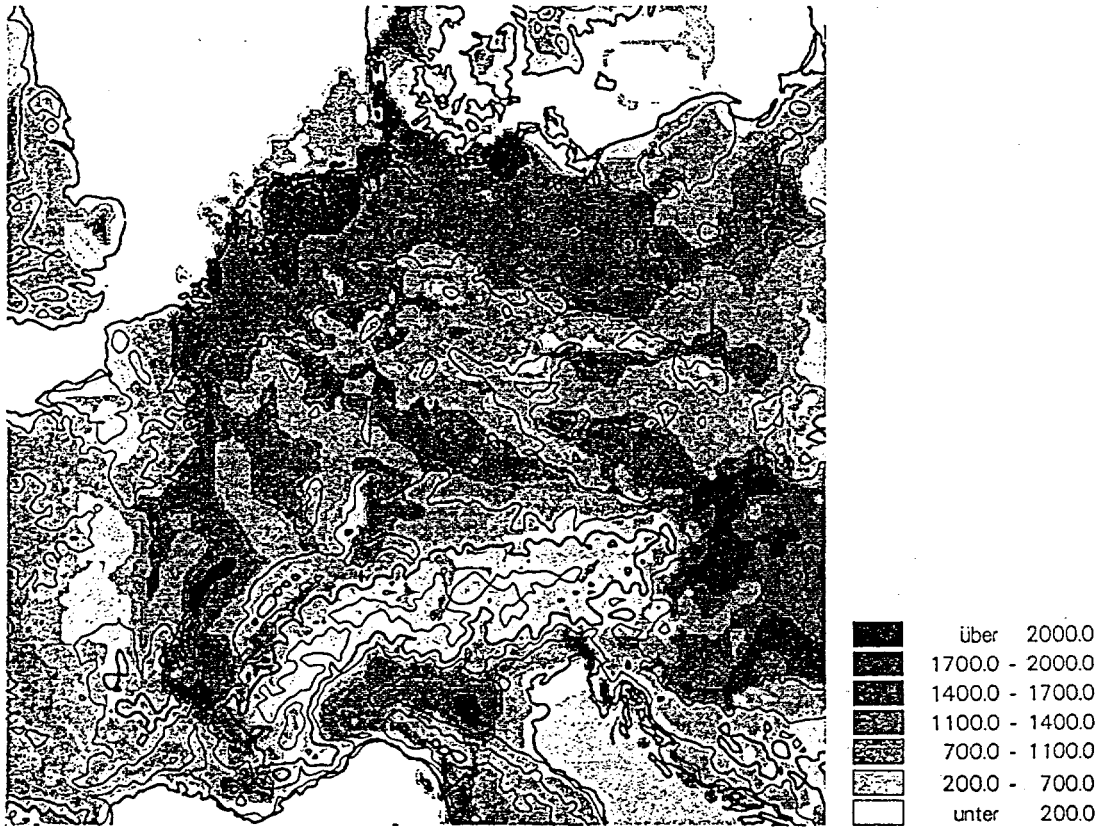


Fig. 1. Forecast PBL (in m above ground) for 12 Aug 1997, 16 UTC, based on DM forecast of 12 Aug 1997, 00 UTC.

The maximum daytime MH derived from experimental wind profiler measurements at Lindenberg (Engelbart(1997)) and the maximum Ri scheme PBL were compared amongst each other and validated against 12 and 18 UTC radiosounding on 22 mainly sunny and 6 cloudy days in August. Calculated PBLs were always equal to or smaller than the profiler ones (within 300m for half the days). This may be partly explained by the profiler evaluation looking for the maximum of the range-corrected received power with respect to height while the Ri scheme determines only the lowest transition from turbulent to laminar layer. Maximum PBLs calculated with the Richardson scheme underestimated the radiosounding heights (within 150m for half the sample). 17 profiler maxima were within $\pm$300m of the radiosoundings while on 6 days the profiler results overestimated the MH. Considering the inherent uncertainties in determining MHs from radiosoundings and profiler measurements, the variability of profiler soundings, and possible forecast errors for the afternoon PBL maxima these results are quite encouraging.

Some sensitivity studies concerning factors influencing MHs were also performed. The DM turbulence parameterisation had been modified some time ago to enhance the turbulent exchange. The improved scheme increased exchange coefficients in cloudy layers of the atmosphere. This resulted in smaller Richardson numbers, a faster morning rise of the PBL, and partially increased afternoon maxima in cloudy regions. The results of the Ri number scheme may be improved also by the introduction of a prognostic turbulence equation currently under development.

A considerable influence on maximum values and area coverage of MHs is exerted from the value of $Ri_c$ used. Increasing $Ri_c$ from 0.38 to 1, 2, 5, and even 10 can largely increase PBL values, and in the evenings these tend to decrease later and to a lesser extent with increasing $Ri_c$. An increased $Ri_c$ might make sense because of the non-local turbulence formulation in NWP models and the complete disappearence of turbulence only at high Ri around 10 (Stull (1988)). In order to stay consistent with the NWP model and its parameters used in dispersion calculations a modification of the NWP model turbulence parameterisation would be required. This might be an example of the results of dispersion-related investigations based on NWP output giving an impulse to the improvement of the actual NWP models themselves.

## Discussion

The preliminary evaluation of MHs calculated with the bulk Richardson number scheme and NWP model input shows an overall realistic temporal and spatial evolution of MHs.

Comparisons with radiosoundings give a trend towards underestimation of turbulent MHs which is generally not serious. The scheme may also underestimate the PBL in situations where there are turbulent layers interspersed with the odd laminar layer. This behaviour can be improved by continuing the calculation beyond 1 or 2 laminar layers if they are topped by turbulent layers. Also the introduction of a prognostic turbulence scheme and a new soil model may improve the PBL calculation by the Ri number scheme.

The determination of the nocturnal MHs poses some problems. RASS measurements will be evaluated to provide improved reference MHs. The present scheme will be tested without a minimum upper level to check whether realistic MHs can be determined especially for cloudy nights. Some earlier evaluations suggest that a vertical maximum of stable Ri numbers may be identified with a stable MH. So far, the assumed upper limit for the PBS seems acceptable for the nocturnal PBS especially on clear nights.

The determination of MHs from vertical profiles of DM horizontal wind speeds, exchange coefficients, humidity, temperature, and virtual potential temperature profiles generally results in MHs comparable to those derived from the Ri number scheme. This is to be expected for reasons of NWP model consistency. Only for some special thermodynamic conditions might a check of these criteria improve the MH calculation.

In future, mechanical and convective MH equations as outlined in Beyrich et al. (1997) will be calculated from the NWP model output and compared to those of the Ri number scheme.

At the moment, MHs calculated with the Ri number scheme are successfully used in the 2-layer trajectory-box model for ozone prediction under development at the DWD.

## References


Beyrich F.,Gryning S.E.,Joffre S.,Rasmussen A.,Seibert P.,Tercier P., 1997: Mixing height determination for dispersion modelling - a test of meteorological pre-processors. Proceedings of 22nd NATO/CCMS,II,367-374.

Engelbart D., 1997: Determination of mixed-layer depth using a 1290MHz windprofiler/RASS. COST76 Profiler workshop, May 1997, Engelberg,Switzerland, ext.abstracts, ed. H.Richner,286-289.

Mellor G.L. and Yamada T., 1974: A hierarchy of turbulence closure models for planetary boundary layers. J.Atm.Sci.31,1791-1806.

Schrodin R., 1995: Bestimmung der Grenzschichthöhe in einem Gitterpunktmodell. Internal work paper.

Stull R.B., 1988: An introduction to boundary layer meteorology. Kluwer Academic Publishers.

# Session IV - Climatology and Global Aspects
# Chairperson: Werner Klug

# A Global Boundary-Layer Height Climatology

Han van Dop, Maarten Krol and Bert Holtslag

Institute for Marine and Atmospheric Research Utrecht (IMAU)
P.O. box 80.005, 3508 TA Utrecht, The Netherlands

## Introduction

Various definitions can be given of the Atmospheric Boundary Layer (ABL). For our purposes we shall define it as the layer which is to some degree turbulent due to processes which are directly related to the presence of the earth' surface: shear and buoyancy generated turbulence. In this layer vertical fluxes are dominated by turbulence, and therefore, the height of the ABL determines to a large extent the vertical spread of substances released. The height of the ABL (*h*) is directly (inversely) proportional to the mean ABL concentrations of all emissions at or near the surface, and in modelling global transport and chemistry the ABL height is thus an essential parameter, also because many parameterizations of vertical transport use the ABL height as a scaling parameter.

The ABL is highly variable in space and time. Over land during daytime the boundary layer is strongly convective, turbulence well-developed and associated mixing strong, leading to small variations with height in the bulk of the layer of e.g.,. wind velocity, (potential) temperature, humidity and mixing ratios of trace substances. In the course of the day the boundary-layer entrains air aloft and may grow substantially. During nighttime the boundary layer is stably stratified, turbulence suppressed and mixing considerably slower. Also its time evolution is moderate. Over sea convective activity is generally small and turbulence is predominantly generated by shear. Also diurnal variations are small. Superimposed on the diurnal variation is the seasonal variation which is strong at high latitudes and moderate in tropical regions.

In principle the ABL height can be retrieved from atmospheric global circulation models since they contain algorithms which determine the intensity of the turbulence as a function of height (e.g. Holtslag and Boville, 1993). However, these data are not routinely available, or on a (vertical) resolution which is too crude in view of the application. This justifies the development of a separate algorithm in order to define the ABL. The algorithm should include the generation of turbulence by both shear and buoyancy and should be based on readily available atmospheric parameters. There is obviously a wide application for boundary heights in off-line global and regional chemistry and transport modelling. It is also a much used parameter in air pollution meteorology.

In this article we shall present a theory which is based on current insights in ABL dynamics. The theory is applicable over land and sea surfaces in all seasons. The theory is (for various reasons) not valid in mountainous areas. In areas where boundary-layer clouds or deep cumulus convection are present the theory does not apply. However, the same global atmospheric circulation models contain parameterizations for shallow and deep convection from which separate estimates can be obtained for the extent of vertical mixing.

## Theory

The equations which describe the dynamical behaviour of the daytime convective boundary layer are well known (Tennekes, 1973; Driedonks, 1982). In this formulation the fluxes $\overline{w\theta}_0$ and $\overline{w\theta}_i$, the surface and downward entrained heatflux at the inversion respectively, as well as $\gamma$, the lapse rate of the stably stratified layer aloft play an important role. The entrainment flux is modelled as

$$\overline{w\theta}_i = c_1 \overline{w\theta}_0 + c_2 \frac{u_*^3}{\beta h} \tag{1}$$

and thus both includes entrainment by buoyancy and shear. The proportionality constants are 0.2 and 5 respectively, $u_*$ is the friction velocity and $\beta = g/T$ the buoyancy parameter. Using this we are able to obtain simple numerical solutions for the development of $h$.
For the parameterisation discussed below, however, we shall use an analytical solutions, along the formulation given by Thomson (1991) treating the heat flux and friction velocity as constant. For pure convection ($u_*$=0) the solution is

$$\left(\frac{h}{h_0}\right)^2 - \left(\frac{h}{h_0}\right)^{-\frac{1}{c_1}} = \frac{2(1+2c_1)}{\gamma h_0^2} \overline{w\theta}_0 \, t. \tag{2}$$

Here $h_0$ is the initial ($t$=0) ABL height, here taken to be equal to 100 m. Note that the second term at the left becomes soon very small and can be neglected in most practical cases. In pure shear turbulence ($\overline{w\theta}_0$=0) we obtain

$$\left(\frac{h}{h_0}\right)^3 = 1 + \frac{6c_2 u_*^3 t}{\beta \gamma h_0^3}, \tag{3}$$

which indicates a slower growth rate ($\sim t^{1/3}$) than in the convective case.

When both mechanical and buoyant turbulence contribute to the ABL growth we can only obtain an analytical solution for the inverse relationship $t(h)$. This solution was applied to evaluate afternoon mixed-layer heights for the parameters given in table 1 and for a number of current values of $u_*$ and $\overline{w\theta}_0$. The results are summarized in Fig. 1.

*Table I. parameters used for the evaluation of the afternoon ABL-height.*

| $c_1$ | $c_2$ | $c_3$ | $t(h)$ | $\beta\left(ms^{-2}K^{-1}\right)$ | $\gamma\left(K\,m^{-1}\right)$ | $N\left(s^{-1}\right)$ |
|---|---|---|---|---|---|---|
| 0.2 | 5 | 10.7 | 10 | 0.03 | $5.10^{-3}$ | 0.012 |

The formula given above can be suitably approximated. Introducing the convective velocity scale, $w_* = \left(\beta \overline{w\theta}_0 h\right)^{1/3}$, and $N = \left(\beta\gamma\right)^{1/2}$, the Brunt-Vaïsala frequency, we may reformulate the limiting expressions (Eqs. 2,3) for $h/h_0 >> 1$ as

$$h_{conv} = \left(2(1+2c_1)t\right)^{1/3}\left(\frac{w_*}{N^{2/3}}\right) \text{ and } h_{shear} = \left(6c_2 t\right)^{1/3}\left(\frac{u_*}{N^{2/3}}\right) \tag{4}$$

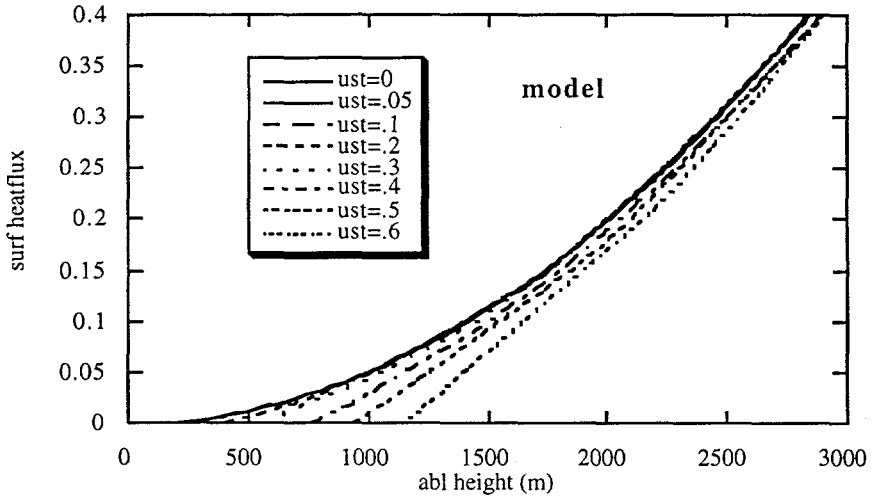


*Fig. 1. Height of theafternoon ABL as a function of the surface heat flux, for a range of values of the friction velocity.*

A cubic interpolation of these expressions according to $h = \left(h_{conv}^3 + h_{shear}^3\right)^{1/3}$ yields for the general case

$$h = \left(\frac{2(1+2c_1)t}{N^2}\right)^{1/3}\left[w_*^3 + c_3 u_*^3\right]^{1/3} \tag{5}$$

where $c_3=3c_2/(1+2c_1)$. The agreement with the exact expression is fair for values of $h/h_0 > 5$.

In the stably stratified boundary layer we adopt Mahrt's suggestion (1981) that the equilibrium height of the nocturnal boundary layer can be estimated by the assumption that the bulk Richardson number reaches a critical value in the SBL. Thus, denoting the critical height with $h$, we have

$$Ri_{bulk} \equiv \frac{\beta\left(\partial\theta/\partial z\right)}{\left(\partial U/\partial z\right)^2} \approx \left(\frac{hN}{G}\right)^2.$$

We have assumed that the wind velocity at the top of the SBL is approximately geostrophic ($G$). When the Richardson number reaches its critical value we get

$$h = \left(c_d Ri_{cr}\right)^{-1/2}\frac{u_*}{N}, \tag{6}$$

The drag coefficient in Eq.(6) is given by $c_d = \left(u_*/G\right)^2$ so that assuming that $Ri_{cr}$=0.2 and $c_d$=1.5 $10^{-3}$ (Stull, 1994) we obtain for the numerical coefficient ~ 18. This estimate is remarkably close to the value given in Zilitinkevich and Mironov (1996) which quote a value of 20, with the caveat that a more rigorous evaluation would be required. Also Vogelezang and Holtslag (1997) and Van Pul et al. (1994) arrive at a similar expression but with a coefficient of the order of 10. Zilitinkevich and Mironov (1996) also list other formulations for the stable boundary layer depth which contain the Coriolis parameter *f*. Since this parameter usually occurs in the denominator these formulations become useless in tropical regions, where $f \rightarrow 0$. Their multi-limit formulation may be an interesting generalisation of Eq. 6, however.

## Results

Based on Eqs. 4 and 6 we are able to determine global ABL heights and its seasonal variation. The only parameters which are required are the friction velocity, the surface heatflux and the free tropospheric potential temperature lapse rate. These data are readily available from global atmospheric circulation models.

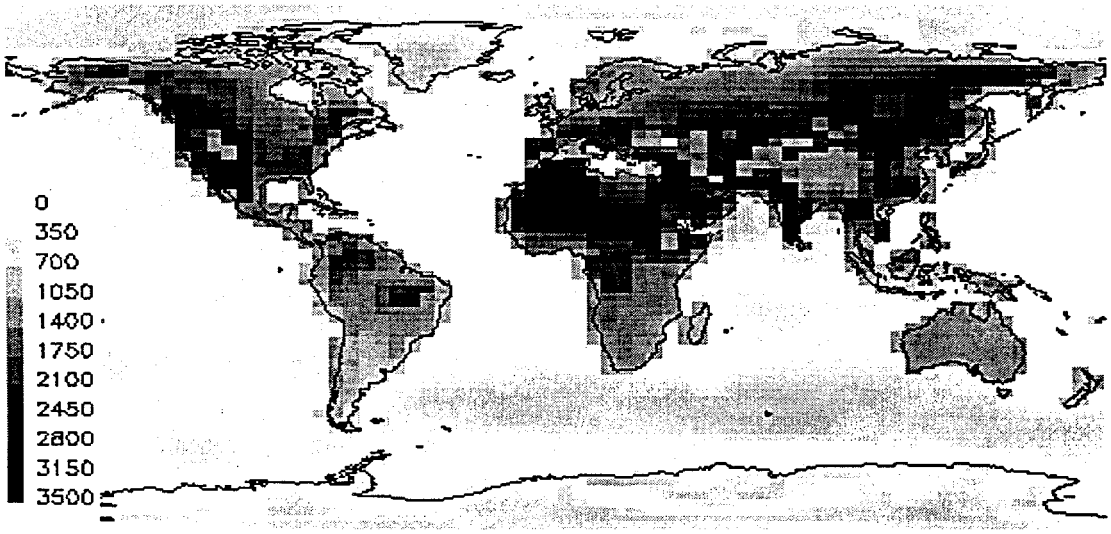


*Figure 2. Global daily afternoon ABL heights for july*

## References

Driedonks, A.G.M.: 1982, Models and observations of the growth of the atmopsheric boundary layer, *Boundary-Layer Meteorol.*, **23**, 283-306.

Mahrt, L.: 1981, Modelling the depth of the stable boundary layer, *Boundary-Layer Meteorol.*, **21**, 3-19.

Stull, R.B.: 1994, An introduction to boundary layer meteorology, Kluwer (Dordrecht).

Tennekes, H.: 1973, A model for the dynamics of the inversion above a convective boundary layer. *J. Atm. Sci.*, **30**, 558-567.

Thomson, D.J.: 1991, An analytical solution of Tennekes' equations for the growth of boundary-layer depth, *Boundary-Layer Meteorol.*, **59**, 227-229.

Van Pul, W.A.J., A.A.M. Holtslag and D.P.J. Swart: 1994, A comparison of ABL heights inferred routinely from Lidar and Radiosondes at noontime, *Bound.-Layer Meteorol,* **68**, 173-191.

Vogelezang, D.H.P. and A.A.M. Holtslag: 1997, Evaluation and model impacts of alternative boundary-layer height formulations., **81**, 245-269.

Zilitinkevich, S. and D.V. Mironov: 1996, A multi-limit formulation for the equilibrium depth of a stably stratified boundary layer, *Boundary-Layer Meteorol.*, **81**, 325-351.

# Climatology and evolution of the mixing height over water

Anna M. Sempreviva[1] and S-E Gryning[2]

[1]Istituto di Fisica dell'Atmosfera, CNR, Rome, Italy
[2]Risø National Laboratory, Roskilde, Denmark

## Introduction

In this paper we present results from an experimental investigation on the height of the mixed layer h, using a meteorological station located on the Danish island of Anholt. The station was operational for two years from September 1990 to October 1992. We present the analysis of two years of radiosounding showing the average daily evolution of h. Furthermore observations of the mixed layer growth under near-neutral and unstable atmospheric conditions during six consecutive days has been modelled using a simple zero-order mixed-layer height model. Finally we have compared the evolution of the mixing height from the model with the evolution of the correlation coefficient between temperature and humidity to study the influence of the deepness of the convective layer on the mechanism of the correlation between temperature and humidity in the surface layer.

## Experimental set-up

A 22 m high mast, placed near the shoreline, on the western part of the island, was equipped with a standard meteorological instrumentation to measure pressure, solar radiation and profiles of wind-speed and temperature. Measurements of the turbulent fluctuations of wind speed components, temperature and humidity were carried out with a three-dimensional sonic anemometer (Kaijo-Denki DAT/TR-61B) and a fast response humidiometer (OPHIR) respectively, mounted at the height of 22 m. The parameters derived from this analysis were averaged over 10-min periods. Here we analyse only data collected under offshore westerly wind cases (240°-360°) representing over water conditions. At westerly winds radiosondes (type RS-80 by Vaisala) were released three times a day all year long, and more frequently during intensive campaigns for a total of 400 profiles of wind direction and speed, temperature, humidity and pressure. The measurements were performed with a frequency of 0.1 Hz until March 1992, and then the frequency was changed to 0.5 Hz. With a radiosonde ascent velocity of 2.5 $ms^{-1}$ the latter frequency corresponds to a vertical resolution of 5m. The mixed layer height has been identified using the temperature and humidity profiles by visual inspection.

## Climatology of the mixing height

Statistics of stability over water indicates that the conditions are predominantly unstable. The seasonal and yearly average daily evolution of the inversion height is shown in figure 1a,b, c, d, e. Over the sea h does not show the same pronounced daily cycle observed over land. Over the sea the warming of the water surface due to solar radiation is small due to the high heat capacity of the water and is further reduced by surface mixing. In our case, the shallow water close to the island could plays a certain role in the slight climatological daily variation of h. From the yearly statistic we estimate the mean yearly height of the mixed layer over the sea to be approximately 800 m whereas a typical mixed layer height over land in Denmark is of 1000 m, Larsen and Jensen (1983). A seasonal cycle of h can be observed comparing figure 1 a and 1b where h results lower during the winter than during the summer.

## Case study of mixing height evolution over the sea

Intensive measurements of the mixed layer height over the sea were carried out during a two-week experimental campaign in June 1992. Figure 2 shows the evolution of the mixing height and other meteorological parameters during six consecutive days. From satellite data it can be seen that the horizontal variation of the sea surface temperature is of 1.6 °C up to 50 km

around the island. The mixed layer height is found to be constant around 400-500 m between June 13 and June 14 then growing slowly until 700 m during June 15. The meteorology is characterised by constant heat flux and sea air temperature difference $\Delta T = T_{sea} - T_{air}$ (figure 2b and 2c) and an almost stationary high pressure on the area. During the night between June 15 and June 16, the mixing height growth responding to the increase of $\Delta T$ following the passage of a cold front from north-west. h continues to grow until the early afternoon of June 16 when a lower inversion starts to develop near the surface while the higher inversion sinks slowly likely due to subsidence. A similar case is found between June 17 and June18, the mixed layer starts to grow just before midnight during the passage of a second front.

**The model**

A zero-order slab model (Batcharova and Gryning, 1991) based on the turbulent kinetic energy budget inside the mixed layer has been used to model the observed evolution of the mixed layer. The model is based the assumption that the consumption of kinetic energy plus potential energy at the top of the mixed layer is related to the production of convective and mechanical turbulent kinetic energy within the mixed layer. It predicts the mixing height using the following equation

$$\left[\left(\frac{h^2}{(1+2A)h-2BkL}\right)+\frac{Cu_*^2T}{\gamma g[(1+A)h-BkL]}\right]*w_e=\frac{(\overline{w'\theta'})_s}{\gamma}$$

where $(\overline{w'\theta'})_s$ is the surface kinematic heat flux, $u_*$ is the friction velocity, g/T is the buoyancy parameter, $\gamma$ is the potential temperature gradient above the mixed layer, L is the Monin-Obukhov length and k is the Von-Karman constant. The details and a discussion on the value of the constants A, B and C can be found in the original paper. The growth rate of the mixed layer, dh/dt, is estimated by

$$dh/dt = w_e + w_s$$

where $w_e$ is the rate at which the mixed layer entrains into the free atmosphere and $w_s$ is the mean vertical motion of the air at the top of the mixed layer, (the so-called subsidence velocity is opposite sign of $w_s$). Input data are derived from the turbulence at the meteorological tower. The potential temperature gradient in the free atmosphere was determined using the profile used to initialise the model. The model was initialised with the mixed layer height that was measured before the arrival of a new air mass. Evidence of subsidence can be observed in the decreasing rate of the inversion height on June 17. As mentioned above during this day a ground based inversion has developed and remains stationary at around 400 m while the upper inversion is sinking. The estimated subsidence velocity of the upper inversion used in this model is around 1.2 $cm^{-1}$ which is a typical value for a high pressure system. In figure 2a the evolution of the modelled mixed layer is compared with the experimental data from radiosoundings.

**Correlation coefficient between Temperature an moisture**

The correlation coefficient between temperature and moisture defined as $R_{qT} = \frac{\overline{q'T'}}{\sigma(q)\sigma(T)}$ gives information about similarity amongst scalars. In the surface layer where scalar are transported by local turbulence $R_{qT} = 1$. During the AMTEX experiment the correlation coefficient between temperature and humidity $R_{qT}$ has been found to decrease with increasing height z and to change sign at around z/h=0.5 because of the entrainment process at the top of the boundary layer. In Sempreviva and Gryning (1996) analysis of the Anholt turbulence data set showed that at the same height and location, $R_{qT}$ assumes values less than 1 also in unstable atmospheric stratification. During the winter campaign for instance although in unstable conditions $R_{qT}$ was found to be less around 0.6. Various authors e.g. Mahrt, (1991), De Bruin et. al. (1993) have suggested that the observed scalar fluctuations near the ground have

two components, one generated by local turbulence and the other one generated by non-local processes as for instance influence of drier and warmer air aloft by entrainment process. We use the simulated data from the model to investigate on this subject. figure 3 show the evolution of h and $R_{qT}$ during the six days and we note that during period with low h $R_{qT}$ is scattered, when h starts to growth $R_{qT}$ is also growing. This result shows a dependence of $R_{qT}$ on the deepness of the mixed layer. We have parametrised the correlation coefficient using both surface and upper layer parameters by $R_{qT} = 1\text{-}z/L + L/h$ the comparison between experimental and parameterised $R_{qT}$ is showed in figure 4. During the period June 13- June 15 the parameterisation overestimate the $R_{qT}$ values. During the period June 15- June 18 the parameterised $R_{qT}$ still overestimates the experimental value but it describes satisfactory the experimental evolution.


## Acknowledgements

The radiosonde station belonged to the Danish Meteorological Institute and we express our thanks to Ole Berknov who was responsible for the operations of the station. The study was supported by the National Agency of Environmental Protection in Denmark as part of the Marine Research Programme-90.


## References


Batchvarova, E. and S.E.Gryning.: 1991, 'Applied model for the growth of the daytime mixed layer', *Boundary-Layer Meteorol.*, **56**, 261-274.

De Bruin, H.A.R., Kohsiek, W. and Van Der Hurk, J.J.M.: 1993, 'A verification of some methods to determine the fluxes of momentum, sensible heat and water vapour using standard deviation and structure parameter of a scalar meteorological quantities'. Boundary-Layer Meteorol., **63**, 231-257.

Jensen N.O. and S.E.Larsen: 1983, 'Summary and interpretation of some danish climate statistics'. Risoe-R-399. 76 pp.

Mahrt, L.: 1991, Boundary-Layer Moisture regimes. Q.J.R.Meteorol. Soc., **117**, 151 - 176.

Sempreviva, Anna M. and Gryning S.E.: 1996, 'Humidity fluctuations in the marine boundary layer measured at coastal site with an infrared humidity sensor'. Boundary-Layer Meteor., **77**, 331-352.


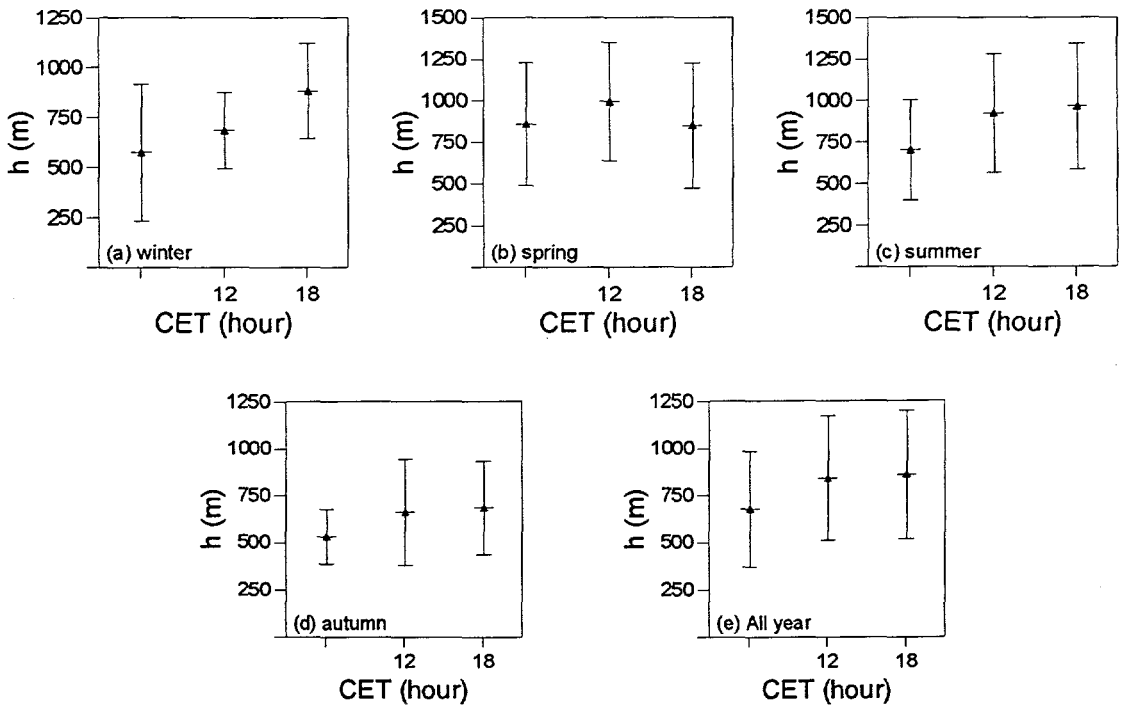


Figure 1. Seasonal and yearly average daily evolution of the mixing height. The standard deviation has been scaled by a factor 0.5.

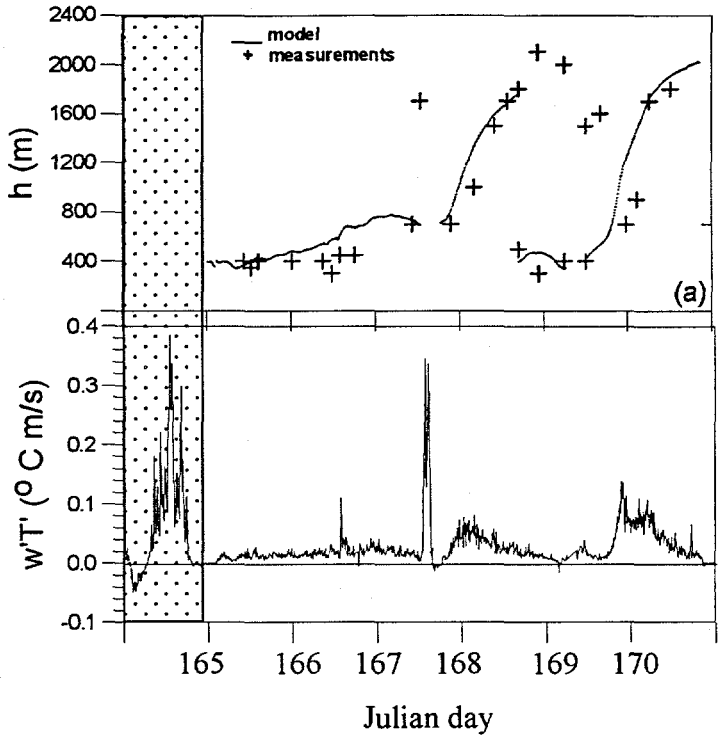


Figure 2. (a) Comparison between the experimental and modelled time evolution of the height of the mixed layer. (b) Time evolution of the surface heat flux. During the first day (rectangle with filling) the flow was onshore, this explain the evident daily cycle of the heat flux and the missing of radiosounding data.

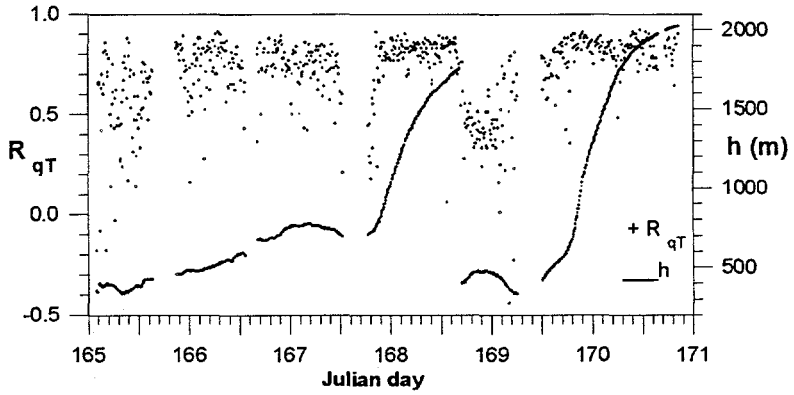


Figure 3. Time evolution of $R_{qt}$ and of h during six days.

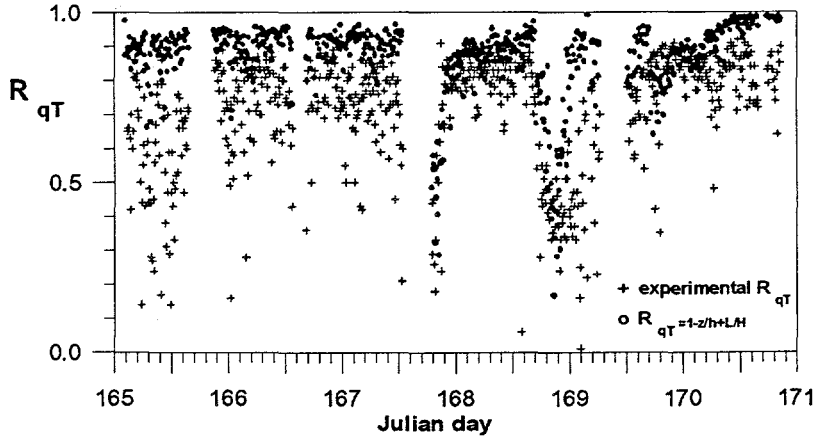


Figure 4. Comparison between modelled and experimental $R_{qt}$.

# Session V - Mixing Height Determination from Remote Sensing Systems
# Chairperson: Werner Klug

# Mixing Height Determination Using Remote Sensing Systems - General Remarks

Frank Beyrich

BTU Cottbus, LS Umweltmeteorologie, PF 10 13 44, D - 03013 Cottbus, Germany

## Introduction

The Mixing Height (MH) is one of the most important parameters governing the dispersion of atmospheric pollutants, and measured concentrations of trace gases and aerosols strongly depend on it. Therefore, MH data are necessary for both operational air quality monitoring and as a direct input to numerical transport and dispersion models. Usually, MH values are derived from profiles of atmospheric parameters which should satisfy the following conditions:

- The profiles should cover a range between the earth's surface and about 2-4 km a.g.l. considering the typical MH variability during its annual and diurnal cycles.
- The profile data should have a vertical resolution of about 10-30 m to avoid relative uncertainties of more than 10-20 % especially for low MH-values (less than 200 m).
- The data should be available with a time resolution of one hour or less in order to properly describe the non-stationary MH-evolution, especially during the morning and evening transition periods.
- The available output parameters should preferably characterize the intensity of turbulence or the result of mixing processes.

Over the last decade, remote sensing systems (sodar, wind profiling radar, lidar) became introduced more and more into operational application. The basic advantages of these systems are the possibility of continuous operation and the fact that they do not cause any distortion to the flow being investigated. On the other side, they do not directly measure standard atmospheric parameters (pressure, temperture, humidity, wind), and the data interpretation is therefore not always straightforward.

## Characterization of the Remote Sensing Systems

In general, the measuring principle of remote sensing systems is based on the scattering of waves in the atmosphere at small-scale inhomogeneities of the acoustic and electromagnetic refractive index fields (described through the refractive index structure parameter, $C_N^2$) or from aerosols (lidar). Backscattered signal intensity (S-) profiles thus provide information on the vertical structure of the lower atmosphere basically with respect to temperature (sodar), humidity (wind profiler) and aerosol content (lidar).

Those inhomogeneities which significantly contribute to the backscatter of sodar and wind profiler signals are normally well within the inertial subrange of the turbulence spectrum. Therefore, S gives some information about the turbulent structure of the ABL. However, S is not an easy-to-interprete parameter, but it reflects in a complex way the contributions of local fluxes and of gradients in the mean profiles. Especially in the SBL, these may be due to different processes and phenomena, and the dominance or negligibility of the one or other may cause similar S-profiles under completely different conditions or completely different profiles in apparently comparable situations.

In addition to S, sodars and wind profilers provide information on the profiles of the horizontal wind vector (V, $\alpha$), vertical velocity (w) and its variance ($\sigma_w^2$), and also temperature if a RASS component is part of the system. $\sigma_w^2$ represents the vertical component of the turbulent kinetic energy. It could be therefore employed for MH estimation either directly or making use of well-established similarity relationships. However, quantitative assessment of both w- and $\sigma_w^2$-data is not without problems since the measurement accuracy achieved up to now is in the range of the typical values of these parameters except for the case of strong convection. The wind profile is also determined from external parameters and seems not to be suitable as the sole indicator for MH-estimation. It may be, however, used as an additional criterion.

Lidar signals directly originate from aerosol backscatter ("pollution"), and the lidar therefore might be considered to provide direct measurements of the MH. But even the interpretation of data from simple aerosol lidars is often not straightforward, since it is difficult to decide whether detected aerosol structures are the result of ongoing mixing or whether they originate from advective transport or past accumulation processes. Under stable conditions, problems in MH estimation from lidar data come from the fact that the vertical gradients in aerosol content are much smaller than those at the top of a convective mixed layer. Moreover, in the evening it usually takes some time until a sufficiently clear discontinuity in the S-profile develops at the SBL-top within a previously mixed layer.

Table I attempts to summarize the advantages and shortcomings of the different remote sensing systems with respect to MH determination.

Table I - Advantages and shortcomings of remote sensing methods for MH-determination

| Method | Advantages | Shortcomings |
|---|---|---|
| ABL Wind-profiler / RASS | • continuous operation<br>• high sampling rate<br>• provides structure information and profiles of basic physical parameters (temperature, wind) | • lowest range gate ≥ 100 m<br>• limited vertical resolution (50-250 m)<br>• relatively expensive<br>• frequency allocation problems in Europe<br>• interpretation not in any case straight-forward (clouds !) |
| (Aerosol-) Lidar | • ground based and aircraft based operation possible<br>• different scan modes for 3D-studies (optional)<br>• high sampling rate<br>• return signals directly originate from aerosols ("pollution") | • expensive<br>• unmanned operation for safety reasons often not possible<br>• tracer necessary (gas, aerosol)<br>• interpretation sometimes ambiguous<br>• strong signal attenuation in clouds / fog layers |
| Sodar | • relatively simple, not very expensive<br>• continuous, unattended long-term operation<br>• high temporal and vertical resolution | • limited sounding range (500-1000 m)<br>• sensitivity to environmental noise<br>• noise contamination to the environment<br>• in (classical) monostatic mode only sensitive to temperature inhomogeneities<br>• interpretation requires experience, sometimes ambiguous |

**Criteria for MH estimation from remote sensing data**

The MH depends on the intensity of buoyant and/or mechanical turbulence production as well as on the background stratification (in particular the existence of stable / inversion layers representing a barrier to the vertical exchange of constituents). Information on both the intensity of turbulence and the presence of stable layers can be derived from the backscatter intensity (S-) profile measurements of sodars and wind profilers.

Experimental as well as numerical modelling studies on the vertical profile of $C_N^2$ (e.g. Wyngaard and LeMone, 1980, Burk, 1980) have shown a pronounced maximum at the top of a well-mixed CBL or slightly above. Therefore, a clearly-defined criterion can be formulated to derive the MH from the S-profiles. The problem is much more complex for the SBL where the profiles of mean and turbulent ABL-parameters may exhibit quite a different shape dependent on the relative importance of radiative cooling, wind shear and other effects such as non-stationarity, baroclinity, advection, breaking gravity waves, and terrain influences. Hence there is no universal shape of the $C_N^2$-profile to be expected under stable conditions (see also Wyngaard and Kosovic, 1994). This is confirmed by a small number of experimental and modelling studies (e.g. Burk, 1980, Cuijpers and Kohsiek, 1989). Interpretation of S-profiles therefore has to consider the actual shape of these profiles and the governing processes. The same holds true for aerosol and trace gas concentration profiles measured by lidar which might be even more difficult to interprete due to the possible relevance of microphysical effects, chemical reactions and others.

A summary of the criteria proposed to derive the MH from remote sensing data is given in Table II (where the letters in brackets indicate the type of system for which the criteria have been suggested - acoustic sounder = A, wind profiler = W, lidar = L).

| Table II - Criteria for the MH - determination from remote sensing data suggested in the literature | |
|---|---|
| Stable Boundary Layer (SBL) | Convective Boundary Layer (CBL) |
| • decrease of S below a certain (absolute / relative) threshold value ⟨**A, W**⟩<br>• elevated (secondary) maximum of S ⟨**A**⟩<br>• (lowest) relative / absolute maximum of $-\partial S/\partial z$, computed from either forward, centered, or backward differences ⟨**A, W, L**⟩<br>• maximum curvature in the zone of strong $-\partial S/\partial z$ ⟨**A, L**⟩<br>• S-minimum above a zone of sharp decrease ⟨**A**⟩<br>• maximum of $\partial V/\partial z$ ⟨**A, W**⟩<br>• axis of a low-level jet (maximum of V) ⟨**A, W**⟩ | • secondary maximum of S ⟨**A, W, L**⟩<br>• maximum of $\pm\,\partial S/\partial z$ ⟨**A, W, L**⟩<br>• strong decrease of $\sigma_w^2$ ⟨**A, W**⟩<br>• similarity methods using measurements of $C_T^2$, $\sigma_w^2$, $\lambda_{max}$ in the mixing layer ⟨**A**⟩<br>• extrapolation of plume parameters (S, w) ⟨**A**⟩ |

Certain attempts have been made to automatically analyze the ABL structure and to determine the MH from remote sensing data for operational application (e.g. Endlich et al., 1979, Holets and Swanson, 1984, Beljaars and Agterberg, 1988, Angevine et al., 1994, Mann et al. 1995). This is a non-trivial problem of automatic pattern recognition which has not been finally solved up to now. Difficulties mainly arise from
- the diversity of observed structure patterns which are not easy to classify,
- the fact that completely different meteorological situations may result in similar instantaneous pictures of the ABL-structure (the S-profile),
- the non-stationarity of the ABL-structure which makes it difficult to derive conclusions from averaged profiles (the standard output of most commercially available remote sensing instruments), and
- the non-ideal shape of most measured profiles making it necessary to objectively differentiate between primary and secondary profile features.

**Intercomparison of MH values derived from remote sensing data**

Comprehensive experiments to compare MH-values derived from different measurement systems (radiosonde, sodar, radar, lidar, aircraft) mainly under convective conditions have been described e.g. by Russell et al. (1974), Noonkester (1976), Coulter (1979), Kaimal et al. (1982), Baxter (1991), and Marsik et al. (1995). These studies show that relative differences of the order of 10 % or less can be noticed provided that the capping inversion is not too weak and has a well-defined base. On the other side, for a weak capping stable layer or a CBL not perfectly mixed, measurements from different systems and even the analysis of the same temperature profile by several experienced meteorologists may easily result in relative differences of 25 % or even larger (Hanna et al., 1985).

Conclusions on possible systematic deviations between different estimates of the MH are not consistent. Often this can be attributed to different criteria applied to analyze the profiles (e.g. height of $S_{max}$ or $(\partial S/\partial z)_{max}$ or the use of different threshold values for the temperature gradient to identify stable layers in the radiosonde profiles) as well as to the often limited number of observations and in some cases also to a spatial separation of the sites where the different systems had been operated.

MH-values derived from lidar measurements have been found to be generally slightly but systematically higher than values derived from temperature profiles or sodar measurements (e.g. Russell et al., 1974, Coulter, 1979, Hanna et al., 1985, Dupont, 1991). This is explained basically by the fact that the most energetic convective plumes penetrate into the stable or inversion layer thereby transporting aerosols up to levels higher than the mean height of the stable layer base.

Comparison of sodar measurements with independent MH-values under stable conditions is much more difficult to assess due to the general difficulty of performing turbulence profile measurements in the SBL and the resulting lack of comprehensive datasets. In many studies, the sodar information has been compared with the nocturnal surface inversion height or other temperature and wind profile based height scales which can not a-priori be considered as appropriate measures for the MH. Consequently, the results of such studies are quite inconsistent. Comparing MH-values derived from simultaneous sodar and lidar operation for a very small number of case studies in a simply structured SBL, Dupont (1991) and Devara et al. (1995) found a good qualitative agreement.

## Summary and Conclusions

1. Remote sensing systems can be considered today as a real alternative to classical soundings with respect to the MH determination. They have the basic advantage to allow continuous monitoring of the ABL. Some technical issues which limit their operational use at present should be solved in the near future (frequency allocation, eye safety, costs).

2. Taking into account specific operating conditions and the formulated-above requirements of a sounding system to be used for MH determination it becomes obvious that none of the available systems meets all of them, i.e., **the "Mixing height-meter" does not exist**. Therefore, reliable MH determination under a wide variety of conditions can be achieved only by integrating different instruments into a complex sounding system.

3. The S-profiles provide a suitable data base for MH estimation from all types of remote sensing instruments. The criteria to deduce MH-values from these profiles should consider the structure type and the evolution stage of the ABL as well as the shape of the profiles. A certain kind of harmonization concerning these criteria should be achieved.

4. MH values derived automatically from remote sensing data appear to be not yet reliable enough for direct operational use, they should be in any case critically examined by a trained analyst. Contemporary mathematical methods (wavelet transforms, fuzzy logics) are supposed to allow considerable progress in this field in the near future.

### References


Angevine W.M., White A.B. and Avery S.K. (1994) Boundary layer depth and entrainment zone characterization with a boundary layer profiler. *Boundary-Layer Meteorol.* **68**, 375-385

Baxter R.A. (1991) Determination of mixing heights from data collected during the 1985 SCCCAMP field program. *J. Appl. Meteorol.* **30**, 598-606

Beljaars A.C.M. and Agterberg R. (1988) Automatische detektie van inversies met sodar. *De Bilt - KNMI Techn. Rep. TR-106*, 17 pp.

Burk S.D. (1980) Refractive index structure parameters: Time-dependent calculations using a numerical boundary layer model. *J. Appl. Meteorol.* **19**, 562-576

Coulter R.L. (1979) A comparison of three methods for measuring mixing layer height. *J. Appl. Meteorol.* **18**, 1495-1499

Cuijpers J.W.M. and Kohsiek W. (1989) Vertical profiles of the structure parameter of temperature in the stable, nocturnal boundary layer. *Boundary Layer Meteorol.* **47**, 111-129

Devara P.C.S., Raj P.E., Murthy B.S., Pandithurai G., Sharma S. and Vernekar K.G. (1995) Intercomparison of nocturnal lower-atmospheric structure observed with lidar and sodar techniques at Pune, India. *J. Appl. Meteorol.* **34**, 1375-1383

Dupont E. (1991) Étude methodologique et experimentale de la couche limite atmospherique par teledetection laser. *Ph.D. Thesis, Univ. Paris VI*, 220 pp.

Endlich R.M., Ludwig F.L. and Uthe E.E. (1979) An automatic method for determining the mixing depth from lidar observations. *Atmos. Environm.* **13**, 1051-1056

Hanna S.R., Burkhart C.L. and Paine R.J. (1985) Mixing height uncertainties. *Proc. 7th AMS Symp. Turb. & Diff., Boulder*, 82-85

Holets S.H. and Swanson R.N. (1984) Estimating mixed layer heights from digitized Doppler acoustic sounder data. *Proc. 77th Ann. Meeting Air Poll. Contr. Assoc., San Francisco*, 84-51.4

Kaimal J.C., Abshire N.L., Chadwick R.B., Decker M.T., Hooke W.H., Kroepfli R.A., Neff W.D., Pasqualucci F. and Hildebrand P.H. (1982) Estimating the depth of the daytime convective boundary layer. *J. Appl. Meteorol.* **21**, 1123-1129

Mann J., Davis K.J., Lenschow D.H., Oncley S.P., Kiemle C., Ehret G., Giez A. and Schreiber H.G. (1995) Airborne observations of the boundary layer top, and associated gravity waves and boundary layer structure. *Pepr. 9th AMS Symp. on Meteorol. Obs. & Instrum., Charlotte*, 113-116

Marsik, F.J., Fischer K.W., McDonald T.D. and Samson P.J. (1995): Comparison of methods for estimating mixing height used during the 1992 Atlanta Field Initiative. *J. Appl. Meteorol.* **34**, 1802-1814

Noonkester V.R. (1976) The evolution of the clear air convective layer revealed by surface based remote sensors. *J. Appl. Meteorol.* **15**, 594-606

Russell P.B., Uthe E.E., Ludwig F.L. and Shaw N.A. (1974) A comparison of atmospheric structure as observed with monostatic acoustic sounder and lidar techniques. *J. Geophys. Res.* **79**, 5555-5566

White A.B. (1993) Mixing depth detection using 915-MHz radar reflectivity data. *Prepr. 8th AMS Symp. on Observations & Instrumentation, Anaheim*, 248-250

Wyngaard J.C. and Lemone M.A. (1980) Behavior of the refractive index structure parameter in the entraining convective boundary layer. *J. Atmos. Sci.* **37**, 1573-1585

Wyngaard J.C. and Kosovic B. (1994) Similarity of structure-function parameters in the stably stratified boundary layer. *Boundary-Layer Meteorol.* **71**, 277-296

# Mixing Height Measurements from UHF Wind Profiling Radar

W.M. Angevine and A.W. Grimsdell

CIRES, University of Colorado, and NOAA Aeronomy Laboratory
Boulder, Colorado USA

## Introduction

Mixing height in convective boundary layers can be detected by wind profiling radars (profilers) operating at or near 915 MHZ (Ecklund et al. 1988; Carter et al. 1995). We have made such measurements in a variety of settings including Alabama in 1992 (Angevine et al. 1994); Nova Scotia, Canada, during the North Atlantic Regional Experiment (NARE) 1993 (Angevine et al. 1996); Tennessee during the Southern Oxidant Study (SOS) 1994; near a 450 m tower in Wisconsin in 1995; and extensively in Illinois during the Flatland95, '96, and '97 experiments, as well as continuous operations at the Flatland Atmospheric Observatory (Angevine et al. 1995, 1998a, 1998b).

## Measurement technique and verification

The mixing height is detected as an enhancement in the radar reflectivity due to strong humidity gradients and turbulence (White et al. 1991). The most basic form of the data is shown in figure 1, where the reflectivity is plotted in psuedocolor for every vertical beam (roughly every 100 s). The boundary layer top is clearly visible as a strong enhancement in the reflectivity. The values of $z_i$ determined by an automated algorithm (Angevine et al. 1994a) for hour averages every half hour are shown as a solid line. The algorithm simply finds the height of peak reflectivity in each 30 s sample, then takes the median of those heights over an hour as $z_i$. Cloud heights found by a laser ceilometer sampling every 30 s are shown as crosses. Day 228 1995 was warm (maximum virtual temperature approximately 37 C) and humid (surface water vapor mixing ratios approximately 22 g/kg). The capping inversion was relatively weak and the lower free troposphere was also humid. Day 219 1996 was also warm and humid, but the capping inversion was much stronger and the free troposphere much drier.

Figure 1 clearly shows that the profiler can measure $z_i$ in well-defined convective boundary layers, but it also illustrates several other points. When a cloud layer of significant depth is present at the BL top, for example after 1300 CST on day 228, the reflectivity gradient is poorly defined or displaced to a cloud top or cloud edge, and $z_i$ is difficult to determine. In fact, the definition of $z_i$ in this case is ambiguous and needs further discussion, so this is more a limitation of our understanding than of our instruments. Shallow BL-top clouds as on day 219 do not have such a strong effect. Other interesting phenomena are also visible in these plots. For example, the capping inversion above a residual layer is visible at approximately 1.3 km on day 219, and several humidity layers are visible above the BL in the morning of day 228. The boundary layer evolution is clearly very different on the two days. On day 228 the BL grows slowly and we see quasi-periodic structure in the BL top until the clouds form. On day 219 the BL grows quickly into the residual layer and then more slowly after reaching the capping inversion. In both cases the entrainment zone has significant depth on both short (a few minutes) and long (hour) scales. Downdrafts entraining air from above the BL and therefore moving the humidity gradient downward are clearly visible. Some of the visible structure may also be due to contamination, but none is clearly identifiable on these two days. Much of the signal in the middle of the boundary layer may be due to insects rather than to clear-air refractive index

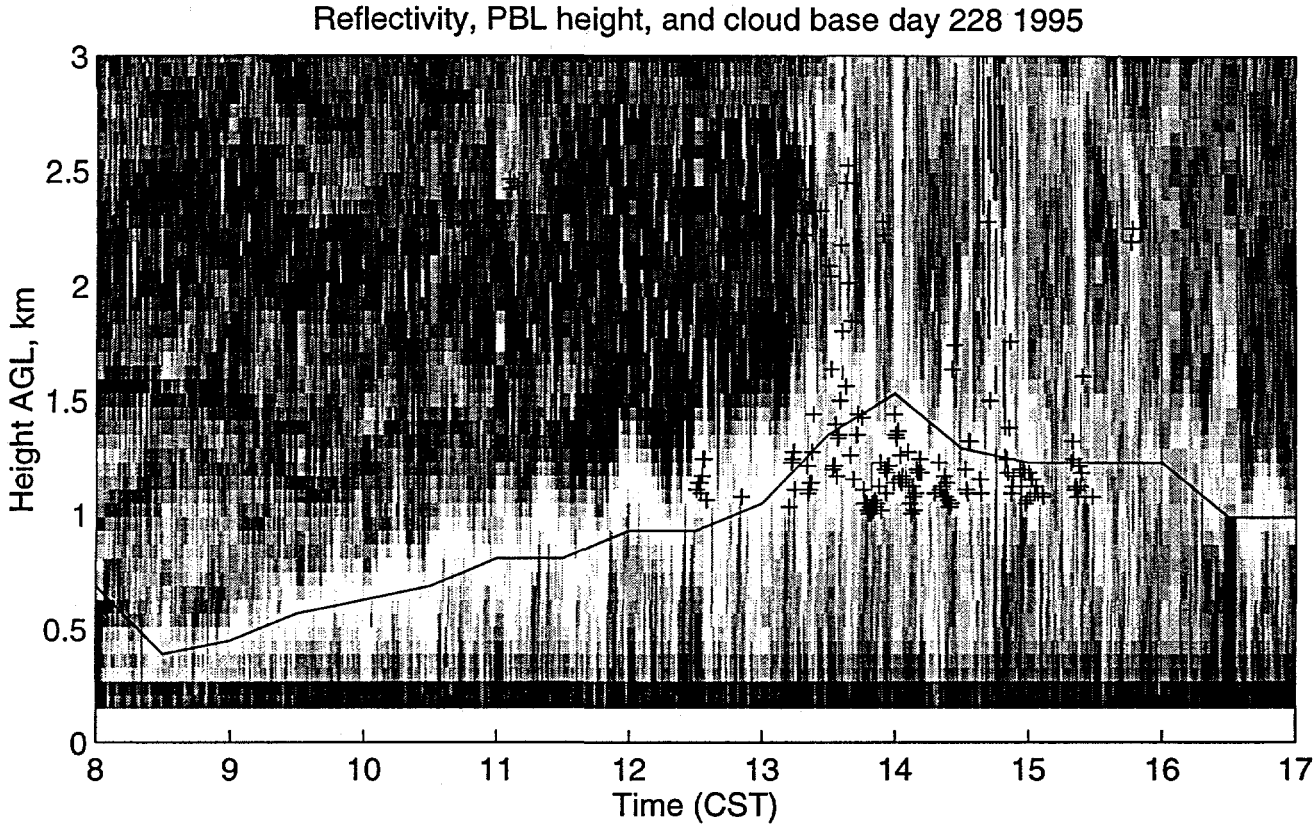
Reflectivity, PBL height, and cloud base day 228 1995
Height AGL, km
Time (CST)
0
0.5
1
1.5
2
2.5
3
8
9
10
11
12
13
14
15
16
17

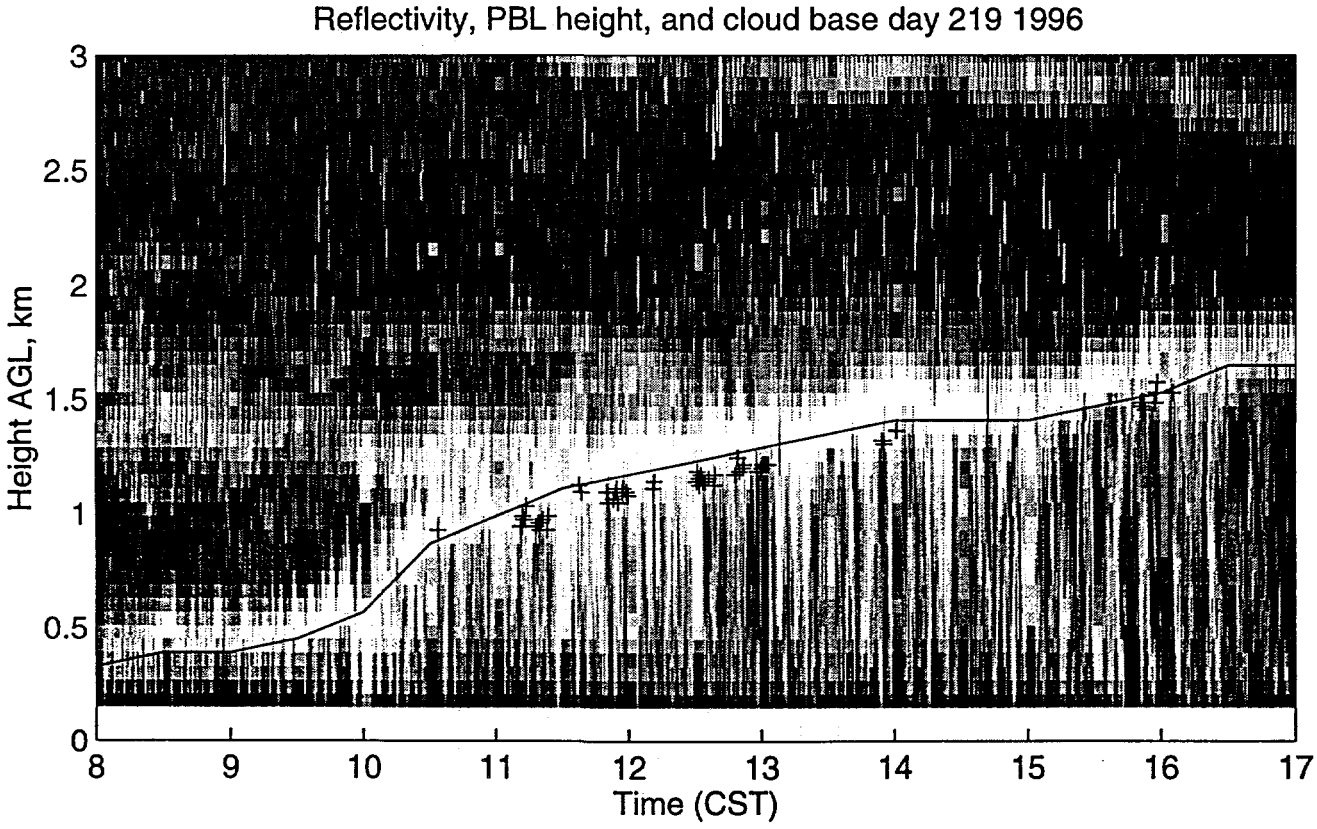
Reflectivity, PBL height, and cloud base day 219 1996
Height AGL, km
Time (CST)
0
0.5
1
1.5
2
2.5
3
8
9
10
11
12
13
14
15
16
17

fluctuations (Clark et al. 1995), but the BL top structure seems to be primarily due to clear-air scattering.

Profiler measurements of mixing height have been compared to measurements from sondes and from aircraft. Here we show a comparison of a large number of measurements

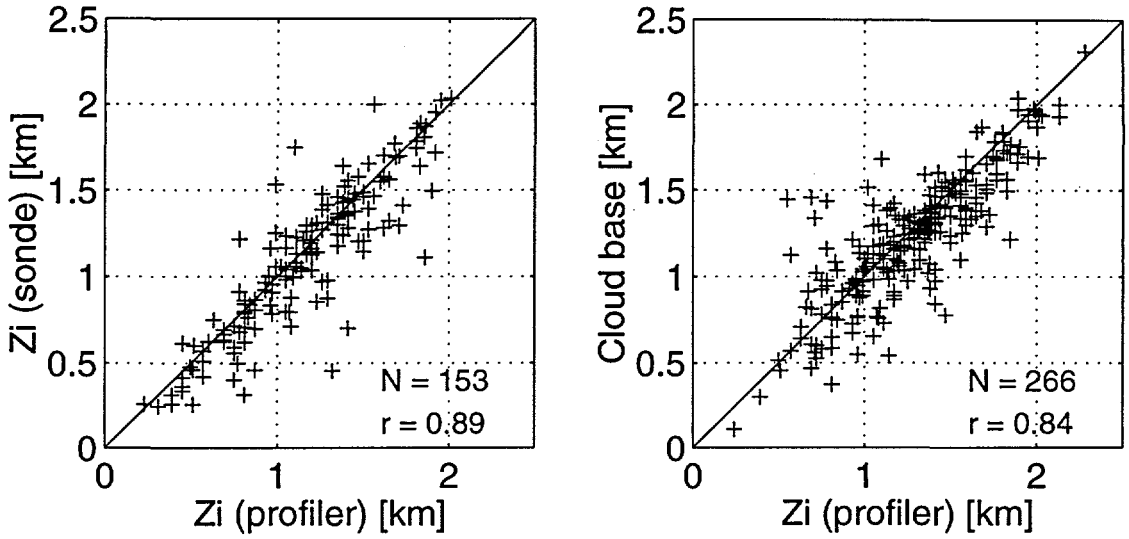


Figure 2: Comparison of profiler mixing height ($z_i$) measurements to measurements from sondes (left) and to cloud base measured by a laser ceilometer (right). Measurements are from the Flatland95 and Flatland96 campaigns.

from the Flatland campaigns in Illinois (figure 2, left panel). For this comparison, the profiler $z_i$ was derived from three profilers in a triangle 5.5-7.5 km on a side. The automated algorithm described above was run for each profiler, and then we compared the results and produced a $z_i$ estimate and a quality control number for each half-hour. The comparison includes only times with reasonably well-defined convective boundary layers and no rain. The sonde $z_i$ shown is subjectively determined to be the middle of the entrainment zone. Most of the sondes were launched at noon CST, but some were launched earlier in the day. The scatter in the comparison is probably primarily caused by the difference in sampling characteristics of the profiler and the sondes; the profiler measurements are hour averages, but the sonde measures only in a single narrow column.

We were also interested in the relationship of clouds to the profiler reflectivity and $z_i$ estimates. The laser ceilometer reports cloud heights every 30 s, but many of these heights do not represent boundary layer cloud bases. Some are cloud edges, some are higher cloud layers, and so on. An algorithm (Grimsdell and Angevine 1998) was devised to filter out the irrelevant cloud heights. The lifting condensation level (LCL) of surface air was calculated, and cloud heights between the lowest reported height and that height plus one half the LCL variation were considered to be boundary layer clouds and included in the hour averages to be compared with the profiler and shown in figure 2 (right panel). This is a fairly loose filter. The scatter in the comparison is caused by the rather different physical mechanisms being measured, but generally the cloud base and the profiler $z_i$ correspond quite well. The profiler $z_i$ is slightly higher (50-60 m) than either the sonde $z_i$ or the cloud base, probably due to a tendency for the profiler measurement to be biased toward the tops and edges of clouds when they are present. Cloud tops and edges have very strong humidity gradients which create strong reflectivity signatures.

**Applications**

We have applied profiler mixing height measurements to atmospheric chemistry and dynamics problems, including case studies and model comparisons. The measurements on

the coast of Nova Scotia (Angevine et al. 1996) were used to determine that surface chemistry measurements were only representative of shallow layers due to the absence of well-mixed layers during most of the experiment period. Mixing height is a basic scaling parameter for boundary layer variables, and profiler measurements were used to scale virtual temperature fluxes and velocity variances measured by profilers and by aircraft (Angevine et al. 1993, 1994b) and to scale fluxes of $CO_2$ (Davis et al. 1996). Measurements of $z_i$ from the Flatland campaigns were a key element in budget analyses to determine the entrainment flux and entrainment velocity at the boundary layer top (Angevine et al. 1998b).

## Conclusions

Profiler mixing height measurements, like all measurements, are subject to some limitations. The most important of these are due to rainfall, minimum height, and height resolution. Profilers are very sensitive to rain, which dominates the reflectivity and prevents the mixing height from being detected. Because the best height resolution is currently 60 m and the minimum height is 120-150 m AGL, the profiler is not suited for detecting mixing height in stable or nocturnal boundary layers. Problems may also arise in very dry or cold environments.

The profiler measurement of mixing height in convective boundary layers is well established. In the absence of rain, profilers provide measurements more often, with better temporal resolution, and more accurately (because of the larger averaging time and volume) than sondes. The information about boundary layer structure provided by profilers is less detailed than lidars can provide, but still quite complex. Under some conditions, particularly in the presence of deep clouds, the concept of mixing height itself may be too simple. Under these conditions, our conceptual models are more limiting than our instruments.

## References


Angevine, W.M., S.K. Avery, and G.L. Kok, 1993: Virtual heat flux measurements from a boundary layer profiler/RASS compared to aircraft measurements. *J. Appl. Meteor.*, **32**, 1901-1907.

Angevine, W.M., A.B. White, and S.K. Avery, 1994a: Boundary layer depth and entrainment zone characterization with a boundary layer profiler, *Boundary Layer Meteor.*, **68**, 375-385.

Angevine, W.M., R.J. Doviak, and Z. Sorbjan, 1994b: Vertical velocity variance and surface virtual heat flux measurements with a boundary layer radar wind profiler, *J. Appl. Meteor.*, **33**, 977-983.

Angevine, W.M., M.P. Buhr, J.S. Holloway, M. Trainer, D.D. Parrish, J.I. MacPherson, G.L. Kok, R.D. Schillawski, and D.H. Bowlby, 1996: Local meteorological features affecting chemical measurements at a North Atlantic coastal site. *J. Geophys. Res.*, **101**, 28,935-28,946.

Angevine, W.M., A.W. Grimsdell, L.M. Hartten, and A.C. Delany, 1998a: The Flatland boundary layer experiments, *Bull. Amer. Meteorol. Soc.*, submitted.

Angevine, W.M., A.W. Grimsdell, S.A. McKeen, and J.M. Warnock, 1998b: Entrainment results from the Flatland boundary layer experiments. *J. Geophys. Res.*, submitted.

Carter, D.A., K.S. Gage, W.L. Ecklund, W.M. Angevine, P.E. Johnston, A.C. Riddle, J. Wilson, and C.R. Williams, 1995: Developments in UHF lower tropospheric wind profiling at NOAA's Aeronomy Laboratory, *Radio Sci.*, **30**, 977-1001.

Clark, W.L., J.M. Warnock, T.E. VanZandt, and K.S. Gage, 1995: Scattering from clear air, precipitation and biological targets: Multiple frequency profiler studies. *Proceedings, 27th Conference on Radar Meteorology, 9-13 October 1995, Vail, Colorado.* Published by AMS. 281-283.

Davis, K.J., P.S. Bakwin, C. Zhao, W.M. Angevine, and D.F. Hurst, 1996: Monitoring regional forest-atmosphere exchanges of carbon dioxide. *Proceedings, 22nd Conference on Agricultural and Forest Meteorology, 28 Jan.-2 Feb. 1996, Atlanta, Georgia.* Published by AMS. 302-305.

Ecklund, W.L., D.A. Carter, and B.B. Balsley, 1988: A UHF wind profiler for the boundary layer: Brief description and initial results, *J. Atmos. Oceanic. Technol.*, **5**, 432-441.

Grimsdell, A.W., and W.M. Angevine, 1998: Convective boundary layer height measured with wind profilers and compared to cloud base, *J. Atmos. Oceanic Technol.*, submitted.

White, A.B., C.W. Fairall, and D.W. Thompson, 1991: Radar observations of humidity variability in and above the marine atmospheric boundary layer, *J. Atmos. Ocean. Technol., 8*, 639-658.

# Variation of Backscatter as an Indicator of Boundary Layer Structure

M. Bennett[1], G.C. Hunter[2]

[1]Department of Chemical Engineering, UMIST, Manchester, M60 1QD, UK
[2]National Power, Swindon, SN5 9PB, UK

## Introduction

The routine measurement of boundary layer (BL) depths with a simple backscatter Lidar is not straightforward since there is no reliable signature in the profile of the mean aerosol concentration which would indicate the transition between a well-mixed layer in contact with the ground and a streamline layer above it. In a previous paper (Bennett 1995) we have argued that the small-scale variation of aerosol concentrations might serve as a marker of the top of the BL. If, by definition, the streamline layer is not well mixed, then differences in the histories of neighbouring packets of air can lead to a 'layer-cake' appearance in the backscatter profile (Stull 1988). The small-scale variance both in time and space should thus be larger outside the nominally well-mixed BL.

In this work we have extended the previous analysis by developing software to display cross-sections of the variance of backscatter over a given sampling period in addition to its absolute mean. We have analyzed a series of Lidar cross-sections of elevated plumes dispersing into a convective BL and have then derived profiles both of the mean backscatter, $<B(z)>$, as a function of height and of its relative, shot-to-shot, variation, $\sqrt{<B'(z)^2>}/<B(z)>$. The latter is a measure of the homogeneity of the aerosol.

There is no cheap device for measuring BL depths so we were interested in comparing depths estimated using our Lidar with those predicted by the current ADMS atmospheric dispersion model (CERC 1995). This is based on integrating an energy budget to predict the BL development and as such relies on values for the initial lapse rate and for the surface sensible heat flux. A major shortcoming of the model appears to be that, in the absence of measurements, it must assume a default value for the former; the latter may be estimated from surface measurements but is very sensitive to the assumed availability of surface moisture.

## Observational Data

The data used for this study were gathered at Staythorpe power station near Newark, Notts. in the summer of 1993 as part of an exercise to measure the final buoyant rise of a plume (Bennett 1993). The Lidar used operates at a wavelength of 532 nm, has a range resolution of 5 m and a pulse repeat frequency of 30 Hz. The beam may be steered with a plane mirror so that cross-sections of a dispersing plume may be obtained: typically 240 such cross sections may be obtained in 20 min.

Local meteorological data (10 m wind speed and direction, temperature, humidity, short-wave radiation) were measured at the Lidar. Wind and temperature data were also available from the Belmont TV mast 55 km to the NE (cf. Bennett 1997).

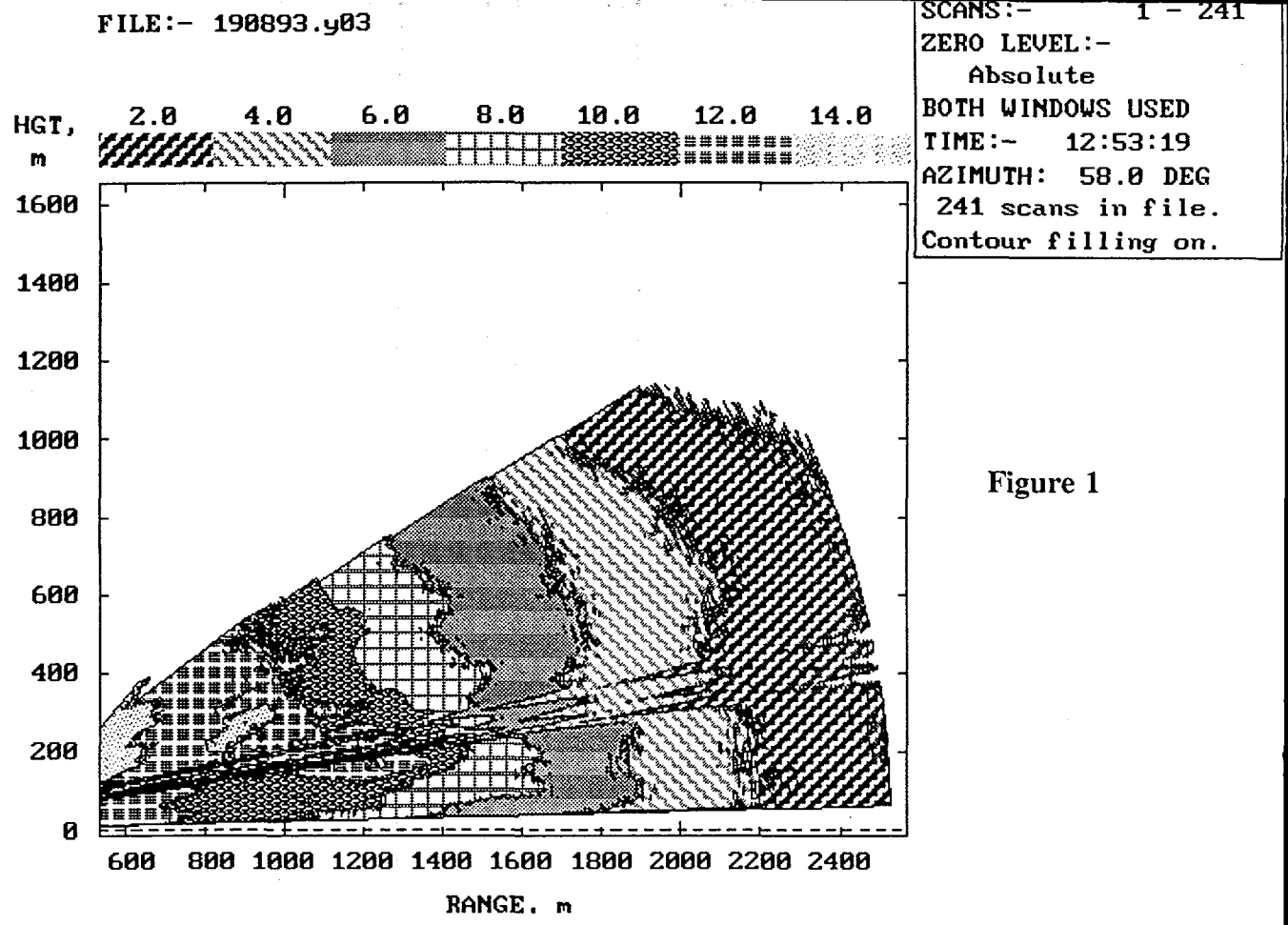


Figure 1

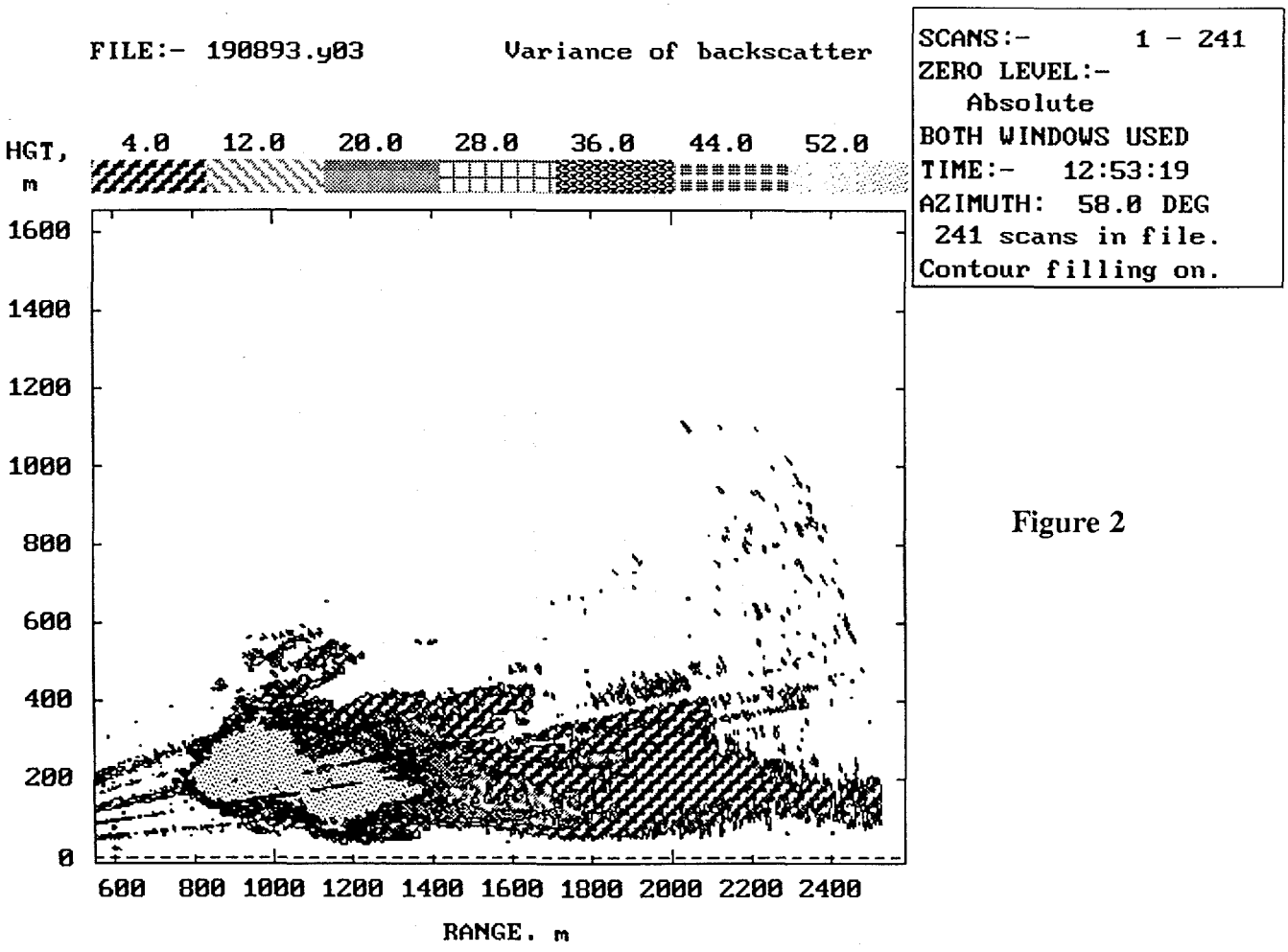


Figure 2

The mean absolute backscatter from a typical series of scans is shown in Figure 1 (the streaks are the shadows of power lines) and its variance in Figure 2. The plume may barely be distinguished above the mean backscatter: for plume dispersion studies we have developed algorithms to subtract the background aerosol. Signal variance arises from the wispiness of the plume; from the discreteness of the scatterers; from shot noise in the background light; and from system noise. We have here treated the zero level of variance as being the 10th percentile of variance at a given range. This then allows the subtraction of system and shot noise without being over-sensitive to problems at a few elevations. Since the plume breaks up into puffs, the backscatter within it has a large variance.

The measured backscatter and its variance can be integrated horizontally to give the profiles shown in Figure 3. The effect of the plume on the relative variation of backscatter (RVB) may be seen very clearly below 400 m. The mean backscatter apparently falls steadily with height: this is an artefact arising from greater heights being sampled at greater ranges and hence being more subject to extinction. The sharp fall at 1100 m appears to mark the top of the BL; the RVB rises towards unity at this point. As the afternoon progressed, this peak in RVB died away, implying that it arose from active mixing across the capping inversion. On later days, with a shallower BL, the RVB greatly exceeded unity outside the BL.

We modelled the BL depth over the 9 days of the survey. Within an energy-budget model, the depth is proportional to the square root of the integrated surface sensible heat flux since dawn, and inversely proportional to the Brunt-Vaisala frequency in the overlying inversion. ADMS assumes a value $N$ = 13 mHz, corresponding to a potential temperature lapse rate of 0.005 K $m^{-1}$. Statistics from Belmont suggest that this is reasonable. The measured value of $N$ at Belmont varied between 12.7 and 21.0 mHz over the survey but inserting the correct value for each day did not improve agreement with the Lidar observations. Of more significance may be the partitioning between latent and sensible surface heat fluxes. Van Ulden and Holtslag (1985) model the availability of surface moisture using a parameter $\alpha$ which may vary between zero for a dry surface and unity for (say) wet grass. ADMS uses a default condition of $\alpha$ =1. The inadequacy of such an approach may be seen from the BL development on 18/8/93. On this day the initial Brunt-Vaisala frequency measured at Belmont was 12.7 mHz, very close to the default value. The measured BL depth, however, topped out at around 1200 m while the predicted value was 730 m. A good simulation of the BL depth is obtained by replacing the default value with $\alpha$ = 0.5. (This corresponds to dry vegetation: rain on 15/8 was followed by several dry days). Thus a rather arbitrary change in input conditions has trebled the surface sensible heat flux.

**Discussion**

At times of active convection, the relative variation of backscatter (RVB) appears to increase rapidly over the top third of the boundary layer. This presumably is a consequence of the folding of over-lying dry, clean air into the BL. Later in the day, as the convection dies away, the RVB tends to drop to a lower, near-constant value. The mean backscatter profile changes little between the two cases. As such, RVB profiles might be useful in distinguishing active boundary layers from the aerosol layers left over from a previous diurnal cycle.

Typical values of RVB appear to be 0.1 - 0.5 in a dry convective BL, rising to perhaps ~1 at the top of the layer; ~1 in a dispersing plume; 2 - 5 in mist; and 5 -

10 in cloud.

Sensitivity analyses show that the ADMS prediction of BL depth can be in error by more than a factor of two, with corresponding errors in the predicted pollutant concentrations. We do not have enough information from these measurements to disentangle the relative importance of the initial lapse rate and the availability of surface moisture.

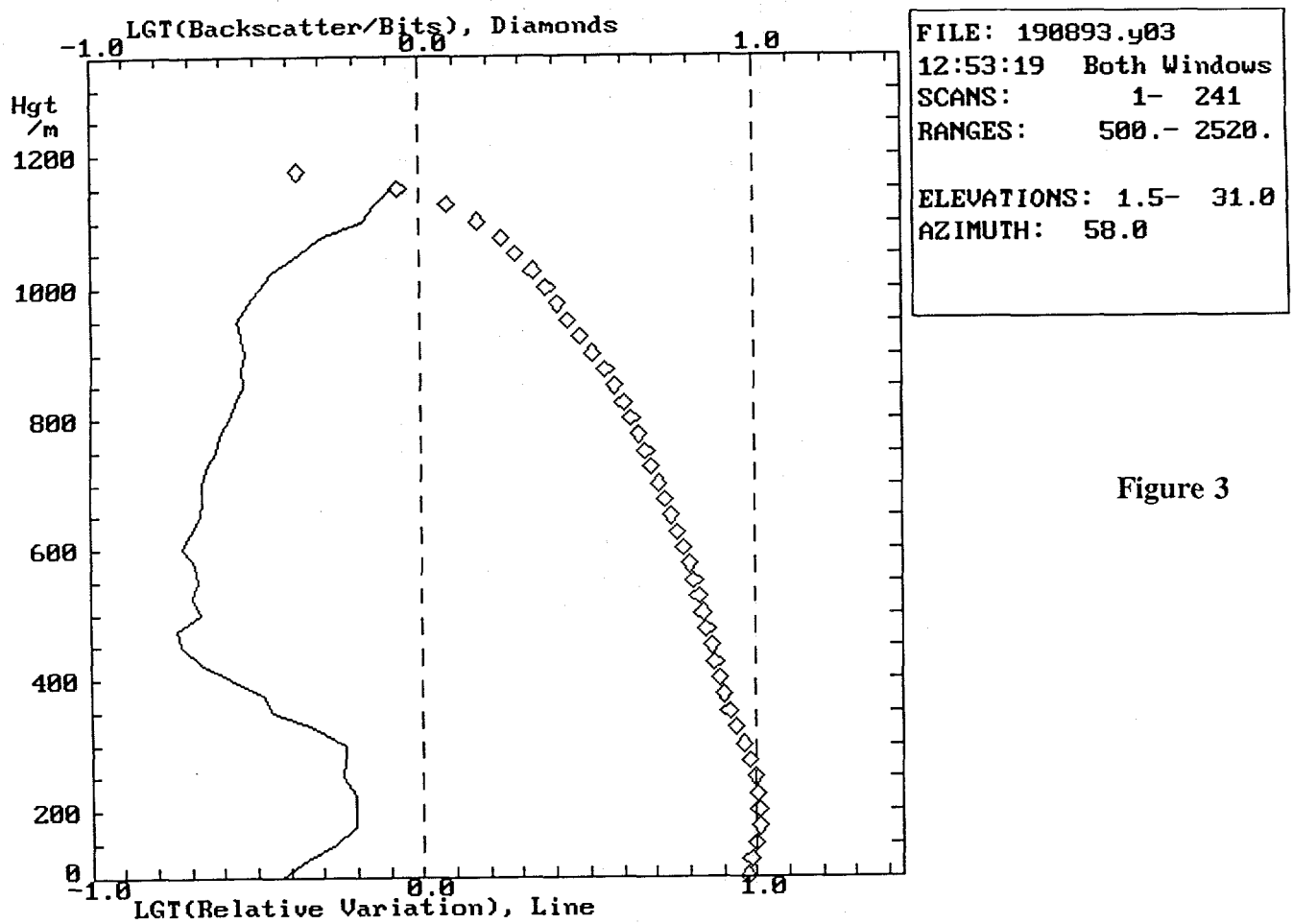


Figure 3


## Acknowledgements

These measurements were made with the help of a grant from the Natural Environment Research Council and with the permission and assistance of National Power.


## References


Bennett M., 1995: A Lidar study of the limits to buoyant plume rise in a well-mixed boundary layer. *Atmos. Environ.*, **29**, 2275-2288.

Bennett M., 1997: Wind shear and the sea-breeze in Lincolnshire. *Weather*, **52**, 198-204.

CERC, 1995: ADMS 2 User Guide. *Cambridge Environmental Research Consultants*, 3d King's Parade, Cambridge, UK

Stull R.B., 1988: An introduction to boundary layer meteorology. *Atmospheric Sciences Library*. Kluwer Academic Publishers, Dordrecht. p413.

van Ulden A.P., Holtslag A.A.M., 1985: Estimation of atmospheric boundary layer parameters for diffusion applications. *J. Climate & Appl. Meteor.*, **24**, 1196-1207.

# A Comparison of Mixing Depths Observed by Ground-based Wind Profilers and an Airborne Lidar

A. B. White[1], C. Senff[1], and R. M. Banta[2]

[1]Cooperative Institute for Research in Environmental Sciences
University of Colorado/NOAA Environmental Technology Laboratory
Boulder, CO, USA

[2]NOAA Environmental Technology Laboratory
Boulder, CO, USA

## Introduction

The mixing depth is one of the most important parameters in air pollution studies because it determines the vertical extent of the "box" in which pollutants are mixed and dispersed. During the 1995 Southern Oxidants Study (SOS95), scientists from the National Oceanic and Atmospheric Administration Environmental Technology Laboratory (NOAA/ETL) deployed four 915-MHz boundary-layer radar/wind profilers (hereafter radars) in and around the Nashville, Tennessee metropolitan area (White et al., 1998). Scientists from NOAA/ETL also operated an ultraviolet differential absorption lidar (DIAL) onboard a CASA-212 aircraft (Alvarez et al., 1998; Banta et al., 1998, Senff et al., 1998). Profiles from radar and DIAL can be used to derive estimates of the mixing depth. The methods used for both instruments are similar in that they depend on information derived from the backscattered power. However, different scattering mechanisms for the radar and DIAL mean that different tracers of mixing depth are measured. In this paper we compare the mixing depth estimates obtained from the radar and DIAL and discuss the similarities and differences that occur.

## Radar Method

The backscattered signal in clear air from the radars is directly proportional to the refractive index structure function parameter, $C_n^2$. Theory and observations show that the profile of $C_n^2$ exhibits a peak at the inversion capping the mixed layer. The radar method relies on finding the peaks in successive profiles of $C_n^2$ (White, 1993). The largest errors associated with this technique are due to real or apparent enhancements in $C_n^2$ that occur in regions other than at the top of the mixed layer. Examples include scattering from clear-air turbulence within or above the boundary layer, insects, birds, and ground clutter. For the SOS95 hourly mixing depths were produced from hourly median profiles of radar backscatter. A median was used instead of an average to reduce the impact of outliers.

Cumulus convection changes the interpretation of the mixing depth, both from a theoretical and observational perspective. The updrafts that feed cumulus convection vent the boundary layer of pollutants. Since these penetrating updrafts originate in the boundary layer, the question becomes what is the relevant mixing depth. Clouds also enhance radar backscatter through turbulent mixing caused by evaporation/condensation processes and entrainment, as well as by Rayleigh scattering from large cloud droplets and precipitation. Therefore, the strongest peak in a profile of radar backscatter may occur inside the cloud or at a cloud boundary, which complicates the interpretation of the radar data for the purpose of deducing the mixing depth (Angevine et al., 1994).

**DIAL method**

The airborne, downward-looking DIAL emits laser pulses at five different ultraviolet wavelengths into the atmosphere. The backscattered return signals are used to retrieve ozone concentration and aerosol backscatter profiles (Alvarez et al., 1998). The retrieved profiles of aerosol backscatter can be used to estimate the mixing depth by detecting the drop in aerosol concentration that often occurs at the top of the mixed layer. One approach is to find the steepest negative gradient in successive backscatter profiles. Other possibilities include using wavelet transforms to detect the relevant structure (Cohn et al., 1997). Regardless of the analysis method used, one of the difficulties associated with using lidar to detect the mixing depth is identifying the gradient at the top of the current day's mixed layer as opposed to a gradient resulting from the mixed layer on a previous day. Clouds present additional problems for the downward looking lidar because the strong backscatter from cloud particles produces an apparent gradient in the aerosol backscatter profile at an altitude near cloud top. Also, the rapid attenuation of the lidar beam in optically thick clouds, such as boundary layer cumulus, prevents measurement of the aerosol structure below this altitude. Because of these and other difficulties, we determined the aerosol mixing depths in this study by visual inspection of the DIAL backscatter profiles.

**Comparison of Methods**

The data used for the comparison were collected during the SOS95 period of 24 June–19 July. Airborne DIAL data were obtained on 16 of these days. The flight patterns varied from day to day and included both morning and afternoon departures. To select data for the comparison, we constrained the flight track to be within 20 km horizontal distance of one of the profiler sites. This criterion yielded 165 time segments. The length of each segment depended on how long the DIAL remained in the vicinity of one of the profiler sites and varied from less than 1 min. to slightly more than 13 min. The mixing depth for the radar was determined by averaging the mixing depths obtained at the endpoints of the segments, which were calculated by linear interpolation over the hourly mixing depth values. Nearly half (78) of the segments were discarded in the analysis because a mixed-layer signature was not found in either the radar or DIAL data. This usually occurred when the mixing depth was below the minimum effective range of the instruments (~200 m) or when the DIAL profiles were obscured by clouds.

Figure 1 is a scatterplot comparing the mixing depth estimates from the radars and DIAL. Correlation statistics are shown in the upper left. The mixing depths are well correlated, but there is significant scatter (12% of the mean), and there is a mean bias (calculated by subtracting the value of Average X from the value of Average Y) of 69 m. Still, given the sampling differences of the two instruments and the spatial inhomogeneity accompanying the criterion we used to specify coincident data, the agreement is quite good.

We segregated the "cloudy" (C) days from the "mostly clear" (MC) days based on the daily cloud fraction data provided by a laser ceilometer deployed at one of the radar sites. The cloud fraction deduced from the ceilometer differs from the standard definition. First, because of instrument range limitations, the ceilometer cloud fraction only includes clouds with base elevations within 4 km of the surface. Second, the ceilometer points vertically and does not scan, so the deduced cloud fraction is based solely on the clouds that pass directly over the instrument. We distinguished the C days from the MC days using an arbitrary threshold of 0.15 for the average daytime (1220–2400 UTC) overhead cloud fraction. Figures 2 and 3 show scatterplots for the C data and MC data, respectively. The

largest difference is in the mean bias, which drops from 148 m for the C data to just 37 m for the MC data. For the MC data there is also an increase in the correlation coefficient (0.87 to 0.94) and a reduction in the root-mean-squared (RMS) scatter (169 m to 146 m).


## Summary

The mixing depth is an important parameter for pollution studies but is difficult to model because of complex interactions between the many physical processes that contribute to its evolution. A variety of remote sensing technologies have been used to detect the mixing depth including sodar, radar, and lidar. We compared the mixing depths deduced by radar and DIAL and found generally good agreement despite the different scattering mechanisms for each instrument (clear-air turbulence for the radar and aerosol backscatter for the DIAL) and given the difficulty and uncertainty associated with comparing data from an airborne sensor with data from a fixed sensor on the ground. Clouds affect both the radar and DIAL measurements but tend to cause the downward-looking DIAL to over predict the mixing depth because of the apparent gradient in aerosol backscatter that results near cloud top.



## Acknowledgments

This research was sponsored by the NOAA Health of the Atmospheres Program.


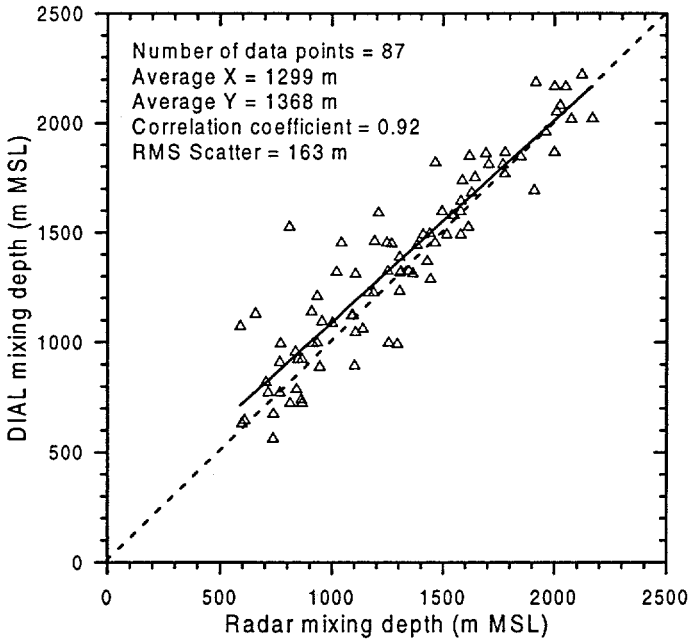


Figure 1. Scatterplot comparing the mixing depths determined by ground-based 915-MHz wind profilers (radar) and an airborne differential absorption lidar (DIAL) deployed during the 1995 Southern Oxidants Study. The solid line and the statistics in the upper left show the results of linear regression analysis. The dashed line shows 1:1 correlation.

## References


Angevine, W.M., A.B. White, and S.K. Avery, 1994: Boundary layer depth and entrainment zone characterization with a boundary layer profiler. *Bound.-Layer Meteor.*, **68**, 375–385.

Alvarez, R.J., R.M. Hardesty, C.J. Senff, D.D. Parrish, W.T. Luke, T.B. Watson, P.H. Daum, and N. Gillani, 1998: Validation of airborne lidar measurements of ozone with airborne in situ measurements during the 1995 Southern Oxidants Study. *J. Geophys. Res.*, submitted.

Banta, R.M., C.J. Senff, A.B. White, M. Trainer, D. Parrish, R.T. McNider, R.J. Valente, P.H. Daum, S.D. Mayor, R.J. Alvarez, and R.M. Hardesty, 1998: Daytime buildup and nighttime transport of urban ozone in the boundary layer during a stagnation episode. *J. Geophys. Res.*, submitted.

Cohn, S.A., C.J. Grund, S.D. Mayor, and W.M. Angevine, 1997: Boundary layer height and vertical velocity measurements at LIFT. Preprint Vol., Twelfth Symp. on Boundary Layers and Turbulence, Amer. Meteor. Soc., Boston, 7–8.

Senff, C.J., R.M. Hardesty, R.J. Alvarez, and S.D. Mayor, 1998: Airborne lidar characterization of power plant plumes during the 1995 Southern Oxidants Study. *J. Geophys. Res.*, submitted.

White, A.B., 1993: Mixing depth detection using 915-MHz radar reflectivity data. Preprint Vol., Eighth Symp. on Observations and Instrumentation, Amer. Meteor. Soc., Boston, 248–250.

White, A.B., C.J. Senff, R.J. Zamora, and R.M. Banta, 1998: Horizontal variation in mixing depth: A case study from the 1995 Southern Oxidants Study. *J. Geophys. Res.*, submitted.

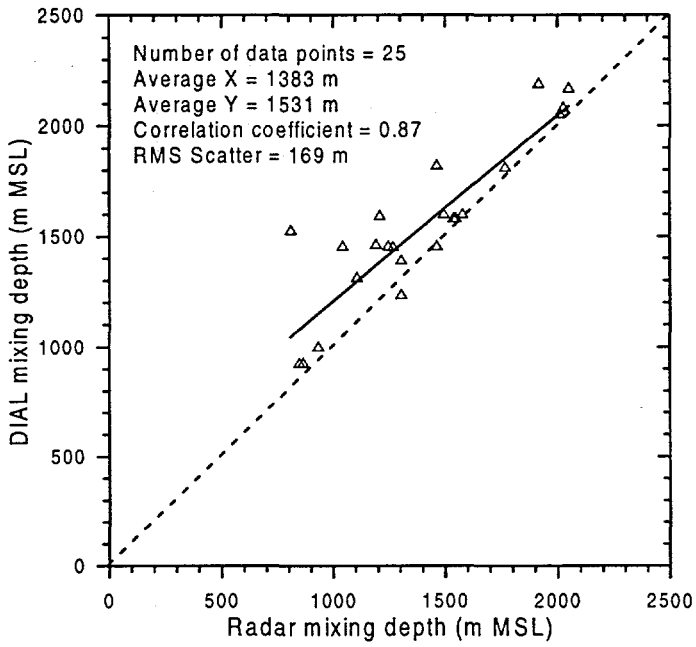


Figure 2. Same as Fig. 1 except for the "cloudy" days as specified by laser ceilometer measurements of the overhead cloud fraction.

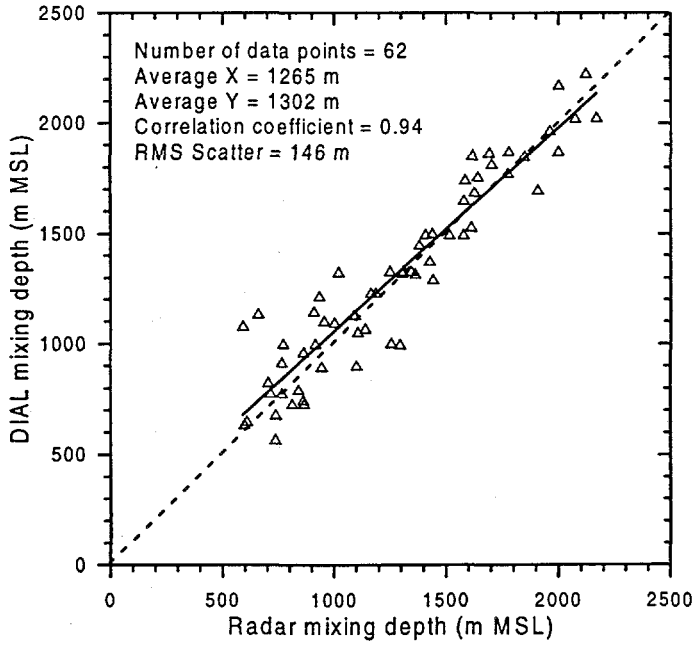


Figure 3. Same as Fig. 1 except for the "mostly clear" days as specified by laser ceilometer measurements of the overhead cloud fraction.

# On determination of the urban mixing height for air quality application

M. A. Kallistratova[1], M. A. Lokoshchenko[2]

[1] Obukhov Institute of Atmospheric Physics, Moscow, Russia
[2] Moscow State University, Russia

## Introduction

The character of height-dependence of all the meteorological and turbulence parameters markedly changes in the MH vicinity. At the same time, there is no a generally accepted definition of MH, and therefore it would be more natural to speak about the estimation of its scale but not about its determination.

Even within some type of the ABL structure, which can be described by a model, it is difficult to choose the best way of the definition of MH. There are more than a dozen of different recommendations in different papers (see, e.g., Elting (1975) and Beirich (1996)). The definition of MH as a height at which the velocity of kinetic energy dissipation $\varepsilon$ rapidly decreases most precisely corresponds to the very meaning of the term "mixing layer"(ML) for the purpose of the air-pollution meteorology.

The upper boundary of the ML is related to changes in the gradient of potential temperature $\theta$, which affects the degree of stability of the vertical air motions. For a long time, the MH was estimated exactly from the profiles of $\theta$ (e.g., Holzworth (1992, 1994), Miller (1967)). However, MH is too sensitive to small changes in $d\theta/dz$ (even smaller than the errors in standard measurements of the latter quantity). As it was shown by Aron (1983), such a method of MH estimating is not quite reliable. New remote sensing techniques give extensive possibilities for operative estimates of MH.

## The behavior of the ABL parameters near MH and admissible errors in its estimates

Fig. 1 gives height dependencies of different parameters under the conditions of developed convection for flat country. This graph was plotted by Kukharets et al. (1980) according to the data obtained from long-term fluctuation measurements from board an airplane; these measurements were carried out in the 1970s by the scientists of the Institute of Atmospheric Physics. Similar dependencies were obtained from the results of complex field experiments in Kansas and Minnesota. Such kind of dependencies can be used to obtain an agreement between different experimental methods of estimating the MH in the convective ABL. But the total period for the existence of developed convection in the European latitudes is only about 15% of the total number of hours in a year. For other types of stratification and nonstationary synoptic conditions it is difficult to obtain such universal dependencies. The table (by data of Pekour and Kallistratova (1993) and Asimakoupolos et al. (1992)) shows that rather complex vertical structure of ABL is observed for about 50% of the whole time, especially for non homogeneous underlying surface. An example of the multilayered structure is given in Fig. 2.

Table. Occurrence of different types of stratification (in %).

| Stratification / Place | Surface inversion | Multi layer inversion | Capped convection | Developed convection | Near neutral |
|---|---|---|---|---|---|
| Moscow | 28 | 15 | 3 | 15 | 28 |
| Southern Greece | 39 | 42 | 8 | 16 | 6 |
| Northern Greece | 27 | 43 | 10 | 15 | 5 |

To determine the validity of this or that method of MH estimation, a criterion is needed for an admissible error in the MH value. For application to air pollution meteorology, this criterion depends on the effect of MH value on the results of calculations of the admixture concentration field. The degree of this effect is determined not only by the type of a dispersion model, but also by the atmospheric stratification itself. Let us clarify this statement using an example of the simplest box-model. The relative error in estimating the "mixing volume" (<v> * MH) is equal to the relative error in estimating the MH value under convective conditions (i.e., when wind velocity remains almost unchanged with height within the ML) and to the double value of this error at inversions (i.e., when wind velocity increases almost linearly with height and <v> ~ MH).

**MH estimates from the results of acoustic sounding**

The MH estimates according to the height variations in the amplitude of an echo-signal of an acoustic locator (sodar) and wind-profiler (radar) are based on an abrupt decrease of $C_T^2$, which usually corresponds to decrease of $\varepsilon$ (Petenko et al., 1996). Height ranges are different for a sodar and a radar: a radar cannot detect low-level inversions, but it reveals the elevated maximum of $C_T^2$ above developed convection. Therefore it is rather attractive to use them both simultaneously, as it was demonstrated in paper of Beyrich (1996).

However, to estimate the convective MH with an admissible accuracy for most of the models, almost all the ways of extrapolation of sodar data are appropriate (see e.g., Singal et al. (1984), Singal (1988)). Beyrich (1993) indicated some restrictions of these methods.

Fig. 3 shows the comparison of sodar estimates of MH with estimates of maximal daily MH from the profiles of $\theta$ (z) according to the Holzworth (1964) method. The scatter of points may be mainly due to uncertainty of the determination of MH from the profiles. It is also necessary to take into account that, when the synoptic processes are nonstationary (e.g., at advection or subsidence of air masses), the errors in sodar estimates may increase. Therefore the synoptic analysis of meteorological conditions is extremely advisable for sodar estimates of MH as well as for any other methods to MH estimate (Lokoshchenko et al. (1994)).

**Estimates of MH over a city by sodar**

The Institute of Atmospheric Physics and the MSU Meteorological Observatory have accumulated a three-year experience of continuous sodar measurements taken at several points of Moscow and its suburbs. This experience has demonstrated that sodars are convenient to be used within of urban area, where there are strong limitations in using other experimental methods for estimating MH. There are essential differences between the values of synchronous estimates of MH over a city and over its suburbs (see Shurygin (1997)). These differences are due to the presence of a heat island over a city and to a time lag of daily variations in the underlying surface heating. This lag noticeably increases at nonstationary synoptic conditions. The available statistical data on such differences allow the results of suburb measurements to be used for climatological estimates of urban MH. However, the scatter of the data is too great to use them for operative purposes even for the same region, where they have been obtained.

Fig. 4 gives an example of an empirical dependence of carbon monoxide concentration at a height of 10 m on the reciprocal value of "mixing volume" (1/ <v>·MH). The measurements of MH values and mean wind velocity <v> were taken by Doppler sodar simultaneously with the measurements of the CO

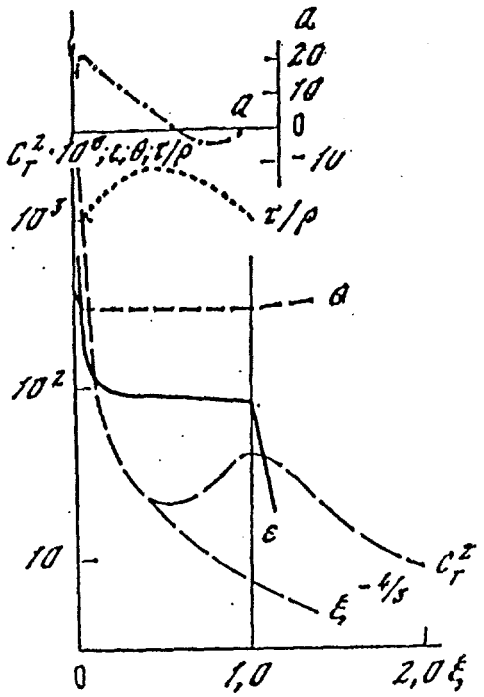


Fig. 1. Schematic profiles of temperature flux Q (°C· cm ·c $^{-1}$ ), momentum flux $\tau/\rho$ (cm$^2$ · c$^{-2}$ ), rate of dissipation $\varepsilon$ (cm$^2$ ·c$^{-3}$ ), temperature structure parameter $C_T^2$ ((°C)$^2$·cm$^{-2/3}$) and potential temperature $\theta$ (°C) as functions of nondimensional height $\xi$= z/h (h=MH) under convection (Kukharets et al., 1980).

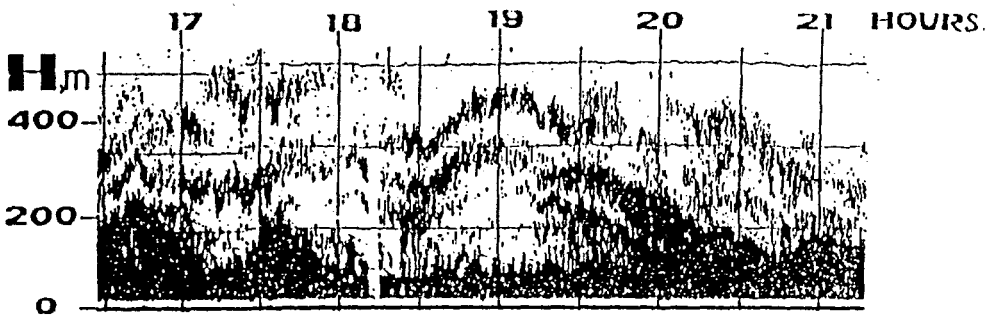


Fig. 2. An example of the multilayered structure of temperature turbulence over Moscow (08 Dec. 1989) accordingly to the sodar facsimile.

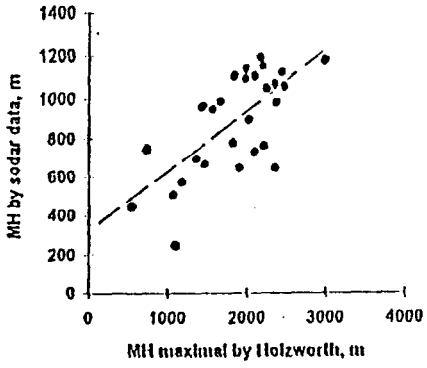


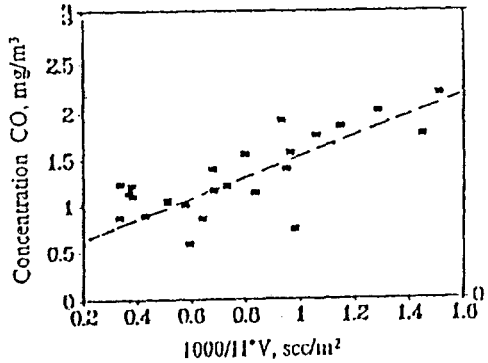


Fig. 3. Comparison of the MH estimates by sodar with the maximal possible values $(MH)_{max}$ determined from profiles of $\theta$ by Holzworth's method.

Fig. 4. Comparison of the local concentrations of CO with the "mixing volume" (<v>MH) by sodar data for the center of Moscow (Fokeeva et al., 1997).

concentrations at one and the same place, in the center of Moscow. This Figure manifests the potentialities of sodar in estimating the level of local atmospheric pollution under urban conditions.

## Conclusion

1. The verification of different estimates of MH through their comparison with the aerological profiles of potential temperature is not reliable due to great errors of this method assumed as a standard one. Only results of complex fluctuation measurements of height dependencies of meteoparameters may serve as a standard.

2. The criterion of admissible relative errors in estimating MH depends on the degree of their effect on final results of calculations of the admixture concentration field. Such criteria can depend essentially not only on the type of a dispersion model but also on the character of atmospheric stratification, underlying surface, and synoptic processes.

3. Sodars are the most cost-effective and accessible means of operative estimation of urban MH. Errors in sodar estimates of MH are admissible for elementary dispersion models.

This work was partially supported by the Russian Foundation for Fundamental Researches, grants nos. 96-05-65741 and 97-05-65697.

## References

Aron R., 1983: Mixing height - an inconsistent indicator of potential air pollution concentrations. *Atm. Environment*, **17**, 2193-2197.

Asimakopoulos D.N., Helmis C.G., Deligiori D.G., 1992: Climatological valuation of sodar recordings over complex terrain. In: D.N. Asimakopoulos (Ed.), *Proc. of 6th Int. Symp. on Acoustic Remote Sensing*, Athens, May 26-29, p. 11-22.

Beyrich F., 1993: On the use of sodar data to estimate mixing height. *Appl. Phys.* **B 57**, 27-35.

Beyrich F., 1996: Mixing height estimation from sodar data - A review. In: M.A. Kallistratova (Ed.), *Proc. of 8th Int. Symp. on Acoustic Remote Sensing*, Moscow, May 27-31, p. 6.11-6.22.

Elting D., Wippermann F., 1975: The height of the planetary boundary layer and the surface layer. *Contribs Atmos. Phys.*, **48**, 250-254.

Fokeeva T.V., Grechko E.I., Pekour M.C., 1997: Study of carbon monoxide contamination at the center of Moscow. *Izvestia RAN, FAO* (in print).

Holzworth G.C., 1962: A study of air pollution potential for the western United States. *Journal of Applied Meteorol.*, **1**, 366-382.

Holzworth G.C., 1964: Estimates of mean maximum mixing depths in the contiguous United States. *Monthly Weather Review*, **92**, 235-242.

Kukharets V.P., Tsvang L.R., Yaglom A.M., 1980: About connection of turbulent characteristics in surface and boundary layers of the atmosphere. In coll.: G.S. Golitsyn, A.M. Yaglom (Eds.) Atmospheric Physics and Problems of Climate, M.: Nauka, p. 162-193 (in Russian).

Lokoshchenko M.A., Semenchenko B.A., Kallistratova M.A., Pekour M.C., 1994: On influence of synoptic conditions on the mixing layer height. *Optics of Atm. and Climate*, **7**, . 976-985.

Miller M.E., 1967: Forecasting afternoon mixing depths and transport wind speeds. *Monthly Weather Review*, **95**, 35-44.

Pekour M.S. and Kallistratova M.A., 1993: Sodar study of the boundary layer over Moscow for air-pollution application. *J. Appl. Phys.* **B 57**, 49-55.

Pekour M.S., Kallistratova M.A., Lokoshchenko M.A., Petenko I.V., 1993: Acoustic sounding study of the mixing layer over a city. *SPIE, 2107, Optical Monit. of the Environment*, p. 169-193.

Petenko I.V., Kallistratova M.A., Bedulin A.N., 1996: Wind turbulence measurements with a mono-bistatic sodar. *Proc. of 8th Symp. on Acoustic Remote Sensing*, Moscow, p. 3.55-3.60.

Singal S.P., Gera B.S., Aggarwal S.K., 1984: Nowcasting by acoustic remote sensing: *Journal of Scientific and Industrial Research.*, **43**, 469-488.

Singal S.P., 1988: The use of an acoustic sounder in air quality studies. *Journal of Scientific & Industrial Research.* **47**, 520-533.

Shurygin E.A., 1997: Sodar measurements of the mixed-layer depth over a large city (see this collection).

# Some aspects of estimation of mixing height using vertical Sodar records

J. Walczewski

Institute for Meteorology and Water Management, Cracow, Poland

## Introduction

Vertical sodar is a comparitevely simple means for obtaining continuous information on the ABL structure. This kind of instrument is relatively inexpensive and reliable, and thus widely used all over the world. There are many types of sodars in use, their technical parameters may differ very much one from another. Consequently, their observation results may become incomparable. This fact is not always conceived and taken into account in the interpretation of sodar data. For convective BL the mixing height may be estimated using the formula, developed by Singal et al. (1984):

$$h = k\, z_c + a \qquad (1)$$

where: h - mixing height, $z_c$ - height of the observed convective plumes, k and a - coefficients determined in empirical way. This formula is applied by some authors because of its simplicity (Beyrich 1996; Lokoshchenko 1995; Walczewski 1989). It is evident that the output of this estimation method will differ depending on the maximal height to which a given sodar type is able to follow the convective processes recorded in the form of convective plumes. This height range depends on sodar performances determined by technical parameters of sodar. Similar problem arises when the mixing layer height is defined as the height at which capping inversion layer is observed. Less powerful sodars may miss the echoes of layers situated beyond their range of recognition; at the other hand, more powerful sodars may record the layers situated at higher levels. The consequences for mixing height estimation are obvious.

Problems mentioned above are demonstrated in this paper on the basis of analysis of sodar data from Cracow, Poland (50° N, 20° E).

## Observational Data

The data used for analysis were collected in the years 1980 - 1996 with use of subsequent versions of Polish sodars of „SAMOS" series (Walczewski 1989), whose technical characteristics have been changed several times in the period of 17 years. The first operational model No.2 was used since October 1979 till 1982, later models were marked: 3A (1983 - 1990), 4 (1991 through the first half of 1993), 4C (digital system used since August 1993). The volumes of data files from different years are different, because in some years development works were interfering with regular soundings, thus the total number of observation hours, equal about 68 000, is distributed in not even way.

For determination of maximal range of convective plumes observations it is essential to consider the records from warm season, in which convective processes are having maximal energy and they are able to penetrate to highest levels. Data selected for analysis are taken from the years, in which sufficient representation was found for the warm season (months April through September): years 1980-1982, 1984, 1987, 1991-1996. This collection was complemented by data from years 1985 and 1988, in which the representation of warm season is reduced to 2 months (June - July in 1985 and August - September in 1988), but the number of hours of free convection records is exceeding 200. Total of 9599 hours of free convection records were analyzed. For separate

analysis, 5183 hours of observations of elevated layers, capping convective plumes, were taken into account. As the unit of information was cosidered: mean maximal height of observed convective plumes in 1 hour interval; or: mean height of the base of elevated layer in 1 hour interval.

**Analysis method and results**

The first part of analysis is concerning the maximal observation range of convective plumes. The frequency distribution of observations in different height ranges, in 50 m height increments, was determined for each year (Fig. 1). The year 1993 was presented

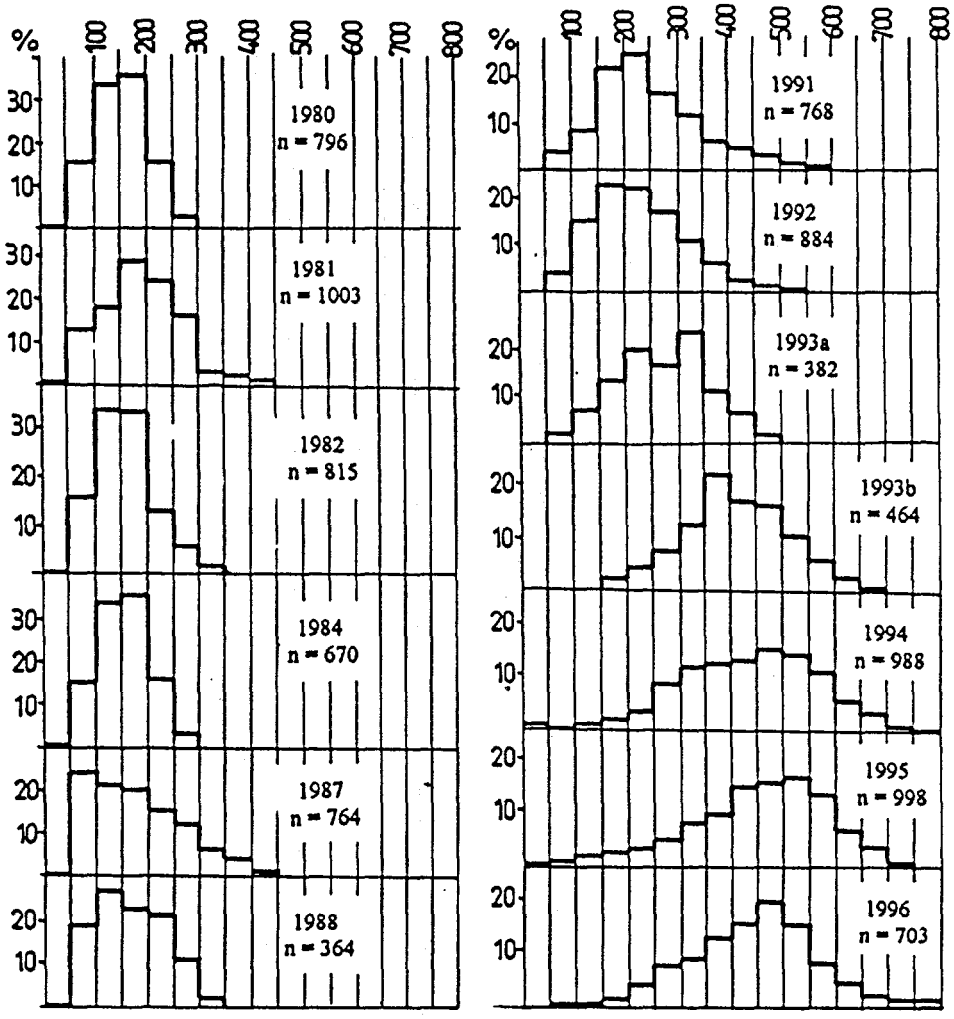


Fig.1. Frequency distribution of convective plumes (free convection) in different height intervals, for different years. Horizontal axis - height in meters, vertical axis - %; n - number of observation hours

in 2 separate graphs: till July (older analog sodar, part „a") and since August (new digital sodar, part „b"). Following indices were determined: $R_{max}$ - height interval reached by the highest recorded plumes (representing not less than 1% of plumes recorded in the year); $z(n_{max})$ - height interval, in which maximal number of plumes was recorded; $z_S$ - center of gravity of the distribution. These indices are presented for individual years on Fig. 2.

In the second part of analysis the same kind of indices (except $z_s$) were determined for elevated layers capping convection (Fig. 3).

Analysis of data, presented on Fig. 2, indicates 3 sodar types, identified by their performances; they may be labelled conventionally: Sodar A (years 1980 - 1988), B (1991 - 1993"a"), C (1993 „b" - 1996). Corresponding indices of vertical range

(calculated as mean values for each group) are as follows (figures in meters):

| | A | B | C |
|---|---|---|---|
| $R_{max}$ : | 357 | 483 | 700 |
| $z_S$ : | 181 | 253 | 439 |
| $z(n_{max})$: | 150-200 | 200-250 | 450-500 |

These characteristics are results of a complex of technical factors, like the magnitude of transmitted power, refinement of antenna design, parameters of electronic circuitry. The most significant improvement of performances was obtained by putting in operation digital sodar „C" with 400 W electric power. What is interesting, further increase of transmitter power to 1000 W (in November 1995) did not contribute in significant way to the increase of the range of recognition of convective structures. This fact suggests an efect of „saturation" or approaching the limits of physical process responsible for backscatter of acoustic wave in convective atmosphere. Below these limits, the range of recorded plume heights depends strongly on technical parameters of sodar - indices $R_{max}$, $z_S$, $z(n_{max})$ are changing in parallel.

Fig. 3. has a different character. It indicates that improvement of sodar performances enables recognition of higher situated layers (increase from 400-500 m up to 900-950 m), whilst the maximum of height distribution does not change its mean position and is oscillating between height intervals 50-100 and 200-250 meters.

The depth of observed ground-based layers seems to be much less affected by sodar performances, because majority of these layers is situated in the height intervals not exceeding 300-400 m.

**Conclusions**

The changes of the vertical range of sodar, depending on technical parameters, were illustrated by resulting changes of the height distribution of convective and elevated layers echoes. The extent of the differences in vertical range may be compratively large.

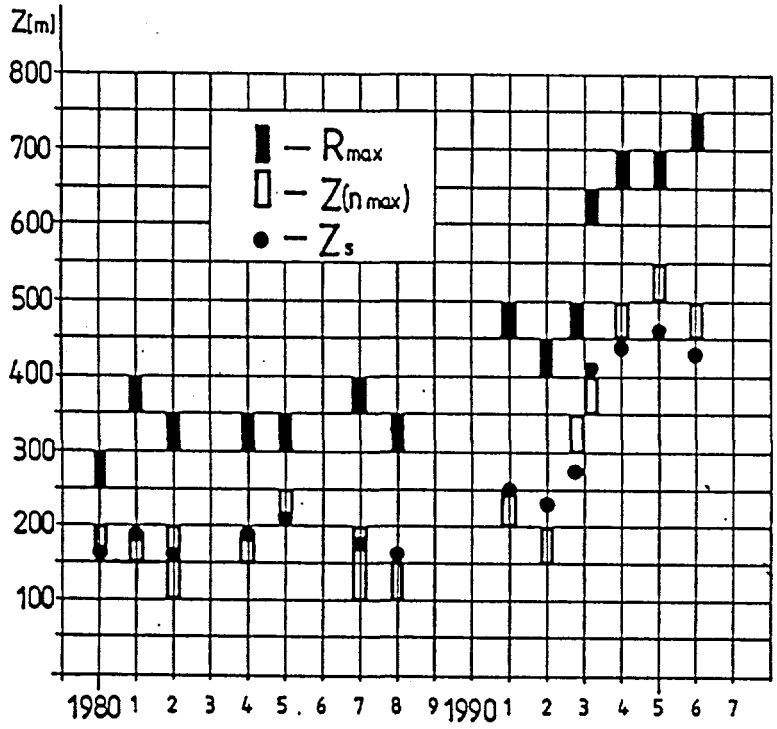


Fig.2. Graphic presentation of indices: $R_{max}$ , z ($n_{max}$), $z_S$ for convective plumes observations in different years; vertical axis - height in meters

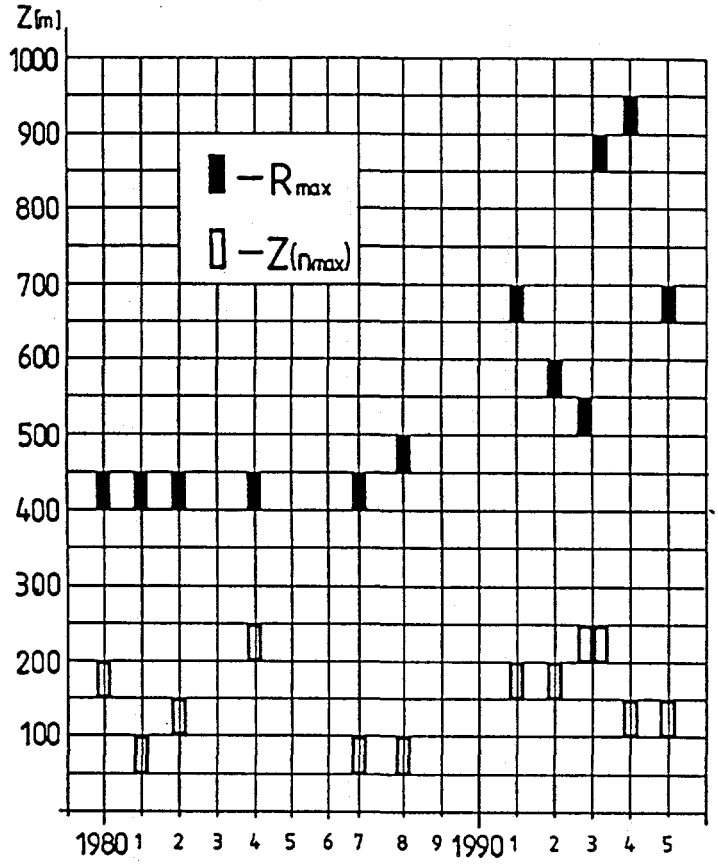


Fig.3. Graphic presentation of indices $R_{max}$ and $z(n_{max})$ for elevated layers capping convective layer, in different years; vertical axis - height in meters

In analyzed case, the maximal heights of convective plumes recorded at the same site with use of 3 types of sodar, were like 1 : 1.35 : 1.96. The relations of mean centers of gravity of frequency distributions were like 1 : 1.4 : 2.4. Consequently, the coefficients in formula (1) have to be matched for each sodar type. Mixing height estimations made with use of formula (1) for different sodars cannot be compared without proper analysis. It has been demonstrated that improvement of sodar performances increased the height of detection of elevated layers by factor of 2. This should be taken into account when mixing height is derived from the observed position of capping layer..

It should be mentioned, that problems indicated above may be related, too, to the methods of stability estimations with use of height characteristics of sodar echoes (Singal et al. 1983; Walczewski 1989).

## References

Beyrich, F., 1996: Mixing height estimation from sodar data - a review.
*8th Int. Symp. Acoust. Remote Sensing, Moscow, May 1996 - Proceedings,* 6.11-6.22

Lokoshchenko , M.A., 1995: On the sodar observations of free convection *(in Russian)*
*Vestnik Moskovskogo Universiteta, Ser.5, No.4.* 43-51

Singal, S.P., Gera, B.S., Aggarval, S.K., 1983: Studies of Boundary Layer at Delhi using sodar.
*2nd Int. Symp. Acoust. Remote Sensing, Rome, Aug.1983 - Proceedings,* XXIII.1-XXIII.8

Singal, S.P., Gera, B.S., Aggarval, S.K., 1984: Nowcasting by acoustic Remote Sensing - experiences with the system established at the NPL, New Delhi.
*J. of Sci. and Industrial Res.,* **43,** *No.3*

Walczewski, J., 1989: Development of sodar and acoustic sounding of the atmosphere in Poland.
*Zeitschrift f. Meteorologie,* **39,** *No.3,* 129-14

Walczewski, J., 1997: Vertical range of recognition of BL structures by sodars with different technical characteristics *(in Polish)*
*Repts. Inst. Meteorol. and Water Mngmt,* **20,** *No.1,* 45-58

# Session VI - Verification of Mixing Height Parameterizations and Models
# Chairperson: Frank Beyrich

# Comparison of Mixed Layer models predictions with experimental data

Paola Faggian[1], Giuseppe Maurizio Riva[1], Giuseppe Brusasca[2]

[1] CISE Spa - Divisione Ambiente, via Reggio Emilia 39, Segrate (MI) - ITALY
[2]ENEL Spa - CRAM, via Rubattino 54, Milano - ITALY

## Introduction

Dispersion models use the concept of Mixed Layer (ML) to determine the turbulent domain in which dispersion takes place. In principle, the depth of the mixed layer can be inferred from vertical profiles of quantities such as wind speed and direction, temperature and humidity, directly influenced by turbulent mixing. However, the actual observed profiles of these atmospheric parameters generally contain complicated structures. As a result, the determination of the mixed-layer depth is often ambiguous under realistic atmospheric conditions, even over relatively homogeneous terrain. Besides, ML values derived from measurements are often available only for limited periods. Then parametrizations are widely used.

In this study, the temporal evolution of the PBL vertical structure for an North Italian rural site (S.Pietro CapoFiume, in the Po Valley about 25Km east far from Bologna), situated within relatively large agricultural fields and almost flat terrain, has been investigated during the period 22÷28 June 1993 by experimental and modellistic point of view. In particular, the results about a sunny day (June 22$^{nd}$) and a cloudy day (June 25$^{th}$) are presented in this paper. Three schemes to estimate mixing layer depth have been compared, i.e. Holzworth (1967), Carson (1973) and Gryning-Batchvarova models (1990), which use standard meteorological observations. To estimate their degree of accuracy, model outputs were analyzed considering radiosounding meteorological profiles and stability atmospheric classification criteria. Besides, the mixed layer depths prediction were compared with the estimated values obtained by a simple box model, whose input requires hourly measures of air concentrations and ground flux of $^{222}$Rn.

## Models considered

The inputs of the applied models were constructed by using meteorological and radiometric data recorded by ENEL Spa and CISE Spa during the experimental campaign in S.Pietro Capofiume throughout 22÷28 June 1993.

The mixed-layer-depth algorithm proposed by **Holzworth** (1967) was selected because of its simplicity as well as its frequent use in air quality modelling studies. In this algorithm, the maximum afternoon mixing height is predicted on the basis of the morning temperature sounding and assuming that the early-afternoon sounding will follow the dry adiabatic lapse rate from the afternoon maximum surface temperature to the point of intersection of the morning sounding. The point of intersection will be the maximum mixed-layer height in the afternoon.

**METPRO (CTDM Meteorological Preprocessor Program)** (Paine, 1988) uses two separate schemes to provide the hourly mixing depths for the two mixing-depth regimes. In particular, during daytime hours, convective and mechanical mixing are assumed to operate independently of one another, and the larger one is selected as the actual value (modified Carson 1973 model). The growth of the convective mixing height depends on the hourly sensible flux H(t):

$$h\,\theta_s(h) - \int_0^h \theta_s dz = (1+2A)\int_0^t \frac{H(\tau)}{\rho c_p} d\tau$$

where A=0.2 (Deardorff, 1980) and $\theta_s$ is the sunrise temperature profile.
In similar manner, mechanical mixing height's formulation is a function of the friction velocity $u_*$:

$$h^2\,\theta_s(h) - 2\int_0^h z\,\theta_s dz = 2\,\frac{BT_0}{g}\int_0^t u_*^3 d\tau$$

where $T_0$ is the surface temperature and B=2.5.

**Gryning and Batchvarova** (1990) proposed an expression for the growth of the internal boundary layer for a range of near neutral and convective conditions, based on parametrizations of the energy balance equation for the boundary layer and the potential jump at the top of it:

$$\left\{\left(\frac{h^2}{(1+2A)h - 2BkL}\right) + \frac{Cu_*^2 T}{\gamma g[(1+A)h - BkL]}\right\}\frac{dh}{dt} = \frac{(\overline{w'\theta'})_s}{\gamma}$$

where $(\overline{w'\theta'})_s$ is the vertical kinematic heat flux at the surface, $\gamma$ is the potential temperature gradient above the internal boundary layer, assumed constant $\gamma$=0.005°K/m for simplicity. A=0.2, B=2.5, C=8 (Tennekes e Driedonks, 1982).

The **$^{222}$Rn box model** considered is based on the following considerations. Atmospheric $^{222}$Rn concentrations exhibit diurnal variations, related to atmospheric vertical diffusion. Within a mixed layer it has frequently been found that $^{222}$Rn concentration are relatively independent of altitude (Lopez et al, 1974). Assuming that $^{222}$Rn concentrations within the mixing layer are homogeneous and variations of $^{222}$Rn concentration in atmosphere depend upon the exhalation rate of $^{222}$Rn $\Phi(t)$ [Bq m$^{-2}$ s$^{-1}$] and radioactive decay (with a decay constant $\lambda=2.1\times10^{-6}$s$^{-1}$), mixing height is evaluated considering mass conservation equation for each time step $\Delta t$ between a given i-hour and the previous one i-1, for the two possible situations:

i) nighttime hours:

$$h_i = \frac{\phi_i \Delta t}{c_i - c_{i-1}e^{-\lambda\Delta t}}$$

ii) daytime hours

$$h_i = \frac{\phi_i \Delta t + h_{i-1}c_{i-1}e^{-\lambda\Delta t}}{c_i}$$

## Results and discussion

Two different thermodynamic situations have been studied:
1) June 22$^{nd}$, a sunny day characterized by a regular solar radiation evolution (with the maximum solar radiation value of 839 W/m$^2$), unstable conditions and typical daily variation of $^{222}$Rn concentrations
2) June 25$^{th}$, a cloudy day characterized by rain during the period 6:30 ÷ 8:30, low solar radiation and absence of daily $^{222}$Rn cycle.

The models have been tested by comparison with data gathered during a field study, to know how reliable the model results are. Information on the vertical structure of wind direction and speed, temperature and humidity were obtained from measurements by radiosonde, rising over 3000m, and tethered balloon flights up to approximately 500m. Radiosoundings, covering about 2-3 Km above ground, provide useful information about PBL thermal structures, whereas tethered balloons are limited by

their inability to penetrate layers above 500m. Anyway, as they provide temperature and wind profiles, they offer the possibility to characterize thermal and mechanical effects in such a layer.

Mixing heights $h$ [m] computed hourly with the different methods have been plotted in the same figures together with profile measurements, for each observation times. In the figures 1÷4 the quantities HO, CA, GB and RN are respectively the mixing height evaluated by Holzworth algorithm, METPRO method, Gryning-Batchvarova model and $^{222}$Rn box model. TPV is the virtual potential temperature [°C], TS is the dry temperature [°C] and R is the water-vapour mixing-ratio [g kg$^{-1}$]. Besides, the dry adiabatic temperature profile is plotted in the same figures. The temperature gradient has been used in conjunction with the humidity profile to determine better the actual depth of the mixed layer.

Generally all three conventional methods describe satisfactory the time evolution of the whole mixed layer, whereas the box model identified substructures of the PBL. Figure 1 illustrates $h$ values calculated by the models at 10:00 together with the radiosounding launched at 9:52. The outputs of METPRO and Gryning-Batchvarova models, even if different (CA=629m, GB=837m), are both related to the variation of TPV gradient, indicating a variation about atmospheric diffusivity characteristic, like it is strengthened by R vertical profile, decreasing from 6.6gkg$^{-1}$ to 4.5gkg$^{-1}$ between 600m and 800m. The box model describes a lower layer (RN=187m), characterized by a very pronounced decreasing with height of water vapour and an adiabatic TPV profile. Figure 2 shows an afternoon situation of the same day: both the conventional models are correctly related with temperature gradient, whereas $^{222}$Rn box model identifies the temperature inversion of about 0.01°Cm$^{-1}$ observed approximately at 400m. Even if such an inversion is not strong enough to be an actual limit for atmospheric motions, it causes obviously a discontinuity about the atmospheric turbulent processes, like it is shown by the R profile.

About the second day, Holzworth, Carson and Gryning-Batchvarova models predict correctly a convective mixed layer. Instead $^{222}$Rn box models calculates a shallower layer characterized by a very pronounced moisture gradient, limited by a change in thermal gradient and related to the surface layer (Figures 3-4).

## Conclusion

The emphasis of the present investigation involves a comparison of well-known and widely used formula for the mixed layer depth with observation obtained from conventional measuring devices. All three conventional models show a satisfactory ability to estimate mixed layer depth, whereas the $^{222}$Rn box model underestimates considerably the PBL height. Such results can be explained considering that the box model request of uniform mixing through the whole mixing layer is not strictly satisfied. Instead, for several situations it gives some information about the surface layer depht.

## References


Carson D.J., 1973: The development of a dry inversion-capped convectively unstable boundary layer. *J.R.Met.Soc., 99, 450-467.*

Deardorff J.W., 1980: Progress in Understanding Entrainment at the Top of the Mixed Layer. *Workshop on the Planetary Boundary Layer J.C. Wyngaard. American Meteorological Society. 36-66.*

Gryning S., Batchvarova E., 1990: Applied Model for the Growth of the Daytime Mixed Layer. *Boundary Layer Meteorology, 56, 261-274.*

Holzworth G., 1967: Mixing depths, wind speeds and air pollution potential from selected locations in the United States. *J.Appl.Meteor., 6, 1039-1044.*

Lopez A., Guedalia D. Servant J., Fontan J., 1974: Advantages of the Use od the Radioactive Traces $^{222}$Rn and $^{212}$Pb for the study of Aiken Nuclei within the Lower Troposphere. *J. Geophys. Res. 79, 1243-1252.*

Paine R.J., 1988: User's Guide to the CTDM Meteorological Preprocessor Program. *EPA Project Report No. 68-02-3421. 149.*

Tenneks H. and Driedonks A.G., 1981: Basic Entrainment Equation for the Atmospheirc Boundary Layer. *Boundary Layer*

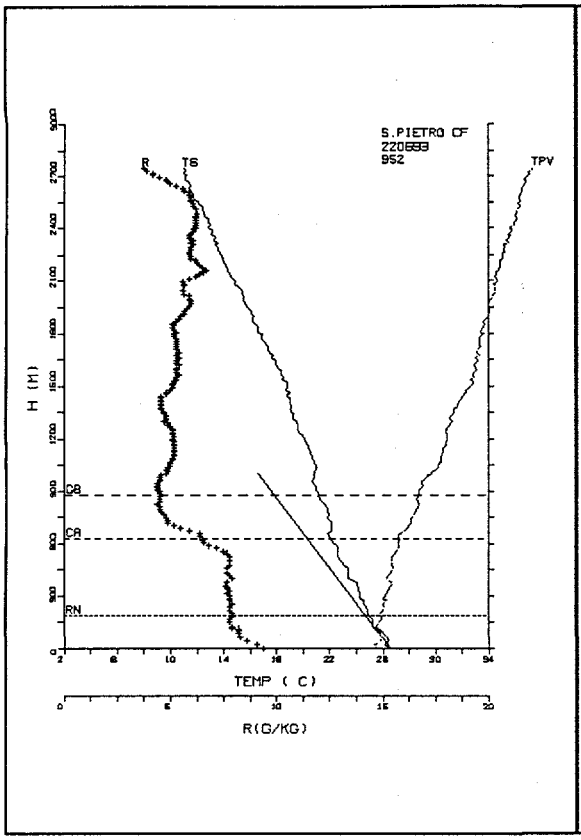


Figure 1

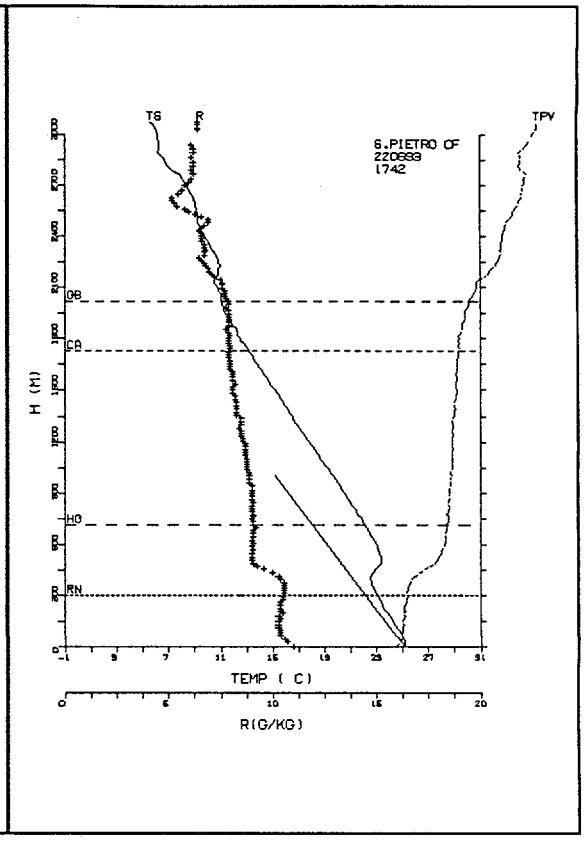


Figure 2

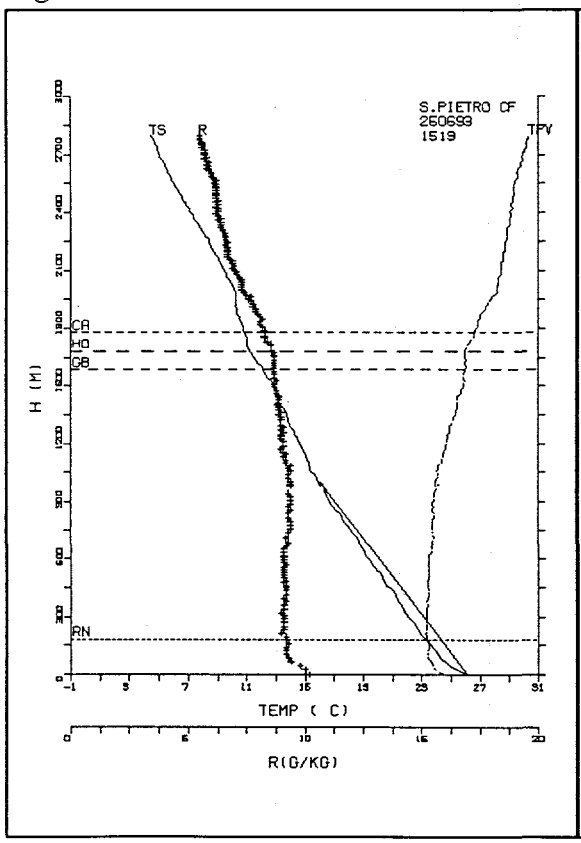


Figure 3

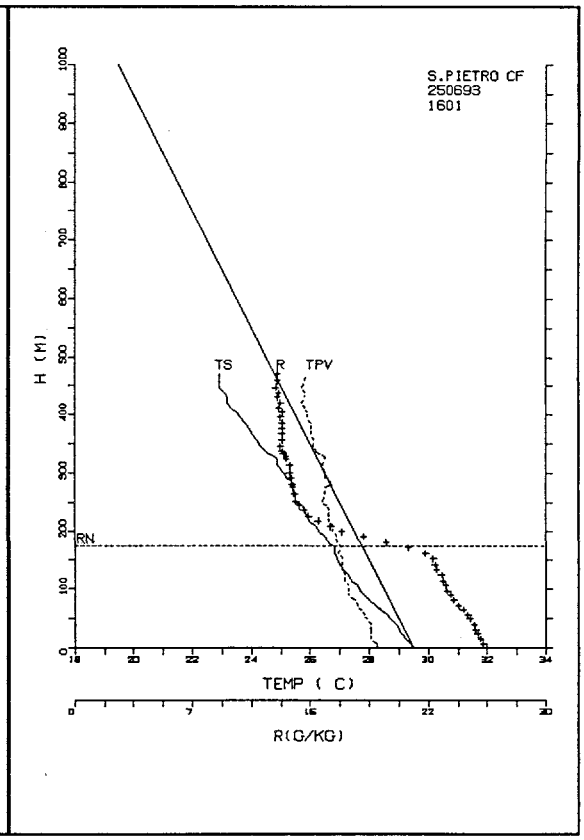


Figure 4

# Validation of Mixing Height Determined from Vertical Profiles of Wind and Temperature from the DMI-HIRLAM NWP Model in Comparison with Radiosoundings

A. Rasmussen, J. H. Sørensen and N. W. Nielsen
Danish Meteorological Institute (DMI), Copenhagen, Denmark

## Abstract

A sensitivity study is performed of vertical profiles from the numerical weather prediction model DMI-HIRLAM (DMI-HIgh Resolution Limited Area Model). The study involves profiles of horizontal wind, temperature and humidity in the lower troposphere up to 2500 meter. Detailed comparisons of analysed as well as forecast profiles are made with measured data from several radisonde stations throughout Europe.

Methods for estimating the Mixing Height (MH) based on a bulk Richardson number method, the Vogelezang and Holtslag method and parcel methods are also studied. The methods are intercompared, and MH based on data from DMI-HIRLAM are compared with the corresponding MH based on radisonde data. For convective conditions the MH estimates are also compared with subjective estimates of the MH.

In this paper preliminary results mainly based on data from Jægersborg (Copenhagen) are presented. Results based on data from 1994-95 show that the resemblance between measured profiles and the DMI-HIRLAM profiles is fairly good in general. Also the estimates of the MH based on DMI-HIRLAM data is in general of nearly the same quality as estimations based on observed data. However, especially in convective conditions there is a tendency by DMI-HIRLAM to underestimate the strength of the mixing and thereby relatively large errors in the estimates of the MH can occur.

## HIRLAM

The HIgh Resolution Limited Area Model (HIRLAM) is an advanced short-range numerical weather forecasting system developed in a joint international research project (Källen 1995).

The analysed and forecast data from DMI-HIRLAM (Sass 1994) are besides the practical dayly applications by duty meteorologists widely used to drive a hierarchy of other models e.g. hydrodynamic models forecasting storm-surge or wave-heights, dispersion modelling for emergency preparedness purposes (Sørensen *et al.* 1997, Sørensen 1997) and air-pollution modelling (Jensen *et al.* 1996). In these latter models wind velocity and direction as well as the mixing height is of crucial importance. The mixing height is estimated by a bulk Richardson number approach (Mahrt 1981, Troen and Mahrt 1986, Sørensen *et al.* 1997).

## Results - profiles

Fig. 1.a-b shows two examples of vertical profiles of temperature, dew point temperature and wind observed at the radisonde station Jægersborg and calculated by DMI-HIRLAM (analysis). For February 27 the observed temperature profile show a well defined boundary layer up to about 600 meter, while the height of the boundary layer from the HIRLAM profile is about 400 meter. Below 400 meter and above 1300 meter the agreement is fairly good. Note the fine agreement for the wind veering from east to west,

but the model wind velocity is too small in the lowest layers. For July 1 again the HIR-LAM boundary layer is more shallow than observed, but the difference is much smaller than for the previous profile. Wind directions and velocities are fairly good.

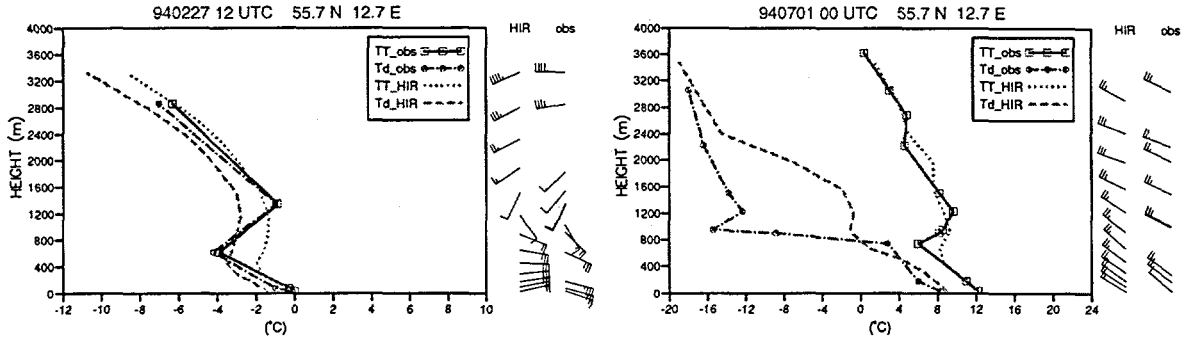


Fig. 1. Profiles of temperature (TT), dew point temperature (Td) and wind (WMO-standard) observed at Jægersborg and calculated by DMI-HIRLAM. (a) February 27, 1994, 12 UTC and (b) July 01, 1994, 00 UTC.

The mean temperature profiles at 00 and 12 UTC for the period July to September, 1994, are shown in Fig. 2.a. Near the ground the HIRLAM temperatures are too low during day, and too high during night, and above 400 meter the HIRLAM temperature is slightly too high both during day and night. Fig. 2.b shows the mean error (ME) and mean absolute error (MAE) for the same period. The MAE is around 1.5 °C near ground decreasing slightly with height. The ME is around -0.8 °C near ground becoming positive above above 300 meter indicating more stable profiles.

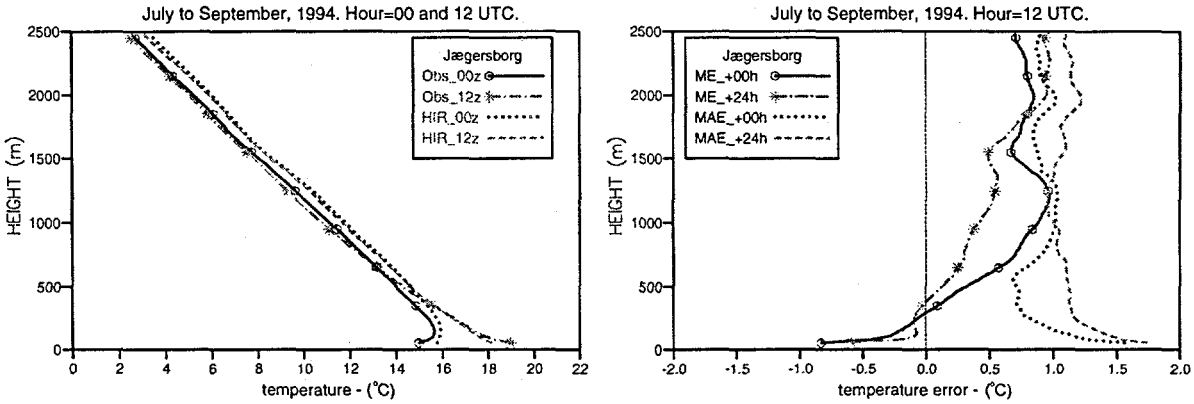


Fig. 2. a) Mean observed and DMI-HIRLAM profiles of the temperature at 00 and 12 UTC for the period July to September, 1994. b) Mean error (ME) and mean absolute error (MAE) for the same period.

The mean profile of wind velocity for the period July to September, 1994, is shown in Fig. 3.a, and the corresponding ME and MAE are shown in Fig. 3.b. Generally the HIR-LAM wind velocity is too high near ground becoming too low higher up, indicting that the vertical gradient of the wind velocity is too small. This is especially important for methods using local gradients of e.g. Richardson numbers. The MAE is around 1.5 m/s for the analysis and 2-3 m/s for the +24 hour forecast.

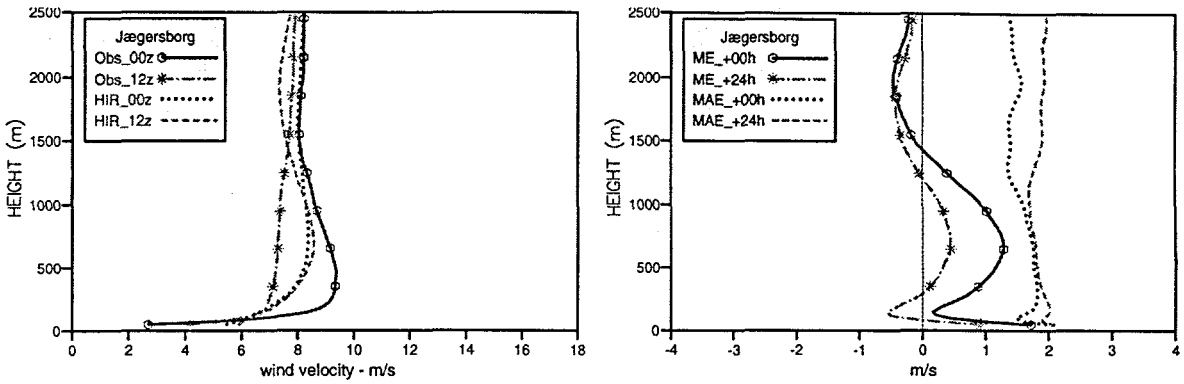


Fig. 3. a) Mean observed and DMI-HIRLAM profiles of wind velocity at 00 and 12 UTC for the period July to September, 1994. b) Mean error (ME) and mean absolute error (MAE) for the velocity profiles for the same period.

Table 1 summarizes the ME and MAE of the temperature profiles at the 50 meter level for 1994-95. The largest errors occur generally in day-time during summer, but the cold weather in autumn '95 resulted in too high model temperatures compared with reality, especially during night.

| Period \ Error | ME 00 UTC | ME 12 UTC | MAE 00 UTC | MAE 12 UTC |
|---|---|---|---|---|
| Jan.-Mar., '94 | 0.4 | -0.7 | 1.2 | 1.3 |
| Apr.-June, '94 | 0.1 | -2.1 | 1.4 | 2.4 |
| July-Sept.,'94 | 1.1 | -1.2 | 1.7 | 2.0 |
| Okt.-Dec.,'94 | 1.7 | 0.3 | 1.8 | 1.0 |
| Jan.-Mar., '95 | 0.4 | -0.5 | 0.8 | 1.0 |
| Apr.-June, '95 | 0.3 | -1.1 | 1.4 | 1.7 |
| July-Sept.,'95 | 0.9 | -1.4 | 1.6 | 1.7 |
| Okt.-Dec.,'95 | 2.4 | 0.6 | 2.5 | 1.5 |

Table 1. ME and MAE of the DMI-HIRLAM temperature profiles at about 50 meter height for Jægersborg 1994-95.

## Results - MH

In the study we are testing 8 different schemes for calculating the MH, cf table 2.

| | **Standard bulk Richardson** | | **Vogelezang-Holtslag bulk Richardson** | | | **Parcel Methods** | | |
|---|---|---|---|---|---|---|---|---|
| | 1 | 2 | 3 | 4 | 5 | 6 | 7 | 8 |
| Lowest level | 2 meter | Lev 31 | Lev 31 | Lev 31 | Lev 31 | 2-meter | Lev 31 | Lev 31 |
| u* | - | - | u*,1 | u*,2 | u*,3 | - | - | - |
| b | - | - | 100 | 100 | 100 | - | - | - |
| $T_{excess}$ | 0 | 0 | 0 | 0 | 0 | 0 | 1.0 K | f(H) |

Comments:

Lev 31: Lowest model level, appr. 33 meter above ground
u*,1 u* calculated by DMI-HIRLAM.
u*,2 u* calculated from wind at 10 meter and at lowest model level (appr. 33 meter) from DMI-HIRLAM assuming logaritmic wind profile
u*,3 u* calculated from wind at 10 meter utilising z0 from the DMI-HIRLAM assuming logaritmic wind-profile
b coefficient in Vogelezang-Holtslag method
f(h) $T_{excess} = 0.5 + 0.003*H$, where H is the sensible heat flux in $W/m^2$

Table 2. Schemes for calcutating the MH

Preliminary results show that the methods (1 and 6) utilising the 2-meter temperature did not give satisfactory results. For the other methods it seems that the standard bulk Richardson gives the most stable results, but it still remains to test over a longer period.

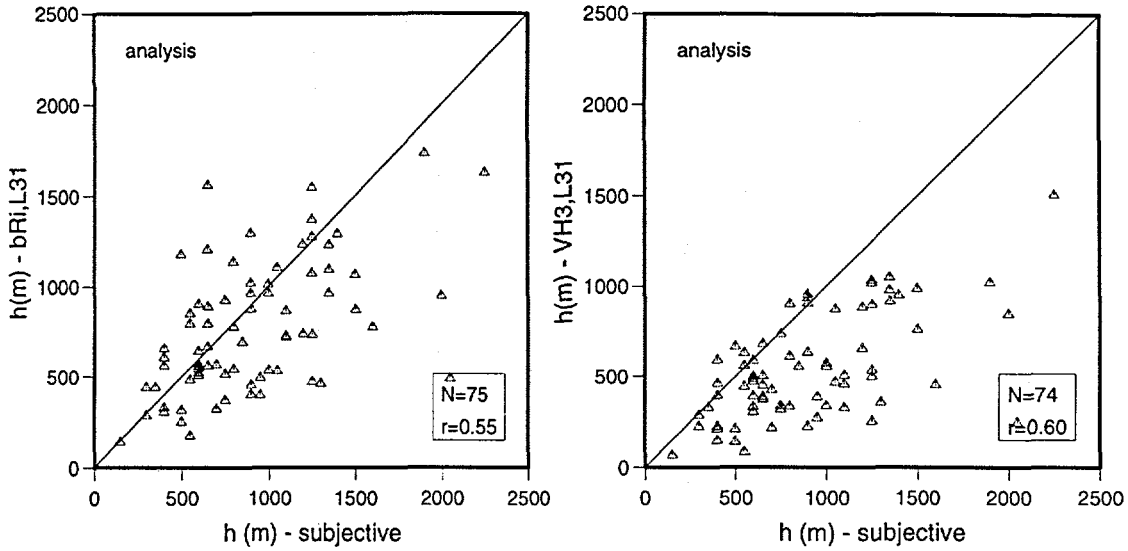


Fig. 4. Scatter plot of subjective MH and a) the MH calculated by standard bulk Richardson method (method 2, cf. table 2) and b) MH calculated by Vogelezang-Holtslag method (5, cf. table 2)

## Conclusion

Preliminary results of a sensitivity study of vertical profiles of temperature and wind from DMI-HIRLAM are presented. In general the resemblance between measurements and the DMI-HIRLAM profiles at Jægersborg is quite good, but especially in unstable and convective conditions there can be large error in the temperature profiles generally caused by too weak development of the boundary layer in this situation.

## References


Jensen, M.H., Rasmussen, A., Svensmark, H. and Sørensen, J. H., 1996: Danish Atmospheric Chemistry Forecasting System (DACFOS), *DMI Technical Report 96-3,* ISSN 0906-897X, DMI, Denmark.

Källen, E. (Ed.), 1996: HIRLAM documentation manual, System 2.5. Available from SMHI, Sweden.

Mahrt, L., 1981: Modelling the depth of the stable boundary-layer. Boundary-Layer Met., **21**, 3-19.

Sass, B.H., 1994: The DMI Operational HIRLAM Forecasting System, Version 2.3. DMI Technical Report 94-8, DMI, Denmark.

Seibert, P., Beyrich, B. Gryning, S.-E., Joffre, S., Rasmussen, A., Tercier, P., 1997: Mixing Height Determination for Dispersion Modelling. COST action 710, WG2. To be published by the CEC.

Sørensen, J. H., Rasmussen, A., Ellerman, T. and Lyck, E., 1997: Mesoscale Influence on Long-range Transport; Evidence from ETEX Modelling and Observations. Accepted for publication in Atmos. Environ.

Sørensen, J.H., Rasmussen, A. and Svensmark H., 1996: Forecasting Atmospheric Boundary Layer Height. Phys. Chem. Earth, Vol. **21**, 435-439.

Sørensen, J.H., 1997: Sensitivity of DERMA to Boundary-Layer Parameters, and Evidence for Mesoscale Influence on Long-Range Transport. I*n: ETEX Symposium on Long-Range Atmospheric Transport.* Ed: Nodop K. Vienna, Austria, EUR 17346 EN pp. 207-210.

Troen, I. and Mahrt, L., 1986: A simple model of the atmospheric boundary layer. Sensitivity to surface evaporation, Boundary-Layer Meteorol., **37**, 129-149.

Vogelezang, D.H.P. and Holtslag, A.A.M., 1996: Evaluation and model impacts of alternative boundary-layer height formulations. Boundary-Layer Meteorol, **81**, 245-269.

# Comparison of Mixing Height parameterizations with profiles measurements

Alain Jaquier, René Stübi and Philippe Tercier

Swiss Meteorological Institute (SMI) – MeteoSwiss
Les Invuardes, CH-1530 Payerne

## Introduction

Different meteorological preprocessors for dispersion studies are available to derive the atmospheric boundary layer mixing height (MH). The analysis of their performances has been reviewed in the framework of the European COST Action 710 (COST-710, 97). In that report, the computed mixing height values have been compared with data derived mostly from aerological sounding analysis and Sodar measurements. Since then, a new analysis of a low-tropospheric wind profiler (WP) data has been performed taking advantage of its high data sampling ($\delta t \sim 30$ sec.). The comparison between these recent results and aerological sounding, Sodar data, as well as to meteorological preprocessors calculations are reported for three periods of several days corresponding to different meteorological situations.

## Meteorological preprocessors

The MH calculations are performed using meteorological preprocessor of the Danish dispersion model (OML) (Olesen, 1987) and of the Hybrid Plume Dispersion Model (HPDM) (Hanna, 1989). Different parameterization levels, required for flux computation, can be use as input. In this contribution for both preprocessors, net radiation measurement additionally to conventional measurements have been used. Some modifications in the programs have been introduced in order to use the sensible heat flux measurements as well. Both preprocessors require the potential temperature profiles from the aerological sounding. The HPDM need the stable nocturnal profile while the OML take advantage of the diurnal profile to update the atmospheric conditions at midday.

## Remote sensing data

The characteristic heights (CHs), measured here with a WP (RADIAN LAP 3000), are defined as heights corresponding to signal to noise ratio (SNR) maxima of the back-scattered electro-magnetic waves profile. The inverse quadratic distance correction is used while the exponential attenuation is not considered. The SNR is proportional to the refractive index structure parameter $C_n^2$ sensitive to turbulence variations and changes of temperature and moisture content. So, most of the CHs are signature of inversion layer, top of the mixing layer or moist layer boundaries.

The method applied (Jaquier, 1997) uses the three beams raw spectrums, internally averaged over 30 s. It exploits the wind components spatial and temporal continuity to pick the clear air signal and combines the beams to obtain the temporal evolution of the CHs. The profiler used in this study runs alternatively on two modes: the low mode has 30 levels with 60 m resolution and the high mode has 22 levels with 200 m resolution.

The Sodar (REMTECH PA1) has 30 levels with a resolution of 20 m and the averaging time was set to 30 minutes. The MH algorithm sold by REMTECH for the Sodar uses the peak frequency in the vertical velocity spectrums (for each measurement level), which are transformed to a wavelength related to the MH.

**Case studies**

The measurement location is nearby Payerne (Switzerland), a site located in a 70km wide hilly basin surrounded in the Northwest by the Jura mountains and in the Southeast by the Alps. Three episodes have been studied, a foggy winter period and two spring sunny episodes with low to high winds in the MH. The Figure illustrates the three time series including the following data:

- the potential temperature profiles (solid lines, inner lower scale: 0 – 30 [°C]) and relative humidity profiles (dashed lines, inner upper scale: 0 – 100 [%]) measured every 12 hours (launch time at 0 UTC - 1 and 12 UTC - 1) by the aerological sounding systems,
- the wind profiler CHs (dots) deduced from both modes data (except upper panel),
- the Sodar MH determined with the REMTECH software (diamonds),
- the MH derived by the HPDM (squares) and the OML (circles) models both computed with parameterized turbulent fluxes.

**Episode 1: Winter fog , 27 - 30 January 1997**

A weak depression above Central Europe was progressively filled from the West. Starting January the 27$^{th}$, a strong anticyclone centered above the British Islands extended to Romania. Since the 28$^{th}$, a northeasterly wind flew, channeled between the Jura Mountains and the Alps, and weakened progressively along this episode. Weak precipitation took place in Payerne in the early morning of the 28$^{th}$. Latter on, a fog layer settled for several days with brief partial fog dispersal in the afternoons.

As seen on the top panel of the figure, the 27$^{th}$ the WP tracks the rising clouds tops until the short precipitation period (top panel of the figure). Subsequently the WP remarkably follows the fog layer top, which is decreasing as the wind weakens, in good agreement with the sounding profiles. Sub-structures appear intermittently. During the daytime of the 28$^{th}$ and the 29$^{th}$, these are partially coinciding with the Sodar MH estimates.

The MH determination by the HPDM preprocessor switched every days to the convective algorithm output as soon as the sensible flux get positive. The OML uses the mechanical algorithm on the 27$^{th}$ and 28$^{th}$. On the 29$^{th}$ and 30$^{th}$, it shifts to the convective algorithm around noon. For these last days, the HPDM convective estimates reach quickly high values due to the almost uniform potential temperature under the fog layer.

**Episodes 2 and 3: Spring clear sky days, 15 - 18 April and 26 - 29 May 1997**

In the April period, the alpine region was under the influence of a strong anticyclone centered over North Atlantic. The 16$^{th}$ and 17$^{th}$ of April are characteristic days of an installed moderate to strong northeasterly flow, with surface temperatures ranging from –2 to 10°C. The wind on the 15$^{th}$ and 18$^{th}$ of April are low and from the southwestern sector, the surface temperatures are slightly higher. The surface specific humidity is low (2-4 g/Kg) during the daytime hours in this period.

In the May period, Switzerland was under the south part of an anticyclone centered on the Great Britain. The winds were low with no well defined direction excepted the 28$^{th}$ and the 29$^{th}$ of May when, in the daytime hours, the northeasterly wind is moderate to high. The surface temperature daily cycle is similar to the April period but 10°C higher. The surface specific humidity is significantly higher (6-8 g/Kg) than in the April period.

For these Spring episodes, the CHs from both low and high WP modes are plotted on the figure and only small differences between them can be observed. In windy conditions, the wind profiler often shows a well-defined MH evolution from the morning convective growth to the nocturnal residual layer. In low wind conditions, the WP determined CHs do not give a clear picture of a growing convective MH. The CHs are linked to stratified structure of the humidity profile which seem to be absent in presence of established wind. The SNR profiles do have more CHs in these low wind conditions than in strong wind conditions. Further adjustments of the filtering algorithms are necessary to see if such CHs could be linked to real phenomena like large eddies.

The mixing height data are significantly higher during the April episode than during the May episode because of a lower Bowen ratio in last period. As a matter of fact, the measured sensible heat flux reached values higher than 250 $Wm^{-2}$ in April but stood below 200 $Wm^{-2}$ in May.

The constant height sub-structures (~950 m and ~1200 m) appearing in the daytime on the 16$^{th}$, 17$^{th}$ April and the 28$^{th}$ May, are linked with ground clutter perturbations occurring by strong winds.

Along both considered episodes, the HPDM selects the convective procedure for daytime hours. The output values are similar in both period and larger than experimental data, especially in the May period. Just after midday, the growth rate of the MH presents a discontinuity, which stays unexplained.

The evaluation of the convective MH out of the Sodar measurements do not correspond to any features in the temperature and humidity profiles. The values of the MH are limited to below twice the measurement range of the Sodar (~1000 m agl), which is probably not realistic.

## Conclusion

In convective conditions, the preprocessors give reasonable level, the mixing height growing rate is in fair agreement with the measured one. In stable cloudy daytime conditions, the modeled mixing height does not correspond to any measured heigth.

The wind profiler data permits to follow the evolution of the mixing height, and others characteristic height, along whole days with high temporal resolution. These heights are in good agreement with those observed on the sounding profiles. They also cover a much wider range than those estimated by the REMTECH Sodar algorithm. This study has shown that the benefit obtained by using the high sampling rate of the wind profiler is large compared to the use of the averaged data (e.g. 30 minutes). Final adjustment of the filtering process to reject the irrelevant maxima (i.e. characteristic heights) has still to be done. However, based on the analysis of such episodes, the perspective of systematic use of WP for tracking the MH evolution is good.

## References


COST-Action 710: *Harmonization in the pre-processing of meteorological data for dispersion models*, (Final report to be published 1997).

Hanna S. R., Paine R. J., 1989: *Hybrid Plume Dispersion Model (HPDM) Development and evaluation.* J. Appl. Meteorol. 28, 206-224.

Jaquier A., Ruffieux D., and Stübi R., 1997. *Multi-Peak Analysis and Determination of Characteristic Heights with a Low-Tropospheric Wind Profiler.* COST-76 Profiler Workshop (PWS-97), 12-16 May, 1997, Engelberg, Switzerland.

Olesen, H. R., Jensen A. B., Brown N., 1987:*An operational procedure for mixing height estimation.* Risoe Nat. Lab. MST-Luft-A96. End edition 1992, 182pp.

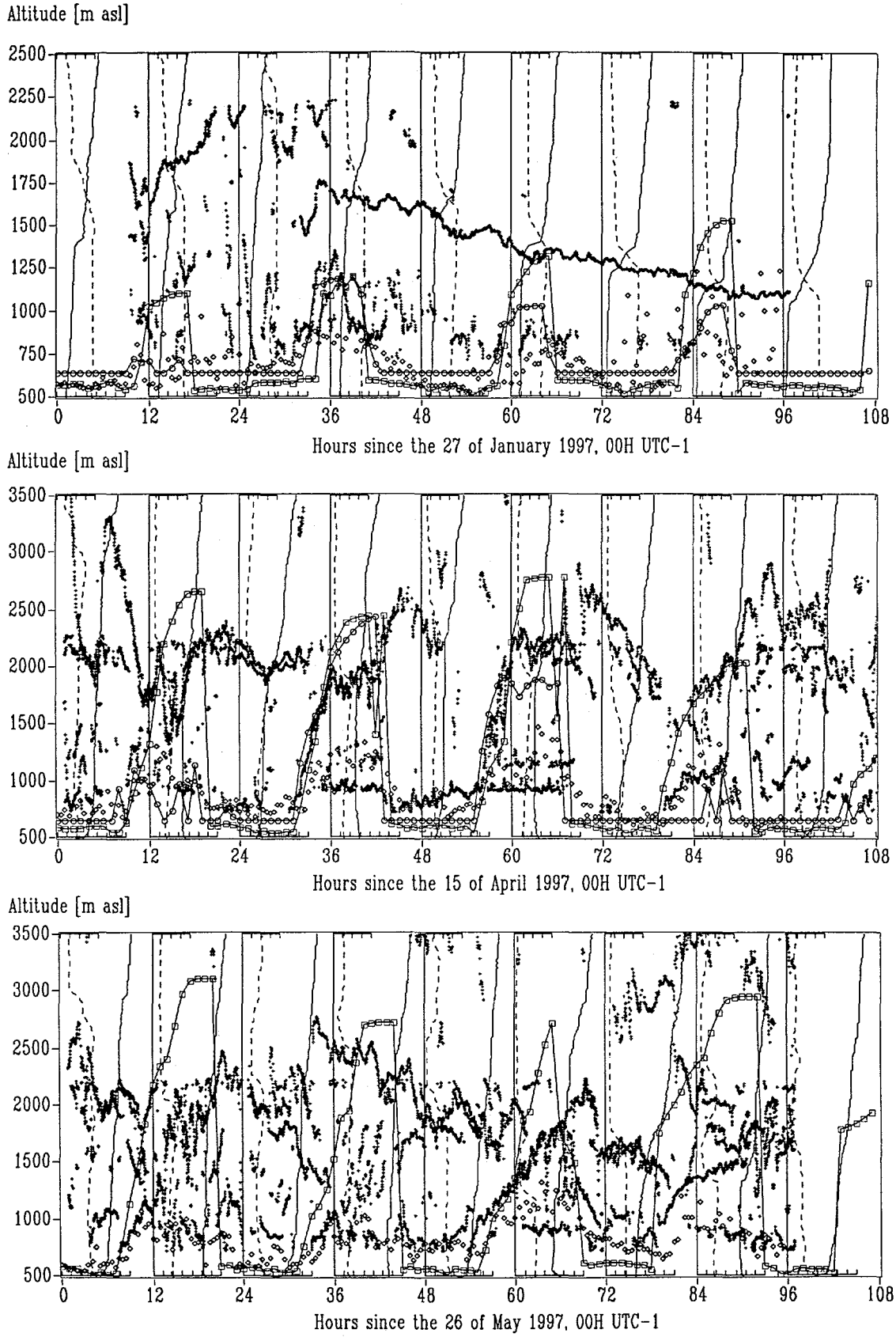


Figure. See text for details.

# Comparison of Measured and Modelled Mixing Heights during the Borex'95 Experiment

T. Mikkelsen[1], P. Astrup[1], H. E. Jørgensen[1], S. Ott[1], J. H. Sørensen[2], P. Løfstrøm[3]

[1]Risø National Laboratory, Roskilde, Denmark
[2]Danish Meteorological Institute, Copenhagen, Denmark
[3]National Environmental Research Institute, Roskilde, Denmark

## Introduction

A real-time modelling system designed for "on-the-fly" assessment of atmospheric dispersion during accidental releases is under establishment within the framework of the European Union. It integrates real-time dispersion models for both local scale and long range transport with wind, turbulence and deposition models. As meteorological input, the system uses both in-situ measured and on-line available meteorology. The resulting real-time dispersion system is called **MET-RODOS**, Mikkelsen et al.(1997), and is integral part of the real-time on-line decision support system for nuclear emergencies, **RODOS** (Ehrhardt 1996; Kelly et al., 1996; Ehrhardt et al., 1997).

This paper focuses on evaluation of the **MET-RODOS** systems build-in local scale pre-processing software for real-time determination of mixing height, - an needless to say important parameter for the local scale dispersion assessments. The paper discusses the systems local scale mixing height algorithms as well as its on-line mixing height acquisition from the DMI-HIRLAM model. Comparisons of the diurnal mixing height evolutions is made with measured mixing heights from in-situ radio-sonde data during the Borex'95 field trials (Jørgensen et al., 1997), and recently also with remote sensed (LIDAR) aerosol profiles measured at Risø.

## Determination of Mixing height in MET-RODOS

The meteorological model chains in **MET-RODOS** runs nested on directly measured or real-time predicted weather data available from local meteorological towers and/or via data coming from remote national or international Numerical Weather Predicting (NWP) centres. **MET-RODOS** is designed to produce estimates of actual (real-time) and forecasted (+36 hour) ground-level air concentrations, wet and dry deposition, and ground-level gamma dose rates on all scales. **MET-RODOS** incorporates in this way both real-time input data from both on-line meteorological towers and high-resolution (pt. 20 km x 20 km grid) NWP data from the Danish **DMI-HIRLAM** model.

## Methods to determine the atmospheric Boundary Layer (ABL) Height

The local scale model chain includes real-time mixing height predictions in basically two independent ways: 1) By use of build-in so-called "**PAD**" mixing height subroutines, one for stable/neutral mechanically-determined mixing height , and one for convective-determined mixing height (Mikkelsen and Desiato, 1993), which calculates the boundary layer height from either in-situ measured or predicted surface layer turbulence ($u_*$ and $T_*$), and: 2) via analysis of the vertical temperature profile in NWP data. While the first method is applicable for **MET-RODOS** in diagnostic mode (now-casting) only, the latter can be used also in forecast mode (+36 Hr).

The **MET-RODOS** pre-processor manages the real-time data handling and storing. It:

- Establishes communication protocols, handshakes and data formats for external data communication with available on-line <point-based > <met-stations>, including <NWP forecast data> for a set of pre-specified <NWP grid-points>, which can be located both inside and outside the local scale domain.
- captures "On-the-fly" (temporal storage) the <point-related primary met-data>, such as mean wind and temperature profiles, coming on-line to the system at random.
- Automatic unpacks, decodes, sorts, time stamps and stores all <point-related primary met-data> into the <Local Scale Preprocessor real-time data base>.
- Archives the corresponding time-independent <point-related stationary data>, such as <latitude>, <longitude> and <elevation> coordinates, including <aero-dynamical roughness $z_0$>, <land use>, etc.

The task of the preprocessor furthermore involves preprocessing of the at any time available measured or predicted *<single point primary met-data>* into corresponding micro-meteorological *<scaling parameters>*, such as turbulent shear-stress ($u_*$) and heat-flux ($T^*$), deposition velocities, mixing heights ($H_{mix}$), and the Monin-Obukhov atmospheric stability parameter (L).

**Mixing height from locally measured - or predicted - values of $u_*$ and $T_*$**

The local scale preprocessor contains two subroutines for determination of mixing height. One for convective conditions called "mixh_con", and one for mechanical turbulence controlled mixing height, called "mixh_mech".

The "mixh_con" subroutine estimates the convective mixing height based on the "slab" model described by Batchvarova and Gryning (1990). In order for this model to initialize properly, we have chosen to start the model integration at the first positive (upward) measured or predicted heat flux after midnight.

The "mixh_mech" subroutine estimates the mechanical mixing height mixh_mech from surface heat and momentum fluxes according to Niewstadt (1981): $hf(1/c_1 + h/c_2L) = u_*$, where h is the mixing height, L is the Monin-Obukov length, f the Coriolis parameter and $u_*$ the friction velocity. In this study we have used $c_1 = 0.3$ and $c_2 = 0.49$ together with a maximum allowable mechanical mixing height of 1500 m.

In the **MET-RODOS** local scale pre-processor, we have chosen to represent mixing height as the largest of the two , i.e.: $H_{mix}$= MAX[mixh_con, mixh_mech].

**Mixing heights in MET-RODOS from analysis of NWP data**

Sørensen et al. (1997) has devised a method suited for use with **DMI-HIRLAM** NWP outputs. The method is based on calculations of bulk Richardson numbers,

$$Ri_B = gz(\theta_v - \theta_s)/\theta_s(u^2+v^2) \qquad (1)$$

Here, $z$ is the height, $\theta_s$ and $\theta_v$ are the virtual potential temperature at the surface and at height $z$, respectively, and $u$ and $v$ are the horizontal wind components at height $z$. The height of the ABL is given by the height at which the bulk Richardson number reaches a prescribed critical value. The method has recently been tested (Sørensen *et al.*, 1997). The optimal value for "the critical" bulk Richardson number turned out to be 0.14. See also the paper by Sørensen and Rasmussen on mixing height determination from NWP data previous in these proceedings.

**Mixing height measurements during the Borex'95 field study**

The Borex'95 field experiment took place in July'95 near the town of Borris in Western Jutland, which is located about 20 km inland from the North Sea coast line. The field study resulted in a directly measured "concentration fluctuation data base" which contains high-resolution spatial and temporal resolved concentration fluctuation measurements from elevated plumes. The dispersion studies were accompanied by detailed micro-meteorological wind and turbulence measurements including daily balloon soundings for in-situ determination of mixing heights.

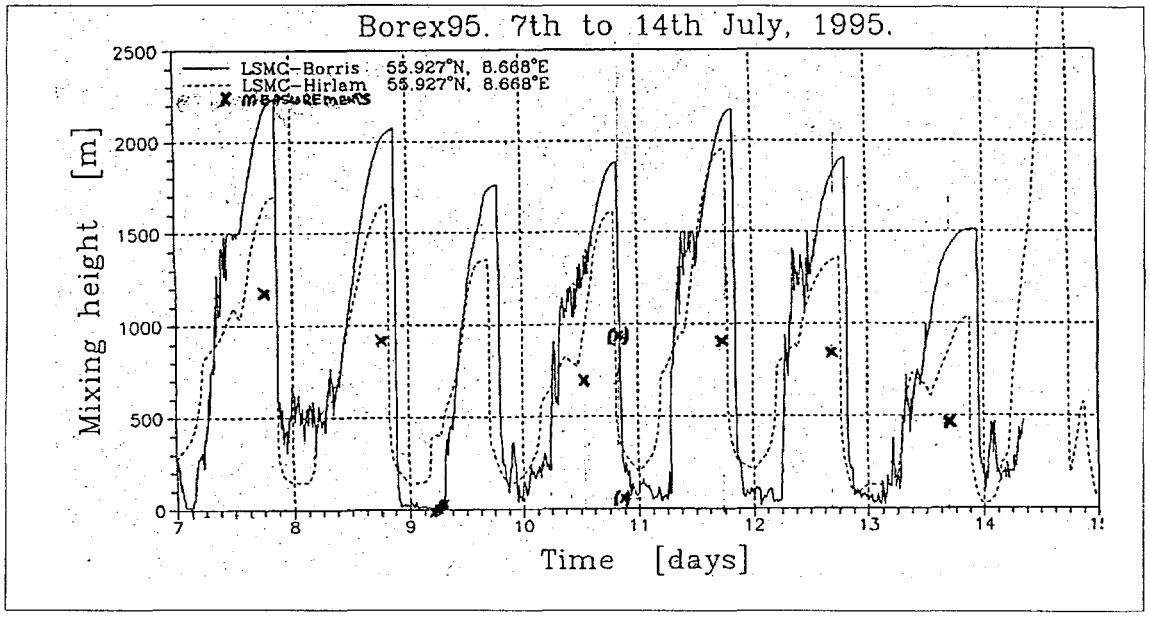


**Figure 1**

Comparison of radio-sonde measured (x) and Local Scale Model Chain (LSMC) predicted Mixing heights during Borex' 95 from July 7 to July 15. The full line represents mixing height calculations based on directly measured momentum and heat fluxes determined from a sonic anemometer at the test site. The dashed line represents "LSMC-PAD"determined -mixing heights during the period based on DMI-HIRLAM predictions of temperature and momentum fluxes at the nearest-by HIRLAM grid point. The values indicated in parentheses (x) have been estimated or extrapolated. In the morning of July 9, a clear ground-based inversion height was measured from a 20 metre tall met-tower equipped with 10 thermocouples. The inversion starts to break up at 5:40 am near the ground (0.23 m) and has grown to 20 metres at 6:50 am.

Figure 1 shows that the **MET-RODOS** local scale build in preprocessor apparently over predicts (by almost a factor of two) the measured mixing heights during Borex'95, both for the mechanical, and also for the convective part, and independent of source of input (in-situ at Borris or Hirlam).

Figure 2 shows comparison of measured and Hirlam-provided mixing heights for the same Borex '95 period. The NWP data shows in this case much better agreement with the mid-afternoon balloon soundings. On the other hand is the July 9. 5:40 am low inversion break-up is not so well predicted as in Figure 1.

**Discussions**

This intercomparison of NWP-based and In-situ-based mixing height determination comes in this study out in favour of the NWP data method. It should be noticed that we have used default coefficients ($c_1$, $c_2$ - and also upper-air lapse rate $\Gamma$=0.005) in this study. Very possible, the in-situ method can be better calibrated for real-time use within the operational met-rodos framework, but more extensive data sets of surface scaling parameters and mixing height are then needed. We have just begun to study continuously (with an averaging time ~ a few seconds) mixing heights at Risø by use of an operational aerosol-backscatter lidar system. An on-line sonic anemometer for surface flux measurements has

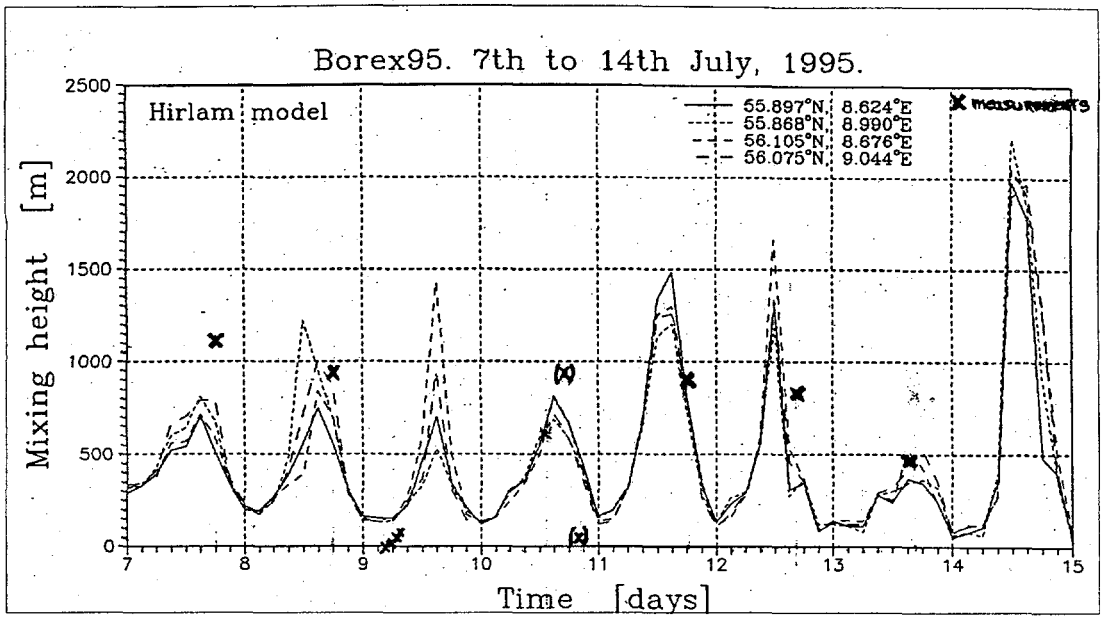


**Figure 2**

Comparison of the radio-sonde measured (x), and LSMC predictions of the mixing height during Borex' 95 from July 7 to July 15. The lines shown are mixing height predictions based on the "Critical Richardson No. Method by Sørensen et al( 1997) available from NWP forecasts for the period (analysed data). The data has been provided to **MET-RODOS** from DMI-HIRLAM.

also been put in continuous operation at the 123 metre tall met-tower at Risø. From such lidar measurements (see Figure 3) we aim at getting more mixing height data for calibration of the in-situ method in **MET-RODOS**.

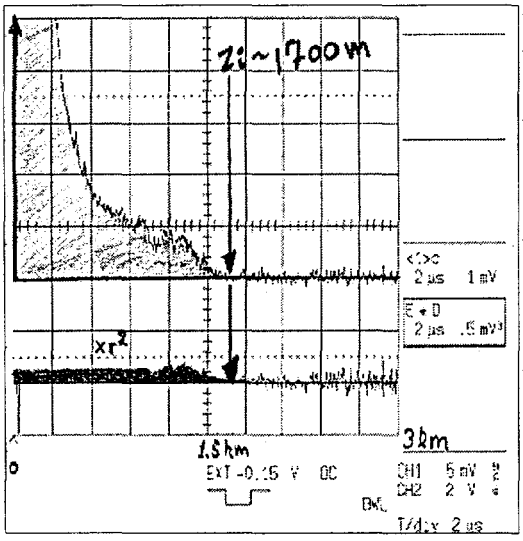


**Figure 3** Lidar-measurement of the aerosol-backscatter profile over Risø on September 18. 1997 at 13:00 UTC. The mixing height based on the aerosol distribution is determined to be~ 1700 metres. The grafs show: 1) (upper curve) the directly measured detector signal, and 2) (lower curve) the range square-corrected backscatter signal. The backscatter is seen to vanish at 1700 metres hight, which is interpreted as the top of the mixing layer. The lidar shoots at 50 Hz rep rate with a ND:YAG laser (1.064 μ, with 2-10 m-Joule pr shot.. 1000 range gates are shown(0- 3 km). A moving average of 1.2 sec has been applied.
The Risø backscatter Lidar will operate during the Eurasap workshop.


## Acknowledgements

This study has been supported by the Danish Environmental Research Program 1992-1996, and by the Forth EU DG XII Radiation Protection Research Program 1996-1999.


## References


Mikkelsen, T., S. Thykier-Nielsen, P. Astrup, H. E. Jørgensen, J. M. Santabárbara, A. Rasmussen, J. Havskov Sørensen, L. Robertson, C. Persson, S. Deme, R. Martens, J.G.Bartzis, P. Deligiannis, N. Catsaros and Jürgen Päsler-Sauer (1997): **MET-RODOS**: a comprehensive atmospheric dispersion module. Radiation Protection Dosimetry, 1997 (In Press).

Sørensen, J.H., Rasmussen, A., and Svensmark, H. (1996): Forecast of Atmospheric Boundary Layer Height Utilised for ETEX Real-time Dispersion Modelling.Phys.Chem Earth, Vol 21, No 5-6, pp 435-439.

Jørgensen, E., Mikkelsen, T., Streicher, J., Herrmann, H., Werner, C. and Lyck, E.: "Lidar calibration experiments". Applied Physics B., Vol. 64, pp 355-361, 1997.

# Some parameterization formulae for mixing height compared with joint Sodar and Lidar observations

A.Bielak, J.Burzyński, W.Kaszowski, J.Walczewski

Institute for Meteorology and Water Management
ul. P.Borowego 14, 30-215 Cracow, Poland

## Introduction

The mixing height (MH) is most frequently defined in terms of the mixing mechanism: atmospheric turbulence and its variability versus height. The MH is described as the height at which the turbulent heat flux obtains minimum value or zero (Taconet and Weil, 1983; Genetay, 1988). The mixing intensity, therefore, is decreasing with height. Consequently, the real mixing of a matter like gas or aerosol may not reach the top of MH determined on the basis of thermodynamic considerations. From the practical point of view it is more important to know the height of mixing of real polluting substances, than the absolute ceiling of turbulent processes. This approach is followed by many Authors, especially those using lidars for observations of aerosol or gas mixing. In this paper effort is made to bring some contribution to these studies; authors were encouraged for this research by some airborne observations of $SO_2$ mixing height reaching only a fraction of the height of capping inversion in convective BL (Walczewski and Orkisz, 1994). The paper presents the results of selected observations of aerosol mixing height, compared with sodar observations of BL structure and with the MH calculated with use of different formulae taken from literature. All measurements were made in Cracow, Poland.

## Observational data

The aerosol MH was estimated on the basis of lidar soundings. The lidar used for measurements was a mobile unit loaned by Dutch company N.V.KEMA. It was implemented with a Nd-Yag laser with doubled frequency (effective $\lambda$ = 532 nm); pulse frequency 10 Hz, pulse length 6 - 7 ns and mean pulse energy 150 mJ. The receiver aperture has diameter 26.6 cm. The sounding beam was inclined at the angle 19 - 60°. Lidar signal was normalised by $R^2$ (square of distance). Obtained backscatter intensity versus distance was projected on the vertical axis and presented in form of darkening of corresponding segments of the time-height record, in 8 steps of grey-tone scale. The aerosol mixing height was defined as the height at which signal drops to zero (end of the grey zone). Layers in the limits of the grey zone (differences in grey scale) are considered as „internal structure". Separate layers above the grey zone are considered as elevated layers. The acoustic soundings were made with use of Polish "SAMOS-4C" vertical sodar with electric power 1000 W, pulse length 30 ms, acoustic frequency 1.6 kHz, antenna dish area 1.13 $m^2$, digital processing system. The output was presented in the form of ordinary sodar echograms (Figs. 2 - 3 ). In the years 1994 - 1996 data from 422 hours of lidar observations were collected; sodar and ground-based observations were practically continuos, and in some periods tethered-balloon soundings were performed (total number 91). Available data were used in MH calculations.

## Parameterization formulae

Formulae used for calculations are listed below; they were taken from papers of following Authors: Blackadar and Tennekes (1968), Nieuwstadt (1981), Tennekes (1970), Zilitenkevich (1972). Formula No. 1.8. was developed by J.Burzyński.

| Nb. | Formulae | coeff. | PGT | used by: |
|---|---|---|---|---|
| 1.1 | $h = c_1(\frac{u_* L}{f})^{1/2}$ | $c_1$=0.22-0.7 | F | S. S. Zilitinkevich |
| 1.2 | $h = c_2 u_*^{3/2}$ | $c_2$=2400 | E,F | |
| 1.4 | $h = c_5 u(10m)^{3/2}$ | c5=28 | E,F | F. T. Nieuwstadt |
| 1.6 | $h = c_6 \frac{u_*}{f}$ | | D | A.K. Blackadar H. Tennekes |
| 1.8 | $h = c_{10} \frac{(u(10m))^{1/2}}{(t(10m) - t(2m))^{1/4}}$ | $c_{10}$=125 | E-F | |
| 1.9 | $h = c_{11} \frac{u_*}{f}$. | $c_{11}$=0.25 | A-C | H. Tennekes |

Authors were also testing formulae of Deardorff (1.3), Erbrink (1.5), van Dop (1.7).

**Discussion of results**

The top of sodar-observed ground-based inversion ($z_g$) is generally in good correlation with the upper limit of ground-based inversion determined by temperature profile (correlation coefficient r = 0.69 for n = 50). Comparing the aerosol MH from lidar observations ($z_L$) with $z_g$ for stable BL and for 142 cases from March, May, June and November, it has been found that generally $z_L$ is higher than $z_g$ . Denoting $z_L/z_g = s$ we have s = 1 - 1.1 for 19% of cases, highest contribution (22.5%) of cases with s = 1.1 - 1.3, and only 7.7% of cases (all from warm season) with s<1. Value of s > 2.1 is for 11.9% of cases; such values are most frequently observed after wave structures recorded by sodar. The impact of wave structures may be extended for several hours after disappearing of waves.

Fig.1. presents an example of comparisons of balloon, sodar and lidar observations in the period of 25 May 1995, 16.00 GMT - 26. May, 10.00 GMT. The top of sodar-observed ground-based layer follows the ground-based inversions on temperature profile. Sudden increases of the wind speed at 50m and 200m height, at 19.30 - 20.00 hrs resulted in jumps of lidar-observed layers at about 21.00 and 22.00 hrs. Ground-based aerosol layer height is variable at night; in the morning hours it is situated above the peaks of sodar-observed convective plumes (in height relations 1.3 - 2).

Fig.2. shows an example of neutral stability. Calculated values of MH are in good agreement with the height of sodar record of wind noises, whilst the lidar-observed aerosol layer is much deeper (by factor of 2 - 2.2). Observation of other cases of neutral stability reveals the effect of „inertia" of aerosol layer which preserves through some time its height obtained during earlier period (for instance, in the phase of convective BL).

Fig.3. refers to unstable case, in which both aerosol layer and calculated MHs are very near to the heights of sodar-observed convective plumes. The same height was indicated by software built-in in the REMTECH PA-2 Doppler Sodar, using parameterization of the vertical turbulent heat flux (Genetay, 1988). This parameterization, by the rule, gives MH equal the peaks of convective plumes recorded by vertical sodar of SAMOS-4C class. However, in many other observations in convective BL, the aerosol MH observed by lidar was much higher than convective plumes, even by factor 2 - 3.

**Conclusions**

The analysis of rather broad material does not give any fixed rules for relations between aerosol MHs from lidar observations and sodar indices of MH, like $z_g$ or peaks of convective plumes. The values of $z_L$ are also often exceeding the heights of sodar-

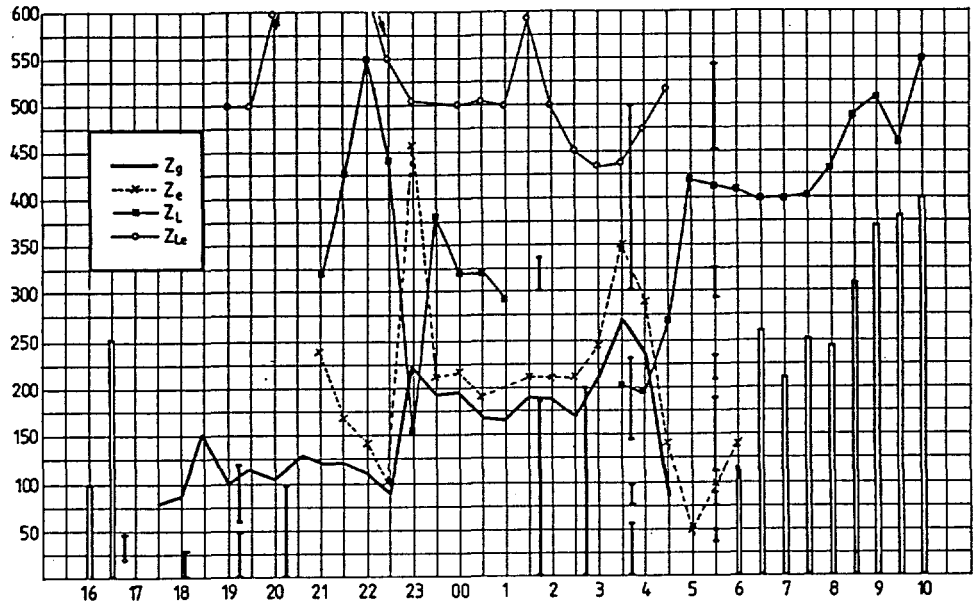


Fig.1. Comparison of different observational indices of MH for the night 25/26 May 1995. Vertical axis - height in meters, horizontal axis - time in GMT. Heavy vertical lines - inversion layers determined by temperature profile from balloon sounding; double vertical lines - height of convective plumes recorded by sodar. $z_g$ and $z_e$ - ground-based and elevated layers (sodar signal); $z_L$ and $z_{Le}$ - the same for lidar signal.

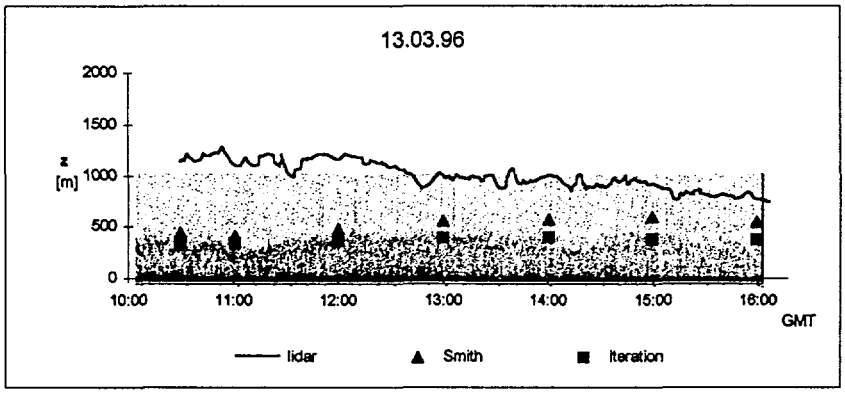


Fig.2. Case of neutral stability ($u_{10m}$ > 4.5 m/s). Sodar record with marked top of aerosol layer („lidar") and calculated values of MH for 2 parameterization methods („Smith", „iteration").

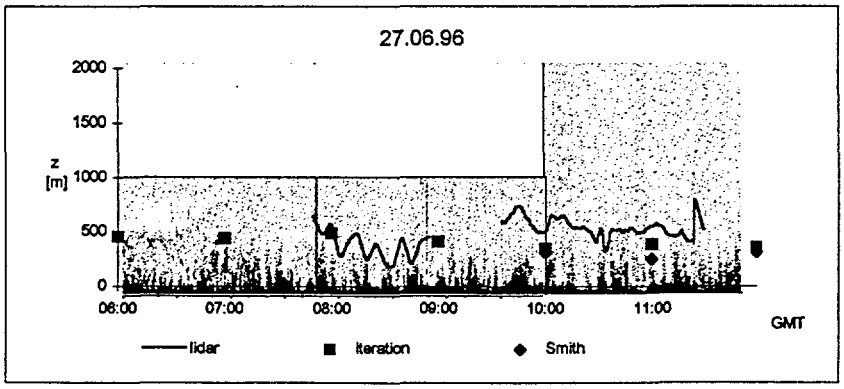


Fig.3. Case of the morning convective layer. Sodar record with marked top of aerosol layer („lidar") and calculated values of MH.

recorded elevated layers, especially in morning hours. For these height relations only some statistical characteristics can be given; they may be helpful in some practical applications, and in planning of more detailed investigations, taking into account categorisation of physical situations. The „inertia" of aerosol layer is a confounding factor in correlation studies and should be taken into account. In this aspect, short-period studies (like one-day experiments) may give misleading results, because time-history of each situation may play important role.

Having in view bigger files of data, it should be stated that generally rather low correlation exists between MH values calculated and estimated on the basis of observations. Comparisons of calculations with observations, performed in different locations, are giving different results, probably because of impact of local conditions. Moreover, different Authors are using different methods for calculation of similarity scales. Comparison of 4 such methods gave results being in poor correlation one to another. Some parameterization formulae seem to overestimate the factor of wind speed, especially in category of low speeds. There are many other problems, too, connected to the estimation of values of coefficients in the formulae.

## References:


Arya S. P. S., 1981: Parameterizing the height of the stable atmospheric boundary layer. *J. Appl. Met.*, 20, 1192-1202.

Berkowicz R., Prahm L.P., 1982: Evaluation of the profile method for estimation of surface fluxes of momentum and heat. *Atmos. Environ.*, 16, no. 12.

Beyrich F., 1995: Mixing height estimation in the Convective Boundary Layer using sodar data. *Bound. Lay. Met.*, 74, 1-18.

Bielak A., Kaszowski W., 1997: The measurements of mixing layer depth obtained from lidar, sodar and tethered balloon data. *Wiad. IMGW*, Vol.20, No.1, 59-65, in Polish.

Blackadar A. K., Tennekes H., 1968: Asymptotic similarity in Neutral Barotropic Planetary Boundary Layers. *J. Atmos. Sc.*, 25, 1015-1020.

Burzyński J., 1994: Preliminary testing of operational models for calculation of mixing layer height. *Wiad. IMGW*, Vol.17, No. 3-4, 45-57, in Polish.

Burzyński J., 1995: Calculations of mixing height for stable layer of the atmosphere. *Wiad. IMGW*, Vol.18, No.3-4, 31-46, in Polish.

CDTM, 1987: User's guide to the CDTM-meteorological preprocesor program, EPA.

Erbrink J.J., 1995: Turbullent diffusion from tall stacks. Thesis Phd., Printed in the Netherlands by KEMA International BV, Arnhem.

Genetay Y., 1988: Mixing height calculations. Remtech Doc. TD -88/020

Holtslag A. A. M., van Westrhenen R. M., 1991: Diagnostic derivation of boundary layer parameters from the outputs of atmospheric models. Air pollution modelling and its applications, VIII edited by H. van Dop, D. G. Steyn Plenum Press, New York.

Irwin J., Paumier J., 1991: Comparison of modified Carson and EPA mixing height estimates using data from five field experiments -preprints of 7-th joint conference on applications of air pollution meteorology with AMWA. *Am.Meteo Soc.*

Kaszowski W., Bielak A., 1996: The estimation of mixing layer depth in unstable and neutral categories of the atmospheric stability. *Wiad.i IMGW*, Vol.19, No.2, 3-12, in Polish.

Koracin D., Berkowicz R., 1988: Nocturnal boundary layer height: observations by acoustic sounders and predictions in terms of surface-layer parameters. *Bound. Layer. Met.*, 43.

Nieuwstadt F.T.M., 1981: The height of the stable boundary layer. Preprints, V Symp. on Turbulence, Diffusionand Air Pollution. *Am.Meteo.Soc.*, Atlanta, 104-105.

Panofsky H., Dutton J., 1983: Atmospheric turbulence. Models and methods for engineering applications. Evan Bugh Research, Aville Interscience Publication John Villey & Sons N.Y.

Taconet, O. Weill A., 1983: Convective plumes in the Atmospheric Boundary Layer as observed with an Acoustic Doppler sodar. Bound. Lay. Met. 25, 143-158

Tennekes H., 1970: Free convection in the Turbulent Ekman Layer of the atmosphere. J. Atmos. Sc., 27, 1027-1034

Walczewski J, Orkisz K., 1994: Application of correlation spectrometer for determining $SO_2$ mixing depth in convective atmosphere. *Wiad. IMGW*, Vol.17, No.3., 71 - 80, in Polish.

Zilitinkevich S., 1972: On the determination of the height of the Ekman boundary layer. *Bound. Layer Meteor.*3.

# On the Parametrization of the Planetary Boundary Layer of the Atmosphere

D. Yordanov[1], D. Syrakov[2], M. Kolarova[2]

[1] Geophysical Institute, Bulgarian Academy of Sciences, Sofia, Bulgaria
[2] National Institute of Meteorology and Hydrology, Bulgarian Academy of Sciences, Sofia, Bulgaria

## Introduction

The investigation of the dynamic processes in the planetary boundary layer presents a definite theoretical challenge and plays a growing role for the solution of a number of practical tasks. The improvement of large-scale atmospheric weather forecast depends, to a certain degree, on the proper inclusion of the planetary boundary layer dynamics in the numerical models. The modeling of the transport and the diffusion of air pollutants is connected with estimation of the different processes in the Planetary Boundary Layer (PBL) and needs also a proper PBL parametrization. For the solution of these practical tasks the following PBL models: i) a baroclinic PBL model with its barotropic version, and ii) a convective PBL model were developed. Both models are one dimensional and are based on the similarity theory and the resistance lows extended for the whole PBL. Two different PBL parametrisations under stable and under convective conditions are proposed, on the basis of which the turbulent surface heat and momentum fluxes are estimated using generalized similarity theory. By the proposed parametrizations the internal parameters are calculated from the synoptic scale parameters as geostrophyc wind, potential temperature and humidity given at two levels (ground level and at 850 hPa) and from them - the PBL profiles. The models consist of two layers: a surface layer (SL) with a variable height and a second (Ekman layer) over it with a constant with height turbulent exchange coefficient.

## The baroclinic planetary boundary layer model

The baroclinic planetary boundary layer (PBL) model is developed on the basis of the similarity theory. Two additional external baroclinicity parameters, which take into account the horizontal temperature gradients are introduced. The resistance laws giving the relation between the external and the internal PBL parameters are numerically solved. The profiles of the meteorological elements are analytically derived using a two-layer PBL structure and the known internal parameters. The outlined methodology may be used at arbitrary conditions of stratification and baroclinicity and contains as an asymptote the barotropic PBL (Yordanov, 1983). The baroclinic PBL model uses as an input information the following meteorological variables, which can be obtained from the large-scale weather forecast models:

1) the geostrophic wind vector $V_g$ which is taken to be equal to the wind at 850 mb;
2) the potential temperature $\theta_h$ at the same level;
3) surface temperature $\theta_0$ which can be calculated from the energy balance equation;
4) the horizontal temperature gradients $\partial\bar{\theta}/\partial x$, $\partial\bar{\theta}/\partial y$, where $\bar{\theta}$ is the average temperature.

The external PBL parameters describing the dynamics of a barotropic PBL are :

(1) $Ro = |V_{g0}| / fz_0, \quad S = \beta\delta\theta / f|V_{g0}|,$

For the baroclinic PBL new external parameters, which depend on the horizontal temperature gradients are added:

(2) $$\eta_{x*} = -\beta \frac{\kappa^2}{f^2}\frac{\partial \theta}{\partial y} = \frac{\kappa^2}{f}\frac{du_{g*}}{dz}, \quad \eta_{y*} = \beta \frac{\kappa^2}{f^2}\frac{\partial \theta}{\partial x_*} = \frac{\kappa^2}{f}\frac{dv_{g*}}{dz}$$

where Ro - Rossby number, $|V_{g0}|$ - the ground level geostrophic wind, $\delta\theta$ - the difference between the geostrophic and ground level temperature, $u_{g*}$, $v_{g*}$ - the geostrophic wind components in coordinate system with $x_*$ axis directed along the ground level geostrophic wind $V_{g0}$.

The similarity theory is used to describe the relation between the external and the internal PBL parameters, namely: $u_*$ - turbulent friction velocity, $\alpha$ - the angle between the geostrophic and surface wind direction, $\mu$ - internal stratification parameter (Yordanov et al., 1983). In the case of baroclinic PBL new internal baroclinicity parameters are added:

(3) $$\lambda_x = -\beta \frac{\kappa^2}{f^2}\frac{\partial \bar{\theta}}{\partial y} = \frac{\kappa^2}{f}\frac{du_g}{dz}, \quad \lambda_y = \beta \frac{\kappa^2}{f^2}\frac{\partial \bar{\theta}}{\partial x} = \frac{\kappa^2}{f}\frac{dv_g}{dz}$$

where $u_g$, $v_g$ are the geostrophic wind components along the coordinate axes x and y; x axis is directed along the surface wind; the horizontal temperature gradients are assumed constant with the height, i.e. $d^2V_g/dz^2 = 0$.

The relation between the external and internal baroclinicity parameters in the PBL model is given by:

(4) $$\lambda_x = \eta_{x*}\cos\alpha + \eta_{y*}\sin\alpha, \quad \lambda_y = \eta_{x*}\sin\alpha + \eta_{y*}\cos\alpha,$$

where $\alpha$ is the angle between the surface and geostrophic wind at ground level, i.e. between x and $x_*$.

In the baroclinic PBL model developed by Iordanov (1975, 1976) on the basis of the hypothesis of automodelity the relationship between the external and internal parameters or the so called resistance laws has been derived. The internal parameters allow to define the wind, temperature and humidity profiles at arbitrary meteorological conditions. The solution of the resistance laws is presented in polynomial form in the paper by Iordanov et al. (1978) :

(5) $$c_g(Ro, S, \eta_{x*}, \eta_{y*}) = c_g(Ro, S) + \frac{\partial C_g}{\partial(\eta_{x*} + \eta_{y*})}(\eta_{x*} + \eta_{y*})$$

$$\alpha(Ro, S, \eta_{x*}, \eta_{y*}) = \alpha(Ro, S) + \frac{\partial \alpha}{\partial(\eta_{x*} - \eta_{y*})}(\eta_{y*} - \eta_{x*})$$

$$\mu(Ro, S, \eta_{x*}, \eta_{y*}) = \mu(Ro, S) + \frac{\partial \mu}{\partial(\eta_{x*} + \eta_{y*})}(\eta_{x*} + \eta_{y*})$$

where $c_g = u_* / |V_g|$ is the geostrophic resistance coefficient.

**The CPBL model**

The convective planetary boundary layer (CPBL), also based on the similarity theory, consists of two layers - surface layer (SL) and Ekman layer over it, in which the turbulent exchange coefficient is assumed constant with height. The turbulent exchange coefficient is determined from the turbulent kinetic energy balance equation under the assumptions about the type of the turbulent kinetic energy and its dissipation (BC-EMEP, 1994).

The turbulent regime in a barotropic PBL capped by an inversion is parametrized on the basis of the similarity theory using the following nondimensional external parameters:

(6) $Ri_B = \frac{\beta(\theta_z - \theta_0)z_i}{V_g^2}$, $Z_0 = \frac{z_0}{z_i}$, and

(7) $Ro_i = \frac{V_g}{fz_i}$,

where $Ri_B$ is the bulk Richardson number, $\beta = g/\overline{\theta}$ - the buoyancy parameter, g - gravity acceleration, $\overline{\theta}$ - mean potential temperature, $(\theta_z - \theta_0)$ - the difference between the potential temperature at the inversion height and the ground, $V_g$ - the geostrophic wind vector, $Z_0$ is the nondimensionless roughness, $z_0$ is the roughness parameter, $z_i$ - the inversion height, $Ro_i$ is the bulk inversion Rossby number, f is the Coriolis parameter.

The turbulent regime in the CPBL is determined by the following internal parameters:

(8) $c_g = \frac{u_*}{|V_g|}$, $\alpha$, $\mu = \frac{z_i}{L}$, $\mu_0 = \frac{\kappa u_*}{fL}$,

where $c_g$ is the drag coefficient, $u_*$ - friction velocity, $\alpha$ - surface wind deviation from the geostrophic wind, $\mu$ and $\mu_0$ - the internal stratification parameters, L - the Monin-Obukhov length.

The relationship between the external and internal CPBL parameters is given by the resistance and heat exchange laws, which in this case are :

(9)
$$\frac{\kappa \cos\alpha}{c_g} = -\ln Z_0 - M_m(\mu)$$
$$\frac{\kappa \sin\alpha}{c_g} = N(Ro_i, c_g) = \frac{\mu_0}{\mu} = \kappa c_g Ro_i$$
$$\frac{\alpha_\theta(0)\kappa^2 Ri_b}{c_g^2} = -\ln Z_0 - M_\theta(\mu)$$

where $\kappa$ is the von Karman constant, $\alpha_\theta(0)=1.35$ is the inverse Prandtl number at the ground. The universal functions $M_m$, $N$, $M_\theta$ for the CPBL are derived in (Kolarova, 1988). The numerical solution of this system is given in Kolarova, Yordanov et al. (1989).

The evolution of the convective PBL height (mixing layer height) at conditions of horizontal homogeneity is calculated using the equation:

(10) $\frac{dz_i}{dt} = \frac{\overline{(w'\theta')_0} - \overline{(w'\theta')_{z_i}}}{\Gamma z_i} = \frac{(1+2c_1)\overline{(w'\theta')_0}}{\Gamma z_i} + c_2 \frac{u_*^3}{\Gamma \beta z_i^2}$

where $\overline{(w'\theta')_0}$, $\overline{(w'\theta')_{z_i}}$ are the normalized by $c_p\rho$ surface fluxes at height $z_i$ and at the ground, $c_p$ is the specific air heat capacity, $\rho$ - air density, $\Gamma$ is the potential temperature gradient above the inversion layer, $c_1 = 0.2$ , $c_2 = 2.5$ . The evolution of the inversion height depends on the surface turbulent heat and momentum fluxes:

(11) $\overline{(w'\theta')_0} = \frac{\mu_0 f u_*}{\kappa^2 \beta} = \frac{\mu u_*^3}{\kappa \beta z_i}$ $u_* = c_g |V_g|$,

i.e. on the internal CPBL parameters.

**Comparison with experimental data**

Comparisons with data approximating the experiments Wangara, Minnesota, O'Neill and Sofia were presented in Yordanov, Kolarova et al., 1990. Some of the results from the comparisons with

climatological data are given in Kolarova, Djolov et al. (1989), where the annual variation of the inversion height over Sofia has been calculated using the CPBL model and favorably compared with the climatological data.

The baroclinic PBL model was compared with some experimental data for the external and internal parameters and velocity profiles, taken from theoretical and experimental investigations as the Meppen data and the experimental results of Orlenko (BC-EMEP, 1994). The analysis of the experimental data show that the PBL height at barotropic and adiabatic conditions defined as the height at which $u = u_g$ , $v = v_g$ is $h_* = 0.4\, u_* / f$ .

## Conclusion

Two computer codes YORDAN and YORCON are developed for an operational use of the PBL models. First, the PBL parametrization was incorporated in the operational weather prediction model in Novosibirsk (see Iordanov at al., 1978). The barotropic version of the PBL model YORDAN (Yordanov et al., 1983) is incorporated in the Bulgarian Long-range air pollution transport model (LED) Syrakov et al., 1983 and was used also to investigate the transport of pollutants over long distances in the region of South-East Europe (Djolov et al., 1987) and the Baltic region (Kolarova, 1988). The PBL parametrization is widely used in the Bulgarian EMAP model - part of the national participation in the EMEP program (BC-EMEP, 1994, 1995, 1996) and also for modeling of the transport of radioactive substances over long distances in the ETEX program (Syrakov, Prodanova, 1997). The convective PBL model YORCON can be used in a limited areas, when a clear day-time convective conditions with an inversion layer exist, to simulate the PBL experimental data. It was used mainly for simulating some experimental data for summer inversions over Sofia and also with some climatic data simulating the development of convective PBL over NIMH at Sofia (Kolarova, 1988).

## References


BC-EMEP, 1994: Bulgarian Contribution to EMEP. Annual Report for 1994, NIMH, Sofia-Moscow, March 1995.

BC-EMEP, 1995: Bulgarian Contribution to EMEP. Annual Report for 1995, NIMH, Sofia-Moscow, March 1996.

BC-EMEP, 1996: Bulgarian Contribution to EMEP. Annual Report for 1995, NIMH, Sofia-Moscow, March 1997.

Djolov G.,.D. Yordanov, D. Syrakov, 1987: Modeling the long-range transport of air pollutants with atmospheric boundary layer chemistry. *Boundary Layer Meteor.*, 41.

Iordanov D.L., 1975: Prostaja baroklinnaja model Planetarnogo Pogranicnogo Sloja. *Izv. AN SSSR, FAO*, 11.

Iordanov D.L., 1976: Ob universalnih funkcii v zakonah soprotivlenija baroklinnogo PPS. *Izv. AN SSSR, FAO*, 12.

Iordanov D.L., V.V.Penenko, A.E.Aloyan, 1978: Parametrizacii stratificirovannogo baroklin-nogo PPS dlja cislennogo modelirovanija atmosfernih procesov. *Izv. AN SSSR, FAO*, 8.

Kolarova M., 1988: A Convective PBL model and its application for modeling of the dispersion in it. A doctorate thesis, Vilnius, 1988. (in russian)

Kolarova M., D.Yordanov, D.Syrakov, G.Djolov, D.Karadjov, L.Aleksandrov, 1989: Paramet-rization of a convective planetary boundary layer. *Izv Acad.Sci. USSR Atmos.Ocean Phys.*, 7.

Kolarova M., G.Djolov, D.Yordanov, D.Syrakov, 1989: Diurnal evolution of the convective planetary boundary layer. *Bulg.Geophys.J.*, XV, 1.

Syrakov D., G. Djolov, D. Yordanov, 1983: Incorporation of PBL dynamics in a numerical model of long-range air pollution transport. *Boundary Layer Meteor.*, 26.

Syrakov D. and M. Prodanova, 1997: Bulgarian LRT models-simulation of ETEX first release. *Proc. of ETEX Symp. on Long-range atmos. transport..*,13-16 May 1997, Vienna, Austria.

Yordanov D., D. Syrakov and G. Djolov, 1983: A Barotropic planetary layer. Boundary-Layer.Meteorol, 25.

Yordanov D., M.Kolarova, D.Syrakov, G.Djolov, 1990: Convective boundary layer - theory and experiment. *Proc. of the 9th Symp. on Turbulence and Diffusion*, RISO, Denmark, April 1990.

# Session VII - Mixing Height over Complex Terrain
# Chairperson: Ekaterina Batchvarova

# A Comparison of Mixing Depths Observed Over Horizontally Inhomogeneous Terrain

A. B. White[1] and C. W. King[2]

[1]Cooperative Institute for Research in Environmental Sciences
University of Colorado/NOAA Environmental Technology Laboratory
Boulder, CO, USA

[2]NOAA Environmental Technology Laboratory
Boulder, CO, USA

## Introduction

During the one-year period from December 1994 through November 1995, the National Oceanic and Atmospheric Administration Environmental Technology Laboratory (NOAA/ETL) operated two 915-MHz boundary-layer radar/wind profilers (Ecklund et al., 1988) and several meteorological towers in the vicinity of the Front Range in Colorado (King, 1996). Figure 1 shows a terrain map of the study region. One important characteristic of this and other similar topographies are thermally forced circulations resulting from the diurnal heating and cooling cycle. In the case of the Colorado Front Range, daytime heating along the eastern slopes of the Front Range produces flow from east to west with upslope flow resulting east of the Continental Divide. These upslope flows occur with notable frequency during the summer and may impact the inter-mountain regional air quality as pollutants from the heavily populated communities east of the Colorado Front Range are transported to the relatively pristine environment to the west (Parrish et al., 1990).

Previous studies have discussed the importance of the mixing depth relative to the mountain height in a thermally induced plain-to-basin circulation (PTBC). For example, in the model results of Kimura and Kuwagata (1993), a PTBC developed only when the maximum mixing depth over the plains was greater than or equal to the altitude of the mountain range. A separate modeling study by deWekker et al. (1997) indicated that the mixing depth on the plains was not critical as long as a horizontal temperature gradient existed above mountain height. In both cases the conclusions were based solely on model results. Therefore, in this paper we analyze measurements of mixing depth deduced from profiler observations on days during the summer of 1995 when a PTBC developed along the Colorado Front Range. The profilers were located at the National Renewable Energy Laboratory's Wind Test Facility (WTF) and in the town of Granby (GBY) (see Fig.1). We used near surface winds measured on a 3-m meteorological tower deployed on the Continental Divide (CDE) to verify PTBC events.

## Mixing Depth Determination

Aside from measuring mean wind profiles in the lower troposphere, wind profilers provide an estimate of the convective mixing depth through the intensity of the backscattered signal, which in clear air is directly proportional to the refractive index structure function parameter, $C_n^2$. Theory and observations show that the profile of $C_n^2$ exhibits a peak at the inversion capping the mixed layer. The radar technique for estimating

mixing depth relies on finding this peak in the measured profiles of radar backscatter (White, 1993).

**Results**

During the period 26 June–5 August, 1995, a PTBC was observed on 17 days. King (1996) gives the criteria used to identify these cases as well as a detailed description of the flow characteristics. A brief summary is given here. On average, thermally induced flows observed at WTF start at approximately 1700 UTC (5 h after local sunrise) and dissipate by 0000 UTC (2 h prior to local sunset). Upslope winds reach their maximum depth of approximately 1 km AGL during the late afternoon hours (2200–2300 UTC). On certain days, these thermally induced flows reach a sufficient depth to pass over the Continental Divide (4 km MSL, ~2 km above WTF). On the west side of the Divide, an abrupt wind shift occurs in the lower levels from prevailing westerlies to easterly flow. During PTBC events, upslope winds start earlier (1500–1600 UTC), extend to greater heights (2 km AGL at WTF), and have a longer duration (10–14 h). The time of transition from westerly to easterly flow at CDE correlates with the time that upslope flow at WTF extends to a depth equivalent to the height of the Divide. The PTCB breaks down between 0100 and 0500 UTC in response to the cessation of daytime heating.

Figure 2 shows a horizontal cross section from GBY to WTF along with the maximum mixing depths determined from the profilers at these sites on the 17 days when a PTBC was observed. Data are not shown for two days at GBY and for one day at WTF because a mixed layer was not readily identifiable in the radar backscatter data. The mixing depths observed at GBY are all well above the mountain barrier for the PTBC days. As a result, the average lapse rate of 9.4 °C $km^{-1}$ calculated using the daily maximum temperatures at GBY and CDE on PTBC days approached a neutral lapse rate (9.8 °C $km^{-1}$). The tops of the mixed layers at GBY are also higher, on average, than at WTF. A horizontal temperature gradient results because the air in the deep mixed layers at GBY is warmer than the air above the shallow mixed layers at WTF. This baroclinic zone is intensified throughout the morning and early afternoon by continued surface heating and convergence of upslope flows at the Continental Divide (Bossert and Cotton, 1994).

On certain days, including those when the top of the mixed layer at WTF was slightly lower than the Divide (Fig. 2), easterly winds were found above the convective bounday layer. This is consistent with the observations and conceptual model of Wolyn and McKee (1994). In Phase II of their model (see Fig. 7 in Wolyn and McKee), drying occurs in the easterly flow above the daytime boundary layer and moistening occurs in the westerly return flow aloft, producing a positive moisture gradient with height. The observed moisture inversion weakens and disappears in the afternoon. Figure 3 shows the hourly winds measured by the profiler at WTF on 17 July along with the mixing depths determined from the radar backscatter data. Easterly winds are present above the developing mixed layer between 1900 and 2200 UTC. Figure 4 is a time-height cross section of the radar backscatter for 17 July. At 915-MHz radar returns in the lower atmosphere are dominated by humidity fluctuations. There is also a weaker dependence on background humidity. The region of reduced backscatter just above the boundary layer in Fig. 4 is consistent with drying and corresponds to the region of upslope flow above the mixed layer in Fig. 3. The moistening in the westerlies is represented in Fig. 4 by the enhanced radar backscatter above 2 km, which weakens after 2100 UTC. These features are consistent with the model of Wolyn and McKee (1994). We observed similar behavior during several other PTBC events analyzed in this study.

## Summary

In this paper we used wind profiler observations to estimate the mixing depth on either side of the Continental Divide on days when a PTBC occurred along the Front Range of Colorado during the summer of 1995. The mixing depths on the basin side were significantly deeper than the mountain barrier for all of the PTBC events we analyzed. On the plains side, the mixed layers often extended to or above the level of the mountain barrier. On certain days upslope flow existed above the mixed layer. We depicted the vertical structure of the flow and features in the humidity profile on one of these days using measurements from a wind profiler. The results were consistent with the conceptual model presented by Wolyn and McKee (1994).

## References

Bossert, J.E., and W.R. Cotton, 1994: Regional-scale flows in mountainous terrain. Part I: A numerical and observational comparison. *Mon. Wea. Rev.*, **122**, 1449–1471.

Ecklund, W.L., D.A. Carter, and B.B. Balsley, 1988: A UHF wind profiler for the boundary layer: Brief description and initial results. *J. Atmos. Ocean. Tech.*, **5**, 432–441.

Kimura, F., and T. Kuwagata, 1993: Thermally induced wind passing from plain to basin over a mountain range. *J. Appl. Meteor.*, **32**, 1538–1547.

C.W., 1996: A climatology of thermally forced circulations in oppositely oriented airsheds along the Continental Divide in Colorado. Ph.D. Dissertation, University of Colorado, Boulder, Colorado, 199 pp.

Parrish, D.D., C.H. Hahn, D.W. Fahey, E.J. Williams, M.J. Bollinger, G. Hübler, M.P. Buhr, P.C. Murphy, M. Trainer, E.Y. Hsie, S.C. Liu, and F.C. Fehsenfeld, 1990: Systematic variations in the concentration of $NO_X$ (NO plus $NO_2$) at Niwot Rdige, Colorado. *J. Geophys. Res.*, **95**, 1817-1836.

deWekker, S.F.J., S. Zhong, J.D. Fast, and C.D. Whiteman, 1997: A numerical investigation of thermally-driven circulations produced by basin topography. Preprint Vol., Twelfth Symposium on Boundary Layers and Turbulence, AMS, Boston, 536–537.

White, A.B., 1993: Mixing depth detection using 915-MHz radar reflectivity data. Preprint Vol., Eighth Symposium on Observations and Instrumentation, AMS, Boston, 248–250.

Wolyn, P.G., and T.B. McKee, 1994: The mountain-plains circulation east of a 2-km-high north-south barrier. *Mon. Wea. Rev.*, **122**, 1490–1508.

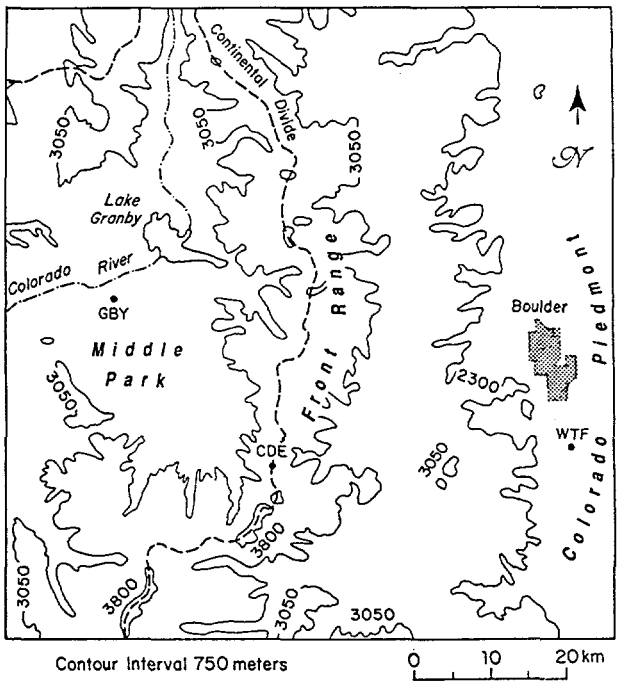


Figure 1. Topographic map of the study region in northern Colorado. A 915-MHz wind profiler was deployed at the National Renewable Energy Laboratory's Wind Test Facility (WTF) and in the town of Granby, Colorado (GBY). A 3-m meteorological tower was placed on the Continental Divide (CDE).

**Acknowledgments.** This work was sponsored by the U.S. Department of Energy through Interagency Agreement No. DE-AI03-95ER61987/A001 and by the NOAA Health of the Atmospheres Program.

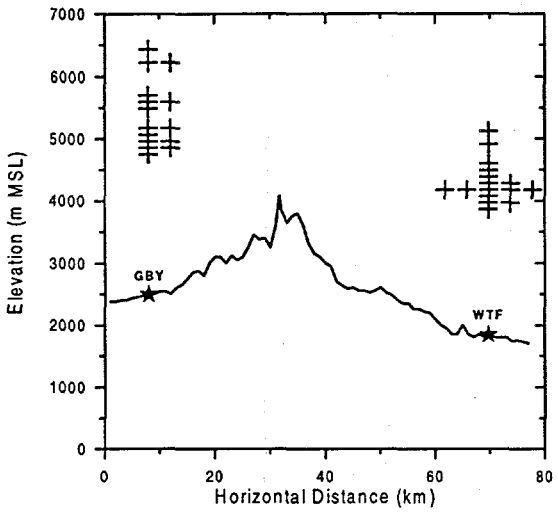


Figure 2. Cross section from GBY to WTF. The maximum mixing depths determined from the wind profilers are denoted by plus symbols above each of the sites.

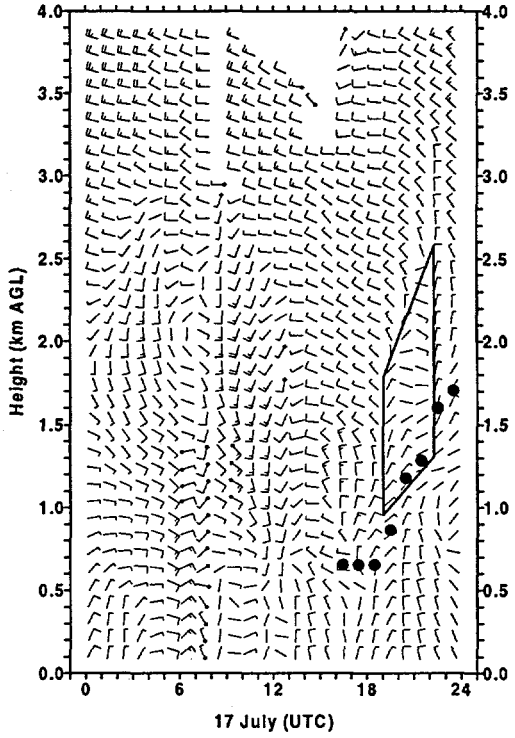


Figure 3. Winds measured by the profiler at WTF on 17 July. A full barb corresponds to a wind speed of 5 m $s^{-1}$. Winds labeled as "suspect" by a quality control program are denoted by a small diamond symbol at the base of the flags. The black dots represent the top of the mixed layer as determined from profiles of radar backscatter. The box encloses a region of upslope flow above the mixed layer.

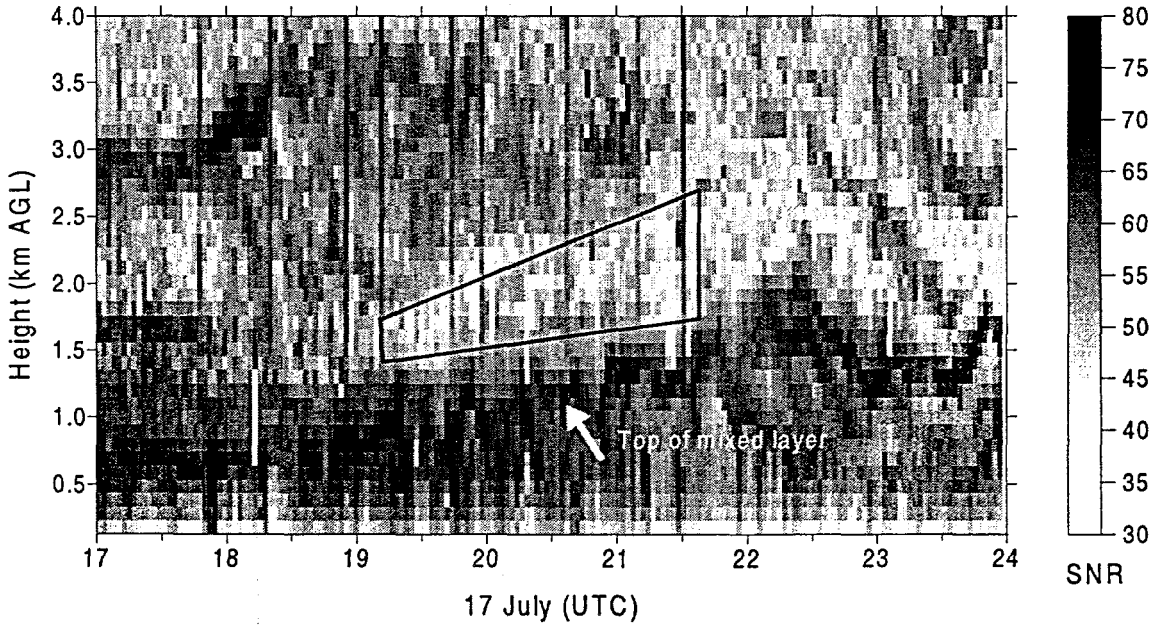


Figure 4. Time-height cross section of radar backscatter in the form of range-corrected signal-to-noise ratio from the profiler at WTF on 17 July. The top of the mixed layer is depicted by the layer of enhanced backscatter identified with the arrow. The box represents a region of drying above the boundary layer associated with upslope flow. Enhanced radar backscatter above the box is associated with moistening in the return westerly flow of the PTBC.

# Mixing heights over hilly terrain - a case study in northern Austria

K. Baumann

Central Institute for Meteorology and Geodynamics (ZAMG), Vienna, Austria

## Introduction

Simultaneous Sodar measurements (Remtech PA2) were conducted from 10 October 1996 to 24 January 1997 at two sites in northern Austria, near the village Allensteig on top of a hill (590 m.s.l.) and in the village Lenzing (460 m.s.l.) near the lake Attersee. The two sites are 145 km apart from each other and differ much according to the complexity of the surrounding terrain, land use and altitude.

Mixing height and inversions height estimations from the Sodar measurements are compared with mixing heights derived from radiosonde potential temperature profiles at the next stations Linz and Vienna using the parcel method of Stull (1991) explained by M. Piringer (this volume).

The information about the static stability at different Sodar heights, which is provided by the new Sodar software in terms of vertical temperature gradients, is dicussed.

## Mixing height estimation from Sodar Data

The Sodar software (Remtech, 1994) includes internal routines for inversion height and convective mixing height detection.

Temperature inversions are generally characterized by strong echo returns below the top of the inversion. But, in cases of very strong ground-based (nocturnal) inversions, the echo intensity may be weak because of weak thermal turbulence. On the other hand, shallow inversions with strong mechanical turbulence lead to strong echo intensities. Thus, inversions are detected from the Sodar data using an echo pattern recognition technique in combination with the standard deviation of the echo strength, the vertical gradient of horizontal windspeed and the standard deviation of the vertical velocity.

According to the Sodar manual (Remtech, 1994), the mixing height determination algorithm is based on spectral analysis of the vertical velocity (time series with a 10 seconds time step). From the power spectra of every single level, a characteristic frequency scale for the most energetic eddies is derived and related to the depth of the mixing layer. Thus, it is possible to estimate the mixing height from Sodar data even if it is well above the maximum range reached by the Sodar (about 650m above ground in the presented case).

In several independent studies (e.g. Kaimal, 1976; Baumann, 1997) it was shown that the size of the most energetic eddies from the spectral analysis is approximately

1.5 the mixing height. The Sodar manual does not tell whether this or a similar value is used in the internal routine, too.

In the latest update of the Remtech Sodar software, a new feature, producing temperature gradients from the Sodar data, is included. A main interest of this study is the verification of these Sodar derived lapse rates.

## Comparison with mixing height estimations from the next radiosounding stations

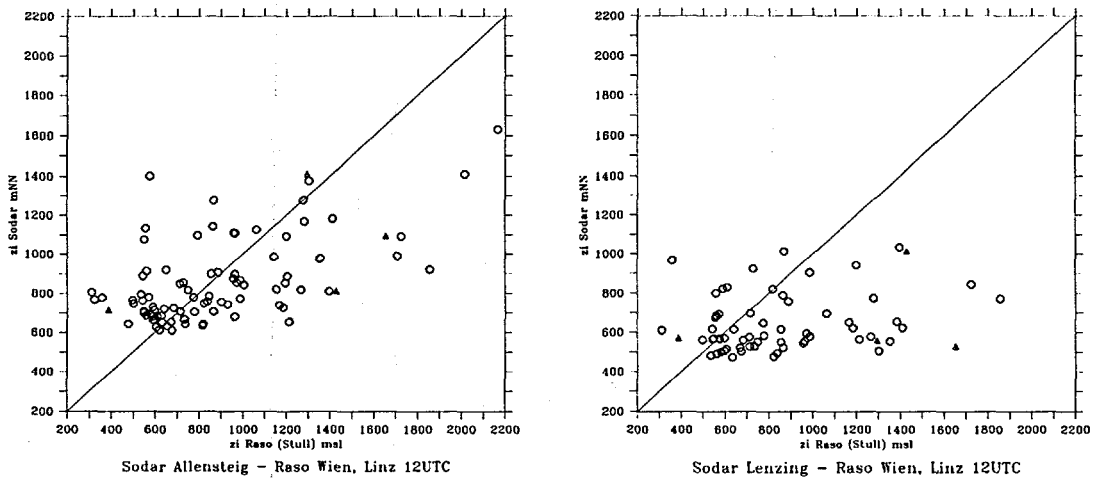


Figure 1: Comparison of mixing heights estimated from Allensteig (left) and Lenzing (right) Sodar data and from Vienna (circles) and Linz (triangles) radiosonde profiles 12 UTC in meters above sea level.

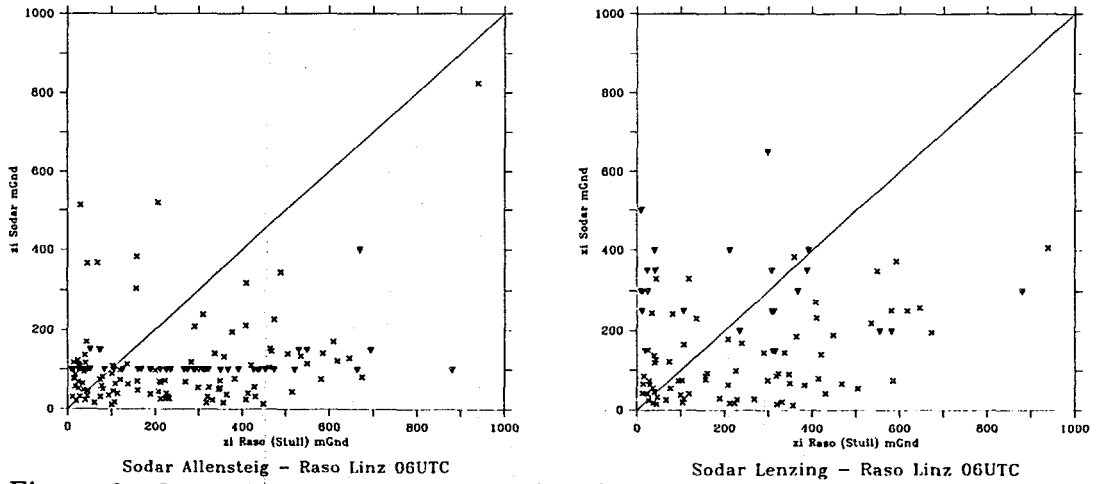


Figure 2: Comparison of mixing heights (stars) and inversion heights (triangles) estimated from Allensteig (left) and Lenzing (right) Sodar data and from Linz radiosonde profiles 6UTC in m above ground.

Noon mixing heights estimated from the Sodar measurements are compared to those derived from the noon radiosonde potential temperature profiles at Vienna. On some days, noon souding data at Linz was available, too. As noon mixing heights

are assumed to be more or less height-constant at least on convective days, the comparison in figure 1 is given in meters above sea level according to the altitudes of the sites.

Some correlation was found for mixing heights between 400 and 1400msl (Allensteig) or 400 and 1000msl (Lenzing). Mixing heights above these values were always underestimated by the Sodars. It turns out that the correlation between the Sodar and radiosonde mixing heights could be improved by multiplying the Sodar values by a factor of 2. It has to be discussed further, whether these findings could lead to a general correction factor which could be applied to the Sodar routine for mixing height estimation.

Morning mixing heights were calculated from the 06 UTC radiosonde profiles at Linz. These are compared to the Sodar mixing heights and inversion heights in figure 2. Low mixing heights (and night-time inversion heights) are expected to be more or less terrain-following. Thus, the morning mixing heights are compared in meters above ground. Morning mixing heights from the Sodar at Allensteig are below 100m gnd in most cases and the inversions were most of the time found at 100m gnd by the Sodar. At Lenzing, larger values were found for the Sodar mixing and inversion heights, but they differ much from the heights derived from the radiosonde data. An explanation for these results can be given by the fact that low nocturnal inversions may occur at the rural site at Allensteig rather often while the site at Lenzing is influenced by the thermal effect of the town and the lake nearby.

## Lapse rate from Sodar Data

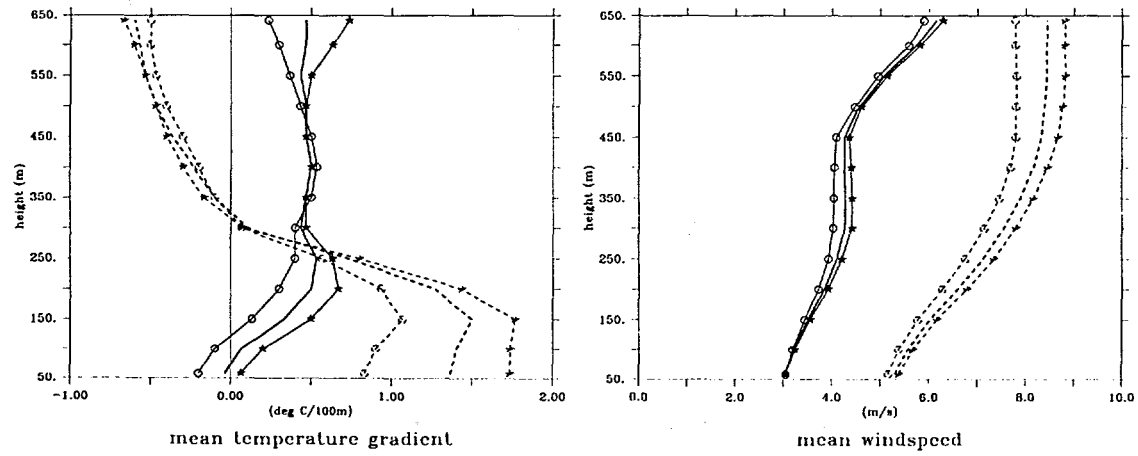


Figure 3: Mean profiles of vertical temperature gradient and windspeed at Lenzing (solid lines) and Allensteig (dotted lines). Daytime mean profiles are marked with circles, nightime profiles with starts.

Mean profiles of the temperature gradient and the windspeed at both sites are shown in figure 3. At Lenzing, the temperature gradients are neutral (between 0. and -0.6 degrees Celsius per 100m) in the lowest 100m above ground and stable (positive) with nearly height-constant mean values above. Night-time temperature

gradients are found to be slightly more stable in the lower levels, daytime temperature gradients are on average less stable. Nocturnal inversions up to 150m gnd in Allensteig result in a mean temperature increase of 1.8 degrees per 100m measured by the Sodar. Mean daytime temperature gradients in the lowest 300m above ground are also found to be stable at Allensteig. Above, the temperature gradients are neutral at Allensteig day and night. The neutral stratification some hundred meters above the hill on which the Sodar is situated, can be explained by usually high windspeeds (see right picture in figure 3) causing mechanical mixing.

The static stability as derived from the Sodar measurements is discussed for different weather patterns. The number of cases with unstable gradients above 400m gnd at Allensteig is higher for variable situations as windspeeds are higher during frontal passages than during weather situations with weak pressure gradients. At Lenzing, stable gradients are hardly observed during weak pressure gradient situations. In this area, fog prevents the evolution of nocturnal inversions rather often and results in the neutral stratification which is observed at Lenzing quite often.

The Sodars render unrealistic maxima and minima of the vertical temperature gradients, but the general information about the stability of the boundary layer given by the Sodar measurements seems to be appropriate.

**Acknowledgements** - This research was funded by the Electricity of Austria (Verband der Elektrizitaetswerke Oesterreichs, VEO), project number 1.20.

**References**

Baumann K., 1997: Plume structures in the convective boundary layer from high-frequency Sodar data. 12th Symposium on Boundary Layer and Turbulence, AMS, Vancouver, Canada.

Kaimal J.C., 1976: Turbulence structure in the convective boundary layer. *J.Atmos.Sci.***33**, 2151-2169.

Langer M., 1995: Ueber die Verwendung von SODAR-Daten zur Mischungshoehenbestimmung. Thesis, Universitaet Muenchen.

Remtech, 1994: Remtech Doppler Sodar Operating Manual. DT94/003, Remtech S.A., BP 101, 78143 Vellzy Cedex, France.

Stull, R.B., 1991: Static stability - an update.*Bull.Am.Met.Soc.***72**,1521-1529.

# Effect on tracer concentrations of ABL depth models in complex terrain

S. Galmarini[1], D. Anfossi[2], P. Salin[1], G. Schayes[3] and S. Trini-Castelli[2]

[1]Joint Research Center Ispra, Italy
[2]CNR-ICGF, Turin, Italy
[3]Univ. Louvain-la-Neuve, Louvain, Belgium

## Introduction

The determination of the atmospheric boundary layer (ABL) depth over complex terrain still is an important and open issue in boundary layer meteorology. All formulations presented up-to-date relate to the diagnostic or prognostic determination of the ABL height based on the assumption of flat-terrain and horizontal homogeneity and little is known about the ABL development and evolution in complex topography. On the other hand, the ABL depth is of fundamental importance for the definition of the turbulence state of the atmospheric flow and in particular for atmospheric dispersion applications. In the present preliminary study we use different ABL depth formulations to study atmospheric dispersion in complex-terrain conditions. The flow in an Alpine valley occurred during the tracer experiment TRANSALP is simulated by means of a mesoscale model and a tracer dispersion is reproduced using a lagrangian particle model. The ABL depth enters as key parameter in particle model turbulent-dispersion formulation. The results obtained using different ABL formulations are compared with the available measurements. Because no direct measurement of the ABL depth in the valley was collected during the experiment, the capability of the model to reproduce the concentration field is considered as indirect estimate of the performance of the ABL depth formulation. Furthermore, since all the formulations selected are based on the above-mentioned flat-terrain assumption and forcibly applied to very complex conditions, scope of the study is to identify the differences between different approaches rather than to point out the best performing one. The result presented here will only concern the daytime ABL.

## Atmospheric flow and dispersion over complex terrain: case study

The flow and the dispersion simulations performed relate to the tracer experiment that took place from the 29 of September to the 30 of Semptember 1990 South of the Gottard Pass. The experiment consisted of the release of a passive tracer at Giornico in the Leventina valley during a southerly wind flow and of the detection of its concentration downstream up to the Gottard pass (Ambrosetti et al., 1994). The concentration was detected in more than 40 sampling sites mainly distributed around the Leventina valley's main axis and in the adjacent valley (Blenio). The general circulation flow and the valley flow is obtained by means of the regional mesoscale model RAMS (Walko et al., 1994) using two nested grids of which the inner one focused on the two above-mentioned valleys geographical region with a resolution of 1x1 km. In Figure 1 the real topography of the inner grid is shown. The different symbols represent the sampling sites and the meteo-stations where the comparison with model results is performed. The turbulence closure adopted is 2.5 Mellor-Yamada closure. The choice of a specific grid resolution imposes a smoothing of the topography. The result of this operation is given in Figure 2 where

two crossections of the Leventina valley are given for the real and the smoothed topography.

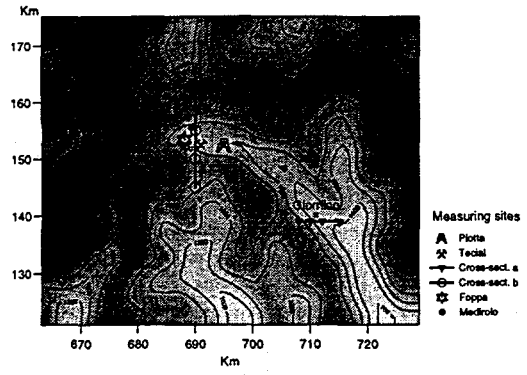


Figure 1: Inner grid topography, sampling and meteorological stations selected for the model evaluation.

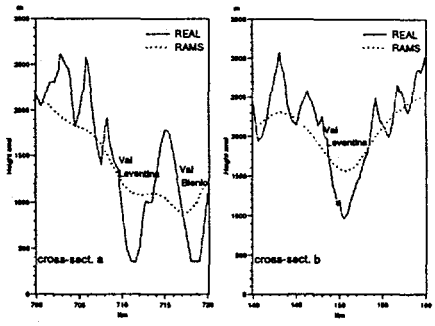


Figure 2: Real and smoothed topography at two different locations of the Leventina valley, see also Fig. 1.

The tracer dispersion is simulated using the lagrangian particle model SPRAY (Tinarelli et al., 1994) based on Thompson (1984) scheme defined on terrain following coordinates. The ABL is used as required external parameter for the determination of turbulent parameters such as the velocity variances ($\sigma_x$,$\sigma_y$,$\sigma_z$) and the Lagrangian timescale, following the scheme proposed by Hanna (Nieuwstadt and vad Dop, 1982).

### Boundary layer depth models: our choice

In order to study the impact of different ABL height parametrisations we have selected three substantially different methods. Namely:

**(ABL1)** Richardson number method according to which the ABL extends up to the height where the Richardson number reaches its critical value (McNider and Pielke, 1981).

**(ABL2)** The prognostic formula proposed by Batchvarova and Gryning (1995) where the external parameters such as stability, surface heat flux and subsidence are take from the mesoscale model.

**(ABL3)** A method based on the vertical profile of the turbulent kinetic energy (TKE) as calculated by RAMS. According to this method the ABL height is taken at the numerical level where TKE is ten percent of maximum value normally located in the bulk of the boundary layer. This method allow us to use the ABL depth explicitly calculated by the mesoscale model and that in principle considers the flat terrain condition only at subgrid level.

These three methods were selected because they allow us to analyse the behaviour of diagnostic (ABL1) against prognostic (ABL2 and ABL3) methods; to consider methods derived from higher order closure as well as local methods (ABL1) against surface-based ones (ABL2).

### Flow simulation and ABL height

We concentrate on the time window that goes from 09:00 (UTC) (release time) to 15:00 hours (UTC) of the September 29th, 1990. The flow simulation is started at

17:00 hours of the 28 of September to initialise the flow. Figures 3(a-c) compare the measured profiles of potential temperature at Tecial with those predicted by the mesoscale model for three different times of the day. Despite a systematic overestimation of the temperature throughout the vertical domain, the model is able to reproduce rather accurately the vertical temperature distribution. A factor which is greatly responsible for this overestimate is the grid resolution and consequently topography smoothing. In Figures 3 the height of the ABL calculated with the three above-listed methods is also displayed. The calculated boundary depths are all based on the result of the mesoscale model. In general we can see that the method which is more consistent with the temperature profile produced by the mesoscale model is ABL2 for all the considered time intervals. Method ABL1 is very sensitive to slight variations of the temperature gradient and wind shear. The TKE method is unable to capture fine ABL structures due to the rapidly decreasing vertical model resolution (in plot (c) the value obtained is larger than 4000 m). Method ABL2 is always consistent with the temperature profile and the potential lifting level of an air parcel having a specified surface temperature. A similar behaviour si found in all other stations where temperature profiles where collected.

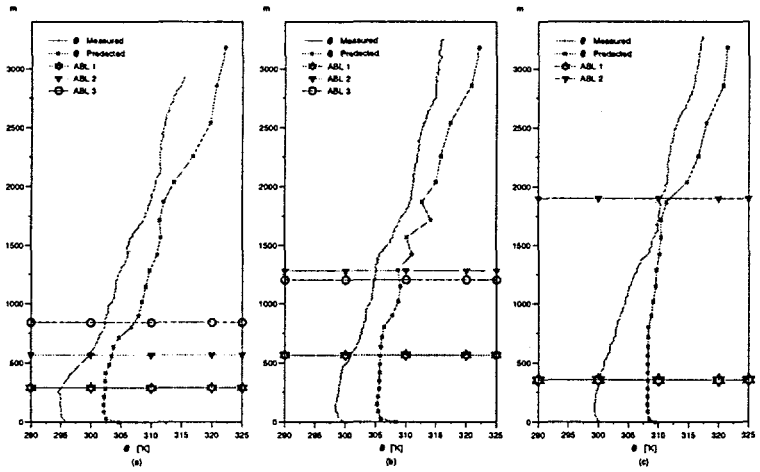

Figure 3:
measured and predicted profiles of potential temperature at Tecial meteorological site:
(a) 09:00 UTC,
(b) 12:00 UTC,
(c) 15:00 UTC

## Dispersion simulation

Figures 4(a-c) shows the comparison between measured and predicted tracer concentrations at three locations placed along the valley's main axis (see Fig. 1). Despite the large differences of the ABL height values present at these stations we can see that the impact on the tracer concentration is not very large at least as far as ABL1 and ABL2 are concerned. Two are the major differences that can be deduced from the figure: the overall underestimate of the predicted concentration ; the similar behaviour given by methods ABL1 and ABL2 and the different time evolution obtained when using method ABL3. The difference obtained between measured and predicted concentration maximum can be explained once again by the smoothing of the real topography. Provided that the same ABL depth is present in the real and in the smoothed valley, the volume of the smoothed valley is much larger than that encompassed by the real valley (as much as a factor 4 for the northen cross section of the valley). The later occurence of the TKE-dependent concentration maximum depends on the fact that the ABL height calculated with method ABL3 is in general larger than the others. The effect is thus a dilution of the particles at higher levels and the occurence of a lower concentration maximum at a later time interval. All methods show an over all capacity of predicting the time of arrival of the plume despite this parameter can be considered to be relatively easy to reproduce since the

flow is channeled and it mainly depends on the capability of the mesoscale model to reproduce the mean flow. An early plume arrival is forecasted for Piotta (approximately 3 hours earlier). This aspect, though, is not related to the ABL depth but rather on the mean flow overestimated intensity at this position of the valley.

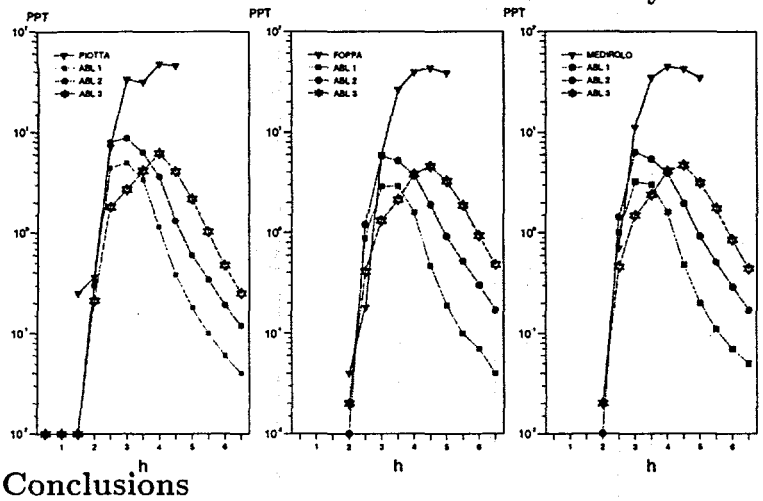


Figure 4:
time evolution
of measured and predicted
concentration
at Piotta (a), Foppa (b)
and Medirolo (c).
Time 0 corresponds to
the release time

## Conclusions

Three typical boundary layer depth parametrisations have been used to simulate the dispersion of a passive tracer in complex terrain conditions. The case considered is the tracer experiment realised during the TRANSALP campaign. The preliminary results reveal that the ABL depth parameter can influence the dispersion process but that in the case of a dispersion in a valley-daytime flow the results depend much more strongly on the model horizontal and vertical resolution. A relatively coarse horizontal resolution implies a considerable smoothing of the topography that largely affects the dispersion characteristics. The vertical resolution does not allow one to resolve with sufficient details the rapid and large variation of the flow characteristic as the terrain feature vary. Two of the methods used to determine the ABL depth depend strongly on the resolution ((ABL1) and (ABL3)). The method that instead depends only on surface parameters like heat flux and surface based stability allowed us to obtain results to be considered satisfactory for what concerns the dispersion process, quite consistent with the flow model results, less numerics dependent and more physically sound.

## References


Ambrosetti, P. et al. (1994). The TRANSALP 90 campaign. European Commission, Report EUR 15952 EN, Luxembourg.

Batchvarova E. and Gryning (1995) .Model of the internal boundary layer formation over inhomogeneous terrain, 21st NATO CCMS meeting, Baltimore USA.

McNider R., R. Pielke (1981). Diurnal Boundary-Layer Development over Sloping Terrain, J. Atmos. Sci, 38, 2198-2212

Nieuwstadt, F.T.M. and H. van Dop (1982). Atmospheric Turbulence and Air Pollution Modelling. Reidel Publishing Company, Dordrecht.

Thomspon, D.J. (1984). Random walk modelling of diffusion in inhomogeneous turbulence. Quarterly J. Roy. Meteor. Soc., **110**, pp. 1107-1120.

Tinarelli, G. et al. (1994). Lagrangian particle simulation of tracer dispersion in the lee of a schematic two-dimensional hill. J. Appl. Meteor., **33**, pp. 744-756.

Walko, R.L. et al. (1995). RAMS the regional atmospheric modeling system -Version 3b- User's Guide. ASTER Division Mission Research Corporation, Fort Collins (Colorado).

# Session VIII - Internal Boundary Layers: Mixing Height in Coastal Areas and Over Cities
# Chairperson: Allen White

# Interactions between the Thermal Internal Boundary Layer and Sea Breezes

D. G. Steyn

*Atmospheric Science Programme*
*Department of Geography*
*The University of British Columbia*
*Vancouver, B. C., Canada, V6T 1Z2*

In the absence of complex terrain, strongly curved coastline or strongly varying mean wind direction, the Thermal Internal Boundary Layer (TIBL) has well known square root behaviour with inland fetch. Existing slab modeling approaches to this phenomenon indicate no inland fetch limit at which this behaviour must cease. It is obvious however that the TIBL cannot continue to grow in depth with increasing fetch, since the typical continental Mixed Layer Depths (MLD) of 1500 to 2000 m must be reached between 100 and 200 km from the shoreline. The anticyclonic conditions with attendant strong convection and light winds which drive the TIBL, also drive daytime Sea Breeze Circulations (SBC) in the coastal zone. The onshore winds driving mesoscale advection of cool air are at the core of TIBL mechanisms, and are invariably part of a SBC. It is to be expected that TIBL and SBC be intimately linked through common mechanisms, as well as external conditions.

In the absence of overriding synoptic winds, the SBC consists of an onshore sea breeze and an upper return flow. Clearly, since onshore winds are needed for the advection which drives the TIBL, the TIBL cannot extend upward beyond the depth of the sea breeze into the return flow layer where warm air advection is important. It is hypothesized that the TIBL will deepen from the shoreline until the point where its depth equals that of the sea breeze, thereafter the depth of the TIBL will be determined by (and equal to) the depth of the sea breeze.

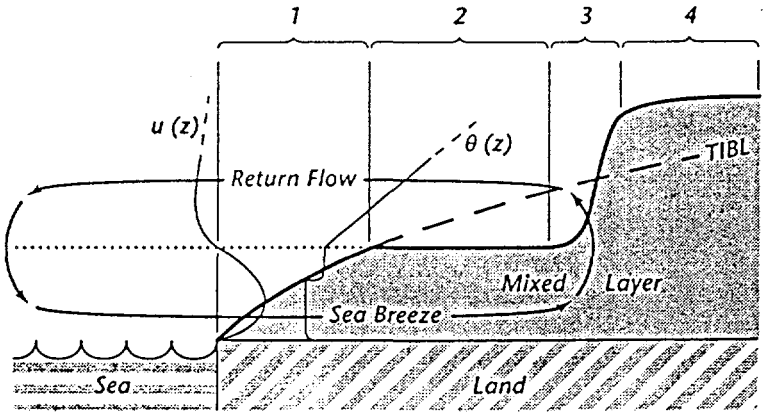


Figure 1. Idealized cross section of atmospheric structures in the coastal zone showing interaction between thermal internal boundary layer and sea breeze circulation. A strongly shaded region indicates MLD. Simplified profiles of velocity and potential temperature are indicated u (z) and θ(z) respectively.

The relation between SBC and TIBL is indicated in Figure 1, which is an idealized cross section of atmospheric structures in the coastal zone. The velocity profile holds at all positions within the sea breeze, while the potential temperature profile only holds in zone 1. In this zone, the TIBL is shallower than the sea breeze depth. This will result in a potential temperature profile with breaks at both TIBL and sea breeze depths. In zone 2, the entrainment zone will coincide with the zero in the sea breeze profile. Entrainment driven deepening of the MDL will be strongly suppressed by the advection of warm air aloft in the sea breeze return flow. In zone 3, entrainment enhanced by vertical motion above the sea breeze front will drive the MLD upward in a very short distance, as well as triggering the convective clouds often associated with the sea breeze front. In zone 4, the MLD has reached its full continental value. The hypothesized interaction between TIBL and SBC results in an MLD in zone 2 that is significantly shallower than the MLD predicted by simple slab TIBL theory. In the upwind portion of zone 4, the MLD will be deeper than that predicted by simple slab TIBL theory.

Observational evidence for the hypothesized interaction between TIBL and SBC is contained in the set of 36 pure sea breeze profiles analyzed by Steyn (1997). The profiles were measured between the coastline and 25 km inland from the coastline. This analysis shows that in all profiles analyzed, the TIBL was either shallower than the SBC (thus representing conditions in zone 1) or of equal depth to the SBC (thus representing conditions in zone 2). Physick et *al.* (1989) show potential temperature profiles at two locations in the coastal zone. They interpret a dramatic shallowing of the MLD in late afternoon as being due to an intrusion of cool marine air by a SBC. This is the same mechanism as outlined above and indicates a transition from zone 2 to zone 1.

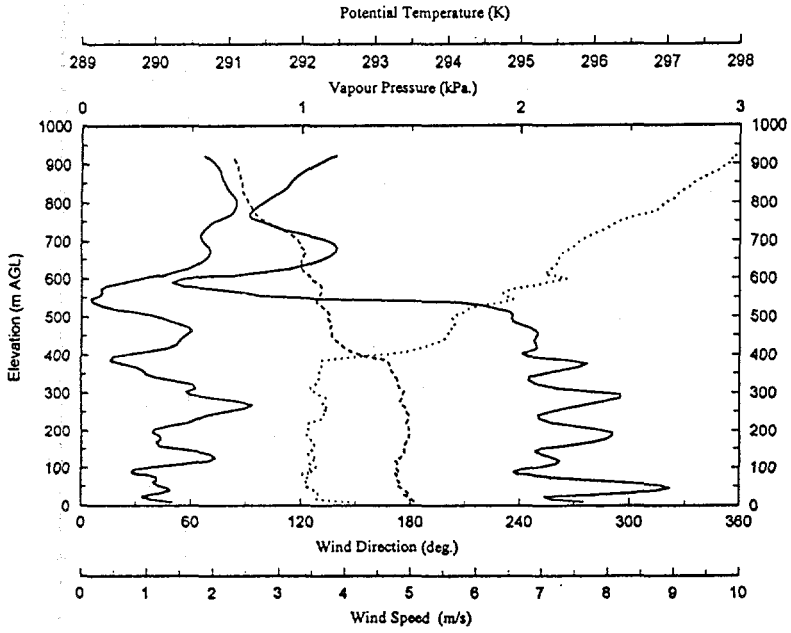


Figure 2. Profiles of wind speed (solid line to left of graph), wind direction (solid line to right of graph), potential temperature (dotted line) and vapour pressure (dashed line) measured at 1001 PST on 1985.08.23. Wind data have been smoothed by application of a seven point, binomially weighted moving average.

The data analyzed by Steyn (1997) contains a number of profiles demonstrating the effect described. Figure 2 is one of the profiles taken when the TIBL was shallower than the SBC (zone 1). The profiles of wind speed and direction indicate (by a sharp switch in wind direction accompanying a minimum in wind speed) that the sea breeze was approximately 550 m deep, while the potential temperature profile shows a TIBL about 380 m deep. The temperature profile between 380 and 440 m shows a sharp increase with height, followed by a transition to nearly isothermal conditions just below the sea breeze depth. Above that (after some variability) the profile reflects the upper capping inversion of synoptic origin. In addition to atmospheric structures in individual profiles, the data presented by Steyn (1977) contains a remarkable sequence of 11 profiles taken on one day at a point roughly 15 km from the coastline. Within the sequence, the TIBL is initially shallower than the sea breeze (zone 1), but grows to equal its depth (zone 2) between 1500 and 1600 LST, thereafter returning to depths shallower than the sea breeze (zone 1 again) in the early evening.

The position of transition between zones and 1 and 2 can be found by determining the fetch distance at which TIBL and SBC have the same depth. The position of zone 3 can be estimated by knowing the depth of penetration of the sea breeze. Estimates of the TIBL depth can be simply obtained from the slab model of Steyn and Oke (1982), while Steyn (1997) provides a scaling scheme for the strength and depth of the sea breeze. The operation of the hypothesized interaction between SBC and TIBL can be quantified from these two diagnostic schemes run in parallel. Input variables for the two schemes are diurnal variation of surface layer turbulent sensible heat flux density and land-sea temperature differences. Smoothed averages for these two variables appropriate for mid-latitude coastal locations are derived from ensemble averaged data. Figure 3 shows the results of the analysis. It shows that the square root TIBL behaviour (and therefore the position of transition between zones 1 and 2) extends from the coastline to roughly 13 km downwind between 0800 and 0900 LAT. This distance grows steadily to reach nearly 20 km by 1500 LAT. From 1500 to sunset (1900 LAT) it decreases quickly to roughly 12 km. The depths of the sea breeze and therefore the MLD in zone 2 never exceed 600 m.

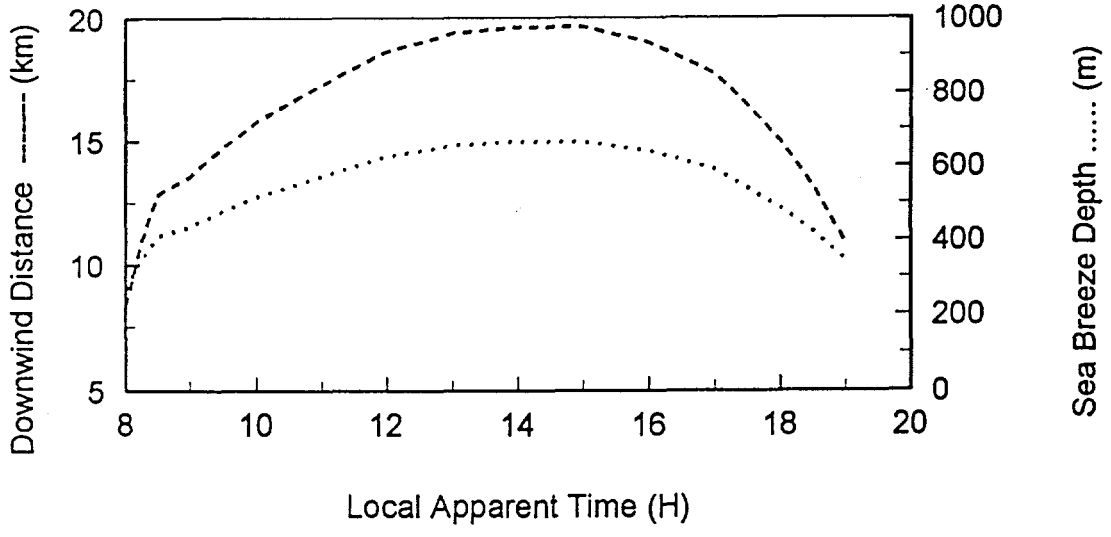


Figure 3: Simulated SBC depth and downwind distance at which TIBL equals SBC depth. The simulation is based on the scaling schemes for depth and strength of SBC of Steyn (1977) while TIBL depth is derived from the simple slab model of Steyn and Oke (1982).

The Steyn (1997) scaling scheme does not allow estimation of the horizontal extent of the sea breeze, and hence position of the sea breeze front, though observations indicate final inland penetration of 90 to 300 km. The sea breeze determined MLD would thus prevail to these inland distances.

## References


Steyn, D.G., 1997: Scaling the vertical structure of sea breezes. *Boundary Layer Meteorology*, Submitted. May, 1997.

Steyn, D. G. and T. R. Oke, 1982. The Depth of the Daytime Mixed Layer at Two Coastal Sites: A Model and its Validation, *Boundary Layer Meteorology*, 24, p. 161-180.

Physick, W.L., D.J. Abbs and R.A. Pielke, 1989: Formulation of the thermal internal boundary layer in a mesoscale model. *Boundary Layer Meteorology*, 49, p. 99- 112.

# Modelling the Internal Boundary Layer over the Lower Fraser Valley, British Columbia.

E. Batchvarova[1,2] , D. Steyn[3] , X. Cai[4],
S.-E. Gryning[1], M. Baldi[5]

[1] *Risø National Laboratory, Roskilde, Denmark*
[2]*National Institute of Meteorology and Hydrology, Sofia, Bulgaria*
[3]*Department of Geography, University of British Columbia, Vancouver, Canada*
[4]*School of Geography, University of Birmingham, Edgbaston, England*
[5]*Institute for Atmospheric Physics, IFA-CNR, Rome, Italy*

## Introduction

The height of the internal boundary layer that develops over land at onshore flow is an important parameter in many theoretical and practical applications. Slab models which assume that the air is well mixed in temperature within the internal boundary layer and is capped by an infinitesimally thin entrainment layer, have successfully been used to predict the internal boundary layer height in coastal areas (Gryning and Batchvarova, 1990, Melas and Kambezidis, 1992; Källstrand and Smedman, 1997). A more complete but also much more demanding modelling effort is to derive the turbulence parameters from higher order turbulence closure models. Then the internal boundary layer can be indirectly determined from the derived profiles.

In this study we use the very extensive data-set on temporal and spatial structure of the internal boundary layer on the Lower Faser Valley, Canada, collected during the so-called Pacific '93 field campaign, to study the ability of the simple applied model by Gryning and Batchvarova (1996) and the CSU-RAMS meso-scale model summarised in Pielke *et al.* (1992) to describe the development and variability of the internal boundary layer depth during the course of a day. Results from the two model simulations are compared with observations and discussed.

## Study area and observational data

In the summer of 1993, an intensive field study was conducted in the Lower Fraser Valley to investigate processes frequently leading to high ground-level ozone concentrations. Steyn et al. (1997) and Pottier et al. (1994) provide an overview of the study and details of all data collected. August 5, 1993 was characterised by warm, dry conditions as the regional weather was dominated by a stationary anticyclone. Data from this day are used for analysis in this study, as the measurements were particularly extense. Figure 1 indicates the location of fixed sensors. Vertical profiles of temperature and specific humidity from all thethered balloon (Harris road) and free balloon (Langley Central) soundings are interpreted to provide information on internal boundary layer height and the warming rate in the air above it. Measurements of turbulence fluxes of heat and momentum were carried out using 20 m tower mounted eddy correlation instrumentation at a location in the residential area of Vancouver about 10 km from the coastline (Sunset observational site, Figure 1). Wind speed and direction were measured on an hourly basis at a large number of routine meteorological stations scattered over the area. In the present study data from 13 stations situated on the valley floor (Figure 1) are used.

## Two models of internal boundary layer depth

*A SIMPLE APPLIED MODEL*

The slab model of Gryning and Batchvarova (1996) is used to model the development of the internal boundary layer during near neutral and unstable atmospheric conditions over land. The spatial and temporal evolution of the internal boundary layer over Lower Fraser Valley on 5 August 1993 was simulated starting at 7 PST when the heat flux at Sunset site became positive. The simulations were based on hourly averages of the model input parameters. The model domain shown in Figure 2 extends 120 km in the west-east direction and 124 km in the south-north direction with a 0.5 km grid resolution. The $u$ and $v$ wind field components in each grid point are derived by inverse distance (to the power 2) interpolation among the wind measurements at the 13 stations. The kinematic heat flux measured at the Sunset observational site was taken as basis for the simulation with a correction applied in each grid point for the actual land use. The heat flux in the urban areas and parks is assumed to be equal to the measured one, in the agricultural fields the value is reduced by 25% and in the mountains it is increased by 25 %. The friction velocity in each grid point was taken as a fraction of the interpolated wind speed for the actual grid point, the fraction being 0.1 for agricultural areas and mountains and 0.13 for urban areas and parks. These corrections were estimated based on earlier investigations in the area (Gryning and Batchvarova, 1996). The land use distribution is shown on Figure 2. Over the sea the height of the boundary layer was kept constant, in the actual simulation arbitrarily chosen as 10 meters. The kinematic heat flux and friction velocity are assumed equal to 0 for all water surfaces. A typical value of 0.007 deg/m is used for the temperature gradient above the internal boundary layer.

*FULLY THREE DIMENSIONAL MESOSCALE MODEL (CSU-RAMS)*

The Colorado State University Regional Atmospheric Modelling System (CSU-RAMS), described by Pielke et al. (1992) can be used to simulate atmospheric phenomena ranging from large eddy simulation of the atmospheric surface layer to mesoscale thunderstorm. When applied to a mesoscale simulation, nesting of model grids is allowed. In the present study, Smagorinsky's deformation turbulence closure scheme is used in the horizontal direction and Mellor-Yamada's second order closure scheme (Mellor et al., 1974) is used in the vertical direction. Three nested grids are used: the largest grid covers most of British Columbia, while the smallest one covers the region shown in Figure 1 and 2. Horizontal mesh spacing are respectively 40 km, 10 km, and 2.5 km for the three grids. Vertical mesh configuration is the same for all three grids. The first vertical mesh point for $u$ and $v$ is at 56.35 m, and the stretching ratio of the vertical mesh spacing is 1.2, with the maximum grid spacing being 2000 m. The top of the domain is at about 18.3 km, and a lid condition is adopted here for all variables. To prevent upward propagating gravity waves being reflected by this lid condition, a nudging layer is imposed from 4 km above with a time scale of 600 sec. At the surface, vertical velocity is specified zero, horizontal velocity components and temperature are given by the Businger-Dyer surface layer similarity relationship, through Louis' scheme (Businger et al.,1971;Louis, 1979). Five soil levels are adopted and their depths are 0.0, 0.1, 0.3, 0.6, 1.0 m. In addition, a vegetation model is used in the present study. The simulation starts at 1600 PST on August 4, 1993, with 12 extra hours to allow non-physical components to be diffused or dissipated. The simulation ends at 0400 PST on August 6 so that total 36 hours results have been obtained. We are only interested in the results in the daytime of 5 August during which observational data are available for comparison. In the present application, the top of the internal boundary layer is diagnosed from the vertical profile of the turbulence kinetic energy (TKE).

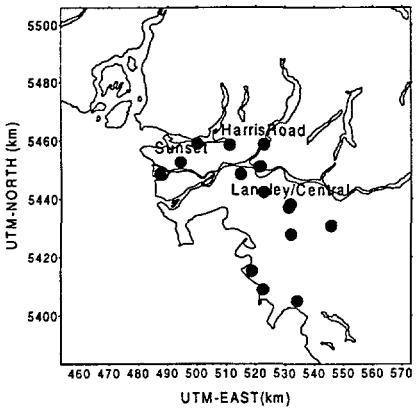


*Figure 1.* Map of the Lower Fraser valley coastline (solid line), tethered balloon (Harris Road), radiosonde (Langley Central), turbulence measuring site (Sunset) and wind measuring sites (balck circles).

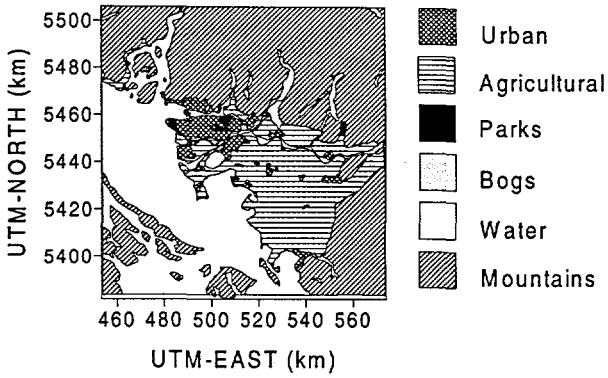


*Figure 2.* Map of the Lower Fraser Valley modellig domain showing the land use pattern.

## Modelling results

Figure 3 shows the evolution of the simulated by the *SIMPLE APPLIED MODEL* (solid line) and measured height of the internal boundary layer at Langley Central (black square) and Harris Road (balck circle). The 1000 PST sounding at Langley Central shows a significantly higher internal boundary layer than simulated, but the next sounding (at 1300 PST) indicates good agreement between model simulations and measurements. At Harris Road the internal boundary layer height was deduced from the tethersoundings carried out throughout the whole day. The agreement between measurements and model simulations is very good.

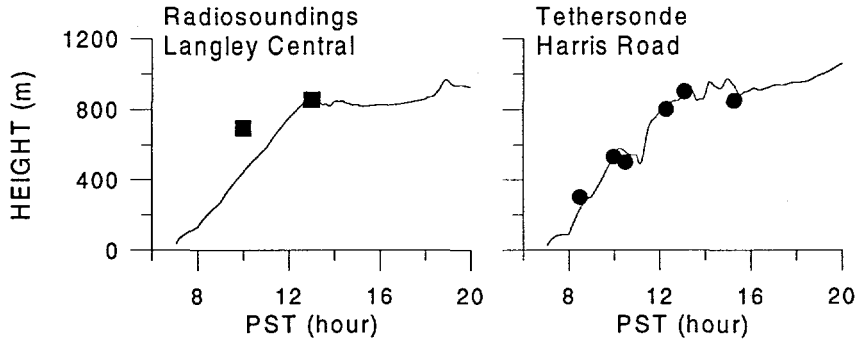


Figure 3. (Reference in the text)

Figure 4 shows the simulated by the *FULLY THREE DIMENSIONAL MESOSCALE MODEL (CSU-RAMS)* (solid line) and measured temporal variation of the internal boundary layer height at Langley Central (black squares) and Harris Road (black circles). For the Langley Central site, the modelled internal boundary layer height closely matches the measurements except for a slight underestimate around mid-day. For Harris Road site, the agreement between the modelled and the observed internal boundary layer height is very good not only during the morning with a developing mixed layer, but also during the afternoon when the mixed layer is decaying.

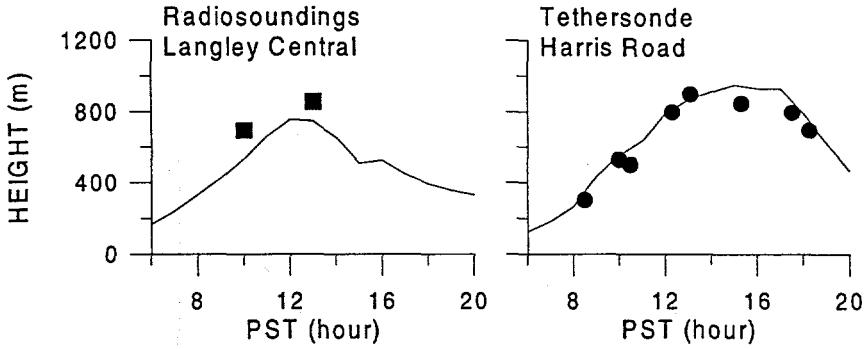


Figure 4. (Reference in the text)

## Conclusions

Given the complexity of topography, coastline and landuse in the Lower Fraser Valley region, both models perform remarkably well. The simple applied model performs extremely well, given its simplicity. It is clear that correct specification of spatially resolved surface sensible heat flux and wind field are crucial to the success of this model which can be operated at very fine spatial resolution. The 3D model performs extremely well, though it too must capture the local wind field correctly for complete success. Its limited horizontal resolution results in strongly smoothed internal boundary layer height fields.


## Acknowledgements

Data was drawn from parts of the Pacific '93 field study funded by Environment Canada, The U.S. National Oceanographic and Oceanic Administration and was partially funded by grants awarded by the Atmospheric Environment Service of Environment Canada and the Natural Science and Engineering Research Council of Canada. The study was supported by the Danish Environmental Research Programme, 1992-1996. Kate Stephens and Roy Hourston analysed some of the data.


## References


Businger, J. A., J. C. Wyngaard, Y. Izumi and E. F. Bradley, 1971: Flux profile relationships in the atmospheric surface layer, *J. Atmos. Sci.*, **28**, 181-189.

Gryning S.E. and Batcharova E.: 1990, 'Analytical model for the growth of the coastal internal boundary layer during onshore flow', *Quart. J. Roy. Met. Soc.*, **116**, 187-203.

Gryning, S. E. and Batchvarova, E.: 1996, 'A model for the height of the internal boundary layer over an area with an irregular coastline', *Boundary-Layer Meteorol.*, **78**, 405-413.

Källstrand, B. and Smedman, A. S.: 1998, 'A case study of the near neutral coastal internal boundary layer growth - Aircraft measurements compared with different model estimates', Accepted for publication in *Boundary-Layer Meteorol.*

Louis, J.-F.: 1979, 'A parametric model of vertical eddy fluxes in the atmosphere', *Boundary Layer Meteorol.*, **17**, 187-202.

Melas, D., and Kambezidis, H. D.: 1992, 'The Depth of the Internal Boundary Layer over an Urban Area under Sea-Breeze Conditions', *Boundary-Layer Meteorol., 61*, 247-274.

Mellor, G., and Yamada, T.: 1974, 'A hierarchy of turbulence closure models for planetary boundary layer', *J. Atmos. Sci.*, **31**, 1791-1806.

Pielke, R., Cotton, W., Walko, R., Tremback, C., Lyons, W., Grasso, L., Nicholls, M., Moran, M., Wesley, D., Lee, T., and Copeland, J., 1992: 'A comprehensive meteorological modelling system - RAMS', *Meteorology and Atmospheric Physics, 49*, 69-91.

Pottier, J., Thomson B., Bottenheim J., and Steyn D.G., 1994: *'Lower Fraser Valley oxidants study and Pacific '93 meta data report'*, Canadian Institute for Research in Atmospheric Chemistry. 50p.

Steyn, D.G., Bottenheim J.W., and Thomson R.B., 1997: 'Overview of tropospheric ozone in the Lower Fraser Valley, and the PACIFIC *'93* field study', *Atmos. Env.* In Press.

# Simulation of the convective mixed layer in Athens

Helmut P. Frank

Risø National Laboratory, Roskilde, Denmark

## Introduction

The region of Athens, Greece, has a highly complicated terrain with irregular coastline and mountains next to the sea. This results in complex flow fields. A case study of a simulation of a sea breeze with the Karlsruhe Atmospheric Mesoscale Model KAMM (Adrian and Fiedler, 1991; Adrian, 1994) is presented together with remarks on the advection of mixed layer air.

The valley of Athens is open to the sea towards the south-west and surrounded by mountains on the other sides. Gaps between the mountains channel the flow into the valley. Simulations were done for 14 September 1994 to compare them with measurements at 6 masts by Risø (Batchvarova and Gryning, 1996) during the MEDCAPHOT-TRACE experiment. It was a day when a stable sea breeze developed in most of the valley. However, another sea breeze from the Mesogia Plain east of the mountains traversed the pass and entered the north-eastern part of the Athens valley.

## Model description and determination of the mixed layer height

The Karlsruhe Atmospheric Mesoscale Model KAMM (Adrian and Fiedler, 1991; Adrian, 1994) is a three–dimensional, non-hydrostatic atmospheric mesoscale model with first order turbulence closure. For the convective mixed layer, i.e. if the surface heat flux is positive, turbulent diffusivities of a non-local closure by Degrazia (1989) are used. The atmospheric model is coupled to a soil-vegetation model as described in Schädler et al. (1990).

Deardorff's (1973) equation is used for the growth of the convective mixed layer. It is frequently written as

$$\frac{dh}{dt} = w_h + w_e \tag{1}$$

with the large-scale vertical motion $w_h$ at the top of the mixed layer and the entrainment velocity

$$w_e = 1.8 \frac{{w_*}^3 + 1.1{u_*}^3 - 3.3{u_*}^2 fh}{\frac{g}{\theta_{v0}} \frac{\partial \theta_{v+}}{\partial z} h^2 + 9{w_*}^2 + 7.2{u_*}^2} \tag{2}$$

Deardorff's parameterization of the entrainment velocity $w_e$ (equ. 2) works well. However, the advection term from the total derivative of $h$ and the mean flow out of the mixed layer is a problem. Shortly, we want to mention the question which advection velocities and which horizontal gradients must be used.

Consider two-dimensional, homogeneous flow of depth $H$. Its continuity equation is (e.g. Gill, 1982, Ch. 5.6) $\frac{\partial H}{\partial t} = -\frac{\partial UH}{\partial x}$. Including entrainment we have for the mixed layer

$$\frac{\partial h}{\partial t} = -\frac{\partial Uh}{\partial x} + w_e \tag{3}$$

where $U$ is the layer-averaged velocity $U(x,t) = \frac{1}{h}\int_s^{s+h} u(x,z,t)dz$, and $s$ is the height of the surface.

Differentiating $U$ we obtain

$$\frac{\partial U}{\partial x} = \left( -\frac{\partial h}{\partial x} U - w(x, s+h, t) + u(x, s+h, t) \frac{\partial (h+s)}{\partial x} \right) \Big/ h \qquad (4)$$

for viscous flow with zero velocity at the surface.

Using (4) in (3) we obtain the, perhaps surprising, result

$$\frac{\partial h}{\partial t} = w(x, s+h, t) - u(x, s+h, t) \frac{\partial (h+s)}{\partial x} + w_e \qquad (5)$$

The advection speed is the speed at the top of the mixed layer. However, it must multiply the gradient of $(h+s)$, the height of the mixed layer above a constant elevation, *not* the gradient of $h$. Which means that (1) is not correct.

If the layer-averaged advection velocity is employed, then the vertical velocity at the top of the mixed layer, $w_h$, drops out, and

$$\frac{\partial h}{\partial t} = -\frac{\partial}{\partial x} \left( \int_s^{s+h} u(x, z, t) dz \right) + w_e \qquad (6)$$

In a numerical model the velocity field is available only at a few discrete levels $z_k$. Therefore $w(x, s+h, t)$ and $u(x, s+h, t)$ must be interpolated. Often there is strong vertical shear at the top of the mixed layer. This means that small errors in $h$ or in the used interpolation functions will give relatively big errors in the advection using (5). Equation (6) is more robust over for these approximations.

Both, equations (5) and (6), face the problem of spatial unsteadiness of $h$, e.g. between stably stratified and unstably stratified regions, or when two separate boundary layers meet as e.g. on a mountain ridge where the mixed layer on the sun-facing slope is expected to be deeper than on the shady side. It is not clear, yet, how to handle this most sensibly.

Convergence zones with high vertical velocities yield very high mixed layer heights. Trying to prevent this, the parcel criterion (Holzworth, 1967) was added. $h$ must not be greater than the height at which a rising parcel becomes neutrally buoyant. However, this limited $h$ only in the late afternoon. Another diagnostic control is that no large positive gradient of the virtual potential temperature $\theta_v$ may exist below the calculated $h$. Otherwise, its height is taken as the mixed layer height.

**Results for a day of MEDCAPHOT-TRACE**

The simulation was done for a domain of 159 × 159 km$^2$ with a grid resolution of 3 km. The model consisted of 26 layers with variable vertical resolution up to 6000 m altitude. The water temperature was 21°C, and the soil temperature at sea level 24°C. The soil temperature decreased 6 K/km with altitude. A uniform land use with dry fields was specified. The model was initialized at 3 local time (LT) with a sounding from Helleniko Airport and run for the rest of the day.

Time series of observed and modeled wind direction, speed, and modeled convective mixed layer height $h$ are shown in Figure 1. Delta Faliro is directly at the coast, NOA further inland and Marousi close to the gap to the Mesogia plain east of the mountains (see also Figure 2 for the positions). The onset of the sea breeze and its development until approximately 16 LT is well captured. The modeled mixed layer height at 12 LT is plotted in Figure 2. It is low in the coastal plains and the Athens valley, and high over the

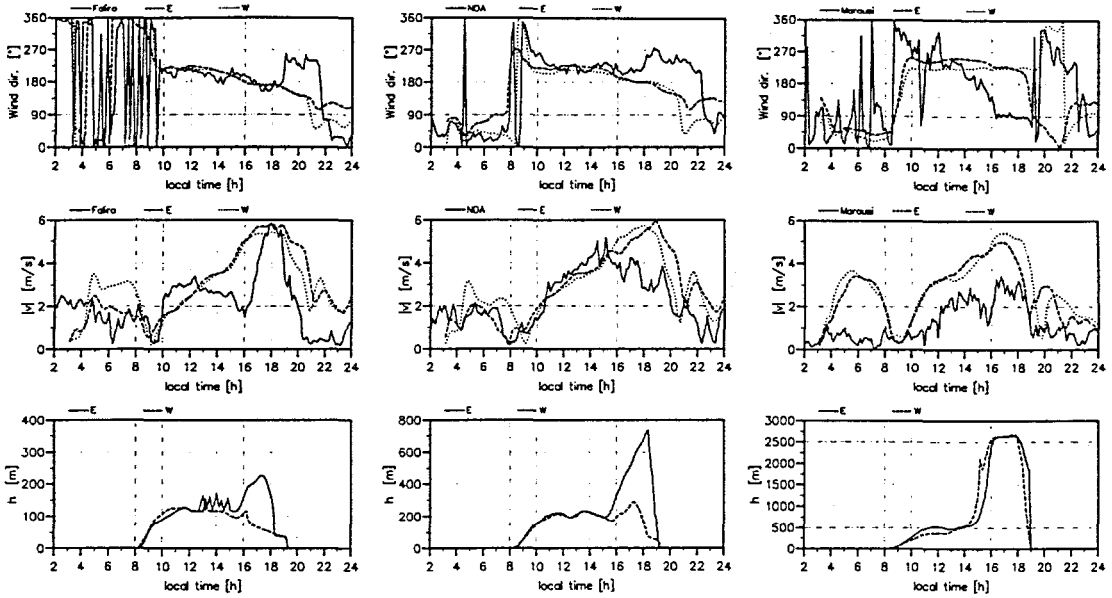


**Figure 1**: Time series of wind direction, wind speed and modeled mixed layer height at Delta Faliro (left), NOA (center), and Marousi (right). The full lines of direction and speed are observations at the Risø masts. The other lines are model results at grid points east (E) and west (W) of the position of the masts.

mountains. Also, the mountains are zones of horizontal confluence where air from the mixed layer is blowing into the free atmosphere.

At about 16 LT the observed wind at Faliro is strengthening rapidly. At 18 LT it turns abruptly west at Faliro and NOA. This is not captured by the model. It might be the effect of a slight change of the large-scale forcing which is not present in the simulation which was performed with fixed large-scale fields. Only the diurnally varying insolation is forcing the simulated mesoscale flow field.

KAMM simulates a gradual backing of the wind near Faliro and NOA. This means that warmer air of a deep mixed layer is advected which yields a much deeper mixed layer in the eastern valley than in the afternoon.

At Marousi the model does not reproduce the easterly winds at 16 LT when the sea breeze from the east enters the Athens basin. In the simulation the confluence zone still is along the pass (Figure 2, right). This is also a result of the deep modeled mixed layer forced by the strong heating of the surface and the rising motion at the mountains. Erroneously, in one experiment the mixed layer advection in equation (5) had been calculated with the layer averaged velocity. Then, the mixed layer was thinner and the eastern sea breeze did enter the Athens basin at approximately 16 LT. This demonstrates how important the correct mixed layer height and its advection can be.

## Further work

The question of how to handle convergence zones and spatially unsteady mixed layer heights needs further investigation. A simulation with finer grid might yield better agreement with the observations as the orography is better resolved.

## Acknowledgments

The author thanks Sven-Erik Gryning and Ekaterina Batchvarova for discussions about this work. KAMM was provided by Franz Fiedler and Gerhard Adrian from the

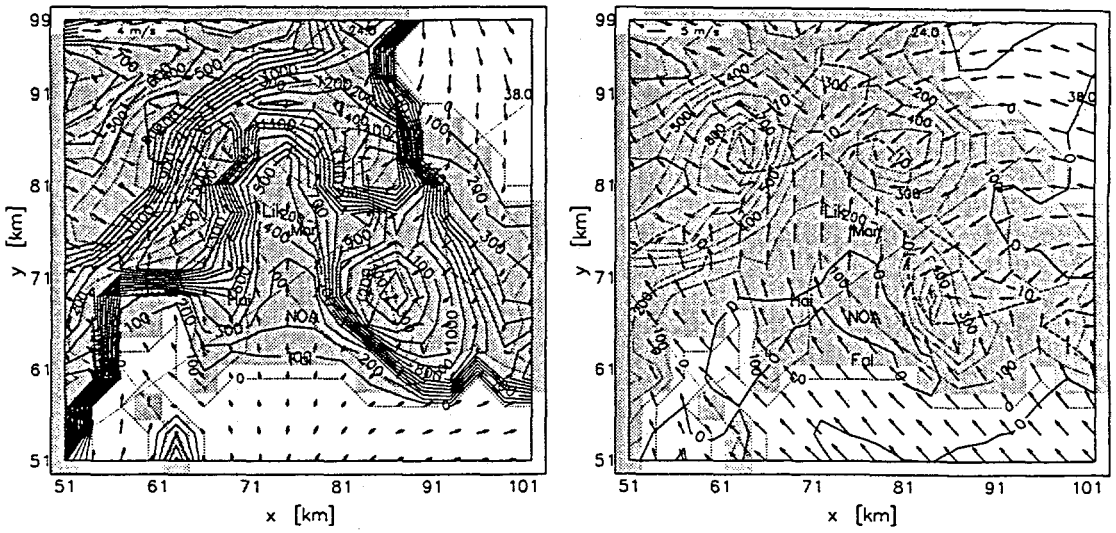


**Figure 2**: Left: Modeled mixed layer height at 12 LT and wind arrows at 15 m agl. The interval of the isolines is 100 m. Right: Confluence $(u_x + v_y)$ in $10^{-4}$ s$^{-1}$ and wind arrows at 50 m agl. at 16 LT. Grid points over land are shaded. Height lines are dotted with 100 m intervals. The model domain is rotated 35° relative to true north. 38° North and 24° East are drawn as dotted lines for orientation. The positions of the Risø masts are indicated by their inital letters.

University of Karlsruhe.

## References

Adrian, G.: 1994, Zur Dynamik des Windfeldes über orographisch gegliedertem Gelände, *Report 188*, Ber. d. Deutschen Wetterdienstes, Offenbach am Main. ISBN 3-88148-295-4.

Adrian, G. and Fiedler, F.: 1991, Simulation of unstationary wind and temperature fields over complex terrain and comparison with observations, *Beitr. Phys. Atmosph.* **64**, 27–48.

Batchvarova, E. and Gryning, S.-E.: 1996, Meteorological measurements, wind climatology, atmospheric turbulence and internal boundary layer development in Athens during the Medcaphot-Trace experiment, *Report Risø-R-877(EN)*, Risø National Laboratory, Roskilde, Denmark. ISBN 87-550-2161-1.

Deardorff, J. W.: 1973, Three-dimensional numerical study of the height and mean structure of a heated planetary boundary layer, *Boundary-Layer Meteorol.* **1**, 81–106.

Degrazia, G. A.: 1989, Zur Anwendung von ähnlichkeitsverfahren auf die turbulente Diffusion in der konvektiven und stabilen Grenzschicht, *Report 12*, Wiss. Ber. Inst. Meteor. Klimaf. Univ. Karlsruhe.

Gill, A. E.: 1982, *Atmosphere-Ocean Dynamics*, Vol. 30 of *International Geophysics Series*, Academic Press.

Holzworth, C. G.: 1967, Mixing depths, wind speeds and air pollution potential for selected locations in the United States, *J. Appl. Meteor.* **6**, 1039–1044.

Schädler, G., Kalthoff, N. and Fiedler, F.: 1990, Validation of a model for heat, mass and momentum exchange over vegetated surfaces using LOTREX-10E/HIBE88 data, *Beitr. Phys. Atmosph.* **63**, 85–100.

# Sensitivity Analysis of the Boundary Layer Height on Idealised Cities (model study)

G. Schayes[1], P. Grossi[2]

[1] University of Louvain, Louvain-la-Neuve, Belgium
[2] Joint Research Center, Ispra, Italy

## Introduction

The behaviour of the typical diurnal variation of the atmospheric boundary layer (ABL) over cities is a complex function of very numerous environmental parameters. Some of them are obvious (city size, roughness elements and their associated roughness lengths, topography, season, state of the atmosphere and meteorological situation), but others have a much less clear effect or are even difficult to describe accurately (e.g. city structure, urban heat island effect, anthropogenic energy waste, etc.). Moreover, most existing cities have a too complex structure to be used for a phenomenological study.

In order to investigate the effect of some of these parameters a model study has been effectuated on idealised cities having a simplified structure defined with few parameters. Also to avoid additional topographic complexities, only flat terrain has been chosen.

Two types of geographical situations have been retained : (i) inland city only surrounded by uniform fields, (ii) coastal city, thus influenced by the sea/land breeze effect.

For this study, we have used the three-dimensional Thermal Vorticity-mode Mesoscale (TVM) model developed jointly by the UCL (Belgium) and JRC (Italy). In this study it has been used in 2-D mode allowing to perform many sensitivity runs. This implies that a kind of infinitely wide city has been effectively simulated, but this does not affect the conclusions for the ABL height.

The sensibility study has been performed for two turbulence closure schemes (those of Therry and Lacarrère (TL), and of Duynkerke (DK)), for various assumptions for the ABL height definition in the model, and for a selected parameter: the soil water content.

## The meso model and surface representation

The TVM model is non-hydrostatic, Boussinesq, and incompressible. The dynamic equations use the vorticity formulation having the advantage of dropping the density and the pressure out of the equations at the expense of a few more computations.

The contact between the atmosphere and the surface is realized with an analytical constant flux surface layer. The temperature and humidity conditions at the ground surface are computed by a soil submodel (SVAT) based on the energy balance at the surface. In this study, the dry version of the code is used (no water vapor saturation). Atmospheric cooling rates due to infra-red radiation flux divergence are computed using the Sasamori radiation scheme.

The turbulence closure uses an additional turbulent kinetic energy (TKE) equation. The dissipation and diffusion mixing lengths are calculated analytically in the Therry-Lacarrère scheme (TL) or via a prognostic equation for the dissipation ε in the Duynkerke scheme (DK).

The Soil-Vegetation-Atmosphere Transfer sub-model (SVAT) of De Ridder et al. (1997) is used. Its main characteristic is the original formulation of the stomatal resistance dependence on visible radiation and leaf water potential, reducing the number of needed empirical formula. In this study, the cities characteristics have been adapted to be simulated by a kind of particular « downtown » and « residential » canopy whose parameters are described here below.

**City representation**

Two of kind idealized cities were considered in this study: a coastal city and an inland city. Both city types comprise a downtown and a residential area. Since the soil and vegetation models included in the TVM code do not provide for a specific description of urban areas, soil and vegetation parameters where adjusted with preliminary runs to match daily heat fluxes evolution that can be considered as characteristic of an European city at 45° latitude during summer. The soil type selected to represent the concrete is clay, a coarse soil with a low heat and water conductivity. The urban canopy was represented using appropriate value of roughness and displacement length, as well as elevated values of minimum stomatal resistance and dead leaf fraction. The most important soil and canopy characteristics are summarized in table I below.

Table I. Main soil and canopy characteristics chosen for the representation of the city parts.

| | Soil type | Soil moisture (%) | Vegetation height (m) | Displacement height (m) | Roughness (m) | Min. stomatal resistance (s/m) |
|---|---|---|---|---|---|---|
| **Down Town** | clay | 25. | 20. | 14. | 1. | 500. |
| **Residential** | clay | 30. | 7. | 5. | 0.40 | 100. |
| **Agricultural** | clay | 35. | 0.50 | 0.35 | 0.05 | 50. |

**Simulated cases**

Three different methodologies are used to calculate the mixing height (MH) in this work.

1. in neutral and convective conditions, MH is assumed to be the level (starting from the model top) where TKE equals 10 % of TKE ground value. For stable conditions MH is assumed to be defined following the well known relation $MH = 0.3u_* / f$ (where $f$ is the Coriolis parameter, and $u_*$ the friction velocity). This definition is applied with the two different turbulence closures used here (TL and DK).
2. same as (1) but one assumes MH to be the level (starting from the model top) where TKE equals 1 % of the ground value, for all atmospheric stability classes.
3. MH determination based on the sensible heat flux (HF) vertical profiles: during the day MH is defined as the level where HF becomes negative, while during the night MH is the height where HF becomes zero.

A second issue of the work is to test the sensitivity of the MH calculation to variations of some surface characteristics. As also shown by Sun et al. (1996), MH is most sensitive to the

amount of soil water content, due to the fact that this parameter controls the surface heat fluxes and hence the atmospheric buoyant turbulence. Three simulations have been performed for each city type, varying the soil water content as shown in Table II. A second ground parameter which is expected to be important in determining MH is the soil roughness, due to its influence on mechanical generated turbulence. The sensitivity at the surface roughness is examined by substituting the most rough urban area (down town) with a smoother ground cover (residential).

Table II. Values of the soil humidity used in the sensitivity runs

| | **Soil water content** | | |
|---|---|---|---|
| | standard | reduced | increased |
| **Down Town** | 25. | 20. | 30. |
| **Residential** | 30. | 25. | 35. |
| **Agricultural** | 35. | 30. | 40. |

**Results**

The model simulation starts at 6:00 LST and lasts for 37 hours. The model is initialized with a standard potential temperature gradient of 3.5 $K.Km^{-1}$ from the ground up to the top of the model and a geostrophic wind of 3 m/s is imposed at the model top. This generates some mechanical turbulence, due to the presence of rough elements at ground level. Figure 1 shows the typical TKE distribution along the simulated vertical plane for the standard run at 1300 LST (MH defined as 10 % of surface value). The highest TKE is naturally to be found close to the downtown area (D), but in the upper levels, the maximum TKE is blown over the western residential area (R) due to advection.

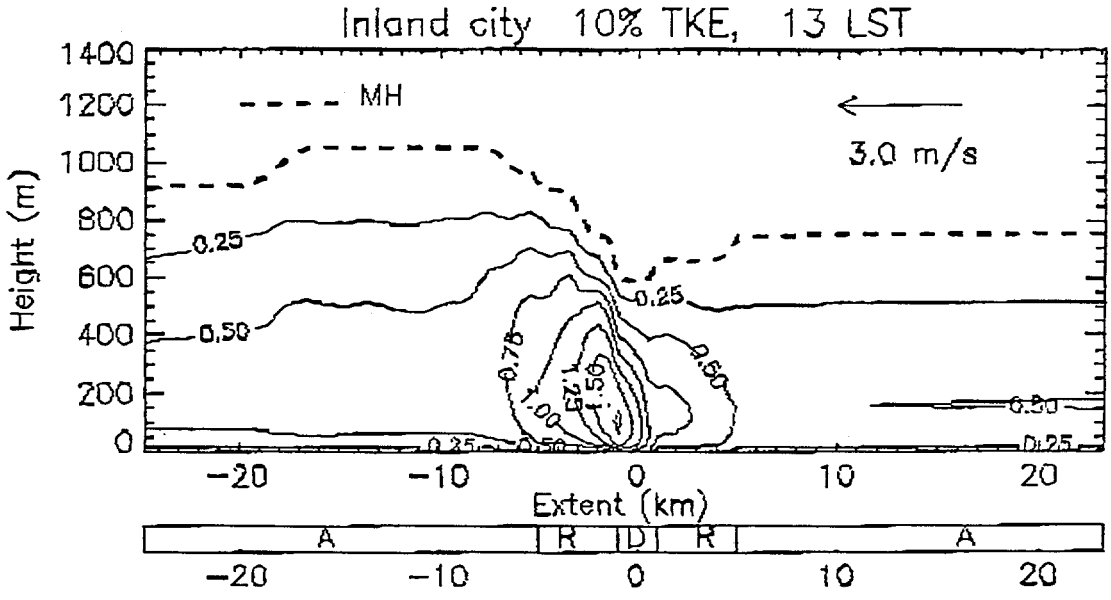


Figure 1. Typical TKE spatial distribution for the standard run at 1300 LST . Letters A, R and D denote respectively the agricultural, residential and downtown part of the idealised city.

The comparison of the different MH definitions is represented on figure 2. Little sensitivity between the different methods is observed. Quite naturally the 1 % TKE definition gives higher

MH values, while HF definition drops to small values sooner at the end of the afternoon. It is interesting to note that the heat flux method, usually applied to pure convective ABL, gives results close to those obtained with the TKE profiles, even though the simulations here concern shear-convective ABL. The MH calculation based on TKE profile, in turn, is shown to be sensitive to the turbulence closure scheme. The DK scheme shows to be more dissipative than the TL scheme; giving weaker TKE and lower MH values. This is mainly evident in the coastal city case, where MH reduces to about 50% from the TL values. For all methods, the maximum development of the MH is obtained about 2-3 km "down wind" to the city, where an internal boundary layer is formed due to the advection of warm air from the city.

As expected, the MH is sensitive to the ground moisture, especially during the second day due to the drying out of the soil.

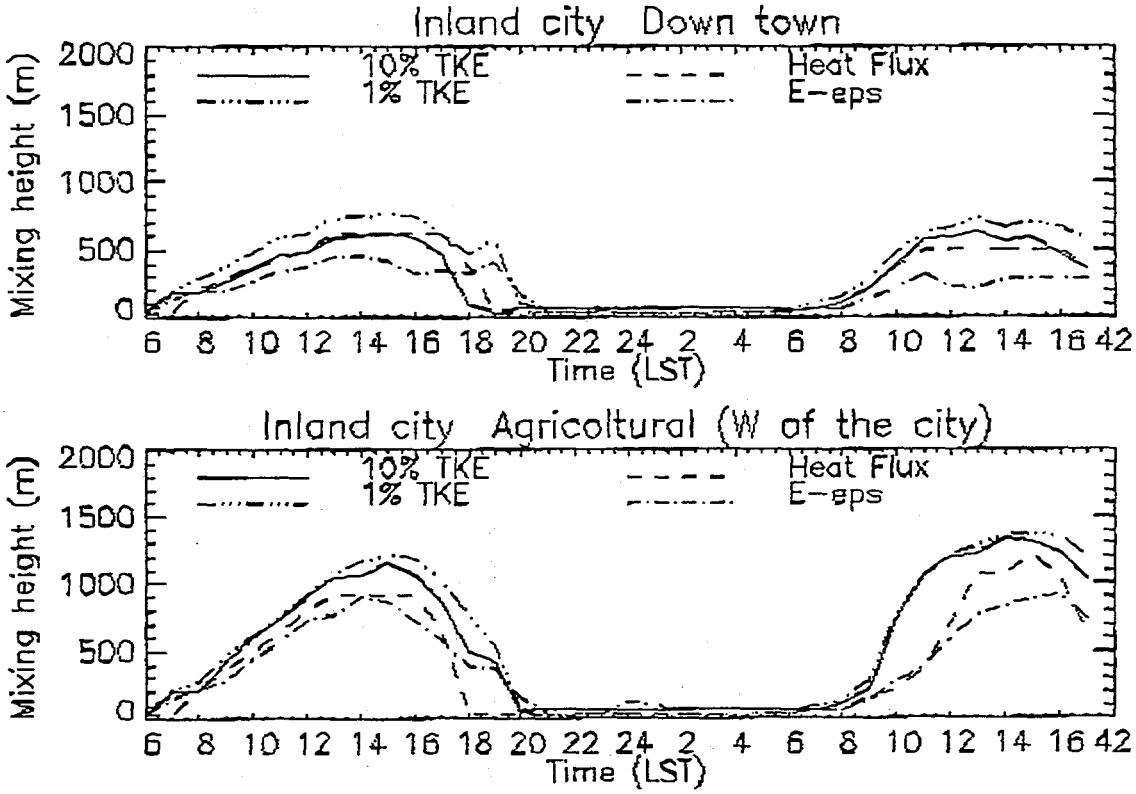


Figure 2. Time variation of the mixing height over the downtown area (upper graph) and the agricultural area (lower graph) using the different assumptions for the mixing height.

## References


Bornstein R., Thunis P., Grossi P., Schayes G., 1996. Topographic Vorticity-Mode Mesoscale-β (Tvm) Model. Part II: Evaluation. *Journ. Appl. Meteor.* **35**, 1824-1834.

De Ridder K., Schayes G., 1996. Description and Validation of the IAGL Land Surface Flux Model. *Journ. Aplied. Meteorol.* **36**, 167-182.

Schayes G., Thunis P., Bornstein R., 1996. Topographic Vorticity-Mode Mesoscale-β (Tvm) Model. Part I: Formulation. *Journ. Appl. Meteor.* **35**, 1815-1823.

Sun Wen-Yih and M. G. Bosilovich, 1996. Planetary Boundary Layer and Surface Layer Sensitivity to Land Surface Parameters, *Boundary Layer Meteorology*, 77, 353-378.

# Sodar Measurements of the Mixed-Layer Depth Over a Large City

E. A. Shurygin

Institute of Atmospheric Physics, Russia Academy of Sciences, Moscow, Russia

## Introduction

For determination of the mixed-layer depth in the last decade the methods of remote sounding of atmosphere, in particular sodars (up to height of 600 m) and wind profiler radars (up to several kilometers) are widely applied. In comparison with WPR the sodars at present have the best space resolution and can find out low inversions, the most dangerous from the point of view of pollution. Application of WPR in urban conditions is also limited because of mutual interference with TV broadcast channels.

The evaluation of the mixed-layer depth by sodar is based on an opportunity of inversion identification (ground based and elevated) and determination of the temperature stratification or degree of stability of the ABL from facsimile records (Beyrich, 1996; Russel, 1978). In given paper the results of determination of a daily and seasonal course of the mixed-layer depth over large city (Moscow) and its vicinities by a method of acoustic sounding are submitted.

## Seasonal and daily course of mixed-layer depth

Measurements of the characteristics of ABL over Moscow were conducted during 1988-1991 years (Pekour, 1993). Figures 1 and 2 shows an annual and daily course of averaged mixed-layer depth. In the spring and summer seasons the depth is grows from 200-250 м up to 600-700 м after sunrise, which is a consequence of high percentage of repeatability of convections. At night time in autumn and winter seasons the mean values of mixed-layer depth exceed the same for spring and summer seasons on 100-150 м.

## Horizontal inhomogeneity of ABL

The realization of the simultaneous sodar measurements in several sites permits to compare an ABL structure in these sites and evaluate a degree of its horizontal homogeneity. For this purpose a 3-dimensional Doppler sodar was placed in a center of the city, on a roof of the Institute of Atmosphere Physics building at height of 13 meters above the ground. Another sodar was located in an agricultural region in 45 km from a center of Moscow on a roof of two-store building.

Results of synchronous sodars measurements during one summer and autumn months have shown that in the winter only about a third of all cases with convect conditions at suburban area are accompanied by the same type of stratification in the city. In summer season practically all cases of convection at the suburban area are accompanied by convection in the centre. But in the centre of the city sometimes exist convection, accompanied by neutral stratification at rural area. The coinsidence of types of stratification were observed between these two places in 40 % from a whole time of synchronous measurements.

On Figures 3-4 the mean daily courses of a difference in repeatability between some types of stratification in Moscow and suburban area for a summer period of measurements (July 1991) are shown. The development of convection begins at the same time, but in the city the processes of erosion of elevated inversion layer proceed faster, so a developed convection (Fig. 3) established early. The values of a difference in repeatability for neutral stratification, ground based and elevated inversions in a day time are near zero, but in a transition time can be 40-60 % (Fig. 4). Thus, both delays in transients of a daily cycle as some constant distinctions of ABL stratification in the center of the city and in the agricultural district were observed.

Comparison of values of height of ground based inversion simultaneously measured by sodars located at two places is submitted on Figure 5. That draws show, that the mean height of inversion layers in the centre of the city is located on 50-150 m higher than in suburban area. At different stratification between the city and periphery the distinction in the mixed-layer depth can reach up to 200 m. That is in accordance with results observed in other large cities (Godowitch, 1985; Dohrn, 1982).

**Summary**

The results of synchronous sodar's measurements on a territory of city and suburban area have shown:

a). The types of stratification over centre of the city and periphery considerably differ, and these distinctions are more often displayed in morning and evening transition period. The agreement between types of stratification in the centre and on the periphery was observed in 40 % of cases;

b). At equal temperature stratification the mixed-layer depth in centre of the city is about 50-150 m higher at inversions in comparison with a periphery, at advanced convection - these depths are identical;

c). At different stratification between the city and periphery the distinction in the mixed-layer depth can reach 200.

**Ascknowledgments**

We thank Russion Foundation for Fundamental Researches (projects 96-05-65741 and 96-05-65351) for supporting our investigations.

**References**

Beyrich, F. 1996: On the Estimation of Mixed-Layer Height from Sodar Data (a review). In M.A. Kallistratova (ed.), *Proceed.Of 8 th Int. Symp on Acoustic Remote Sensing and Associated Techniques of the Atmosphere and Oceans*, Moscow 27-31 May 1996, part 6, pp. 11-22.

Dohrn, R., Raschke E., Warmbier G. 1982: Inversion Structure Heights above the City of Cologne (Germany) and a Rural Station nearby as Measured with two Sodars. *Meteorol. Rdsch.*, **35**, 5, 133-144.

Godowitch, J.M., Ching J.K., Clarke J.F. 1985: Evolution of the inversion layer at an urban and nonurban location. *J. Climate and Applied Meteorology*, **24**, 791-804.

Pekour M.S. and Kallistratova M.A. 1993: Sodar study of the boundary layer over Moscow for air-pollution application, *Appl. Phys.*, **B 57**, 49-55.

Russel, P.B., Uthe E.E.. 1978: Regional patterns of mixing depth and stability: sodar network measurements for input to air qua lity models. *Bull. Amer. Meteorol. Soc.*, **54**, 1275-1287.

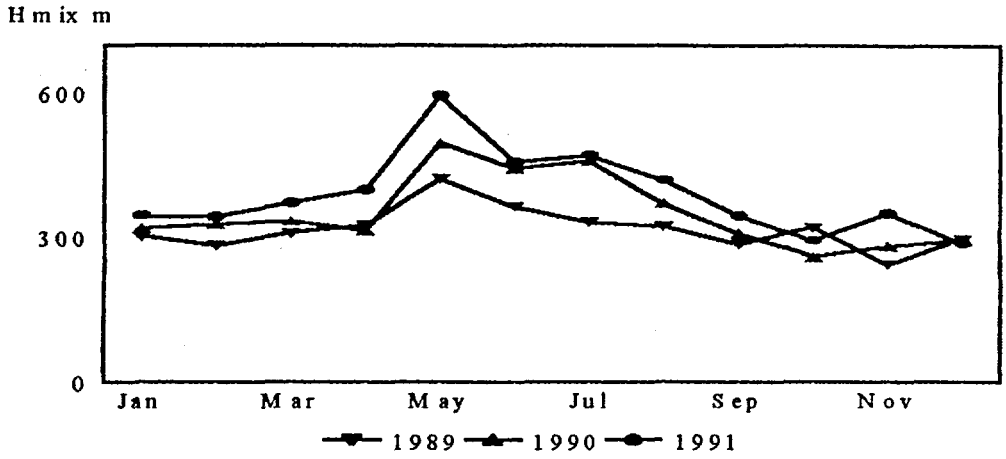


**Figure 1.** Annual course of mean mixed-layer depth.

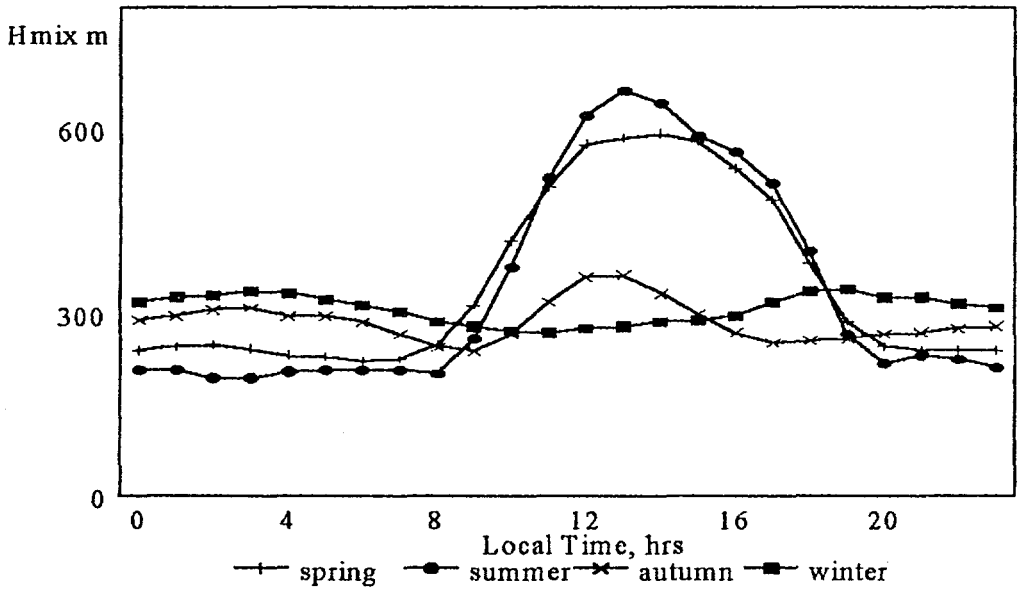


**Figure 2.** Seasonal course of mean mixed-layer depth

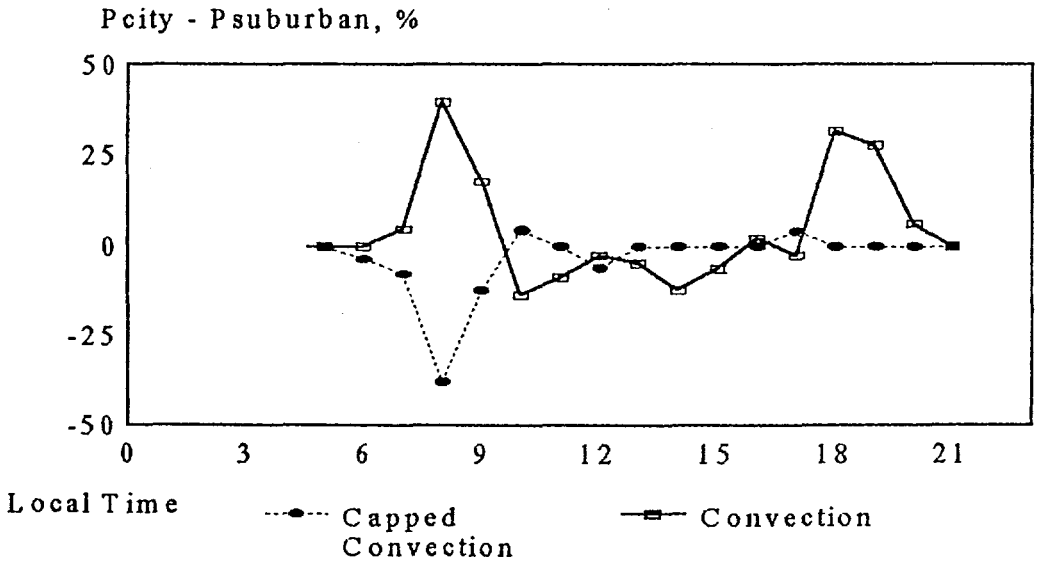


**Figure 3.** Mean daily courses of a difference in repeatability between unstable types of stratification in Moscow and suburban area for a summer period

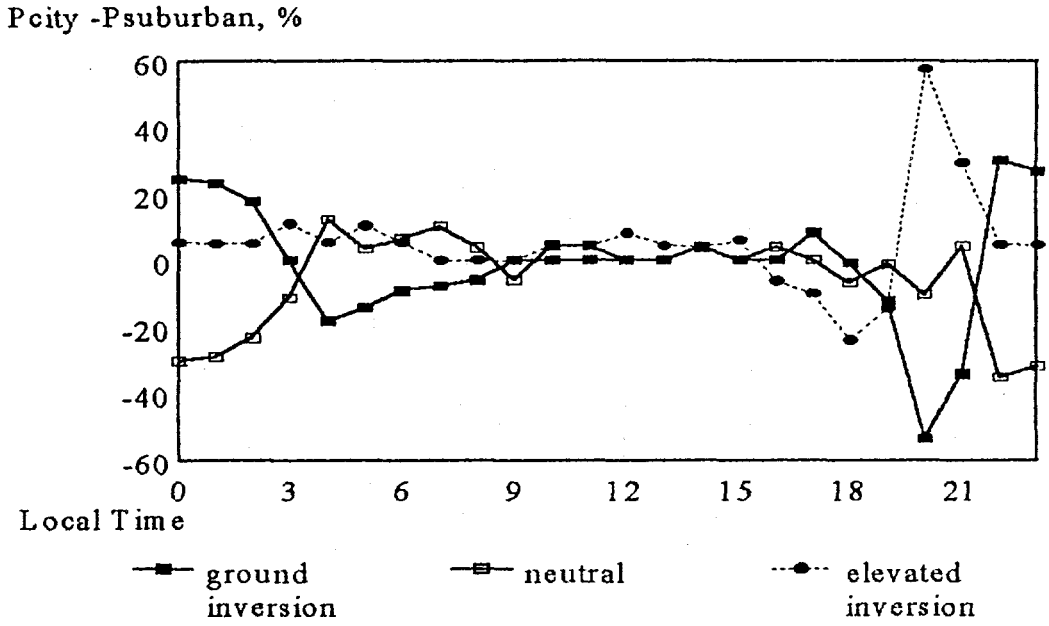


**Figure 4.** Mean daily courses of a difference in repeatability between stable types of stratification in Moscow and suburban area for a summer period

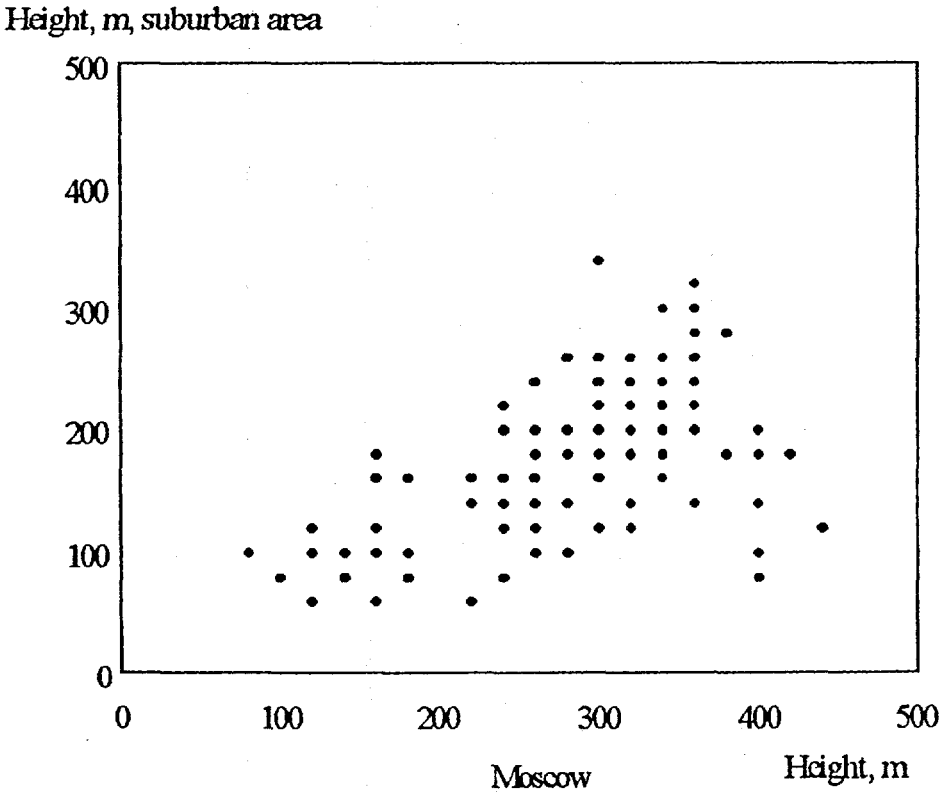


**Figure 5.** Heights of ground based inversions simultaneously measured by sodars at two locations

# Turbulent Structure of the Nighttime Atmospheric Boundary Layer and its Application to Vertically Dependent Mixing Heights

Frank R. Freedman[1,2] and Robert D. Bornstein[2]

[1]*Environmental Fluid Mechanics Laboratory Department of Civil Engineering Stanford University Stanford, CA 94305-4020, U.S.A.*
[2]*Department of Meteorology San Jose State University San Jose, CA 95192-0104, U.S.A.*

## Abstract

The atmospheric mixing height (MH) can be defined as the height to which pollutants emitted at an arbitrary emission height (EH) within the atmospheric boundary layer (ABL) vertically mix. During daytime, clear sky, weak wind conditions, buoyantly driven turbulence engulfs the entire ABL, and MH is independent of EH with its value approximated by the height of the elevated temperature inversion base. In situations where strong buoyant coupling is not present, decoupled regions of turbulence within the ABL can develop. An example of this is the nighttime, clear sky ABL over land. Here, the ABL is commonly described by a turbulent, surface based nocturnal boundary layer (NBL), a non-turbulent region capping the NBL in the vicinity of the nocturnal wind speed maximum, and a weakly turbulent residual layer (RL) above the speed maximum and capped by the base of the elevated inversion. The height to which pollutants mix for emissions in each of these regions will be different.

For this work, results of a 1-D numerical model simulation of Wangara Day 33 will be presented to illustrate the vertical variation of turbulent mixing within the nighttime ABL. It was found that turbulence within the NBL and RL was strongly decoupled by the non-turbulent region near the wind speed maximum. It was additionally found that, although RL turbulent kinetic energy was small (~ 0.1 m2s~2), RL diffusion coefficients were high (~ 1.0 m2s~l). Results suggest a value of MH near the turbulent depth of the NBL for EH within the NBL, and a value of MH that could extend up to the base of the elevated inversion for EH within the RL. Although results directly pertain to the vertical variation of MH within the nighttime, clear sky ABL over land, they are also applicable to daytime cases in which buoyant coupling is either weak (e.g. cloudy and/or windy conditions) or has been eliminated (e.g. in coastal regions in which a cool sea-breeze advects over the surface). Results from the study could help in the construction of analytical expressions to describe the dependence of MH on EH.

**Bibliographic Data Sheet** **Risø-R-997(EN)**

Title and author(s)

The Determination of the Mixing Height - Current Progress and Problems
EURASAP Workshop Proceedings, 1-3 October 1997, Risø National Laboratory

Sven-Erik Gryning, Frank Beyrich and Ekaterina Batchvarova


| ISBN | ISSN |
|---|---|
| 87-550-2325-8 | 0106-2840 |

| Dept. or group | Date |
|---|---|
| Wind Energy and Atmospheric Physics | October 1997 |

| Groups own reg.number(s) | Project/contract No. |
|---|---|
| | |

| Pages | Tables | Illustrations | References |
|---|---|---|---|
| 157 | | | |



Abstract (Max. 2000 char.)

This report contains extended abstracts of presentations given at a EURASAP Workshop on The Determination of the Mixing Height - Current Progress and Problems. The Workshop, initiated from discussions with Peter Builtjes, was held at Risø National Laboratory 1-3 October 1997 within the framework of EURASAP (European Association for the Sciences of Air Pollution). The specific topics and chairpersons of the Workshop were: Theoretical Considerations (Sven-Erik Gryning), Mixing Height Estimation from Turbulence Measurements and In-Situ Soundings (Douw Steyn), Mixing Height Determination from NWP-Models (Han van Dop), Climatology and Global Aspects (Werner Klug), Mixing Height Determination from Remote Systems (Werner Klug), Verification of Mixing Height Parameterizations and Models (Frank Beyrich), Mixing Height over Complex Terrain (Ekaterina Batchvarova), Internal Boundary Layers: Mixing Height in Coastal Areas and Over Cities (Allen White). The discussion at the end of the Workshop was chaired by Robert Bornstein.



Descriptions INIS/EDB

AIR POLLUTION, BOUNDARY LAYERS, MATHEMATICAL MODELS, METEOROLOGY, REMOTE SENSING, TURBULENCE, URBAN AREAS, WIND

Available on request from:
Information Service Department, Risø National Laboratory (Afdelingen for Informationsservice, Forskningscenter Risø)
P.O. Box 49, DK-4000 Roskilde, Denmark
Phone (+45) 46 77 46 77, ext. 4004/4005 · Fax (+45) 46 77 40 13